AD-A073 010 IMPERIAL COLL OF SCIENCE AND TECHNOLOGY LONDON (ENGLA--ETC F/G 13/2
RESPONSE AND STABILITY OF EARTH DAMS DURING STRONG EARTHQUAKES.(U)
JUN 79 S K SARMA DA-ERO-75-G-010

UNCLASSIFIED WES-MP-GL-79-13 NL

1 OF 3
AD A073010

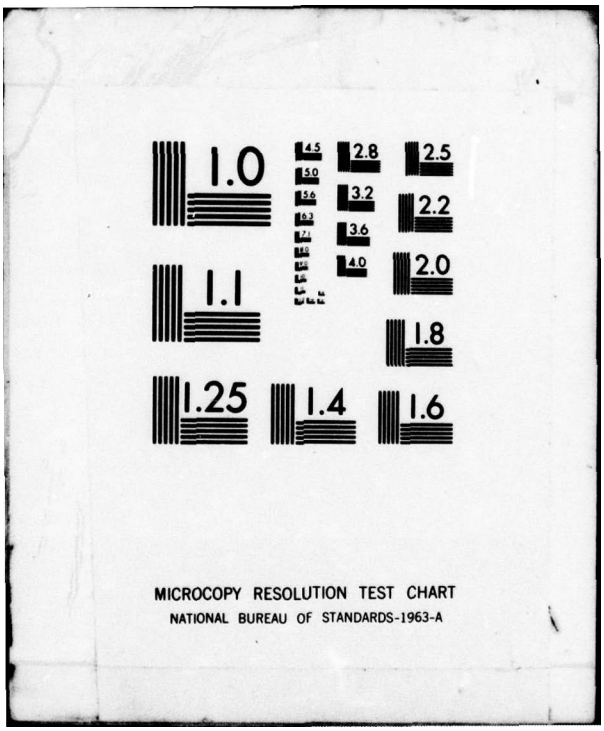
1.0
1.1
1.25
1.4
1.6
1.8
2.0
2.2
2.5
2.8
3.2
3.6
4.0
4.5
5.0
5.6
6.3
MICROCOPY RESOLUTION TEST CHART
NATIONAL BUREAU OF STANDARDS-1963-A

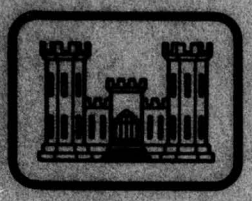

MISCELLANEOUS PAPER GL-79-13

RESPONSE AND STABILITY OF EARTH DAMS DURING STRONG EARTHQUAKES

by

S. K. Sarma
Department of Civil Engineering
Imperial College of Science and Technology, London, U. K.

LEVEL II

June 1979
Final Report

Prepared for Office, Chief of Engineers, U. S. Army
Washington, D. C. 20314

Under Grant Agreement No. DAERO-75-G-010

Monitored by Geotechnical Laboratory
U. S. Army Engineer Waterways Experiment Station
P. O. Box 631, Vicksburg, Miss. 39180

Destroy this report when no longer needed. Do not return it to the originator.

The findings in this report are not to be construed as an official Department of the Army position unless so designated by other authorized documents.

(18) WES

Unclassified
SECURITY CLASSIFICATION OF THIS PAGE (When Data Entered)

REPORT DOCUMENTATION PAGE	READ INSTRUCTIONS BEFORE COMPLETING FORM
1. REPORT NUMBER (19) Miscellaneous Paper GL-79-13	2. GOVT ACCESSION NO. / 3. RECIPIENT'S CATALOG NUMBER
4. TITLE (and Subtitle) (6) RESPONSE AND STABILITY OF EARTH DAMS DURING STRONG EARTHQUAKES	5. TYPE OF REPORT & PERIOD COVERED (9) Final report. / 6. PERFORMING ORG. REPORT NUMBER Nov 74 – Nov 76
7. AUTHOR(s) (10) S. K. Sarma	8. CONTRACT OR GRANT NUMBER(s) (15) Grant Agreement No. DAERO-75-G-010
9. PERFORMING ORGANIZATION NAME AND ADDRESS Department of Civil Engineering / Imperial College of Science and Technology London, United Kingdom	10. PROGRAM ELEMENT, PROJECT, TASK AREA & WORK UNIT NUMBERS CWIS Work Unit 31144
11. CONTROLLING OFFICE NAME AND ADDRESS Office, Chief of Engineers, U. S. Army Washington, D. C. 20314	12. REPORT DATE (11) June 1979 / 13. NUMBER OF PAGES 269
14. MONITORING AGENCY NAME & ADDRESS (if different from Controlling Office) U. S. Army Engineer Waterways Experiment Station Geotechnical Laboratory P. O. Box 631, Vicksburg, Miss. 39180	15. SECURITY CLASS. (of this report) Unclassified / 15a. DECLASSIFICATION/DOWNGRADING SCHEDULE

16. DISTRIBUTION STATEMENT (of this Report)

Approved for public release; distribution unlimited. (12) 278p.

17. DISTRIBUTION STATEMENT (of the abstract entered in Block 20, if different from Report)

18. SUPPLEMENTARY NOTES

19. KEY WORDS (Continue on reverse side if necessary and identify by block number)

Earth dams
Earthquakes
Dam stability
Earthquake resistant structures
Earthquake engineering

20. ABSTRACT (Continue on reverse side if necessary and identify by block number)

This earth dam study considers the response of an earth dam resting on a layer underlain by a rigid base and subjected to a strong ground motion. The dam and the layer are assumed to be elastic, homogeneous, and of simple geometric form. The properties of the dam and the layer may be different. Several combinations of the properties of the dam and the layer, as well as several ratios of the height of the dam to the depth of the layer, are studied.
(Continued)

CONT →

DD FORM 1 JAN 73 1473 EDITION OF 1 NOV 65 IS OBSOLETE

Unclassified
SECURITY CLASSIFICATION OF THIS PAGE (When Data Entered)

S/N 391986

4/B

20. ABSTRACT (Continued).

CONT'

All of these are subjected to nine strong motion acceleration records, and their response is calculated. At the same time, seismic coefficients for various sizes of sliding wedges are computed. The results of individual cases and their envelopes are presented in the spectral form for design purposes.

Methods of stability analysis for static and pseudostatic conditions are examined, and two new methods are presented. One of these methods is suitable for analyzing existing slip surfaces, and the other for quick computation of the critical acceleration for a given surface.

Since pore water pressure developed in the dam during an earthquake is an important factor, a method of stability analysis is developed that takes the excess dynamic pore water pressure into account. The method is based on limit equilibrium principle. Pore water pressures are introduced in the form of dynamic parameter A_n. The result is obtained in the form of a critical acceleration required to cause failure as a function of the number of cycles of earthquake load.

A sub n

Also shown is the computation of displacements of sliding wedges when the earthquake load is greater than the critical acceleration. Then the study is concluded with an example of the analysis of the effects of the San Fernando earthquake of 9 February 1971 on the Lopez Dam in California.

PREFACE

The work reported herein was performed by Dr. S. K. Sarma, of the Department of Civil Engineering, Imperial College of Science and Technology, London, United Kingdom, under Grant Agreement No. DAERO-75-G-010, dated 6 November 1974. This grant was sponsored by the Civil Works Directorate, Office, Chief of Engineers, U. S. Army, under CWIS Work Unit 31144, and administered by the U. S. Army Procurement Agency (Europe).

The research was conducted during the period from November 1974 to November 1976 under the direction of Drs. F. G. McLean, former Chief, and A. G. Franklin, Research Civil Engineer, Earthquake Engineering and Vibrations Division, Soils and Pavements Laboratory (now designated Geotechnical Laboratory (GL)). General guidance was provided by Mr. J. P. Sale, Chief, and Mr. S. J. Johnson (retired), Special Assistant, GL.

The research in this document was made possible through the support and sponsorship of the U. S. Government through its European Research Office. The various computer programs were developed on the CDC 6400 computer at Imperial College. Special acknowledgement is due to Professor N. N. Ambraseys for several discussions during the course of the project.

Directors of the WES during the performance of this work and preparation of the report were COL G. H. Hilt, CE, and COL J. L. Cannon, CE. The Technical Director was Mr. F. R. Brown.

CONTENTS

CONVERSION FACTORS, U. S. CUSTOMARY TO METRIC (SI) UNITS OF MEASUREMENT

U. S. customary units of measurement used in this report can be converted to metric (SI) units as follows:

Multiply	By	To Obtain
inches	2.54	centimetres
feet	0.3048	metres
pounds (mass) per cubic foot	16.01846	kilograms per cubic metre
pounds (force)	4.448222	newtons
pounds (force) per square inch	6894.757	pascals
pounds (force) per square foot	47.88026	pascals
feet per second	0.3048	metres per second
degrees (angle)	0.01745379	radians

RESPONSE AND STABILITY OF EARTH DAMS DURING STRONG EARTHQUAKES

PART I: INTRODUCTION

Background

1. With the failure of the Lower San Fernando Dam during the San Fernando earthquake of 9 February 1971, the attention is directed towards the problem of rational design of earth and rockfill dams against strong earthquake ground motion. With the aid of a high-speed computer and a very sophisticated method of finite element analysis using the nonlinear properties of the materials at the time of failure and knowing the ground motion characteristics of the San Fernando earthquake, it is possible to back-analyze and give the cause of this failure, Seed et al. (1973). But for the designer, who has yet to fix a dam section, to satisfy himself about the soil properties obtained from laboratory tests and assume the ground motion characteristics of a future event, the use of the finite element method is not economical. Moreover, the results obtained by a sophisticated method with doubtful input data are equally doubtful. Therefore, the use of a sophisticated method with doubtful input cannot be justified unless, of course, the method is equally costly and can be used with equal ease--not the case with the finite element method. On the other hand, simplified methods, such as those based on linear analysis of response and limit equilibrium analysis of stability, have produced results comparable to those of the finite element method. What is needed, therefore, is further refinement of the simplified approach without adding extra cost or time to the designer but with a more extensive use of information about the process of analysis. Thus, within the bounds of present-day knowledge regarding the soil parameters and the ground motion input, a simplified method of approach to the design of earth dams is desirable.

Purpose

2. The purpose is to provide a comprehensive method for such an analysis. In order to analyze the stability of a dam during an earthquake, the following information is needed:

a. The inertia forces that are being generated in the dam during an earthquake.

b. The resistance of the dam against these forces, along with the preexisting static forces.

c. The possible consequences when the resistance is not sufficient to withstand these forces temporarily.

These three factors are discussed in Parts II, III, and IV, respectively. In Part V, the proposed method is used to study the effect of the San Fernando earthquake on the Lopez Dam in California, United States of America.

PART II: INERTIA FORCES AND SEISMIC COEFFICIENTS IN EARTH DAMS

Inertia Forces

3. Earth dams are not absolutely rigid, and when excited into oscillations by strong earthquakes, they will respond in a manner that will be dictated by (a) the geometry of the dam, (b) the material properties of the dam and its foundation, and (c) the nature of the ground movements. Depending on circumstances, the ground movements may cause accelerations to develop in the body of the dam with associated fluctuating stresses, which may be larger or smaller than those of the ground.

4. During a strong earthquake, which may last from a few seconds to a few minutes, the ground accelerations will fluctuate with time in magnitude and direction. A dam to which this excitation is applied will respond in a manner that is determined by its resilience and its capacity to dissipate energy. The lower its capacity to dissipate energy, the greater will be its response. Moreover, the dam will seek out the periods of ground movements and respond strongly to those with which it can resonate. Consequently, an earthquake cannot be specified by an acceleration alone, nor can a dam be assumed to be rigid.

5. To make the problem amenable to analysis, it is necessary to make assumptions to obtain such solutions as various authors have done. For instance, Ambraseys and Sarma (1967) give a table of these solutions, which is reproduced here for easy reference (Table 1). Ambraseys and Sarma (1967) and Sarma (1968) deal with the problem of the dam on the rigid foundation and present design curves. Since it is not always possible to assume the foundation to be rigid, it is thought better to produce another set of curves which will take the depth and the shear modulus of the foundation into consideration.

6. Thus, for the sake of analysis, the following assumptions are made regarding the geometric configuration of the dam. We define the geometry by Figure 1:

Table 1

Solutions for Dam Response Problem

One-Dimensional Solutions: Length of Dam L	Width of Crest b	Side Slopes ϕ	Thickness of Overburden d	Ground Acceleration $\ddot{g}$	Shear Modulus G(y)	References
L	b	$\phi_1 = \phi_2$	0	$\ddot{g}(t)$	constant	Ambraseys (1960a, 1960b, 1960c)
L	0	$\phi_1 = \phi_2$	0	$\ddot{g}(t, x)$	constant	Hatanaka (1952, 1955)
L	0	$\phi_1 \neq \phi_2$	0	sine	constant	Minami (1960)
∞	0	$\phi_1 = \phi_2$	d	$\ddot{g}(t)$	constant	Ambraseys (1960a)
∞	0	$\phi_1 = \phi_2$	0	$\ddot{g}(t)$	$y^{1/3}$	Rashid (1961)
L	b	$\phi_1 = \phi_2$	0	$\ddot{g}(t, x)$	y^2	Ambraseys (1963)*
∞	b	$\phi_1 = \phi_2$	0	$\ddot{g}(t, x)$	y^n	Ambraseys (1963)* ($n \neq 2$)

Two-dimensional solutions: Yokoo et al. (1957)
Ishizaki and Hatakeyma (1962)
Medvedev and Sinitsym (1965)
Clough and Chopra (1965)

* Unpublished reports. $G(y) = s(y)^2 p$.

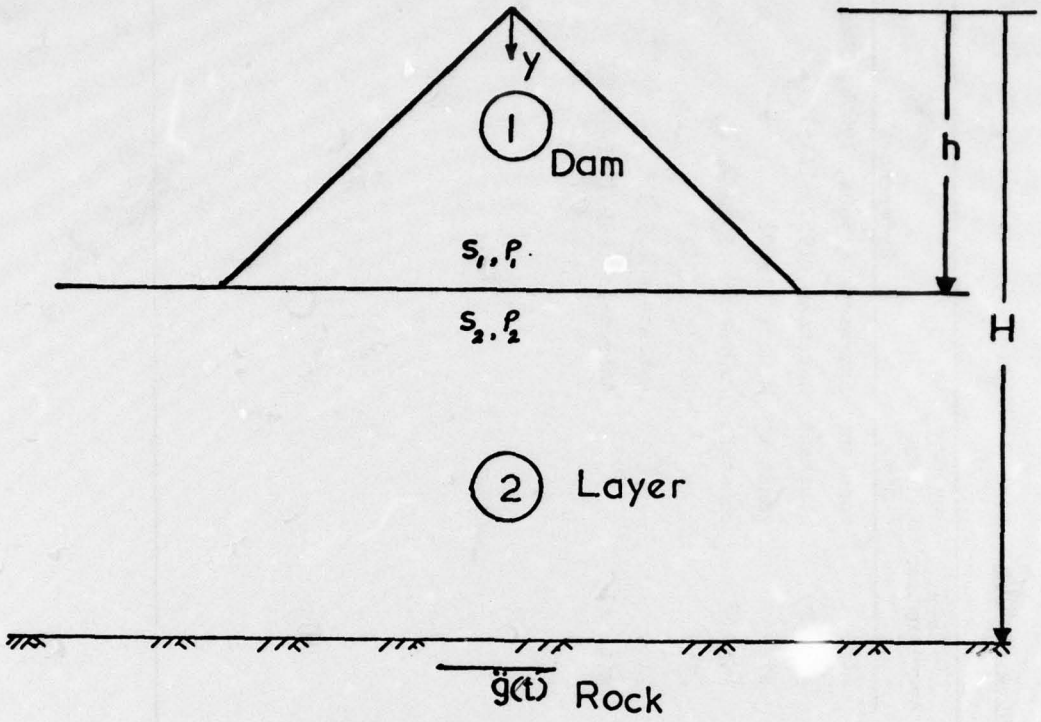

Figure 1. Geometry of dam-foundation system

a. A triangular untruncated wedge is resting on a layer underlain by base rock.

b. The length of the dam is much greater than its height.

c. The dam is symmetrical about a vertical axis.

d. The slopes are flat.

e. It vibrates in shear only.

7. Under these assumptions, a one-dimensional shear beam analysis can be applied. Slight deviations from these assumptions do not affect the result. For example, Ambraseys (1960) has shown that when the top width of the dam is less than 10 percent of the base width of the dam, the wedge behaves as an untruncated wedge. The same author has also shown that when the length of the dam is larger than four times the height, a one-dimensional solution applies. Two-dimensional solutions by Clough and Chopra (1965) and Hatanaka (1955) have shown that for slopes flatter than 1:1.5 a shear beam solution applies.

8. Regarding the properties of the material, we assume that the material for both the dam and its foundations are linearly elastic, homogeneous, and isotropic but that the properties of the dam and the foundations are different. Also, the material has an energy dissipating capacity or damping.

9. For small values of inertia forces, the dam behaves elastically, but the stress-strain behaviour of the material over the stress range in question is not elastic. However, with proper use of damping values, an average linear relationship may be used. The elastic properties of the dam are most conveniently introduced in terms of the shear wave velocity of the material. For zoned dams, when more than one type of soil is used, a weighted average value may be used. Elastic properties of soil generally vary with depth, but the actual variation is not exactly known; therefore, its use cannot be justified in a simplified solution.

Energy dissipating mechanisms

10. The various kinds of energy dissipating mechanisms present in the dam foundation system are as follows:

a. Viscous damping. In this case, energy loss is proportional to the velocity. With pure viscous damping in elastic material, there is no residual displacement at the end of vibrations. In the vibration problems for analysis, this is the most convenient form of damping.

b. Hysteretic damping due to nonlinearity. This is the energy loss due to nonrecoverable work done when the material is strained into an inelastic zone. In this case, there may be permanent deformations of the structure at the end of vibrations. This kind of damping varies with the level of strain.

c. Radiation damping. This is the energy loss due to nonrigidity of the base rock when some of the vibrational energy is filtered back into the base rock. This depends on the relative properties of the structure and the base rock.

In reality, all three energy-dissipating mechanisms are present. Since viscous damping provides an easy method of solution, we lump all of these into one equivalent viscous damping term. As a result, the displacement that is computed is much less than the real one. On the other

hand, the stresses and, therefore, the inertia forces that are computed with equivalent viscous damping become realistic. Even though the pure viscous damping is a frequency-dependent characteristic, in vibration problems this damping is assumed to be constant for all frequencies.

11. There is no direct way to estimate the equivalent viscous damping. The only possible way is vibrating real structures and recalculating the damping from the response of the structure. Alternatively, it may be possible to separate the radiation damping from the other two. In this case, the radiation is considered to be part of the problem, but the solution to this problem does not exist at present.

12. The nature of ground movements depends on various factors, such as the source mechanism, the distance of the site from the source, and the geological conditions of the wave path from the source to the site. The radiation of energy from the structure to the base rock also affects the input ground motion.

13. The earthquake parameter that can be predicted with some confidence is the maximum ground velocity. Otherwise, there is no way of predicting a future ground motion. One possible method is to look through the library of existing records of strong motion earthquakes and find the one that was produced under similar conditions of source, distance, and geology. An alternative is to select a few records that have different frequency characteristics and normalize the amplitudes to obtain the expected ground velocity. For the purpose of this analysis, we assume that the earthquake ground motion is an arbitrary disturbance.

Derivation of governing equations and solutions

14. Let us consider the response of an elastic untruncated wedge, resting on an elastic foundation layer underlain by a rigid base (Figure 1). We consider the vibrations to be in shear in one dimension only, i.e., perpendicular to the y-axis and in the plane of the paper. It can be shown that the equations governing the vibrations of the dam foundation system when the base of the system is

subjected to a ground acceleration $\ddot{g}(t)$* are:

a. For the dam

$$\frac{\partial^2 u_1}{\partial y^2} + \frac{1}{y}\frac{\partial u_1}{\partial y} = \frac{1}{S_1^2}\left[\ddot{u}_1 + c\dot{u}_1 + \ddot{g}(t)\right] \ldots \quad (1)$$

b. For the foundation layer

$$\frac{\partial^2 u_2}{\partial y^2} = \frac{1}{S_2^2}\left[\ddot{u}_2 + c\dot{u}_2 + \ddot{g}(t)\right] \ldots \quad (2)$$

where

$u_1 u_2$ = displacement in the dam and the layer, respectively, measured relative to the base

y = vertical coordinate

S_1, S_2 = shear wave velocity in the dam and the layer, respectively

$\ddot{u}_1, \ddot{u}_2$ = absolute acceleration of a point on the dam and the layer, respectively

c = damping coefficient for both dam and layer

$\dot{u}_1, \dot{u}_2$ = velocity of a point in the dam and the layer relative to the rock, respectively

15. These assume that the damping coefficient for both the dam and the foundation layer is the same. The boundary conditions are

$$u_1(h,t) = u_2(h,t) \quad (3)$$

$$u_2(H,t) = 0 \quad (4)$$

$$\frac{\partial u_1}{\partial y} = 0 \quad \text{at} \quad y = 0 \quad (5)$$

---

* For convenience, symbols and unusual abbreviations are listed and defined in the Notation (Appendix G).

$$G_1 \frac{\partial u_1}{\partial y} = G_2 \frac{\partial u_2}{\partial y} \quad \text{at} \quad y = h \tag{6}$$

where

h = height of dam

t = time

H = total height from crest of dam to rock level

G_1, G_2 = shear modulus of the material of the dam and the layer, respectively

The initial conditions are at rest, i.e.

$$u_1(y,0) = u_2(y,0) = \dot{u}_1(y,0) = \dot{u}_2(y,0) = 0 \tag{7}$$

16. The solutions of these equations give (Ambraseys (1960b) and also Appendix A):

$$u_1(y,t) = \sum_{n=1}^{\infty} \frac{2J_o\left(\bar{a}_n y/h\right)}{\bar{a}_n P_o(q,m,n)} S_{dn} \; ; \; 0 \leq y \leq h \tag{8}$$

$$u_2(y,t) = \sum_{n=1}^{\infty} \frac{2M_o(y)}{\bar{a}_n P_o(q,m,n)} S_{dn} \; ; \; h \leq y \leq H \tag{9}$$

where

J_o, J_1 = Bessel function of the first kind of order zero and the first kind of order one, respectively

$$\bar{a}_n = n^{th} \text{ root of the equation } m \tan q\left(\bar{a}_n\right) \Big/ J_1\left(\bar{a}_n\right) \tag{10}$$

$$P_o(q,m,n) = \frac{J_1\left(\bar{a}_n\right)}{\cos\left(q\bar{a}_n\right)} \left[mq + m^2 \sin^2\left(q\bar{a}_n\right) + \cos^2\left(q\bar{a}_n\right) - \frac{m}{\bar{a}_n} \sin\left(q\bar{a}_n\right) \cos\left(q\bar{a}_n\right) \right] \tag{11}$$

$$M_o(y) = \frac{mJ_1(\bar{a}_n)}{\cos(q\bar{a}_n)} \sin\left(q\bar{a}_n \frac{H-y}{H-h}\right) \tag{12}$$

$$q = m(H-h)P_2/(hP_1) \tag{13}$$

$$m = S_1P_1/S_2P_2 \tag{14}$$

$$S_{dn} = -\frac{S_1}{\omega_n} \int_o^t \ddot{g}(\tau) e^{-\lambda\omega_{on}(t-\tau)} \sin\left[\omega_n(t-\tau)\right] d\tau \tag{15}$$

$\omega_n = \omega_{on}\sqrt{1-\lambda^2}$ = damped and undamped circular frequency, respectively, of the dam foundation system (16)

$\omega_{on} = \frac{S_1}{h}\bar{a}_n$ = undamped circular frequency of the n^{th} mode of the dam foundation system (17)

$\lambda = \frac{C}{2\omega_{on}}$ = damping as a factor of critical, assumed the same for all modes (18)

τ = variable of integration

17. There is no way of proving, at least not to the knowledge of the author, that the solutions $u_1(y,t)$ and $u_2(y,t)$ obtained by applying the Laplace transform technique satisfy the governing equations. Therefore, we apply the limit tests. For $H=h$, the solution $u_1(y,t)$ converges to the well-known case of the dam on the rigid base, which is

$$u_1 = \sum_{n=1}^{\infty} \frac{2J_o(a_n y/h)}{a_n J_1(a_n)} S_{dn} \tag{19}$$

where a_n represents n^{th} root of the equation $J_o(a_n) = 0$. For $h=0$, the solution u_2 converges to the well-known case of the layer on a rigid base, which is

$$u_2 = \sum_{n=1}^{\infty} (-1)^n \cdot \frac{4 \cos [(2n-1)\pi/2\ y/H]}{(2n-1)\ \pi} S_{dn} \qquad (20)$$

18. There is another indirect test that can be applied to test the solution, which is based upon the transient part of the solution. The solution obtained through the Laplace transform technique includes the transient part of the solution. For the undamped solution, the relative displacements u_1 and u_2 should equal the ground displacement at any time before the first arrival of the wave to the point in question. Solution u_1 is obtained as convolutions of two functions F_1 and $\ddot{g}$, and u_2 is obtained as convolutions of F_2 and $\ddot{g}$, where for the undamped case

$$F_1(y,t) = \sum \frac{2J_o(\bar{a}_n y/h)}{\bar{a}_n P_o(q,m,n)} \left[- \frac{\sin \left(S_1 \bar{a}_n t/h \right)}{S_1 \bar{a}_n/h} \right]; \quad h \geq y \geq 0 \qquad (21)$$

$$F_2(y,t) = \sum \frac{2M_o(y)}{\bar{a}_n P_o(q,m,n)} \left[- \frac{\sin \left(S_1 \bar{a}_n t/h \right)}{S_1 \bar{a}_n/h} \right]; \quad H \geq y \geq h \qquad (22)$$

If the solution is true, then

$$F_2(y,t) = t \quad \text{for} \quad 0 \leq t \leq (H-y)/S_2 \qquad (23)$$

and

$$F_1(y,t) = t \quad \text{for} \quad 0 \leq t \leq \left[(H-h)/S_2 + (h-y)/S_1 \right] \qquad (24)$$

19. For a set of typical values of m, q, and y, these two functions are evaluated numerically for t increasing from zero. Function F_2 was found to converge rapidly to t during the period concerned. For values of $y/h > 0.2$, the function F_1 also converged to

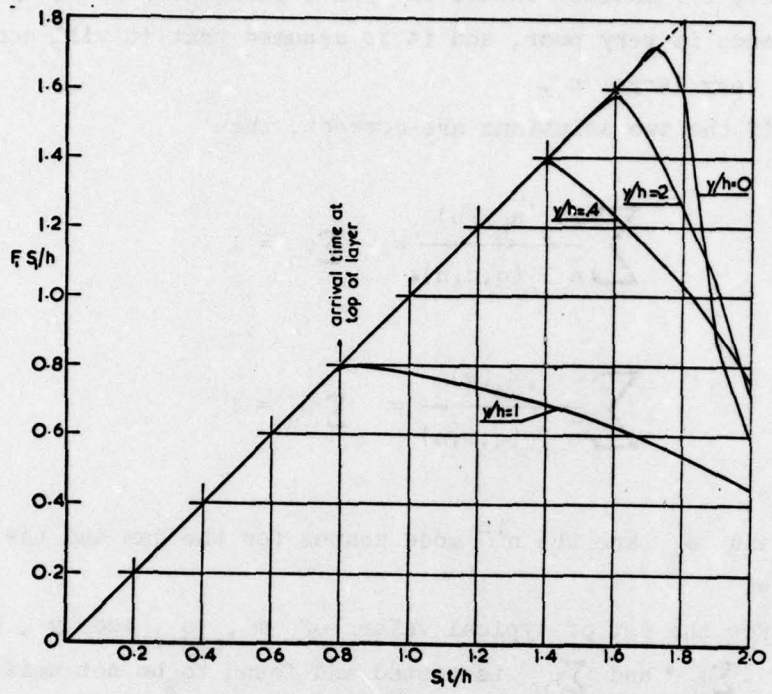

a. Untruncated wedge on a layer

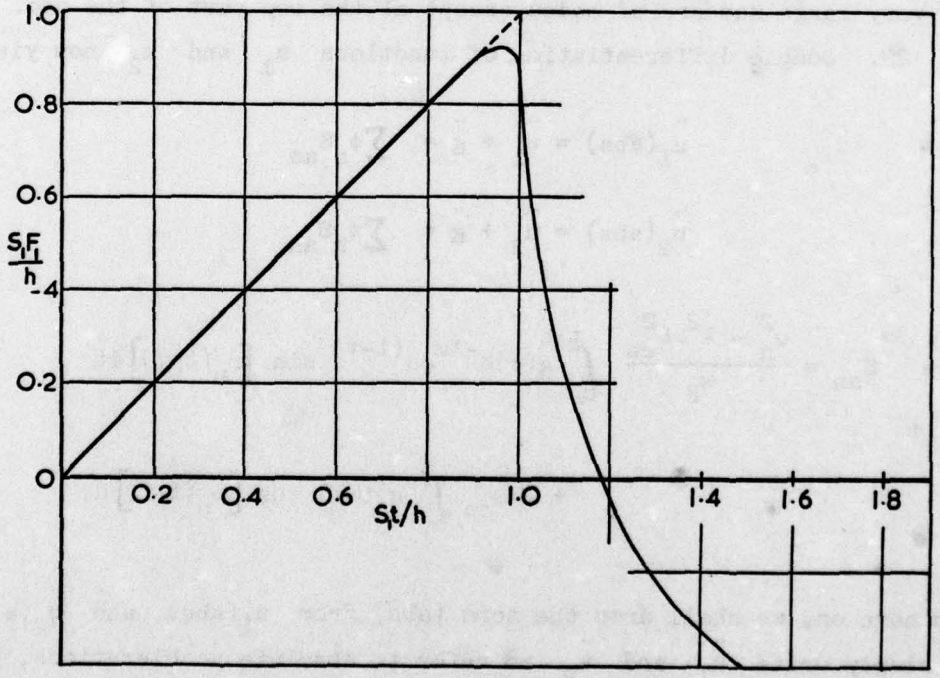

b. Untruncated wedge on rigid base

Figure 2. Convergence test for the function $F_1(y,t)$

t (Figure 2); for smaller values of y/h , particularly for y = 0 , the convergence is very poor, and it is assumed that it will converge to t with very large n .

20. If the two solutions are correct, then

$$\sum \frac{2J_o(\bar{a}_n y/h)}{\bar{a}_n P_o(q,m,n)} = \sum \phi_n = 1 \qquad (25)$$

$$\sum \frac{2M_o(y)}{\bar{a}_n P_o(q,m,n)} = \sum \psi_n = 1 \qquad (26)$$

where ϕ_n and ψ_n are the n^{th} mode shapes for the dam and the layer, respectively.

21. For the set of typical values of m , q , and y , the convergence of $\sum\phi_n$ and $\sum\psi_n$ is tested and found to be not uniform at all points of the dam (Figure 3). However, convergence can be achieved with very large numbers of modes except at the top part of the dam.

22. Double differentiation of functions u_1 and u_2 now yields

$$\ddot{u}_1(abs) = \ddot{u}_1 + \ddot{g} = \sum \phi_n S_{an} \qquad (27)$$

and

$$\ddot{u}_2(abs) = \ddot{u}_2 + \ddot{g} = \sum \psi_n S_{an} \qquad (28)$$

where $$S_{an} = \frac{\omega_n^2 - \lambda^2 \omega_{on}^2}{\omega_N} \int_o^t \ddot{g}(\tau) e^{-\lambda\omega_{on}(t-\tau)} \sin\left[\omega_n(t-\tau)\right] d\tau$$

$$+ 2\lambda\omega_{on} \int_o^t \ddot{g})t-\tau) \cos\left[\omega_n(t-\tau)\right] d\tau \qquad (29)$$

From here on, we shall drop the term (abs) from $\ddot{u}_1(abs)$ and $\ddot{u}_2(abs)$, and simply write $\ddot{u}_1$ and $\ddot{u}_2$ to refer to absolute accelerations, but

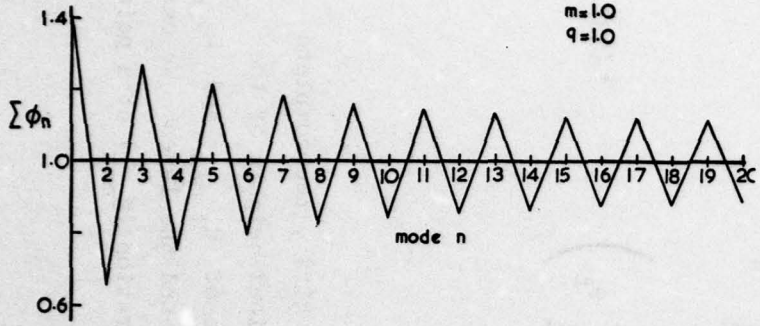

a. Test for $\Sigma\phi_n$ at y/h = 0

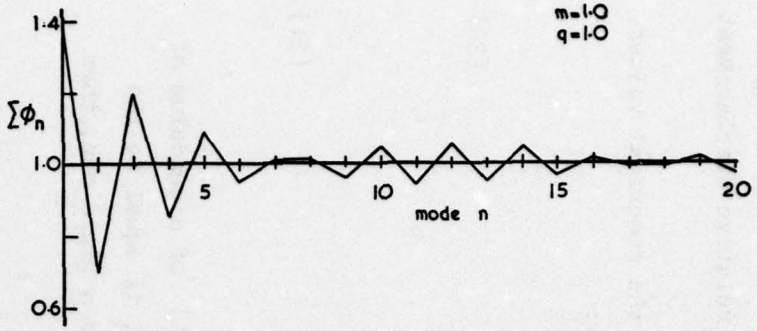

b. Test for $\Sigma\phi_n$ at y/h = 0.2

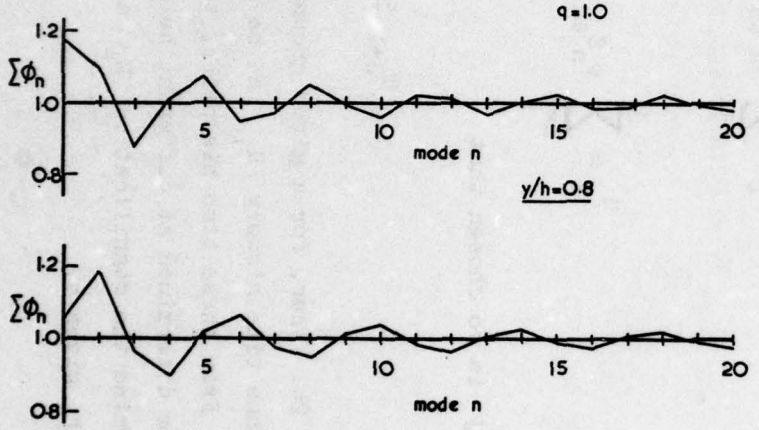

c. Test for $\Sigma\phi_n$ at y/h = 1.0

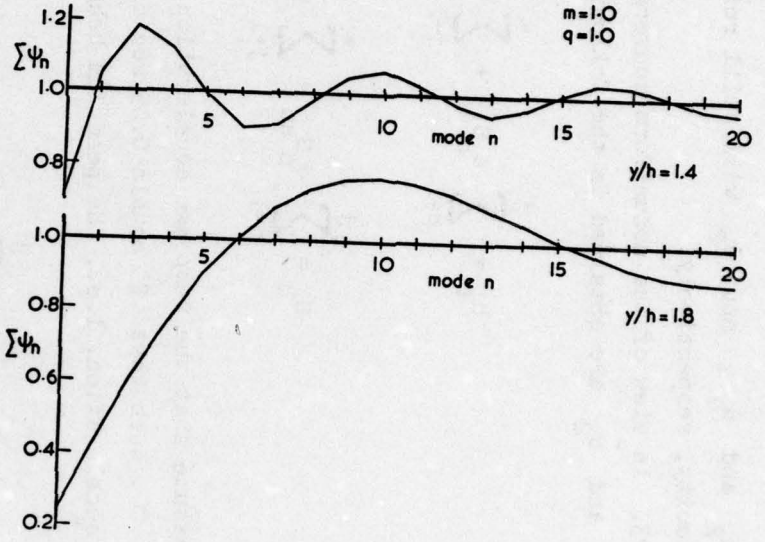

d. Tests for $\Sigma\psi_n$ at y/h = 1.4 and y/h = 1.8

Figure 3. Convergence tests for $\Sigma\phi_n$ and $\Sigma\psi_n$

u_1 , u_2 and $\dot{u}_1$, and $\dot{u}_2$ will still refer to relative displacement and velocity, respectively.

23. In view of the nonuniform convergence, the numerical values of $\ddot{u}_1$ and $\ddot{u}_2$ are obtained in the following way:

$$\ddot{u}_1 = \sum_{n=1}^{j} \phi_n S_{an} + \sum_{j+1}^{\alpha} \phi_n S_{an} \tag{30}$$

and

$$\ddot{u}_2 = \sum_{n=1}^{j} \psi_n S_{an} + \sum_{j+1}^{\alpha} \psi_n S_{an} \tag{31}$$

If we assume that the response acceleration $S_{an}(t)$ of a pendulum of period T , such that T equals 0.05 sec or less, is equal to the ground acceleration, i.e., the pendulum behaves as a rigid one, then

$$\ddot{u}_1 = \sum_{n=1}^{j} \phi_n S_{an} + \ddot{g}_{(t)} \left(1 - \sum_{n+1}^{j} \phi_n\right) \tag{32}$$

$$\ddot{u}_2 = \sum_{n=1}^{j} \psi_n S_{an} + \ddot{g}(t) \left(1 - \sum_{n=1}^{j} \psi_n\right) \tag{33}$$

and j is so chosen that

$$T_{j+1} \leq 0.05 \text{ sec}$$

24. Thus, for a given ground acceleration $\ddot{g}(t)$, the complete response time history $\ddot{u}_1$ can be computed at various heights of the dam. From these time histories, the maximum value of $\ddot{u}_{1\,max}$ and $\ddot{u}_{2\,max}$ can be determined at different heights of the dam and the layer. We can determine the magnification M_α of ground acceleration (g_{max}) at a point $y = \alpha h$ given by

$$M_\alpha = \frac{\ddot{u}_{1\ max}}{g_{max}} \text{ or } \frac{\ddot{u}_{2\ max}}{g_{max}}$$

Seismic Coefficients

25. From the solutions of $\ddot{u}_1$ and $\ddot{u}_2$, it is seen that the accelerations induced in the dam and in its foundations are not constant with respect to height or in time. However, most of the stability analysis techniques prefer to have the accelerations constant with height. According to Seed and Martin (1966), Ambraseys and Sarma (1967), and Sarma (1968), if the potential sliding surface can be defined in advance, then an average seismic acceleration can be computed for that surface that will be a function of the ground vibrations and periods of the dam.

26. The "average seismic coefficient" is defined as that factor which, when multiplied by the weight of the sliding mass, gives the maximum inertia force that will act on the mass during a particular earthquake. Thus

$$K = \frac{F_{max}}{W} \tag{34}$$

where

K = average seismic coefficient

F_{max} = maxiumum inertia force on the potential sliding mass

W = weight of the sliding mass

For convenience of comparison, we shall express the seismic coefficient in terms of the maximum ground acceleration instead of the acceleration due to gravity as

$$\overline{K} = \frac{Kg}{g_{max}} = \frac{F_{max}}{Mg_{max}} \tag{35}$$

where M represents total mass of the sliding body. In order to

compute $\overline{K}$, therefore, we have to determine the total inertia force F and the total mass M of the sliding body.

27. In Figure 4a, consider an element of the sliding mass of thickness dy and width $b(y)$ at a depth y from the crest. The mass of the elemental slice is

$$dm = \rho b(y)\, dy \tag{36}$$

where ρ is the mass density. The corresponding absolute acceleration at the depth y at an instant t is $\ddot{u}(y,t)$ where $\ddot{u} = \ddot{u}_1$ if $y \leq h$, and $\ddot{u} = \ddot{u}_2$ if $y > h$. Then the inertia force on this elemental slice is

$$dF = \ddot{u}\, dm$$

$$= \rho b(y)\ddot{u}(y,t)\, dy \tag{37}$$

Then, the total mass M of the sliding body is

$$M = \int_0^{\alpha h} \rho b(y)\, dy \tag{38}$$

and the total force F is

$$F = \int_0^{\alpha h} \rho b(y)\ddot{u}(y,t)\, dy \tag{39}$$

As can be seen from Equation 39, F is a function of both α and t. We can evaluate the complete time history of the function F and find the absolute maximum value of it at some instant that will give F_{max}, for a given base motion. Thus, knowing F_{max}, M, and the maximum value of the ground acceleration g_{max}, we can determine $\overline{K}_\alpha$, which will be a function of α. For convenience of computation, we may determine a quantity

$$A(\alpha,t) = \frac{F}{M} \tag{40}$$

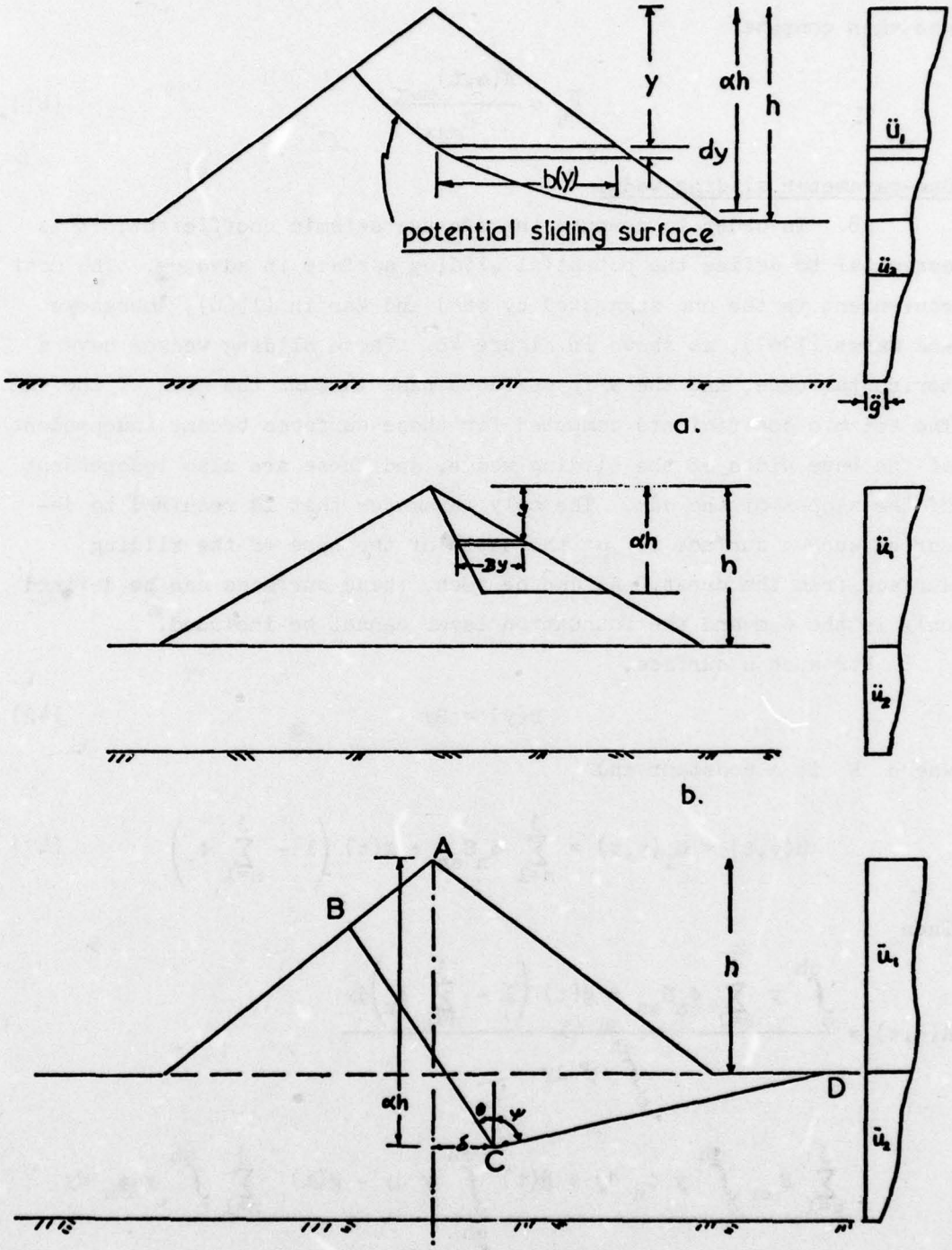

Figure 4. One-parameter and four-parameter sliding wedges

and then compute

$$\overline{K}_a = \frac{A(\alpha,t)_{max}}{g_{max}} \tag{41}$$

One-parameter sliding wedge

28. In order to compute the average seismic coefficient, it is essential to define the potential sliding surface in advance. The most convenient is the one suggested by Seed and Martin (1966), Ambraseys and Sarma (1967), as shown in Figure 4b. These sliding wedges have a horizontal base, and the slip surfaces pass through the apex of the dam. The seismic coefficients computed for these surfaces become independent of the base width of the sliding wedge, and these are also independent of the slopes of the dam. The only parameter that is required to describe such a surface is α the depth of the base of the sliding surface from the crest. As can be seen, these surfaces can be defined only in the dam and the foundation layer cannot be included.

For such a surface,

$$b(y) = By \tag{42}$$

where B is a constant and

$$\ddot{u}(y,t) = \ddot{u}_1(y,t) = \sum_{n=1}^{j} \phi_n S_{an} + \ddot{g}(t)\left(1 - \sum_{n=1}^{j} \phi_n\right) \tag{43}$$

Then

$$A(\alpha,t) = \frac{\int_0^{\alpha h} y \sum_{n=1}^{j} \phi_n S_{an} + \ddot{g}(t)\left(1 - \sum_{n=1}^{j} \phi_n\right) dy}{\int_0^{\alpha h} y\, dy}$$

$$= \frac{\sum_{n=1}^{j} S_{an} \int_0^{\alpha h} y\, \phi_n\, dy + \ddot{g}(t) \int_0^{\alpha h} y\, dy - \ddot{g}(t) \sum_{n=1}^{j} \int_0^{\alpha h} y\, \phi_n\, dy}{\int_0^{\alpha h} y\, dy}$$

Then

$$A(\alpha,t) = \sum_{n=1}^{j} \phi l_n(\alpha) S_{an} + \ddot{g}(t)\left[1 - \sum_{n=1}^{j} \phi l_n(\alpha)\right] \tag{44}$$

where

$$\phi l_n(\alpha) = \frac{\int_0^{\alpha h} y\phi_n \, dy}{\int_0^{\alpha h} y \, dy} \tag{45}$$

As shown in the Appendix B

$$\phi l_n(\alpha) = \frac{4J_1(\alpha\bar{a}_n)}{\alpha\bar{a}_n^2 P_o(q,m,n)} \tag{46}$$

Four-parameter sliding wedge

29. Because of the inability of the one-parameter sliding wedge to include a part of the foundation layer, Ambraseys and Sarma (1967) devised the four-parameter sliding wedge as shown in Figure 4c. In these wedges, the four parameters are the depth of the point C from the crest (α), the slope of the dam, and the two angles θ and ψ. It was assumed that the position of the point C is fixed. But in reality, the position of the point C can also be changed, which of course increases one parameter and seems unnecessary.

30. For such a surface, assuming $\rho_1 = \rho_2 = \rho$

$$F = \int_0^{\alpha h} \rho b(y)\ddot{u}_1 \, dy \qquad 0 \leq \alpha \leq 1 \tag{47}$$

or

$$F = \int_0^{h} \rho b(y)\ddot{u}_1 \, dy + \int_h^{\alpha h} \rho b(y)\ddot{u}_2 \, dy \quad \text{if} \quad \alpha > 1 \tag{48}$$

and

$$M = \int_0^{\alpha h} \rho b(y) \, dy \tag{49}$$

Therefore, using Equations 32 and 33 for $0 \leq \alpha \leq 1$,

$$A_\alpha = \frac{\int_0^{\alpha h} b(y)\left[\sum_{n=1}^{j} \phi_n S_{an} + \ddot{g}(t)\left(1 - \sum_{n=1}^{j} \phi_n\right)\right] dy}{\int_0^{\alpha h} b(y)\, dy} \tag{50}$$

This yields

$$A_\alpha = \sum_{n=1}^{j} \phi 4_n(\alpha) S_{an} + \ddot{g}(t)\left[1 - \sum_{n=1}^{j} \phi 4_n(\alpha)\right] \tag{51}$$

where

$$\phi 4_n(\alpha) = \frac{\int_0^{\alpha h} b(y)\phi_n\, dy}{\int_0^{\alpha h} b(y)\, dy} \quad \text{for} \quad \alpha \leq 1 \tag{52}$$

Similarly, when $\alpha > 1$,

$$A_\alpha = \frac{\int_0^{h} b(y)\left[\sum_{n=1}^{j} \phi_n S_{an} + \ddot{g}(t)\left(1 - \sum_{n=1}^{j} \phi_n\right)\right] dy + \int_h^{\alpha h} b(y)\left[\sum_{n=1}^{j} \psi_n S_{an} + \ddot{g}(t)\left(1 - \sum_{n=1}^{j} \psi_n\right)\right] dy}{\int_0^{\alpha h} b(y)\, dy} \tag{53}$$

This also yields,

$$A_\alpha = \sum_{n=1}^{j} \phi 4_n(\alpha) S_{an} + \ddot{g}(t)\left[1 - \sum_{n=1}^{j} \phi 4_n(\alpha)\right] \tag{54}$$

where

$$\phi 4_n(\alpha) = \frac{\int_0^{h} b(y)\phi_n\, dy + \int_h^{\alpha h} b(y)\psi_n\, dy}{\int_0^{\alpha h} b(y)\, dy} \quad \text{for} \quad \alpha > 1 \tag{55}$$

See Appendix B for $\phi A_n(\alpha)$.

Discussions and Design Curves

31. The single parameter by which a dam-layer system can be represented is its fundamental period. The fundamental period and the higher modes are functions of four factors - S_1 , h , m , q . These represent

(a) The shear wave velocity of the material of the dam = S_1 .

(b) The height of the dam = h .

(c) The shear wave velocity of the foundation layer = $\frac{\rho_1 S_1}{\rho_2}$ m .

(d) The height of the layer on which the dam is situated = $\frac{q}{m}\frac{\rho_1}{\rho_2}$ h .

The fundamental period of the dam-layer system is then given by

$$T_1 = 2\pi \frac{h}{\bar{a}_1 S_1} \tag{56}$$

where $\bar{a}_1$ is the 1st root of the equation

$$m \tan(q\bar{a}_n) = \frac{J_o(\bar{a}_n)}{J_1(\bar{a}_n)} \tag{57}$$

32. The higher roots of the equation give the higher mode periods of the system. These periods are given by

$$T_n = T_1 \bar{a}_1 / \bar{a}_n \tag{58}$$

Figure 5 gives the values of $\bar{a}_1$ for a combination of values of m and q . These curves can be used to determine the fundamental period of the dam-layer system. Some higher roots of the equation are given in a tabular form in the Appendix C.

33. The following earthquake acceleration records are chosen in order to determine the maximum accelerations at various heights of the dam. These records were chosen mainly because of their differences in frequency characteristics. The ground motions, acceleration, velocity,

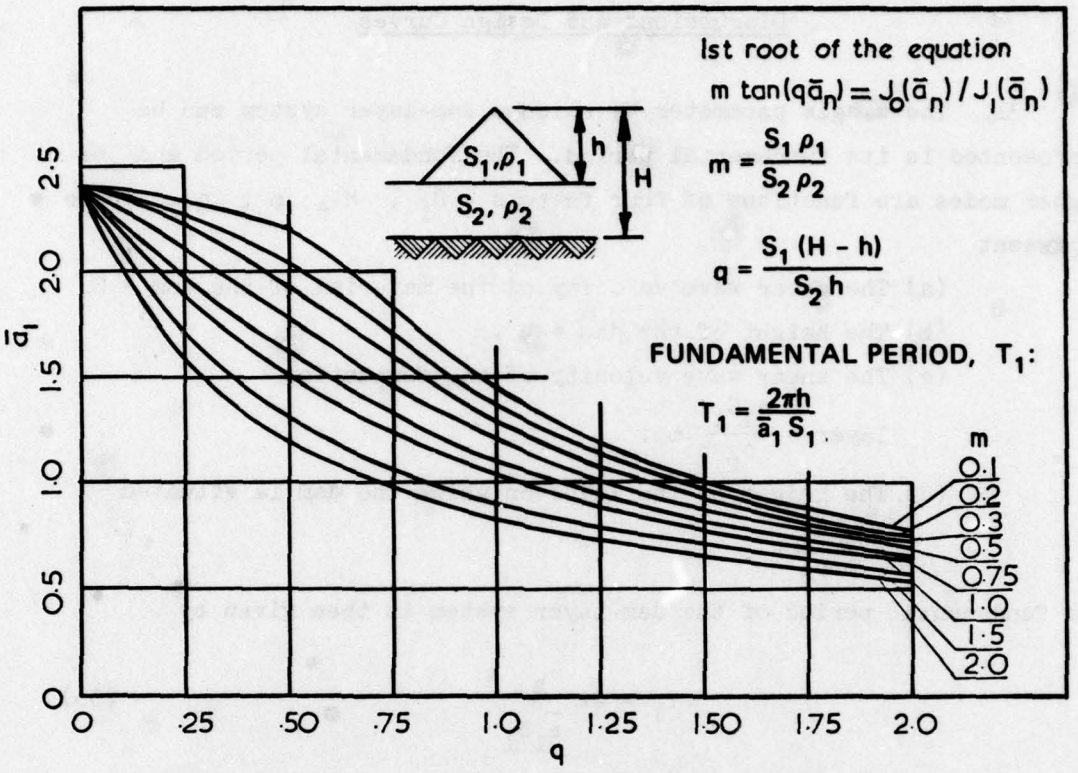

Figure 5. Fundamental period of dam-foundation system

and displacement spectra of these records are shown in Figures D1 through D9 (Appendix D). An example (the Port Hueneme record) is shown in Figure 6. The records are

a.	San Fernando Earthquake 1971 - Pacoima Dam	3 components
b.	Imperial Valley Earthquake 1940 - El-Centro Record	2 components
c.	Koyna (India) Earthquake 1967 - Koyna Dam Record	2 components
d.	Parkfield Earthquake 1966 - Cholame, Shandon Array No. 2	1 component
e.	Port Hueneme Record 1957	1 component

Another record, which is used for the study of the Lopez Dam is added later. This record is

f. San Fernando Earthquake 1971 - Deconvoluted and modified version.

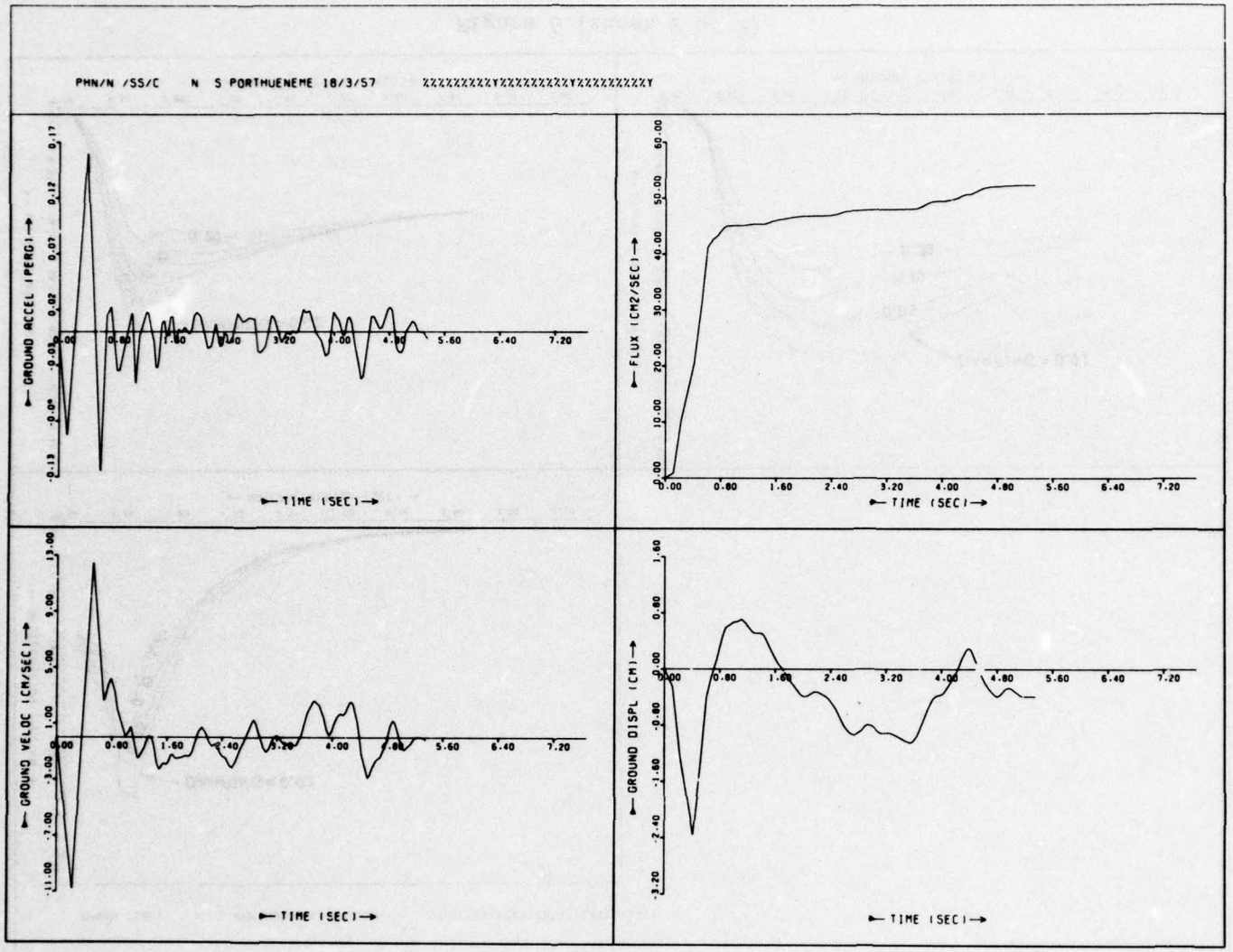

Figure 6. Ground motion records and spectra: Port Hueneme record of 1957 (sheet 1 of 2)

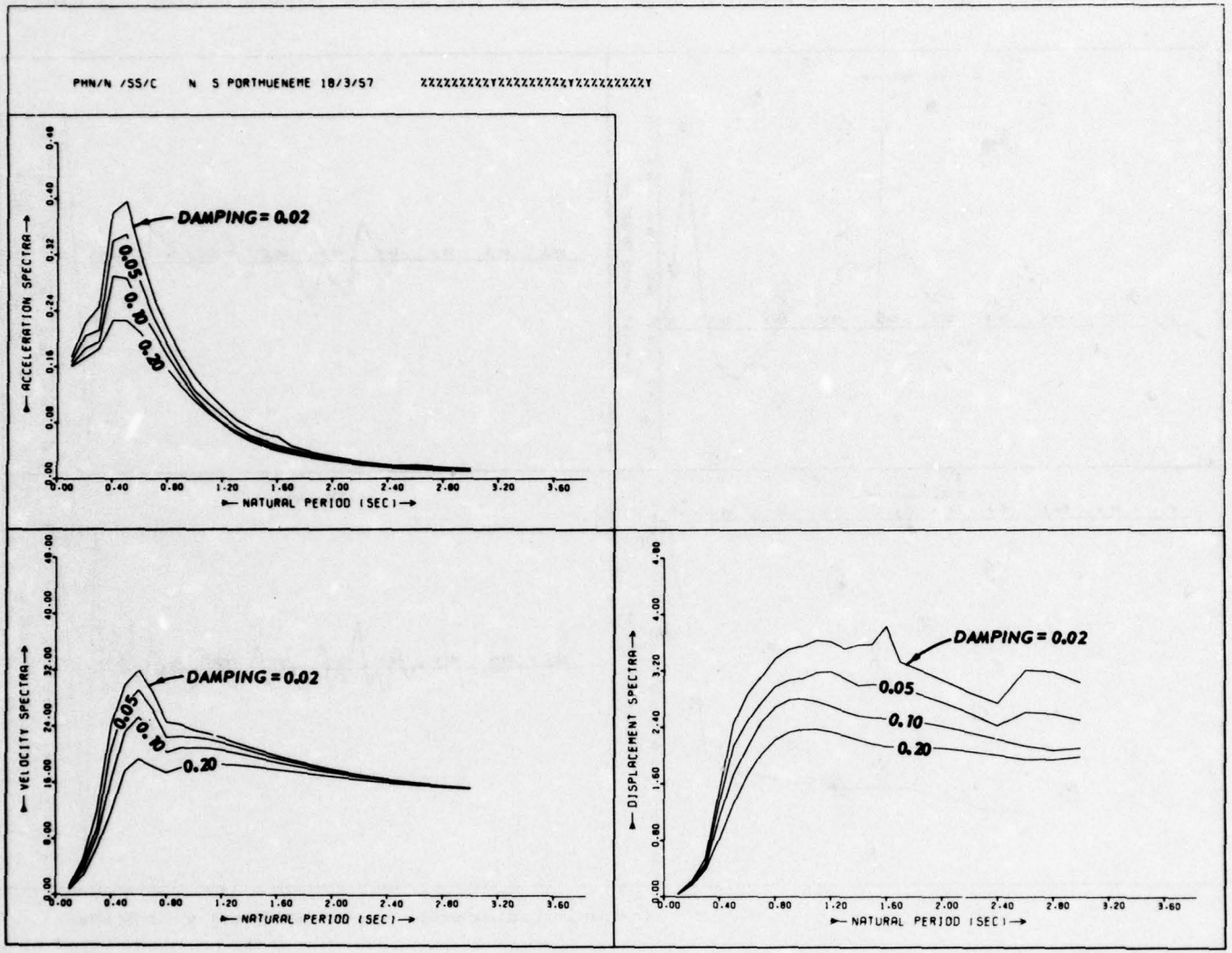

Figure 6 (sheet 2 of 2)

34. In Figures 7 and 8 the effects of m and q are shown. It appears that for m less than 0.2, there may be some convergence problems, particularly in the upper part of the dam, when the predominant period of the earthquake ground motion nearly coincides with the fundamental period of the dam-layer system. For values of m less than 0.7, there is some magnification in the response of the dam, compared with the response of the dam on the rigid base. The magnification is largest for values of m about 0.25. The magnification is also affected by the value of q/m as shown in Figure 8. The magnification is different at different heights of the dam and at different periods of the dam-layer system.

35. Figure 9 is an explanation of Figures E-2 through E-127 (Appendix E) that show, in spectra form, the maximum response of dams of various fundamental periods, and m and q factors subjected to the first nine of the earthquake records listed above. The responses are calculated for a damping value of 20 percent critical for all modes. A maximum of 20 modes was used. The values of m and q that are chosen are

m =	0	0.5	1.0
q =	0	0.125	0.25
		0.25	0.50
		0.375	0.75
		0.50	1.00
		0.75	1.50
		1.0	2.00

36. These sets of q values correspond to depth of layer to height of dam ratios of

$$\frac{H - h}{h} = 1/4,\ 1/2,\ 3/4,\ 1,\ 1\text{-}1/2 \text{ and } 2 \text{ for } \rho_1 = \rho_2$$

At the same time, the seismic coefficients for one-parameter and four-parameter sliding wedges are computed and shown in Figure 9 in spectra form. In this figure, Figure 9a gives the values of the amplication factor M_α (the maximum acceleration at a point divided by the maximum ground acceleration), for values of $\alpha = 0, 0.2, 0.4, 0.6, 0.8, 1.0, 1.2, 1.4, 1.6, 1.8$ if the depth of the layer is greater than, or equal to

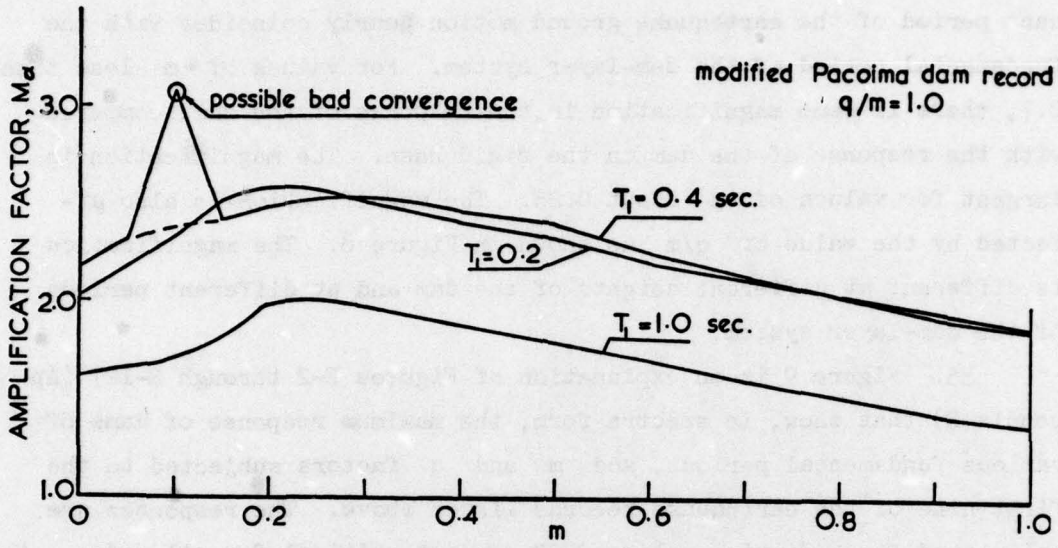

Figure 7. Response at crest of dam versus m

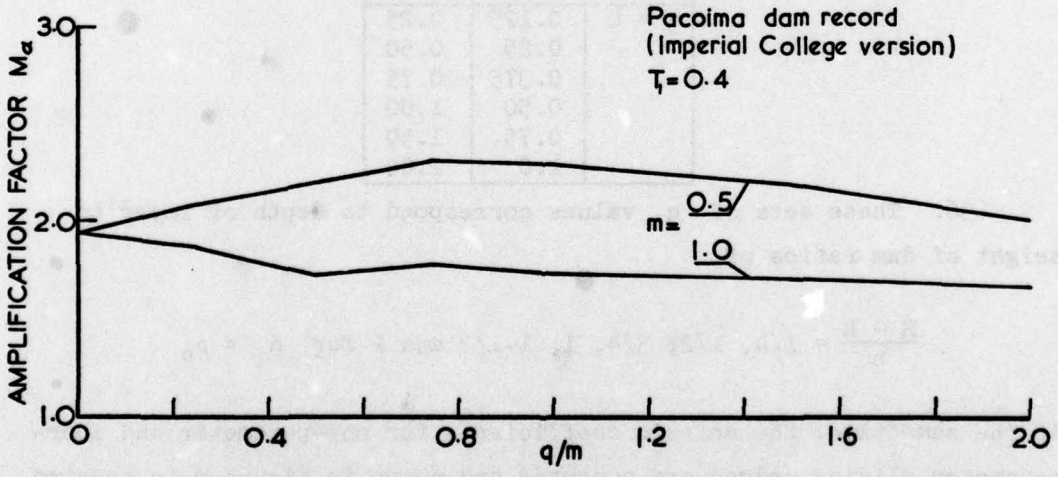

Figure 8. Response at crest of dam versus q/m

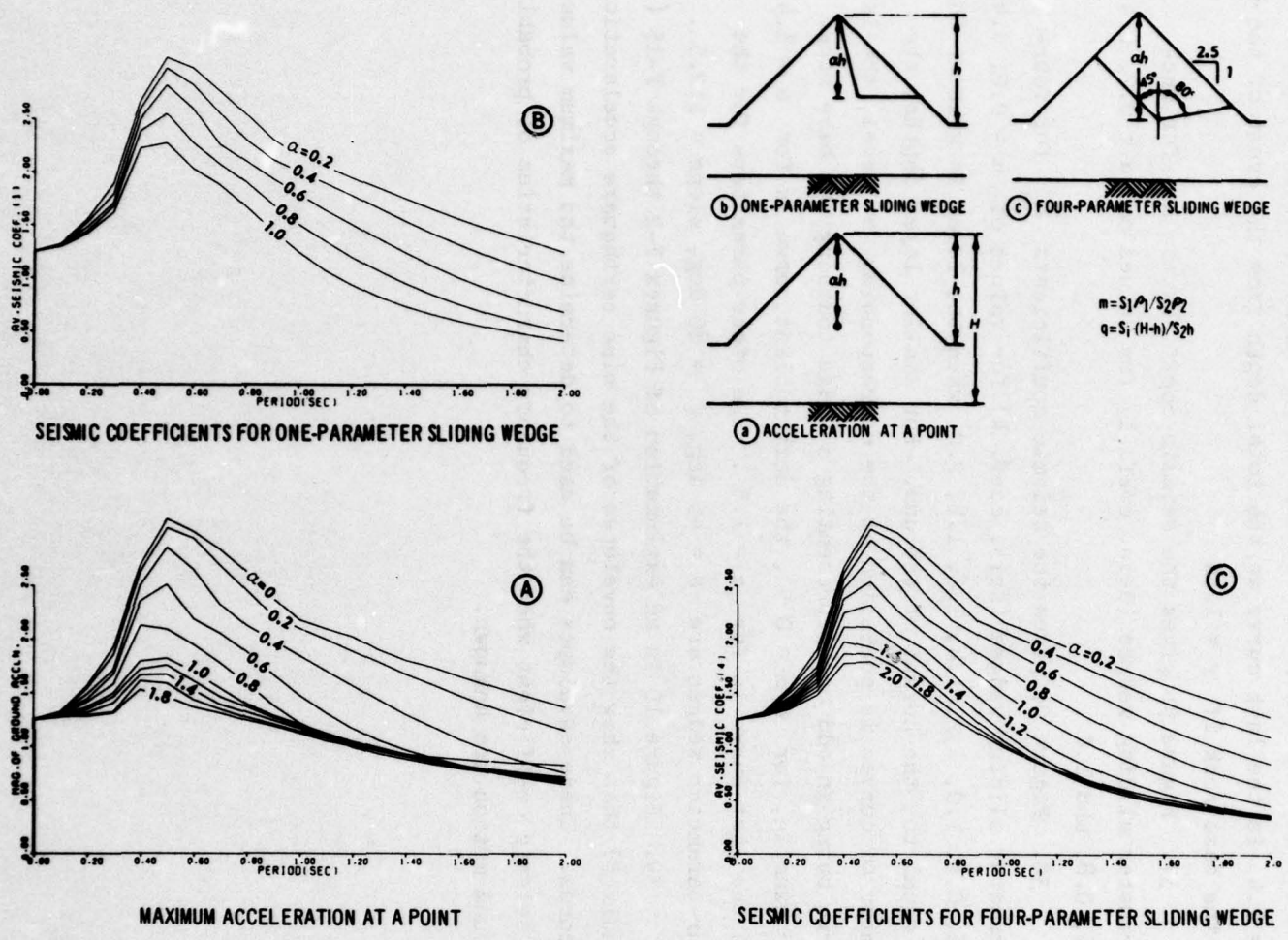

Figure 9. Explanations for Figures E-2 through E-127

the height of the dam. For smaller depths of layer, the number of curves is curtailed at the corresponding point. For example, $q/m = 0.5$ represents a layer depth which is half the height of the dam. Therefore, $\alpha = 1.4$ is the last curve as the total depth from the crest of the dam to the base rock if $y = 1.5h$.

37. Figure 9b gives the seismic coefficients $\overline{K}_\alpha$ for one-parameter sliding wedges (seis. coef. 1) for values of $\alpha = 0.2, 0.4, 0.6, 0.8$, and 1.0 .

38. Figure 9c gives the seismic coefficients $\overline{K}_\alpha$ for four-parameter sliding wedges (seis. coef. 4) for values of $\alpha = 0.2, 0.4, 0.6, 0.8, 1.0, 1.2, 1.4, 1.6, 1.8, 2.0$ when the layer is greater than, or equal to, the height of the dam. For smaller layer depths, the number of curves is curtailed at the corresponding α level, the last curve being an odd one representing a wedge touching the base rock. For example, for $q/m = 0.5$, the next to last curve is for $\alpha = 1.4$, and the last curve is for $\alpha = 1.5$. The other parameters for the four-parameter wedges are $\theta = 45$ deg, $\psi = 80$ deg, slope = 1:2.5 .

39. Figure 10 is an explanation of Figures F-2 through F-15 (Appendix F) that show the envelopes of the nine earthquake acceleration records. These envelopes can be used to determine the maximum values of seismic coefficient when the frequency characteristics of probable ground motion are unknown.

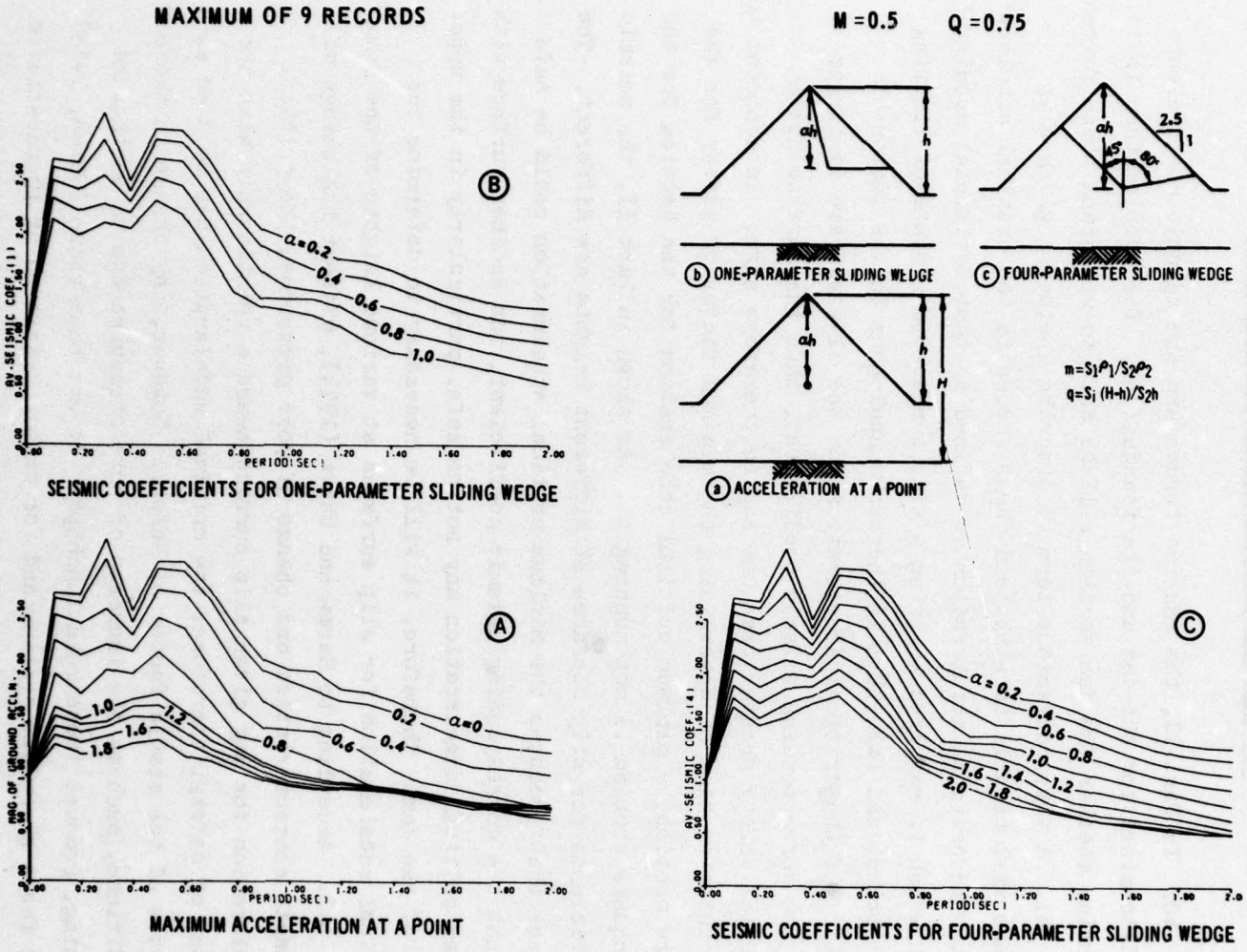

Figure 10. Explanation of Figures F-2 through F-15

PART III: STABILITY ANALYSIS

Critical Acceleration of Slip Surfaces

40. In Part II, the inertia forces and the seismic coefficients are determined for the dam and its foundations. The problem then is to determine whether the dam section will be able to withstand these forces.

41. A very convenient term to describe whether a given slip surface will be able to withstand these forces is the critical acceleration. The critical acceleration is defined as that horizontal acceleration which is required to bring a slip surface to a state of limiting equilibrium, and this term is therefore analogous to the factor of safety. If the critical acceleration for the slip surface is larger than the corresponding seismic coefficient, then the surface has a factor of safety greater than one and is therefore safe. In contrast to the static problem of determining the minimum factor of safety for the entire section, a minimum critical acceleration for the section for the earthquake problem is not meaningful. As shown in Part II, the seismic coefficients for slip surfaces at different heights are different. The surface that produces the minimum critical acceleration could be safe against the corresponding seismic coefficient, but another surface with a higher critical acceleration may not be safe, particularly in the upper part of the dam. Therefore, it will be necessary to determine the critical acceleration for slip surfaces at various heights of the dam.

42. According to Sarma and Bhave (1974), without the change of strength characteristics and change of pore pressures, the critical acceleration for any given slip surface bears a relationship with the factor of safety; therefore, the critical acceleration can be used as a measure of the static factor of safety. However, any change in these conditions, such as the increase of pore pressures due to earthquake loading, removes these relationships. It has been shown (Sarma, 1973) that for a given dam section and for static condition or pseudo-static condition of earthquake loading with horizontal accelerations, the determination of the critical acceleration is easier than the determination

of the factor of safety. The advantages of using a critical acceleration solution instead of a direct factor of safety solution are mentioned in Sarma and Bhave (1974).

43. In this analysis, it is assumed that the earthquake acceleration is constant along the height. It is known that the earthquake acceleration is not constant along the height, and that is why the seismic coefficient was defined in Part II. Therefore, an analysis is made to study the effect of the acceleration distribution on the critical earthquake load (Valenzuela, 1975). From this limited study, it is found that the critical earthquake load for a given slip surface is minimum when the acceleration distribution is constant and is not minimum when the accelerations are increasing towards the crest. Thus, the use of a constant acceleration with the seismic coefficients for that surface produces conservative results. But the use of the critical acceleration with constant distribution cannot produce the critical surface, whereas the use of varying acceleration can. However, the use of varying acceleration for design purposes is not suggested, for the variation is not known in advance.

Existing Methods of Stability Analysis

44. It is accepted that the pore water pressures in a dam increase with cyclic loading induced by earthquakes. Since increase in pore pressures reduces the total strength, this plays an important part in the stability of the dam section. But before going into the solution of the problem for earthquake loading, it is necessary to examine the problem of the stability analysis both for static and earthquake conditions. What follows below is an assessment of this problem. From this we will see that different techniques can be developed that will be suitable for specific types of problems. For example, to analyze an existing slip surface in a dam or a slope, the technique of solution should be different from that required for designing a dam. Since in the design of dams, one can reject a slip surface on the basis that the surface is not kinematically admissible, the existing slip surface

must produce a kinematically admissible solution. Thus, the assumptions may be varied to suit the problem. But whatever the technique, the solution is based on the limit equilibrium principle.

45. There are several methods of stability analysis in existence. All of these have certain things in common:

a. These methods are based on the limit equilibrium principle which defines the factor of safety or the critical acceleration.

b. They employ the Mohr-Coulomb failure criterion with rigid-plastic models.

c. All of these apply a method of slices.

d. They are based on assumed slip surfaces.

These methods differ in

e. The shape of the assumed slip surfaces.

f. The handling of the indeterminancy of the problem as shown later.

46. Before proceeding further, we need to define a few terms.

a. Simplified solution. A solution which does not satisfy all the static equilibrium conditions. Assumptions are made to obtain the solution in a simple form. Most of the available solutions, including Bishop's simplified method (1955), Kenney's method (1956), and even Janbu's generalized method of slices (1957), fall into this category.

b. Rigorous solution. A solution which satisfies the complete equilibrium condition of statics. The implied forces obtained from the solution may not be acceptable.

c. Acceptable solution. A rigorous solution which has the added criterion of the implied forces satisfying the criterion of acceptability. The basic criteria are: the forces must not violate the Mohr-Coulomb failure law, no tension is implied, and the direction of forces must be kinematically admissible.

Our aim is to obtain an acceptable solution with the least possible effort.

47. In the method of slices, the possible failure mass is divided into n slices (Figure 11). For each slice, the known and unknown forces and their points of applications are shown. For n slices, we have the following (6n-2) unknowns:

n	numbers of the normal force N
n	numbers of the shear force T
(n-1)	numbers of the body force E
(n-1)	numbers of the body force X
(N-1)	numbers of the point of application of E
n	numbers of the point of application of N
1	in the form of factor of safety or critical accelerations

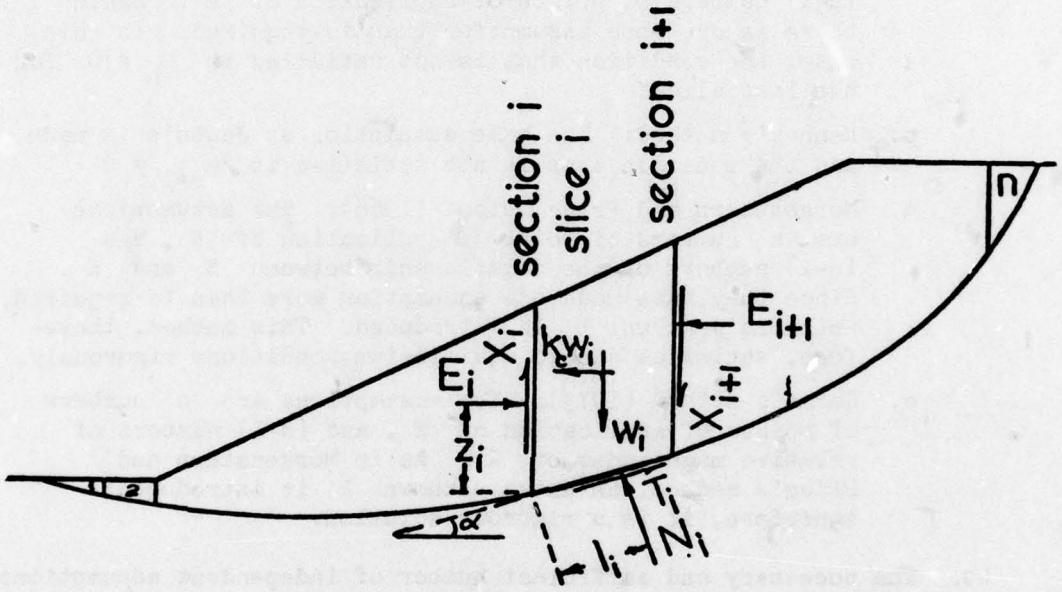

Figure 11. Stability analysis by method of slices

48. From the static equilibrium conditions of each slice, we have the following equations:

$$\sum \text{Moment} = 0$$
$$\sum \text{Vertical forces} = 0$$
$$\sum \text{Horizontal forces} = 0$$

The Mohr-Coulomb failure criterion gives $T = f(N)$; hence, for n slices we have 4n equations. In order to obtain a rigorous solution, therefore, one has to make 2n-2 assumptions. If more assumptions are made, more unknowns must be introduced. Now let us look into the various

available solutions and see how these assumptions are made.

a. Bishop's simplified method: In this method, the assumptions are n numbers of points of application of N, and $(n-1)$ numbers of the magnitude of X ($X = 0$). Since one more assumption is made than required and no unknown is introduced, one known condition must be sacrificed. In this case, the condition that is not satisfied is $E_{n+1} \neq 0$. For circular slip surfaces this error is small, and the result is therefore mostly acceptable.

b. Janbu's generalized method of slices: The assumptions are n numbers of points of application of N, and $(n-1)$ numbers of points of application of E. Again there is one more assumption than is required. In this case, the condition that is not satisfied is $M_n \neq 0$ for the last slice.

c. Kenney's method: The same assumption as Janbu's is made, and the equation that is not satisfied is $E_{n+1} \neq 0$.

d. Morgenstern and Price method (1966): The assumptions are n numbers of point of application of N, and $(n-1)$ numbers of the relationship between X and E. Since they have made one assumption more than is required, an extra unknown λ is introduced. This method, therefore, satisfies static equilibrium conditions rigorously.

e. Sarma's method (1973): The assumptions are n numbers of points of application of N, and $(n-1)$ numbers of relative magnitudes of X. As in Morgenstern and Price's method, an extra unknown λ is introduced; therefore, it is a rigorous solution.

49. The necessary and sufficient number of independent assumptions that are required are $(2n-2)$. If one can make these assumptions satisfactorily, a rigorous solution can be obtained. Some possible combinations of assumptions that one can make are given below.

a. $(n-1)$ numbers of relationship between X and E, and $(n-1)$ numbers of point of application of E or N. A method of solution based on these assumptions is provided herein.

b. $(n-1)$ numbers of point of application of E, and $(n-1)$ numbers of point of application of N. This means that Janbu's method can be a rigorous one by assuming that the point of application of the last N is unknown and then determining it as part of the solution.

c. $(n-1)$ numbers of magnitudes of X, and $(n-1)$ numbers of point of application of E or N. This method is not

recommended, as the solution depends on the absolute magnitude of X, which may be very difficult to guess.

d. n numbers of relative magnitude of N and $(n-1)$ numbers of point of applications of E or N introduce an extra unknown in the form of λ. Since this is a very simple solution, it is also provided here.

New Methods of Stability Analysis

50. It may be possible to find other sets of assumptions, but whether any one of these assumptions will provide acceptable solutions is debatable. What follows below are two new methods of solutions of stability of slopes.

Method 1

51. Figure 12 shows a slip surface in a given slope. The slip surface is formed of segments of n straight lines. We subdivide the sliding mass into n slices, but the slices need not be vertical and the edges of the slices need not be parallel. The force on the slice i

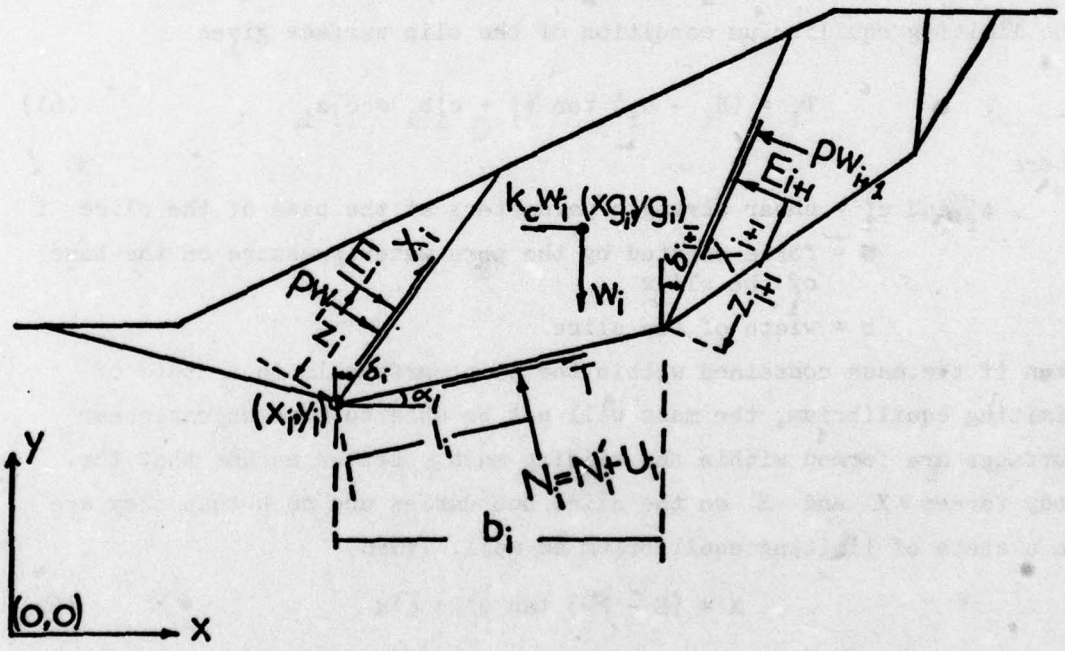

Figure 12. Stability analysis - method 1

is shown in the inset. We assume that under the action of the horizontal acceleration $k_c g$, the slip surface is in limiting equilibrium.

52. From the vertical and horizontal equilibrium of the slice,

$$N_i \cos \alpha_i + T_i \sin \alpha_i = W_i + X_{i+1} \cos \delta_{i+1} - X_i \cos \delta_i - E_{i+1} \sin \delta_{i+1} + E_i \sin \delta_i \quad (59)$$

where

α = the slope of the base of the slice with respect to the horizontal

δ = slope of the side of the slice with respect to the vertical

$$T_i \cos \alpha_i - N_i \sin \alpha_i = k_c W_i + X_{i+1} \sin \delta_{i+1} - X_i \sin \delta_i + E_{i+1} \cos \delta_{i+1} - E_i \cos \delta_i \quad (60)$$

where k_c is the critical acceleration required to bring the stresses on the probable failure surface to a state of limiting equilibrium. The limiting equilibrium condition of the slip surface gives

$$T_i = (N_i - U_i) \tan \phi_i' + c_i' b_i \sec \alpha_i \quad (61)$$

where

ϕ_i' and c_i' = shear strength parameters at the base of the slice i

U = force exerted by the pore water pressure on the base of the slice

b = width of the slice

Even if the mass contained within the slip surface is in a state of limiting equilibrium, the mass will not be able to move unless shear surfaces are formed within the sliding mass. Let us assume that the body forces X and E on the slice boundaries are such that they are in a state of limiting equilibrium as well. Then

$$X = (E - PW) \tan \overline{\phi}' + \overline{c}' d \quad (62)$$

where

$\bar{\phi}'$ and $\bar{c}'$ = the average strength parameters at the slice edges

PW = the force exerted by the pore water pressure on the side of the slice

Putting Equations 61 and 62 in Equations 59 and 60 and eliminating N_i, T_i, X_i, and X_{i+1}, we obtain

$$E_{i+1} = a_i - b_i k_c + E_i e_i \tag{63}$$

where

$$a_i = \frac{W_i \sin(\phi_i' - \alpha_i) + R_i \cos \phi_i' + S_{i+1} \sin(\phi_i' - \alpha_i - \delta_{i+1}) - S_i \sin(\phi_i' - \alpha_i - \delta_i)}{\cos(\phi_i' - \alpha_i + \bar{\phi}_{i+1}' - \delta_{i+1}) \sec(\bar{\phi}_{i+1}')} \tag{64}$$

$$b_i = \frac{W_i \cos(\phi_i' - \alpha_i)}{\cos(\phi_i' - \alpha_i + \bar{\phi}_{i+1}' - \delta_{i+1}) \sec \phi_{i+1}'} \tag{65}$$

$$e_i = \frac{\cos(\phi_i' - \alpha_i + \bar{\phi}_i' - \delta_i) \sec \bar{\phi}_i'}{\cos(\phi_i' - \alpha_i + \bar{\phi}_{i+1}' - \delta_{i+1}) \sec \bar{\phi}_{i+1}'} \tag{66}$$

$$R_i = c_i' b_i \sec \alpha_i - U_i \tan \phi_i' \tag{67}$$

$$S_i = (\bar{c}_i' d_i - PW_i \tan \bar{\phi}_i') \tag{68}$$

Thus

$$E_{n+1} = a_n - b_n k_c + E_n e_n = (a_n + a_{n-1} e_n) - (b_n + b_{n-1} e_n) k_c + E_{n-1} e_n e_{n-1}$$

Therefore, proceeding further with the recurrence relation

$$E_{n+1} = (a_n + a_{n-1}e_n + a_{n-2}e_n e_{n-1} + \ldots \text{ to } n \text{ terms})$$

$$- k_c(b_n + b_{n+1}e_n + b_{n-2}e_n e_{n+1} + \ldots \text{ to } n \text{ terms})$$

$$+ E_1 \cdot e_n \cdot e_{n-1} \cdot e_{n-2} \cdots e_i$$

Since in the absence of external forces

$$E_1 = E_{n+1} = 0$$

$$k_c = \frac{a_n + a_{n-1}e_n + a_{n-2}e_n e_{n-1} + \ldots \text{ to } n \text{ terms}}{b_n + b_{n-1}e_n + b_{n-2}e_n e_{n-1} + \ldots \text{ to } n \text{ terms}} \tag{69}$$

Once the value of k_c is determined, all E forces can be determined from the recurrence relation (Equation 63) and then Equation 62 gives all the X forces. Equations 59 and 61 will give

$$N_i = (W_i + X_{i+1} \cos \delta_{i+1} - X_i \cos \delta_i - E_{i+1} \sin \delta_{i+1} + E_i \sin \delta_i - R_i \sin \alpha_i) \frac{\cos \phi_i'}{\cos (\phi_i' - \alpha_i)} \tag{70}$$

and then Equation 61 will give all values of T_i .

53. In order to complete the solution, we have to obtain the points of applications of N and E forces. For this we make the second set of assumptions. Let us assume the point of application of all E forces is known. Then taking moment about the corner of the slice, we obtain

$$l_i = \left\{W_i(xg_i - x_i) - k_c W_i(yg_i - y_i) + E_i z_i - E_{i+1}\left[z_{i+1} + b_1 \sec \alpha_i \sin (\alpha_i + \delta_{i+1})\right] + X_{i+1} b_i \sec \alpha_i \cos (\alpha_i + \delta_{i+1})\right\} \Big/ N_1 \tag{71}$$

where (xg_i, yg_i) are the coordinates of the center of gravity of the slice.

54. Alternatively, we may determine z_i by assuming l_i as known, in which case the last l_n should be determined as part of the solution.

55. For acceptability, all forces (i.e., N_i, X_i, and E_i) must have a positive result, and l_i must be within the slice, preferably within the middle third.

56. In obtaining the solution, it is assumed that shearing exists between the slices. The assumed angle δ_i may not be the critical one, and it is therefore necessary to try various angles of δ_i. The set of δ_i that will produce minimum k_c will be the critical set. The technique of achieving this minimum value will be: fix all but one δ_i, and change this δ_i gradually to obtain the minimum. Then, fixing this angle δ_i, proceed to another point until all the δ_i's are tried and the smallest value of k_c is reached. It is assumed that the changing of the order of δ_i will not produce a different result. However, this point is not checked. It is seen that the assumption of $\delta_i = 0$ for all slices produces a nonconservative result, but only slightly. Hence, for routine procedure, $\delta_i = 0$ can be used.

57. This solution can be converted to another form: fix $\delta_i = 0$ and introduce a local factor of safety F_L in $\overline{\phi}'$ and $\overline{c}'$. It is seen that as F_L is increased from 1.0, the critical acceleration drops. The minimum k_c value obtained previously corresponds to a local factor of safety of about 1.1 in the homogeneous case. However, this is an observation from a very small number of test cases and requires further observation.

58. In this method of solution, $\overline{\phi}'$ and $\overline{c}'$, which represent the internal strength of the material of the sliding mass, play an important part. The higher the values of $\overline{\phi}'$ and $\overline{c}'$, the higher the critical acceleration is. In other words, the higher the shear strength of the material inside the sliding body is, the lower the shear strength required at the base of the slip surface to maintain static limiting equilibrium. Thus, in the stability analysis of the existing slip

surfaces where the strength on the slip surface may be in the residual state, instead of in the peak state which may exist inside the sliding body, it will be found that the required residual strength is lower than that obtained with the assumption that the peak strength is equal to the residual strength. The effect of the internal strength of the material could not be studied in any of the previous stability analysis methods.*

59. Since the moment equilibriums of the slices do not play any part in the determination of k_c (they are essential for the complete solution), the slices can be as big as possible and, in fact, are controlled by the change of the angle of the slip surface. Also, the position of the point of applications of E or N forces has no effect on k_c, whereas all previous methods are dependent on this assumption. The comparison of this method with the Sarma (1973) method has shown that changing the point of applications has more effect on the production of acceptable results than on the value of k_c.

60. In the strictest sense, this method is not applicable to determining the factor of safety of any surface except the probable failure surface. For any given surface, a factor of safety exists, but the surface may not fail. However, for the probable failure surface, we may use the factor of safety to mean actual reduction of the strength parameters of the material and not just the strength along the slip surface. In this case, the method is applicable. It is best suited for existing slip surfaces where kinematic considerations are already satisfied.

61. Figure 13 presents an example of this method, and gives its comparison with results from the Sarma (1973) method for a homogeneous case.

Method 2

62. This method is given here to show the ease with which a rigorous solution of the stability analysis of earth dams and slopes can be obtained in terms of the critical acceleration factor. Therefore, the method will not be developed completely; and no examples will be given.

---

* Sarma's (1973) method determines the shape of the X force distribution on the basis of the internal strength. Because of the factor λ involved in the solution, the exact effect is not deterministic.

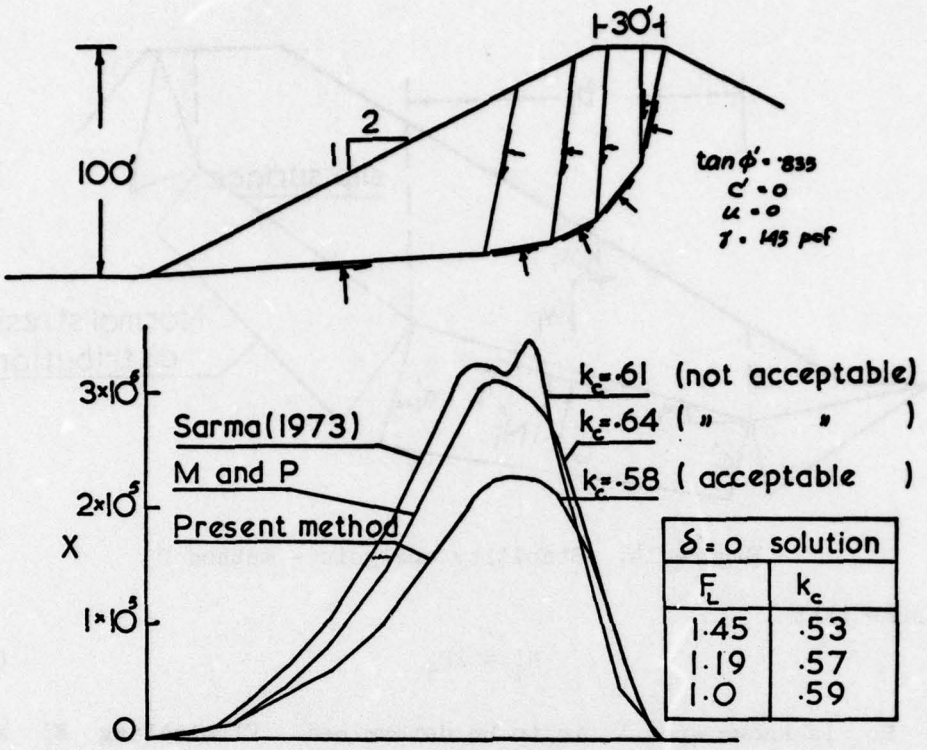

Figure 13. Comparison of method 1 with Morgenstern-Price and Sarma methods

63. The method is based on the assumption that the shape of the normal force distribution on the slip surface is known, but the magnitude is not known. The slip surface is formed of segments of straight lines, and the forces on the base of the slip surface are as shown in Figure 14. From the vertical and horizontal equilibrium of the whole sliding body,

$$\sum (N_i' + U_i) \cos \alpha_i + \sum T_i \sin \alpha_i = \sum W_i \tag{72}$$

$$\sum T_i \cos \alpha_i - \sum (N_i' + U_i) \sin \alpha_i = k_c \sum W_i \tag{73}$$

The Mohr-Coulomb failure criterion gives

$$T_i = N_i' \tan \phi_i' + c_i' b_i \sec \alpha_i \tag{74}$$

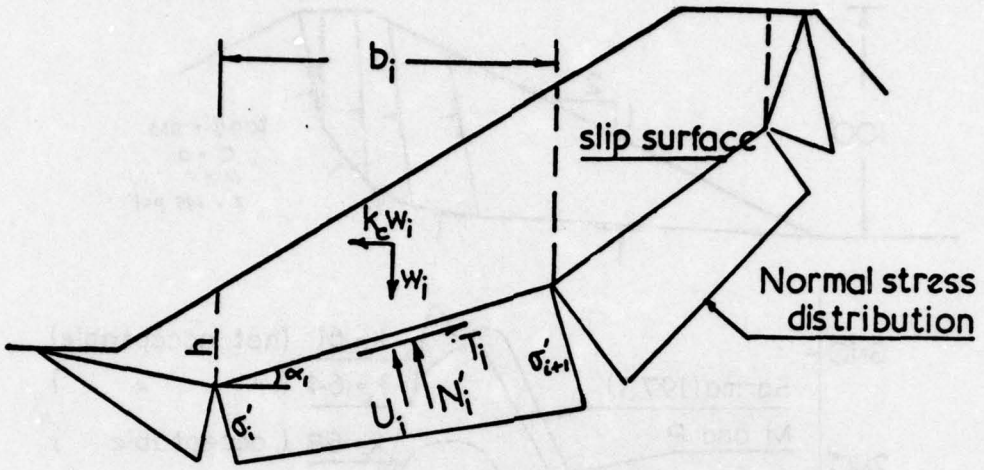

Figure 14. Stability analysis - method 2

We assume that

$$N'_i = \lambda P_i \tag{75}$$

where P_i is known and λ is to be determined. Eliminating N'_i and T_i from Equations 72, 73, 74, and 75, we obtain

$$\lambda = \frac{\sum (W_i - c'_i b_i \tan \alpha_i - U_i \cos \alpha_i)}{\sum P_i \cos (\phi'_i - \alpha_i) \sec \phi'_i} \tag{76}$$

$$k_c = \frac{\sum (c'_i b_i - U_i \sin \alpha_i) + \lambda \sum P_i \sin (\phi'_i - \alpha_i) \sec \phi'_i}{\sum W_i} \tag{77}$$

64. Since the solution depends on P_i, the following expression for P_i gives acceptable results in many cases. If σ'_i and σ'_{i+1} are the normal stresses on the two edges of the slip line segment, then

$$P_i = \frac{\sigma'_i + \sigma'_{i+1}}{2} b_i \sec \alpha_i \tag{78}$$

where

$$\sigma' = \left[\cos \phi' \gamma h (1 - R_u) - c' (\sin \beta + \sin \phi')\right] \frac{\cos \phi'}{1 + \sin \beta \sin \phi'} \tag{79}$$

and

$$R_u = \frac{u}{\gamma h} \tag{80}$$

u = pore pressure at the point under consideration

$$\beta = 2\alpha - \phi' \tag{81}$$

65. In order to compare the result with that obtained from the other method of slices, it is necessary to divide the sliding body into vertical slices as in Figure 11 and then to determine the interslice forces and their points of application. From the vertical and horizontal equilibrium of the slice

$$X_{i+1} = (N_i' + U_i) \cos \alpha_i + T_i \sin \alpha_i - W_i + X_i \tag{82}$$

$$E_{i+1} = T_i \cos \alpha_i - (N_i' + U_i) \sin \alpha_i - k_c W_i + E_i \tag{83}$$

Since λ is known from the solution, N_i from Equation 75 , and T_i from Equation 74, starting from known initial condition of $X_1 = E_1 = 0$, all X and E forces can be calculated.

66. After determining the X and E forces, the points of applications of E and N' forces can be determined by assuming the position of one of these quantities as in method 1.

67. This method appears to be suitable for quick computation of k_c for a slip surface and should give acceptable results for existing slip surfaces. However, it is not easy to see whether it will give acceptable results for any assumed slip surface. Thus, it appears that for design of dams where one has to start with assumed failure surfaces, Sarma's method (1973) is most preferable and that for the analysis of existing slips, the first method presented herein is preferable.

Stability of Slopes Under Earthquake Conditions with Dynamic Pore Pressure

68. Under the earthquake loading conditions, the inertia force

as well as the excess pore pressure generated by the earthquake play an important part in the stability of the dam and its foundations. Until now, this excess pore pressure was introduced into the analysis as equivalent static pressure. Seed and Martin (1966) proposed using the total strength determined under appropriate cyclic loading conditions for the stability analysis. Seed et al. (1969) extended this idea to develop the finite element method for studying the liquefaction potential of the dam during an earthquake, and Seed et al. (1973) used this method for the analysis of the Lower San Fernando Dam in California, which was affected by the San Fernando earthquake of 1971. However, since this is a finite element method, it is outside the scope of this report.

69. The method presented herein is an effective stress method which can take into account the excess pore pressures developed during cyclic loading. This method uses the concept of the pore pressure parameters which was originally defined by Skempton (1954) for static loading conditions.

Dynamic pore pressure parameter A_n

70. Cyclic loading tests on saturated samples of cohesionless soil show that the pore pressures increase with every cycle of loading until failure by large strain or liquefaction occurs (Lee and Seed, 1967a; Lee and Seed, 1967b; Peacock and Seed, 1968; Martin et al., 1975). This pore pressure depends primarily on the applied cyclic shear stress and the number of cycles. Martin et al. (1975) proposed a set of formulas to determine the change of pore pressure ratio $\Delta u/\sigma'_{vo}$ against the number of cycles for a given stress ratio $\Delta\tau/\sigma'_{vo}$ in a simple shear test, where Δu is the pore pressure, σ'_{vo} is the effective consolidation pressure, and $\Delta\tau$ is the applied shear stress. The same relationships are replotted in Figure 15 to show the variation of $\Delta u/\sigma'_{vo}$ against $\Delta\tau/\sigma'_{vo}$ for a given number of cycles. From these curves we see that

$$\frac{\Delta u}{\sigma'_{vo}} = A_n \frac{\Delta\tau}{\sigma'_{vo}} \tag{84}$$

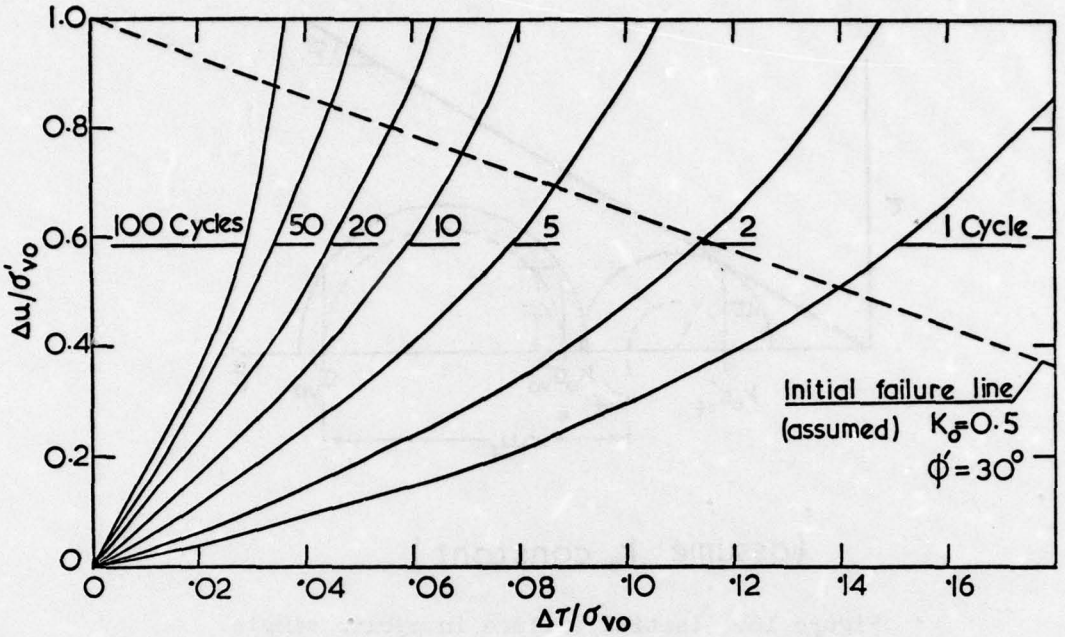

Data from Martin et al (1975)

Figure 15. Pore pressure response in simple shear test (data from Martin et al., 1975)

where A_n is the pore pressure parameter that is a function of the number of cycles and the level of stress ratio. However, for the initial part of the curve, the curves appear linear; and A_n is a function of the number of cycles only. Higher order equations for these curves can easily be found if desired.

71. Initial failure is defined as that state in which the Mohr's circle of stress first touches the failure envelope. From the geometry of the Mohr's circle, Figure 16, we obtain

$$\frac{\Delta u_f}{\sigma'_{vo}} = 1 - \frac{1}{R}\frac{\Delta\tau}{\sigma'_{vo}} \tag{85}$$

where

$$R = \frac{(1 + k_o)^2}{2} \sin^2 \phi' - \frac{(1 - k_o)^2}{2} \tag{86}$$

72. This relationship is shown dotted in Figure 15 . Equations

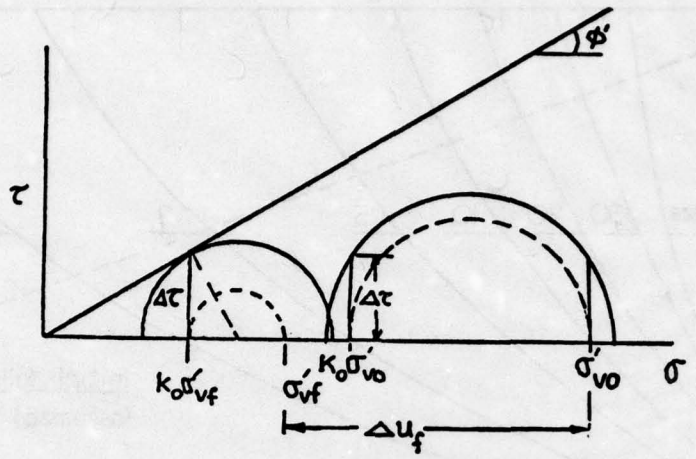

(assume k_o constant)

Figure 16. Initial failure in cyclic simple shear test

Equations 84, 85, and 86 are derived for simple shear tests where the initial stress conditions are represented by σ'_{vo} and $k_o\sigma'_{vo}$ in which k_o is the coefficient of earth pressure at rest. Equations 85 and 86 are derived assuming that k_o remains unchanged until the initial failure.

73. In the slope stability problem involving dams and slopes, simple shear conditions do not represent the true state. Neither does the triaxial test condition where either no rotation of the principal stresses are allowed or they are rotated through 90 deg.* However, in the dam during earthquakes, the rotation will be small (Seed, 1968). Therefore, the consolidated, undrained, triaxial test with anisotropic consolidation appears to be nearer the truth, and we may assume that the pore pressure parameters will not be affected by the rotation of the principal stresses. From the limited test data available in the literature on triaxial cyclic test results, utilizing both isotropically and anisotropically consolidated samples, we see a similar pattern to the simple shear tests; and we may write for the initial part

* A table of factors for converting U. S. customary to metric (SI) units of measurement is presented on page 3.

$$\frac{\Delta u}{\sigma'_{3c}} = A_n \frac{\Delta\sigma_1}{\sigma'_{3c}} \tag{87}$$

and for the anisotropic consolidations, perhaps

$$\frac{\Delta u}{\sigma'_{3c(1+\bar{k}_c)}} = A_n \frac{\Delta\sigma_1}{\sigma'_{3c(1+\bar{k}_c)}} \tag{88}$$

where

σ'_{3c} = confining cell pressure for consolidation

$\Delta\sigma_1$ = change in axial stress

$$\bar{k}_c = \sigma'_{1c}/\sigma'_{3c} \tag{88}$$

However, Equation 88 will need extensive laboratory verification to see whether or not A_n is independent of $\bar{k}_c$. The parameters A_n in triaxial tests are different from those of the simple shear tests.

74. Equations 87 and 88 suggest that the Skempton (1954) equation can be adopted for dynamic pore pressure as well, and we may write

$$\Delta u = B\left[\Delta\sigma_3 + A_n(\Delta\sigma_1 - \Delta\sigma_3)\right] \tag{90}$$

where B is a pore pressure parameter.

The analysis

75. In this analysis, the suffix o denotes the preearthquake conditions, the suffix d for dynamic loading conditions. The method is based on Sarma's (1973) technique of determining k_c, the critical acceleration factor.

76. Let us consider a possible slip surface in a slope as shown in Figure 17. We subdivide the sliding body into n vertical slices. Before the earthquake the slice is acted upon by forces as shown in the figure. Let us assume that there is a factor of safety F_o under static conditions for this surface. We may find this value of F_o, the interslice body forces E_o and X_o, and the normal and shear forces at the base of the slices N_o and T_o by any of the rigorous analysis methods.

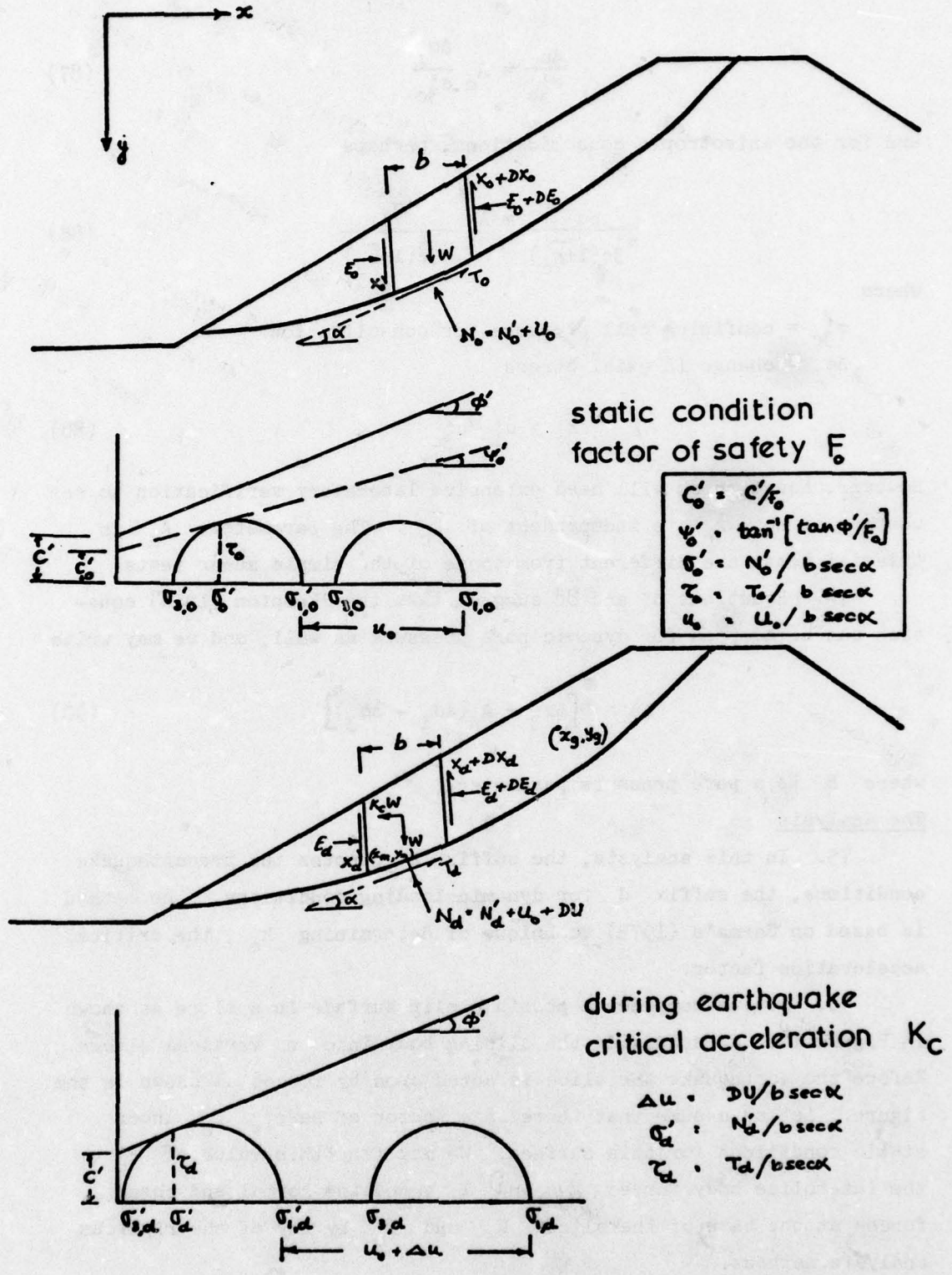

Figure 17. Stability analysis by Sarma method

77. Let us now assume that a horizontal earthquake load kW is applied, under the influence of which limiting equilibrium is achieved. In that case, k is equal to k_c. From Figure 17c, we may then write

$$N_d \cos \alpha + T_d \sin \alpha = W - DX_d \tag{91}$$

$$T_d \cos \alpha - N_d \sin \alpha = k_c W + DE_d \tag{92}$$

$$T_d = (N_d - U_o - DU_d) \tan \phi' + c'b \sec \alpha \tag{93}$$

where

DU_d = the dynamic pore pressure developed under the influence of $K_c W$

W = weight of the slice

DX and DE are as shown in Figure 17.

78. At this stage, let us introduce the hypothesis proposed by Sarma (1975). This hypothesis states that if a possible failure plane is acted upon by a normal stress σ' and a shear stress τ and the shear stress has a factor of safety F, then the state of stress in all planes will be the same as that in which the material has a strength property given by $\psi' = \tan^{-1}(\tan \phi'/F)$ and $\bar{c}' = c'/F$. Under this hypothesis, it is possible to draw the Mohr's circle of stress for static conditions, Figure 17b. From the geometry of the circle,

$$\sigma'_{1,0} = \sigma'_o + \tau_o(\tan \psi'_o + \sec \psi'_o) \tag{94}$$

$$\sigma'_{3,0} = \sigma'_o + \tau_o(\tan \psi'_o - \sec \psi'_o \tag{95}$$

where

$c'_o = c'/F_o$

$\psi'_o = \tan^{-1}(\tan \phi'/F_o)$. Adding u_o (u = pore pressure at the base of the slice) to both sides

$$\sigma_{1,0} = \sigma_o + \tau_o(\tan \psi'_o + \sec \psi'_o) \tag{96}$$

$$\sigma_{3,0} = \sigma_o + \tau_o(\tan \psi'_o - \sec \psi'_o) \tag{97}$$

σ = stress component

Similarly, for the dynamic loading conditions, we shall have

$$\sigma_{1,d} = \sigma_d + \tau_d(\tan \psi'_d + \sec \psi'_d) \tag{98}$$

$$\sigma_{3,d} = \sigma_d + \tau_d(\tan \psi'_d - \sec \psi'_d) \tag{99}$$

We define

$$\Delta\sigma_1 = \sigma_{1,d} - \sigma_{1,0} \tag{100}$$

and

$$\Delta\sigma_3 = \sigma_{3,d} - \sigma_{3,0} \tag{101}$$

and therefore Equation 90 gives

$$\Delta u = B\left[\Delta\sigma_3 + A_n(\Delta\sigma_1 - \Delta\sigma_3)\right]$$

Multiplying both sides by b sec α , we have, with $\psi'_d = \phi'$

$$DU_d = B\Big\{(N_d - N_o) + T_d\left[\tan \phi' - \sec \phi'(1 - 2A)\right] - T_o\Big[\tan \psi'_o - \sec \psi'_o(1 - 2A)\Big]\Big\} \tag{102}$$

79. Eliminating N_d and T_d from Equation 102, with Equations 91 and 93, we obtain

$$DU_d = \bar{a} - \bar{b}\, DX_d \tag{103}$$

where

$$\bar{a} = \frac{B(a - N_o) + dq - T_o q_o}{1 - Bb_o - eq} \tag{104}$$

$$\bar{b} = B(C + fq)/1 - B(b_o - eq) \tag{105}$$

$$a = (W + U_o \sin\alpha \tan\phi' - c'b \tan\alpha \cos\phi' \sec(\phi' - \alpha) \tag{106}$$

$$b_o = \tan\alpha \tan\phi'/(1 + \tan\alpha \tan\phi') \tag{107}$$

$$C = \cos\phi' \sec(\phi' - \alpha) \tag{108}$$

$$d = (c'b + W \tan\phi' - U_o \cos\alpha \tan\phi') \cos\phi' \sec(\phi' - \alpha) \tag{109}$$

$$e = \tan\phi'/(1 + \tan\alpha \tan\phi') \tag{110}$$

$$f = \sin\phi' \sec(\phi' - \alpha) \tag{111}$$

$$q = \tan\phi' - \sec\phi'(1 - 2A_n) \tag{112}$$

$$q_o = \tan\psi_o' - \sec\psi_o'(1 - 2A_n) \tag{113}$$

$$N_o = (W + U_o \sin\alpha \tan\psi_o' - c_o'b \tan\alpha) \cos\psi_o' \sec(\psi_o' - \alpha) - DX_o \cos\psi_o' \sec(\psi_o' - \alpha) \tag{114}$$

$$T_o = (c_o'b + W \tan\psi_o' - U_o \cos\alpha \tan\psi_o') \cos\psi_o' \sec(\psi_o' - \alpha) - DX_o \sin\psi_o' \sec(\psi_o' - \alpha) \tag{115}$$

$$\psi_o' = \tan^{-1}\left(\tan\frac{\phi'}{F_o}\right) \tag{116}$$

$$c_o' = \frac{c'}{F_o} \tag{117}$$

Now eliminating N_d and T_d from Equations 91, 92, and 93, we obtain

$$DX_d \tan(\phi' - \alpha) + DE_d = W \tan(\phi' - \alpha) + (c'b \sec\alpha \cos\phi' - U_o \sin\phi') \sec(\phi' - \alpha) - (\bar{a} - \bar{b}DX_d) \sin\phi' \sec(\phi' - \alpha)$$

and rearranging terms

$$DX_d \left[\tan (\phi' - \alpha) - \bar{b} \sin \phi' \sec (\phi' - \alpha)\right] + DE_d = \bar{D} - k_c W \quad (118)$$

where

$$\bar{D} = W \tan (\phi' - \alpha) + (c'b \sec \alpha \cos \phi' - U_o \sin \phi') \sec (\phi' - \alpha) - \bar{a} \sin \phi' \sec (\phi' - \alpha) \quad (119)$$

summing for all slices and since $\sum DE_d = 0$

$$\sum DX_d \left[\tan (\phi' - \alpha) - \bar{b} \sin \phi' \sec (\phi' - \alpha)\right] + K_c \sum W = \sum \bar{D} \quad (120)$$

80. Let us assume that the point of application of N_d forces are known and that the coordinate of this point is x_m, y_m which, for practical purposes, can be the middle point of the base of the slice. Then taking moment about the centre of gravity of the whole sliding body (x_g, y_g) and remembering that the net moment of W and kW about the centre of gravity is zero, we have

$$\sum (N_d \cos \alpha + T_d \sin \alpha)(x_m - x_g) + \sum (T_d \cos \alpha - N_d \sin \alpha)(y_m - y_g) = 0 \quad (121)$$

and using Equations 91, 92, and 118 in Equation 121,

$$\sum DX_d \left\{(x_m - x_g) + (y_m - y_g)\left[\tan (\phi' - \alpha) - \bar{b} \sin \phi' \sec (\phi' - \alpha)\right]\right\} = \sum W(x_m - x_g) + \sum \bar{D}(y_m - y_g) \quad (122)$$

The problem now is to find a set of X_d forces which will satisfy Equation 122.

81. Let us assume that the shape of the X_d force distribution

is known but not the magnitude. Then we can say that

$$X_d = \lambda Q \tag{123}$$

where Q is known but λ is unknown. Then $DX_d = \lambda(Q_{i+1} - Q_i)$ for the i^{th} slice $= \lambda P$ Then Equations 120 and 122 become

$$\lambda \sum P \left[\tan (\phi' - \alpha) - \bar{b} \sin \phi' \sec (\phi' - \alpha) \right] + k_c \sum W = \sum \bar{D} \tag{124}$$

$$\lambda \sum P \left\{ (x_m - x_g) + (y_m - y_g) \left[\tan (\phi' - \alpha) - \bar{b} \sin \phi' \sec (\phi' - \alpha) \right] \right\}$$

$$= \sum W(x_n - x_g) + \sum \bar{D}(y_m - y_g) \tag{125}$$

Therefore, λ and k_c can be solved. The rest of the solution will follow the same pattern as in Sarma (1973) and is not shown here.

Procedure

82. A procedure for applying the above method of analysis can be summarized as follows:

a. Determine A_n parameters for various cycles, say 1 cycle, 5 cycles, 10 cycles, 20 cycles, etc., from anisotropically consolidated, undrained tests for different materials of the dam.

b. For each set of A_n values, determine the k_c values for the possible slip surface. Therefore, we obtain the critical accelerations for a corresponding number of cycles.

c. From the strong motion record and the average seismic coefficient for the sliding mass, find the equivalent number of uniform cyclic seismic coefficient of k_c (Seed et al., 1969). If the available number of cycles is more than the number of cycles required for failure, the factor of safety will drop below one. Since the available number of cycles will depend primarily on the choice of the record, it is better to consider the critical acceleration for 10-20 cycles as the most critical value and to compute the probable displacement on the basis of it.

PART IV: DISPLACEMENT CRITERION OF DESIGN

83. Within the limit equilibrium principle, a factor of safety smaller than one represents failure. This signifies that when the factor of safety is less than one, the mean strength along the failure surface is less than that required to maintain equilibrium. Therefore, a section of the dam or embankment will slide along the failure surface and will come to rest again at a time and place when the new mean stresses do not exceed the strength. Depending on the amount of relative displacement, which may vary from a fraction of an inch to a few yards, the structure will be said to be safe or to have failed. It is therefore obvious that a factor of safety less than one cannot be permitted under the static conditions, as the stresses producing this stage will exist until large displacements change the geometry of the structure.

84. However, under earthquake conditions, it may be possible to allow the factor of safety to drop below one, as this state will exist only for a very short time. Nevertheless, the consequences of allowing the factor of safety to drop below one must be known, and this can be measured in terms of relative displacements of the sliding mass relative to the main body of the structure. Newmark (1965) proposed the sliding block technique to measure this displacement, later Ambraseys (1973) proposed the upper bound formula, and Sarma (1975) showed that displacements can be computed on the basis of simple pulses once the critical acceleration is known.

85. Sarma's (1975) work is based on the effective stress principle. The displacements were computed on the basis of the assumption that the pore pressures at the base of the sliding block remain constant during movement. In contrast to laboratory testing, where pore pressures continue to rise after the factor of safety has become equal to one in cyclic loading, any attempt to increase the earthquake load only increases the displacement, creating dilatency in the slip zone and thereby reducing the pore pressure. In the case of slope failures, therefore, the assumption that pore pressures remain constant during movement is rather conservative.

86. It is also assumed that the critical slip surfaces can be converted into plane slip surfaces. The shear strength properties of this plane surface which separates the sliding block from the main body of the structure are the average ϕ' and c'. The pore pressure is equal to that at incipient failure (Figure 18).

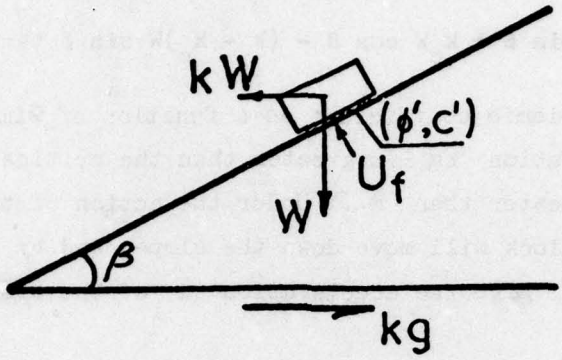

Figure 18. Sliding block model

87. The sliding block is subjected to a horizontal earthquake acceleration kg, which imparts a horizontal load kW on the sliding block, as shown in the figure. The earthquake acceleration is greater than the critical acceleration $k_c g$, which was determined for the original slip surface.

88. The driving force D on the sliding block is

$$D = W \sin \beta + kW \cos \beta \tag{126}$$

where

W = the weight of the sliding block

β = the slope of the sliding plane

and the resisting force R is

$$R = (W \cos \beta - kW \sin \beta - U_f) \tan \phi' + c'L \tag{127}$$

where L is the length of the sliding block. When the earthquake acceleration is $k_c g$, the driving and the resisting forces are equal, which gives

$$W \sin \beta + k_c W \cos \beta = (W \cos \beta - k_c W \sin \beta - U_f) \tan \phi' + c'L \qquad (128)$$

where U_f is the force due to pore pressure at failure.

Using Equation 128 in Equation 127

$$R = W \sin \beta + k_c W \cos \beta - (k - k_c) W \sin \beta \tan \phi' \qquad (129)$$

where k is the seismic coefficient as a function of time. Since the earthquake acceleration kg is greater than the critical acceleration, D is therefore greater than R . Under the action of the net driving force (D-R), the block will move down the slope; and by Newton's Law, this net force will give the acceleration $\ddot{x}$ of the block relative to the base. Thus

$$\frac{W}{g} \ddot{x} = D - R$$

$$= W \frac{\cos (\phi' - \beta)}{\cos \phi'} \quad (k - k_c) \qquad (130)$$

or

$$\ddot{x} = \frac{g \cos (\phi' - \beta)}{\cos \phi'} \quad (k - k_c) \qquad (131)$$

Since the earthquake acceleration kg is a function of time, Equation 131 can be evaluated to determine the total displacement x at the end of the earthquake.

89. For a rectangular pulse of duration T/2 and amplitude $k_m g$, Figure 19a, the solution of Equation 131 gives

$$\frac{4x_m}{k_m g T^2} \cdot \frac{\cos \phi'}{\cos (\phi' - \beta)} = \frac{1}{2} (k_m/k_c - 1) \qquad (132)$$

where

x_m = permanent displacement of the block relative to the base

k_m = maximum value of the seismic coefficient

T = predominant period of an accelerogram or twice the duration of the pulse

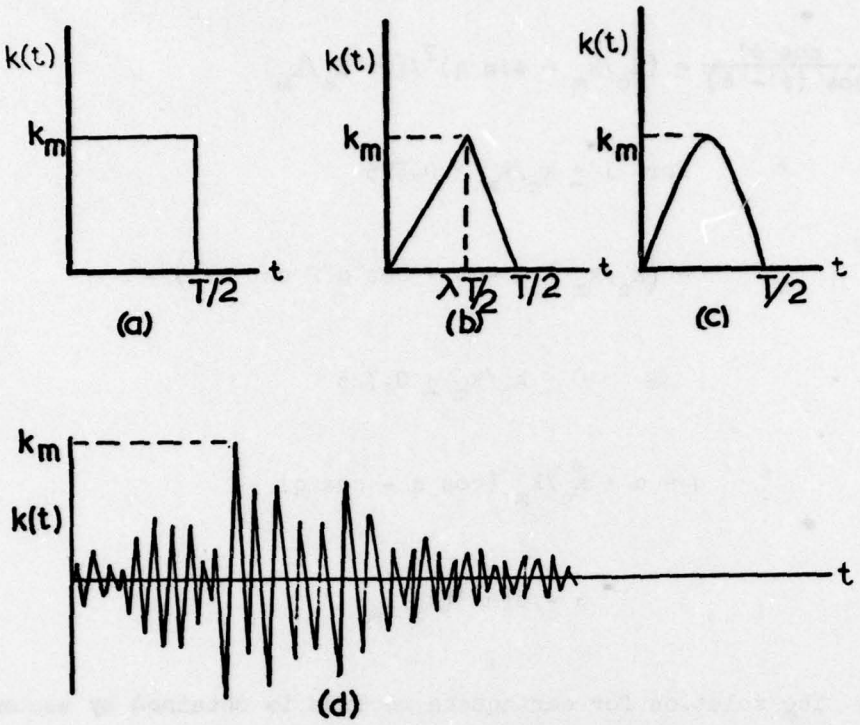

Figure 19. Forms of acceleration pulses used for computation of displacement

For a triangular pulse of duration $T/2$ and amplitude $k_m g$, with a peak at time $\lambda T/2$, Figure 19b,

$$\frac{4x_m}{k_m g T^2} \cdot \frac{\cos\phi'}{\cos(\phi' - \beta)} = \frac{1}{24}\left\{4(1 - k_c/k_m)(1 - \lambda\, k_c/k_m) - \left[1 - \lambda(k_c/k_m)^2\right]^2\right\}(k_c/k_m)$$

$$\text{for } 0 \le k_c/k_m \le \left[1 - \sqrt{(1-\lambda)}\right]/\lambda \qquad (133)$$

$$= \frac{1}{6}\left[(1 - k/k_m)^3\left(2+2\sqrt{1-\lambda} - \lambda\right)\right.$$

$$\text{for } \left(1 - \sqrt{1-\lambda}\right)/\lambda \le k_c/k_m \le 1 \qquad (134)$$

For a half/sine pulse of duration $T/2$ and amplitude $k_m g$, Figure 19c,

$$\frac{4x_m}{k_m g T^2} \cdot \frac{\cos \phi'}{\cos (\phi' - \beta)} = (K_c/k_m - \sin q)^2/(2\pi^2 k_c/k_m)$$

$$\text{for } 1 \geq k_c/k_m > 0.725$$

$$= \left(k_c/k_m + \alpha - \pi + \cos^2 \alpha/2 \cot \alpha/2\right)/\pi^2 \tag{135}$$

$$0 \leq k_c/k_m \leq 0.725 \tag{136}$$

where

$$q = \alpha + k_c/k_m (\cos \alpha - \cos q) \tag{137}$$

and

$$\alpha = \sin^{-1}(k_c/k_m) \tag{138}$$

90. The solution for earthquake records is obtained by assuming piece-wise linear acceleration. Since the problem is that of a slope failure, the critical acceleration required to move the body up the slope is assumed to be very large, and no reversal of displacements occurs.

91. Between the times t_{i-1} and t_i, the acceleration k_g can be written as

$$k(t) = k_{i-1} + \frac{k_i - k_{i-1}}{t_i - t_{i-1}} (t - t_{i-1}) \tag{139}$$

then the solution of Equation 131 gives

$$\frac{\cos\phi'}{\cos(\phi'-\beta)} \cdot \frac{\dot{x}}{g} = (k_{i-1} - k_c)(t - t_{i-1}) + \frac{k_i - k_{i-1}}{t_i - t_{i-1}} \cdot \frac{(t - t_{i-1})^2}{2} + \dot{x}_{i-1} \tag{140}$$

$$\frac{\cos\phi'}{\cos(\phi'-\beta)} \cdot \frac{x}{g} = (k_{i-1} - k_c) \frac{(t - t_{i-1})^2}{2} + \frac{k_i - k_{i-1}}{t_i - t_{i-1}} \cdot \frac{(t - t_{i-1})^3}{6}$$

$$+ \dot{x}_{i-1}(t - t_{i-1}) + x_{i-1} \tag{141}$$

where $\dot{x}$ is the downslope velocity of the sliding block relative to its original position.

92. The procedure for determining the displacement for earthquake record will then be to

a. Scan the earthquake record from the beginning until the pulse is bigger than k_c. This will give the initial conditions. Determine the velocity and displacement at the end of the linear pulse, which provides the initial conditions for the next pulse.

b. It is possible that the movements may stop in the middle of a decreasing pulse. This will be indicated by the change of the sign of the velocity; in which case, the time for zero velocity is interpolated, and the displacement is computed up to that time only.

c. Once the movement is stopped, it will not start unless the pulse is bigger than k_c. Therefore, we are back in step a.

93. The total displacement at the end of the record gives x_m. The maximum acceleration in the record gives k_m, and the predominant period of the acceleration spectrum gives T. We can therefore compute $4x_m/k_m g T^2$. The earthquake acceleration time history is not symmetric about the zero axis, and it is therefore necessary to compute the displacement x_m by changing the signs of the accelerations.

94. Figure 20 shows the quantity $(1/C)(4x_m/k_m g T^2)$ computed against k_c/k_m for the four cases mentioned above. This figure shows that for $k_c/k_m > 0.5$, the triangular pulse and for $k_c/k_m < 0.5$, the rectangular pulse effectively give the displacement from an earthquake record, where k_m for the pulse is the maximum of the acceleration record and T for the pulse is the predominant period of the record. Also, it is seen that the absolute displacement for $k_c/k_m > 0.5$ is very small for real earthquake records. C represents $\cos(\phi' - \beta)/\cos\phi'$.

95. The use of the sliding block technique for computing the displacement demands the following from the dam:

a. A critical acceleration $k_c g$.

b. An average σ'.

c. An average slope angle β.

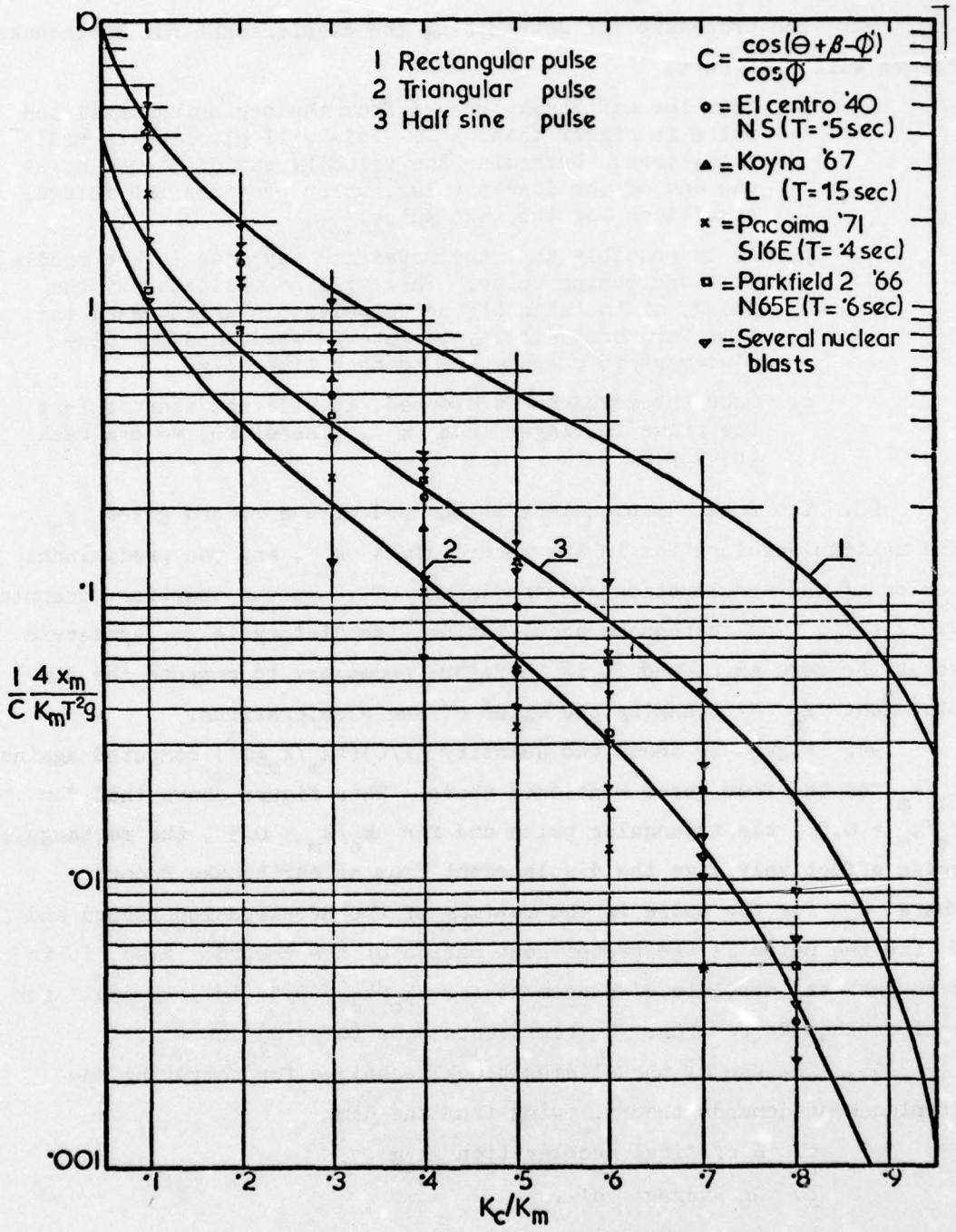

Figure 20. Computed permanent displacements

96. The methods presented in Part III will give the critical acceleration $k_c g$. From this solution we can draw the force-polygon for the entire sliding surface, as shown in Figure 21. The slope of the shear force vector can be used as the slope angle β . From the same solution, we can obtain the average shear stress τ and the average effective normal stress n' on the slip surface. Since we can compute c'_{av} , the average angle ϕ' can be obtained from

$$\phi'_{av} = \tan^{-1} \frac{\tau - c'_{av}}{n'} \tag{142}$$

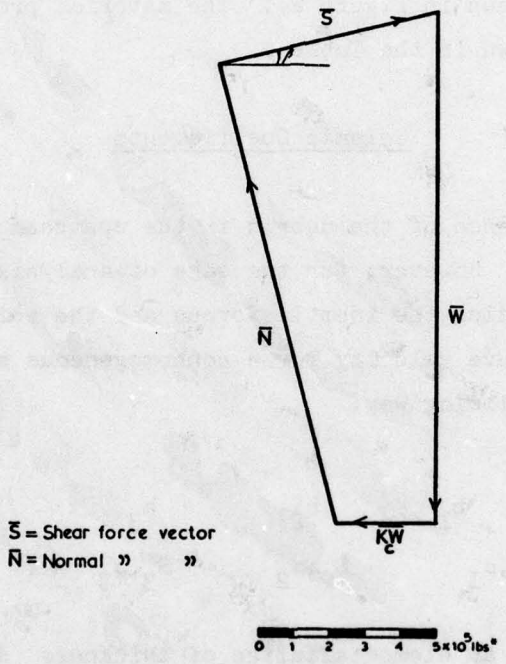

Figure 21. Vector diagram of forces

PART V: ANALYSIS OF THE LOPEZ DAM

97. In this part, the Lopez Dam of California is analyzed by the method mentioned in the previous chapters, and the stability of the dam is checked against the San Fernando Earthquake of 9 February 1971. The probable ground motion at the Lopez damsite during this earthquake is supplied by the U. S. Army Engineer Waterways Experiment Station (WES). This record is a modified version of the Pacoima Dam record. The record is shown in Figure 22, along with the integrated velocity and displacement records. The three spectra are shown in Figure 23. The cross section of the Lopez Dam is shown in Figure 24. The material properties, as supplied by the WES, are shown in the Table 2.

Seismic Coefficients

98. The presence of the debris in the upstream side creates an asymmetric section. However, for the sake of analysis, the debris will be neglected in finding the inertia forces and the seismic coefficients. The average shear wave velocity for a nonhomogeneous section can be computed in the following way:

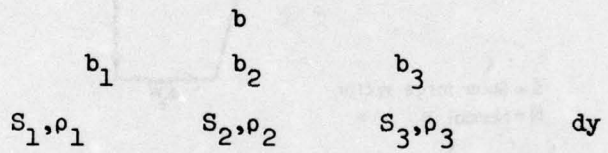

99. Consider an elemental slice of thickness dy. Assuming constant strain along the entire width, the net shear force T across the section is

$$T = (G_1 b_1 + G_2 b_2 + G_3 b_3) \frac{du}{dy}$$
$$= \frac{du}{dy} \sum S_i^2 \rho_i b_i \qquad (143)$$

The average shear stress is therefore

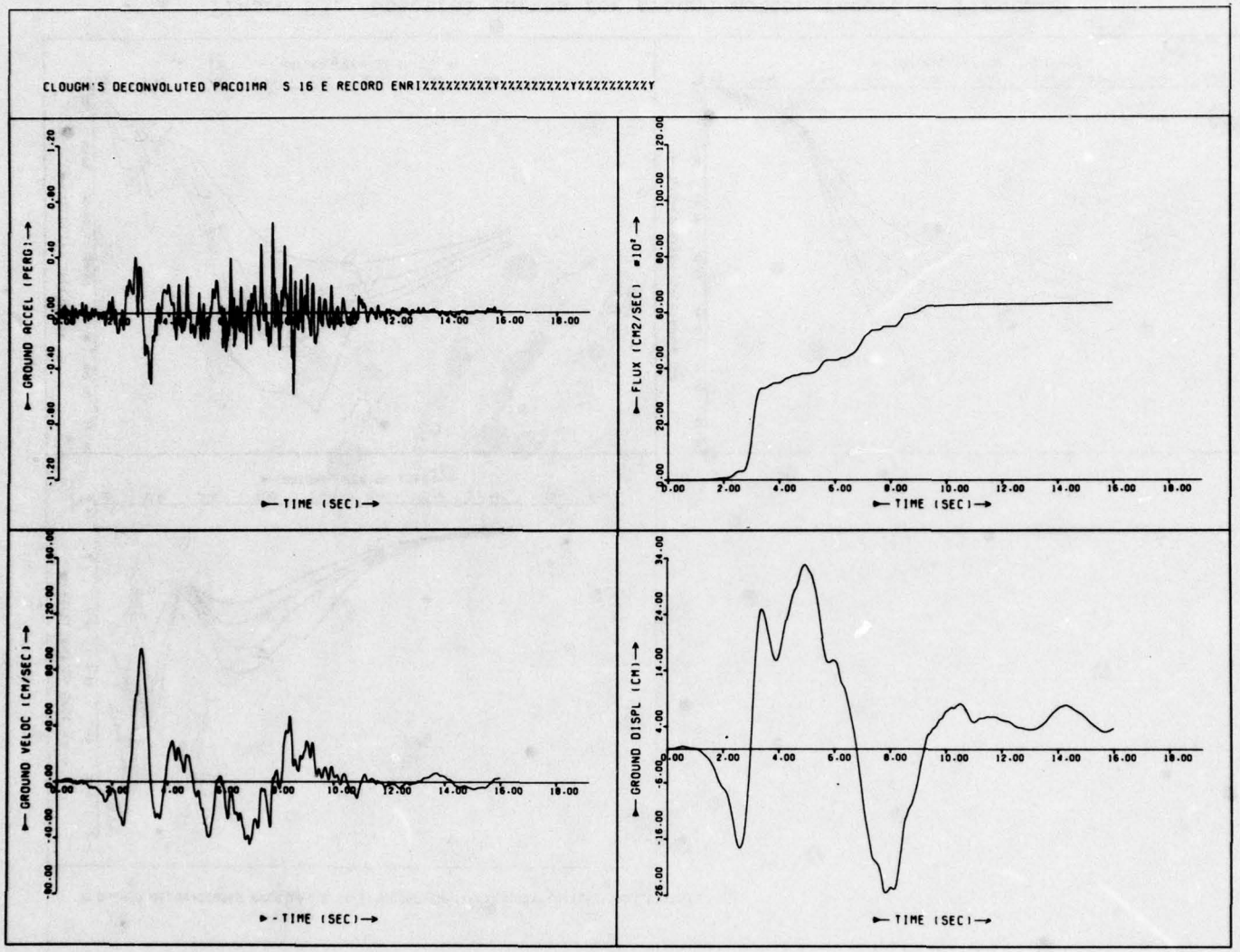

Figure 22. Ground motion record used in analysis of Lopez Dam

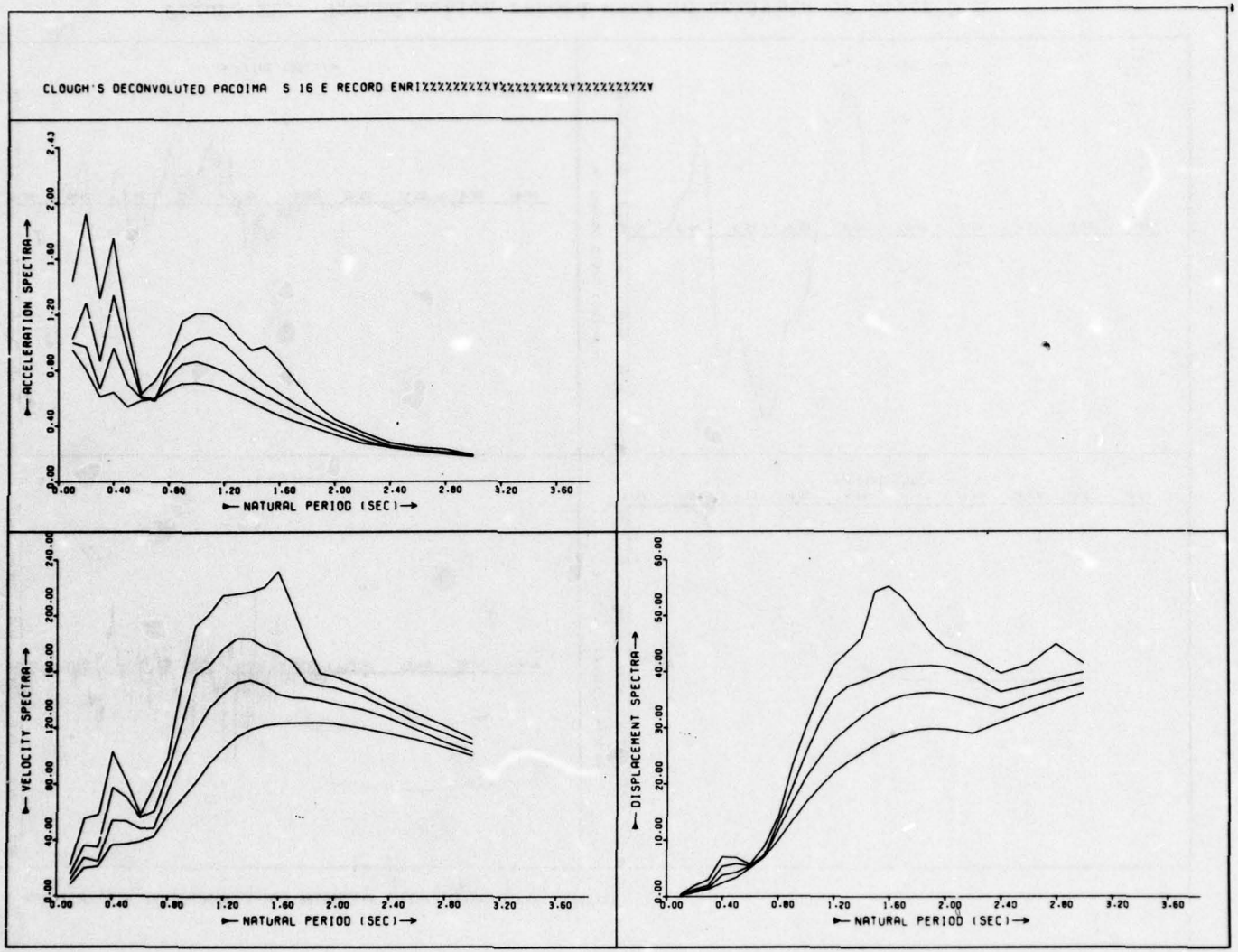

Figure 23. Spectral curves for ground motion record of Figure 22

ZONE	γ_{moist} (pcf)	γ_{sat} (pcf)	v_s (fps)
DEBRIS	107·0	130·0	700
SLOPE	133·0	146·8	750
CORE	123·0	139·3	850
FOUND.	127·5	142·4	1000

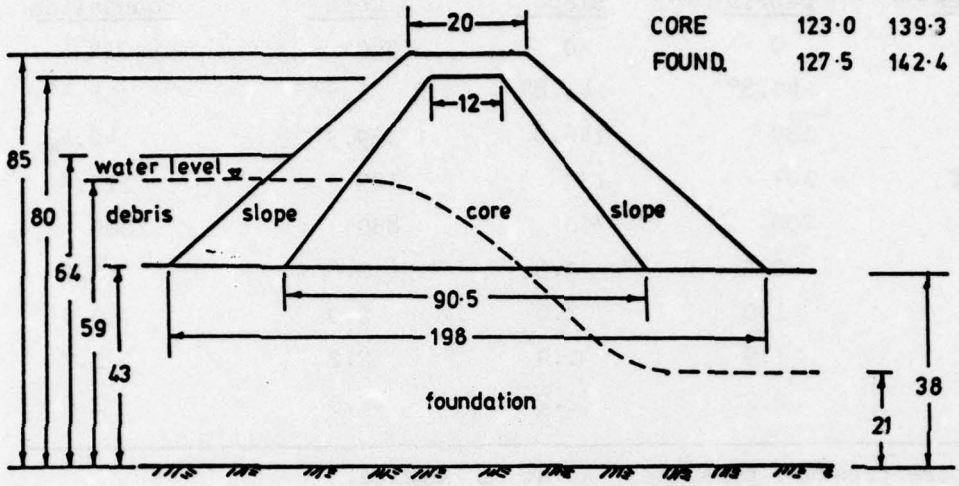

Figure 24. Lopez Dam

$$\tau_{av} = \frac{t}{b} \tag{144}$$

and therefore the average shear modulus is

$$G_{av} = \frac{1}{b} \sum S_i^2 \rho_i b_i \tag{145}$$

The average shear wave velocity is therefore

$$S_{av} = \left(\frac{G_{av}}{\rho_{av}} \right)^{1/2} = \left(\frac{\sum S_i^2 \rho_i b_i}{\sum \rho_i b_i} \right)^{1/2} \tag{146}$$

However, for all practical purposes, a linear average can be assumed, so that

$$S_{av} = \frac{1}{b} \sum S_i b_i \tag{147}$$

Thus for the Lopez Dam section, considering the moist densities, the

Table 2

Lopez Dam - Material Properties

Properties	Zone 1 Debris	Zone 2 Slope	Zone 3 Core	Zone 4 Foundation
c' , psf	0	0	560	224
ϕ'	40.8°	41.8°	27.5°	38.5°
γ_{sat} pcf	130	146.8	139.3	142.4
γ_{moist} pcf	107	133	123	127.5
S ft/sec	700	750	850	1000
A_1*	0.3	0.3	0.6	0.2
A_5*	1.0	1.0	2.0	0.9
A_{10}*	1.9	1.9	2.2	1.7
A_{20}*	2.2	2.2	2.5	2.0

* A_n = pore pressure parameter A at n cycles.

average shear wave velocity is 795 ft/sec; and the average density is 128 lb/ft^3. The shear wave velocity of the foundation layer is 1000 ft/sec, and the density is 127.5 lb/ft^3. Therefore, $m = S_1\rho_1/S_2\rho_2 = 0.8$ and $q = m(H - h)\rho_2/h\rho_1 = 0.71$. For this pair of values of m and q , the first root of the transcendental equation

$$m \tan (q\bar{a}_n) = \frac{J_o(\bar{a}_n)}{J_1(\bar{a}_n)} \tag{148}$$

is $\bar{a}_1 = 1.34$, which is obtained from Figure 5 of Part II (also computed numerically in this case).

100. Thus, the fundamental period of the dam-layer system is

$$T_1 = \frac{2\pi h}{S_{av}\bar{a}_1} = 0.27 \text{ sec} \tag{149}$$

Figure 25 shows the seismic coefficient spectra for the period to range from 0.2 to 0.4 sec for the modified version of the Pacoima Dam record for the pair of values of m and q mentioned above.

101. If, on the other hand, the debris is not neglected but is

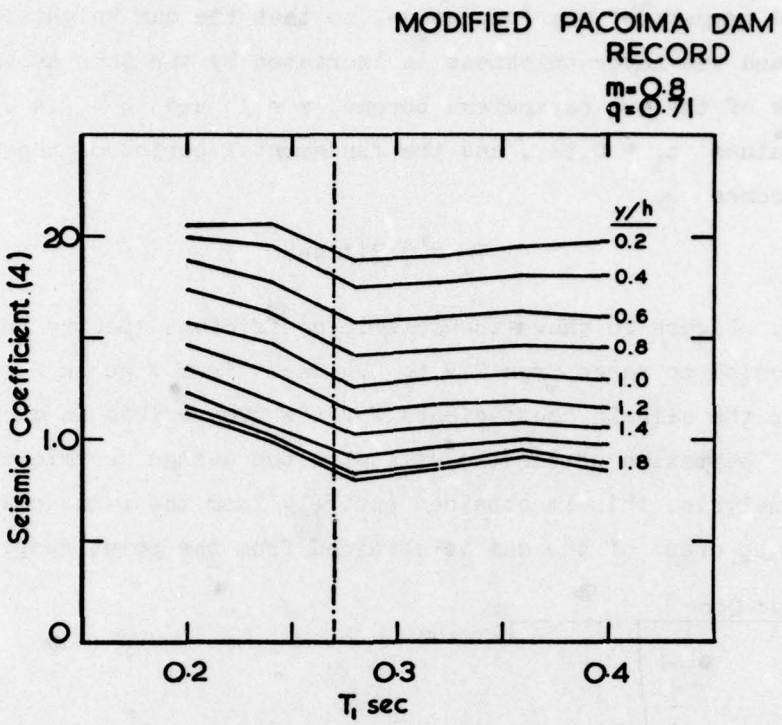

Figure 25. Seismic coefficients if debris is neglected

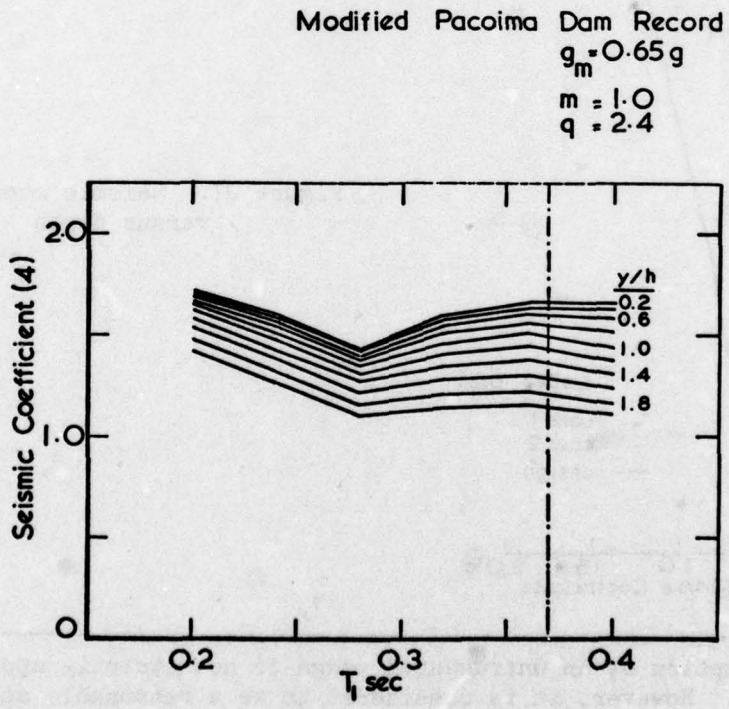

Figure 26. Seismic coefficients if debris is considered part of foundation

considered as part of the foundation, so that the dam height is reduced by 20 ft and the layer thickness is increased by the same amount, then the values of the two parameters become $m = 1$ and $q = 2.4$. For this pair of values $\bar{a}_1 = 0.54$, and the fundamental period of the dam-layer system becomes

$$T_1 = 0.37^* \text{ sec} \tag{150}$$

102. Figure 26 shows the seismic coefficient spectra for this case for the period to range from 0.2 to 0.4 sec. From Figures 25 and 26, we can replot the seismic coefficients for the two periods in question (Figure 27). The maxima of the two will give the design seismic coefficients. In this analysis, this is obtained entirely from the first case. The point at the crest of the dam is obtained from the point response.

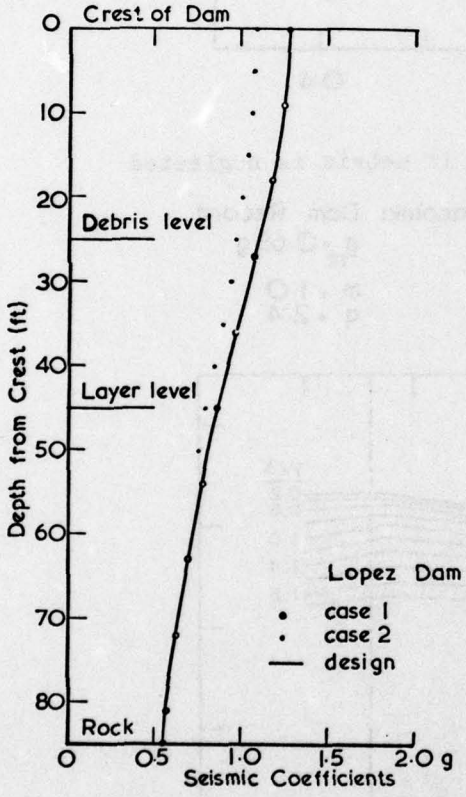

Figure 27. Seismic coefficient versus depth

* The assumption of an untruncated wedge is not strictly applicable in this case. However, it is considered to be a reasonable approximation.

Critical Accelerations

103. The Lopez Dam section is analyzed by the limit equilibrium principle using the Sarma (1973) method, with the computer program written by the author for the CDC 6400-6600 computer at the Imperial College of Science and Technology, London. The various probable slip surfaces and their critical accelerations are shown in Figure 28.

104. WES supplied cyclic triaxial test data indicating the probable values of the pore pressure parameter A_n for various cycles, shown in Figure 29; and the results are tabulated in Table 2. These A_n values are used to determine the critical accelerations for a few upstream surfaces which were considered critical. As far as the dynamic pore pressures were concerned, only the material below the water table is assumed to be affected by the earthquake loading. The results of the analysis are also tabulated in Table 3.

105. From the results we can see the following:

a. There will not be any postearthquake slope failure due to liquefaction. Even the worst case can withstand a critical acceleration of 0.2 g with 20 cycles of pore pressure development, which means, in other words, that without an earthquake, there will be a factor of safety greater than one (a critical acceleration of 0.2 g corresponds to a static factor of safety of approximately 1.6 without earthquake).

b. Even without any dynamic pore pressure development, the critical accelerations of some surfaces are smaller than the design seismic coefficients (Figure 30). Therefore, during the earthquake, the factor of safety of the structure will drop below one; and some slip surfaces will develop.

Displacements

106. Figure 31 shows the dimensionless displacement graph for the modified version of the Pacoima Dam record. The assumed predominate period is 0.4 sec. There are two peaks in the acceleration spectra, one at 0.2 sec and the other at 0.4 sec; however, the velocity spectra shows that 0.4 sec is perhaps more important than 0.2 sec. Table 4

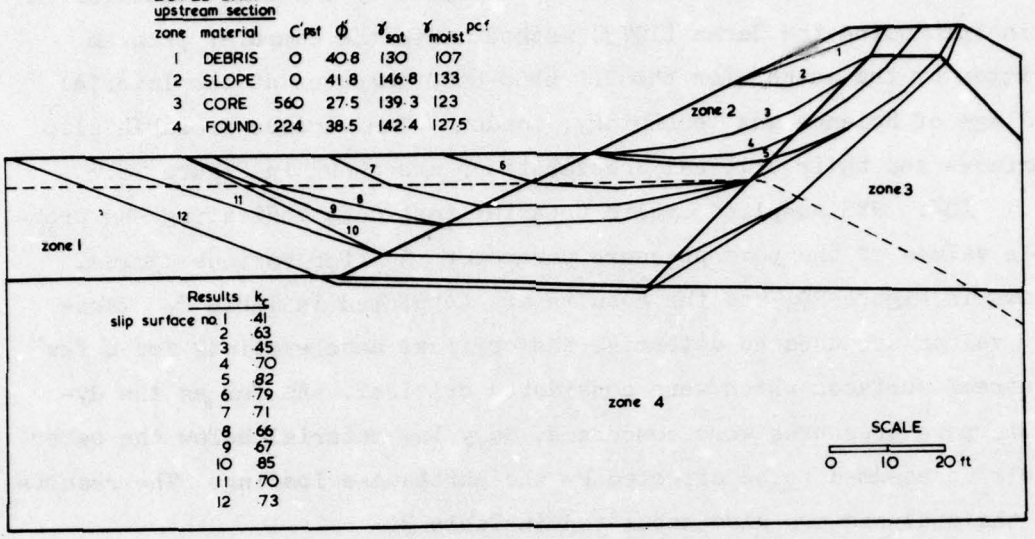

a.

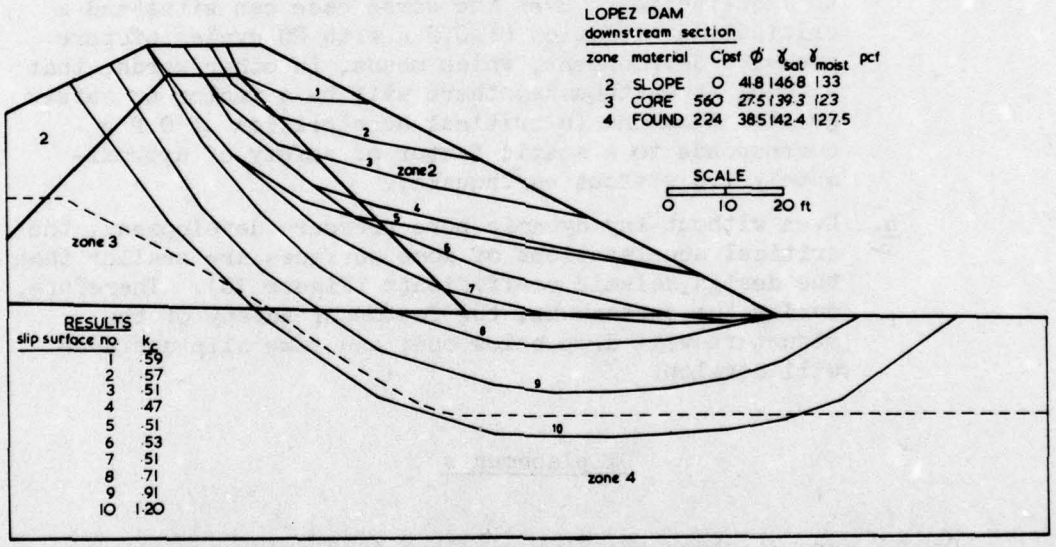

b.

Figure 28. Trial slip surfaces and critical accelerations k_c

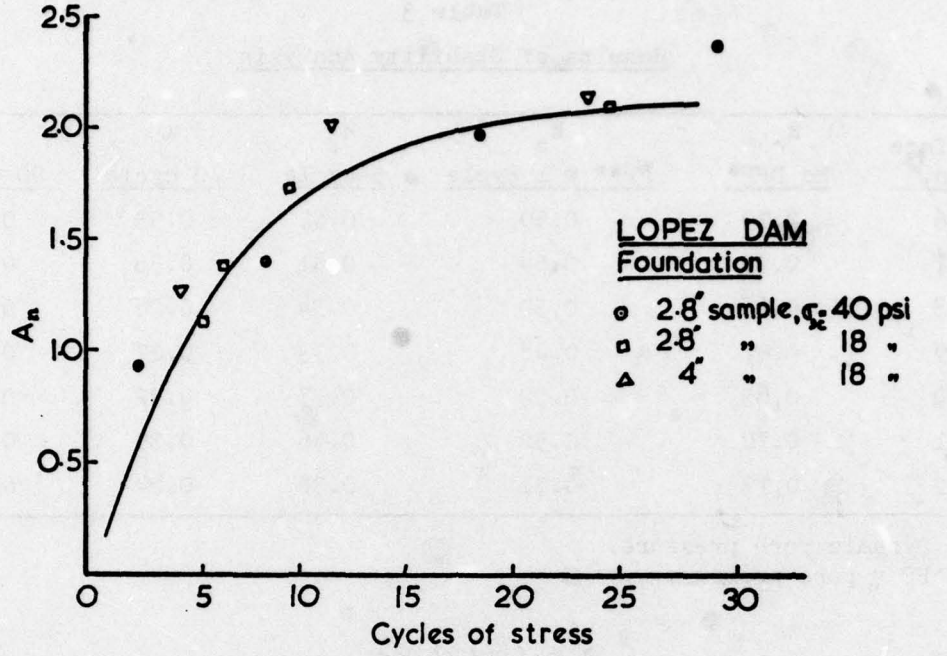

a.

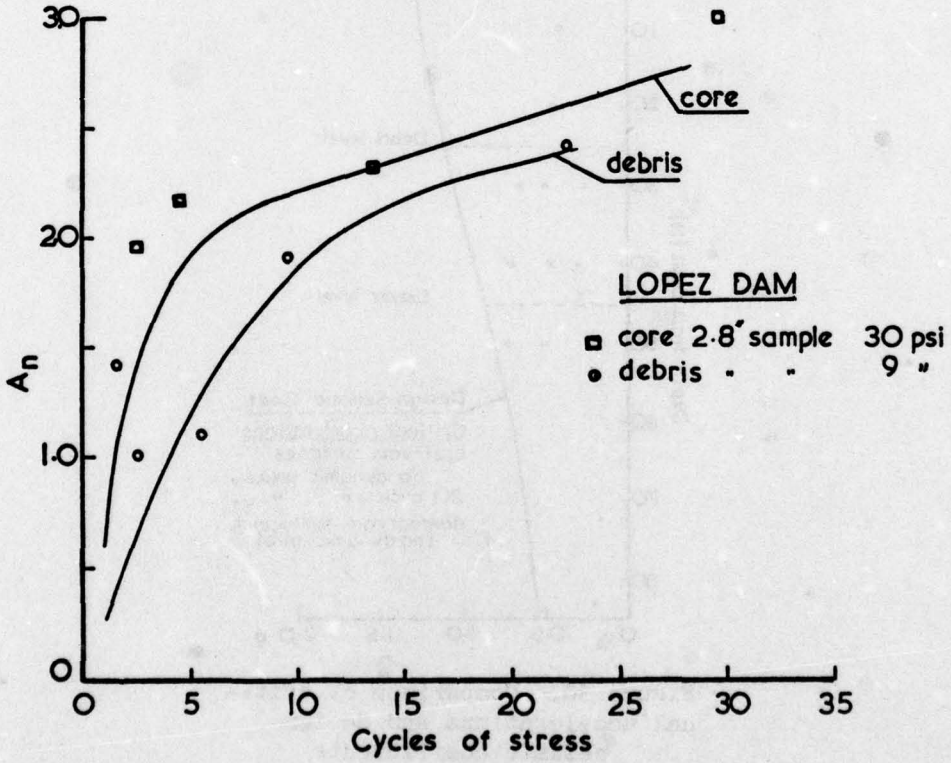

b.

Figure 29. Probable values of pore pressure parameter A

Table 3

Results of Stability Analysis

Surface No.	k_c No DPP*	k_c PP** = 1 cycle	k_c 5 cycle	k_c 10 cycle	k_c 20 cycle
6	0.79	0.59	0.55	0.53	0.53
7	0.71	0.54	0.41	0.36	0.35
8	0.66	0.50	0.34	0.28	0.27
9	0.67	0.48	0.33	0.27	0.26
10	0.85	0.52	0.37	0.32	0.30
11	0.70	0.50	0.46	0.39	0.37
12	0.73	0.51	0.30	0.24	0.22

* Dynamic pore pressure.
** PP = pore pressure.

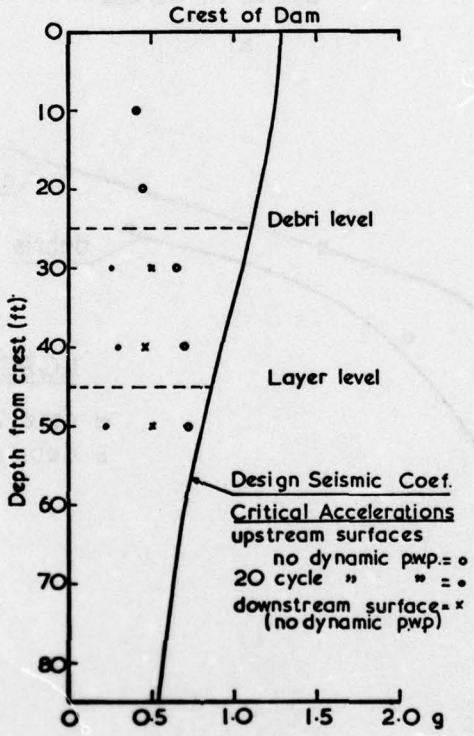

Figure 30. Comparison of critical accelerations and design seismic coefficients

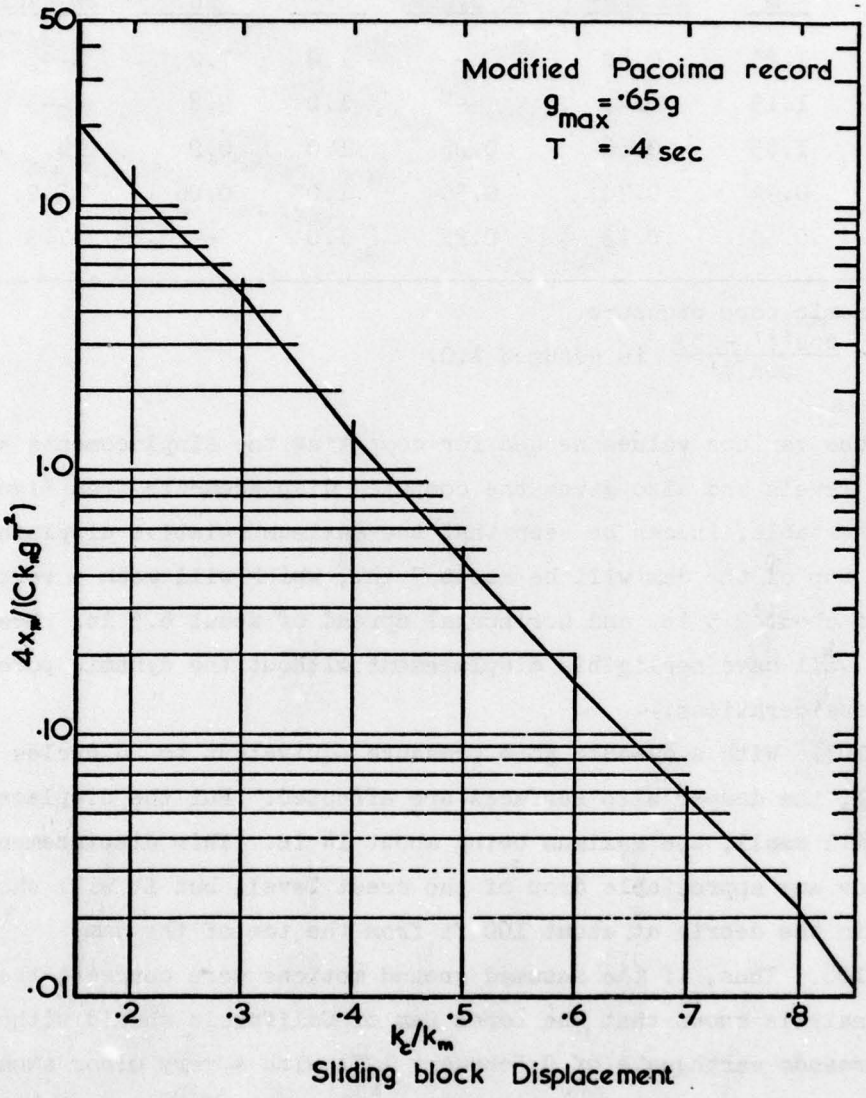

Figure 31. Sliding block displacement from modified Pacoima Record

Table 4

Computed Displacements

$y = \alpha h$ ft	k_m	k_c No DPP*	k_c 20 cycle	C**	Displacement No DPP* in.	Displacement 20 cycle	β deg
10	1.25	0.40	--	1.0	7.2	--	20
20	1.15	0.45	--	1.0	2.8	--	17
30	1.05	0.66	0.25	1.0	0.2	14	7
40	0.94	0.70	0.30	1.0	0.06	5.2	2
50	0.80	0.73	0.22	1.0	--	7.3	0

* Dynamic pore pressure.

** $C = \frac{\cos(\phi' - \beta)}{\cos \phi'}$ is assumed 1.0.

shows the various values needed for computing the displacements at different levels and also gives the computed displacements from Figure 31. From the table, it can be seen that the maximum relative displacement at the top of the dam will be about 7 in., which will mean a vertical drop of about 2.5 in. and horizontal spread of about 6.5 in. Deeper slides will have negligible displacement without the dynamic pore pressure considerations.

107. With a dynamic pore pressure equivalent to 20 cycles of loading, the deeper slip surfaces are affected. But the displacements are still small, the maximum being about 14 in. This displacement does not show any appreciable drop of the crest level, but it will show as a crack in the debris at about 100 ft from the toe of the dam.

108. Thus, if the assumed ground motions were correct, the simplified analysis shows that the Lopez Dam of California should withstand the San Fernando earthquake of 9 February 1971 with a very minor amount of damage. There would be about a 2.5-in. slumping of the crest with a corresponding bulge on the side near the top 10 ft of the dam. There should be some cracking of debris about 100 ft away from the dam, which would be caused by a small movement of a deeper slide.

PART VI: CONCLUSIONS

109. The method of analysis and design of earth dams under earthquake loading conditions, which is developed in this report, is a simple one. The work in the second part is an extension of the original work done by Ambraseys and Sarma (1967), which now includes the presence of a foundation layer. The presence of this layer does seem to affect the response instead of merely changing the fundamental period. The rest of the conclusions that can be drawn are the same as those in the original paper mentioned above. For example, the upper part of the dam is affected more than the lower part, and a deeper slide has a smaller seismic coefficient than a slide on top of the dam. The various seismic coefficient spectra will help the designer in computing the seismic coefficients for his dam.

110. The stability analysis method with the dynamic pore pressure parameters is a simple method and is appropriate for design purposes. However, the dynamic pore pressure parameters need further study. Perhaps a high order curve would be more appropriate than a linear one; but with the present available data, this is superfluous.

111. The displacement criterion of design is still a matter of opinion. However, the displacements computed for the Lopez Dam do not seem to disagree with the field behaviour.

112. The analysis of the Lopez Dam is used more as an example of the concept of this method of analysis than as an attempt to analyze it in detail. For example, the response of the dam and the seismic coefficients are not shown in the time history sequence; only the maximum values are picked up. The seismic coefficients for particular slip surfaces are not computed but are taken from appropriate graphs. Thus, the analysis shows that the concept is a simple one.

REFERENCES

Ambraseys, N. 1960a. "The Seismic Stability of Earth-Dams," Proceedings, Second World Conference on Earthquake Engineering, Vol 2, pp 1345-1363.

_____. 1960b. "On the Shear Response of Two-Dimensional Truncated Wedge Subjected to an Arbitrary Disturbance," Bulletin, Seismological Society of America, Vol 50, pp 45-46.

_____. 1960c. "Uber die Berechnung von erdbebensicheren Erddammen," Ver Deutsch Ing. Zeitsch, Vol 102, pp 1241-1243.

_____. 1973. "Dynamics and Response of Foundation Materials in Epicentral Region of Strong Earthquakes," Proceedings, Fifth World Conference on Earthquake Engineering, Vol 1, pp 124-141.

Ambraseys, N. and Sarma, S. K. 1967. "The Response of Earth Dams to Strong Earthquakes," Geotechnique, Vol 17, pp 181-213.

Bishop, A. W. 1955. "The Use of the Slip Circle in the Stability Analysis of Slopes," Geotechnique, Vol 5, No. 1, pp 7-17.

Clough, R. and Chopra, A. 1965. "Earthquake Stress Analysis in Earth Dams, Report No. 65-68, Structural Engineering Laboratory, University of California, Berkeley, Calif.

Hatanaka, M. 1952. "Three Dimensional Consideration on the Vibration of Earth Dams," Transactions, Japan Society of Civil Engineers, Vol 37, No. 10, pp 423-428.

_____. 1955. "Fundamental Considerations on the Earthquake Resistant Properties of the Earth Dam," Bulletin, Disaster Prevention Research Institute, Kyoto University, Kyoto, Japan, Vol 11.

Ishizaki, H. and Hatakeyama, N. 1962. "Considerations on the Vibrational Behaviour of Earth Dams," Bulletin, Disaster Prevention Research Institute, Kyoto University, Kyoto, Japan, Vol 52.

Janbu, N. 1957. "Earth Pressures and Bearing Capacity Calculations by Generalized Procedure of Slices," Proceedings, Fourth International Conference, Soil Mechanics and Foundation Engineering, Vol 2, pp 207-212.

Kenney, T. C. 1956. "An Examination of the Methods of Calculating the Stability of Slopes," M.S. Thesis, University of London, London, England.

Lee, K. L. and Seed, H. B. 1967a. "Cyclic Stress Conditions Causing Liquefaction of Sand," Journal, Soil Mechanics and Foundations Division, American Society of Civil Engineers, Vol 93, No. SM1, pp 47-70.

_____. 1967b. "Dynamic Strength of Anisotropically Consolidated Sand," Journal, Soil Mechanics and Foundations Division, American Soxiety of Civil Engineers, Vol 93, No. SM5, pp 169-190.

Martin, G., Finn, W. D. L., and Seed, H. B. 1975. "Fundamental of Liquefaction Under Cyclic Loading," Journal, Geological Engineering Division, American Society of Civil Engineers, Vol 101, No. GT5, pp 423-438.

Medvedev, S. and Sinitsym, A. 1965. "Seismic Effects on Earth Fill Dams," Proceedings, Third World Conference on Earthquake Engineering, Paper IV/M/18.

Minami, I. 1960. "A Consideration of Earthquake-Proof Design Method of Earth Dams," Proceedings, Second World Conference on Earthquake Engineering, Vol 3, pp 2061-2074.

Morgenstern, N. R. and Price, V. E. 1966. "The Analysis of the Stability of General Slip Surfaces," Geotechnique, Vol 15, pp 79-93.

Newmark, N. 1965. "Effects of Earthquakes on Dams and Embankments," Geotechnique, Vol 15, No. 2, pp 139-160.

Peacock, W. H. and Seed, H. B. 1968. "Sand Liquefaction Under Cyclic Loading Simple Shear Conditions," Journal, Soil Mechanics and Foundations Division, American Society of Civil Engineers, Vol 94, No. SM3, pp 689-708.

Rashid, Y. 1961. "Dynamic Response of Earth Dams to Earthquakes," Report Graduate Student Research, University of California, Berkeley, Calif.

Sarma, S. K. 1968. Response Characteristics and Stability of Earth Dams During Strong Earthquakes, Ph. D. Dissertation, University of London, London, England.

_____. 1973. "Stability Analysis of Embankments and Slopes," Geotechnique, Vol 23, No. 3, pp 423-433.

_____. 1975. "Seismic Stability of Earth Dams and Embankments," Geotechnique, Vol 25, No. 4, pp 743-761.

Sarma, S. K. and Bhave, M. V. 1974. "Critical Acceleration Versus Static Factor of Safety in Stability Analysis of Earth Dams and Embankments," Geotechnique, Vol 24, No. 4, pp 661-665.

Seed, H. B. 1968. "The Fourth Terzaghi Lecture: Landslides During Earthquakes Due to Liquefaction," Journal, Soil Mechanics and Foundations Division, American Society of Civil Engineers, Vol 94, No. SM5, pp 1053-1122.

Seed, H. B. and Martin, G. 1966. "The Seismic Coefficient on Earth Dam Design," Journal, Soil Mechanics and Foundations Division, American Society of Civil Engineers, Vol 92, No. SM3.

Seed, H. B., Lee, K. L., and Idriss, I. M. 1969. "Analysis of Sheffield Dam Failure," Journal, Soil Mechanics and Foundations Division, American Society of Civil Engineers, Vol 95, No. SM6, pp 1453-1490.

Seed, H. B. et al. 1973. "Analysis of the Slides in the San Fernando Dams During the Earthquake of February 9, 1971," Report No. EERC 73-2, Earthquake Engineering Research Center, University of California, Berkeley, Calif.

Skempton, A. W. 1954. "Pore Pressure Parameters A and B," Geotechnique, Vol 4, No. 4, 954, p 143.

Valenzuela, L. 1975. "Influence of the Distribution of Seismic Acceleration on the Analysis of Stability of Earth Dams and Embankments," M.S. Thesis, Imperial College of Science and Technology, University of London, London, England.

Yokoo et al. 1957. "Vibration Characteristics of Earth Dams," Transactions, Japan Society of Civil Engineers, No. 49, pp 17-18.

APPENDIX A: SOLUTION OF THE GOVERNING EQUATIONS FOR A DAM-FOUNDATION SYSTEM

1. The equations of motion of a dam-layer system subjected to a ground motion are:

$$\frac{\partial^2 u_1}{\partial y^2} + \frac{1}{y} \cdot \frac{\partial u_1}{\partial y} = \frac{1}{S_1^2} \left[\ddot{u}_1 + c\dot{u}_1 + \ddot{g}(t) \right] \tag{A-1}$$

$$\frac{\partial^2 u_2}{\partial y^2} = \frac{1}{S_2^2} \left[\ddot{u}_2 + c\dot{u}_2 + \ddot{g}(t) \right] \tag{A-2}$$

The boundary conditions are:

$$\frac{\partial u_1}{\partial y} = 0 \quad \text{at} \quad y = 0 \tag{A-3}$$

$$u_2 = 0 \quad \text{at} \quad y = H \tag{A-4}$$

$$u_1 = u_2 \quad \text{at} \quad y = h \tag{A-5}$$

$$G_1 \frac{\partial u_1}{\partial y} = G_2 \frac{\partial u_2}{\partial y} \quad \text{at} \quad y = h \tag{A-6}$$

The initial conditions are at rest:

$$u_1 = u_2 = \dot{u}_1 = \dot{u}_2 = 0 \quad \text{at} \quad t = 0 \tag{A-7}$$

Applying Laplace transforms to Equations A-1 and A-2 with the conditions in Equation A-7,

$$\frac{d^2 \bar{u}_1}{dy^2} + \frac{1}{y} \cdot \frac{d\bar{u}_1}{dy} = \frac{1}{S_1^2} (p^2 + cp)\bar{u}_1 + \frac{\bar{\ddot{g}}(t)}{S_1^2} \tag{A-8}$$

$$\frac{d^2 \bar{u}_2}{dy^2} = \frac{1}{S_2^2} (p^2 + cp)\bar{u}_2 + \frac{\bar{\ddot{g}}(t)}{S_2^2} \tag{A-9}$$

where the bar signifies the Laplace transform of the function. Let

$$\frac{p^2 + cp}{S_1^2} = k^2 \text{ , and } \frac{\bar{g}(t)}{S_1^2} = \bar{g} \qquad \text{(A-10)}$$

Equations A-8 and A-9 then become

$$\frac{d^2\bar{u}_1}{dy^2} + \frac{1}{y}\frac{d\bar{u}_1}{dy} = k^2\bar{u}_1 + \bar{g} \qquad \text{(A-11)}$$

$$\frac{d^2\bar{u}_2}{dy^2} = \frac{S_1^2}{S_2^2} k^2\bar{u}_2 + \bar{g} \qquad \text{(A-12)}$$

The transformed boundary conditions are

$$\frac{d\bar{u}_1}{dy} = 0 \quad \text{at} \quad y = 0 \qquad \text{(A-13)}$$

$$\bar{u}_2 = 0 \quad \text{at} \quad y = H \qquad \text{(A-14)}$$

$$\bar{u}_1 = \bar{u}_2 \text{ at } y = h \qquad \text{(A-15)}$$

$$G_1 \frac{d\bar{u}_1}{dy} = G_2 \frac{d\bar{u}_2}{dy} \quad \text{at} \quad y = h \qquad \text{(A-16)}$$

Solution of Equation A-11 with Equation A-13 gives

$$\bar{u}_1 = CI_o(ky) - \frac{\bar{g}}{k^2} \qquad \text{(A-17)}$$

and solution of Equation A-12 with Equation A-14 gives

$$\bar{u}_2 = \frac{B \sinh\left[\frac{S_1}{S_2} k(y - H)\right]}{\cosh\left(\frac{S_1}{S_2} kH\right)} + \frac{g}{k^2} \frac{\cosh\left(\frac{S_1}{S_2} ky\right)}{\cosh\left(\frac{S_1}{S_2} kH\right)} - 1 \qquad \text{(A-18)}$$

where B and C are unknown constants and $I_o()$ is the modified Bessel function of order 0 .

Equation A-15 then gives

$$C = \frac{B}{I_o(kh)} \cdot \frac{\sinh\left[\frac{S_1}{S_2} k(h - H)\right]}{\cosh\left(\frac{S_1}{S_2} kH\right)} + \frac{\bar{g}}{k^2} \frac{\cosh\left(\frac{S_1}{S_2} kH\right)}{I_o(kh) \cosh\left(\frac{S_1}{S_2} kH\right)} \qquad \text{(A-19)}$$

Equation A-16 gives

$$S_1^2 \rho_1 \frac{d\bar{u}_1}{dy} = S_2^2 \rho_2 \frac{d\bar{u}_2}{dy} \quad \text{at} \quad y = h$$

$$\frac{S_1^2}{S_2^2} \cdot \frac{\rho_1}{\rho_2} \cdot \frac{d\bar{u}_1}{dy} = \frac{d\bar{u}_2}{dy} \qquad \text{(A-20)}$$

$$C \frac{S_1 \rho_1}{S_2 \rho_2} I_1(kh) = B \frac{\cosh\left[\frac{S_1}{S_2} k(h - H)\right]}{\cosh\left(\frac{S_1}{S_2} kH\right)} + \frac{\bar{g}}{k^2} \frac{\sinh\left(\frac{S_1}{S_2} kh\right)}{\cosh\left(\frac{S_1}{S_2} kH\right)} \qquad \text{(A-21)}$$

where $I_1()$ is the modified Bessel function of order 1.

Put

$$\frac{S_1 \rho_1}{S_2 \rho_2} = m \qquad \text{(A-22)}$$

$$\frac{S_1(h - H)}{S_2} = a \qquad \text{(A-23)}$$

$$\frac{S_1}{S_2} h = b \tag{A-24}$$

Equations A-19 and A-21 therefore give

$$B = \frac{\bar{g}}{k_2}\left[\frac{I_o(kh)\sinh(bk) - mI_1(kh)\cosh(bk)}{mI_1(kh)\sinh(ak) - I_o(kh)\cosh(ak)}\right] \tag{A-25}$$

Substituting Equation A-25 into Equation A-19 yields

$$C = \frac{\bar{g}}{k^2} \cdot \frac{1}{mI_1(kh)\sinh(ak) - I_o(kh)\cosh(ak)} \tag{A-26}$$

Putting Equation A-26 back into Equation A-17 yields

$$\bar{u}_1 = \frac{\bar{g}}{k^2}\left[\frac{I_o(ky)}{I_o(h)\cosh(ak) - mI_1(kh)\sinh(ak)} - 1\right] \tag{A-27}$$

Similarly, substituting Equation A-25 into Equation A-18 yields

$$\bar{u}_2 = \frac{g}{K^2}\left[\frac{I_o(kh)\cosh\frac{S_1}{S_2}k(y-h) + mI_1(kh)\sinh\frac{S_1}{S_2}k(y-h)}{I_o(kh)\cosh\frac{S_1}{S_2}k(h-H) - mI_1(kh)\sinh(ak)} - 1\right] \tag{A-28}$$

2. The inversion of Equation A-27 and Equation A-28 can be obtained by applying Melin's inversion theorem. We can write

$$\bar{u}_1 = \bar{g} \cdot \bar{F}_1 \tag{A-29}$$

and

$$\bar{u}_2 = \bar{g} \cdot \bar{F}_2 \tag{A-30}$$

where $\bar{F}_1$ and $\bar{F}_2$ are Laplace transforms of F_1 and F_2, and therefore

$$u_1 = \int_0^t \frac{\ddot{g}}{S_1^2}(\tau) F_1(t - \tau)\, d\tau \qquad \text{(A-31)}$$

$$u_2 = \int_0^t \frac{\ddot{g}}{S_1^2}(\tau) F_2(t - \tau)\, d\tau \qquad \text{(A-32)}$$

Therefore, the problem is to obtain F_1 and F_2 from

$$\overline{F}_1 = \frac{1}{k^2}\left[\frac{I_o(ky)}{I_o(kh)\cosh(ak) - mI_1(kh)\sinh(ak)} - 1\right] \qquad \text{(A-33)}$$

$$\overline{F}_2 = \frac{1}{k^2}\left[\frac{I_o(kh)\cosh\frac{S_1}{S_2}k(y-h) + mI_1(kh)\sinh\frac{S_1}{S_2}k(y-h)}{I_o(kh)\cosh(ak) - mI_1(kh)\sinh(ak)} - 1\right] \qquad \text{(A-34)}$$

From the inversion theorem

$$F_1 = \frac{S_1^2}{2\pi i}\int_{\gamma-i\infty}^{\gamma+i\infty} \frac{e^{pt}}{(p^2+cp)}\left[\frac{I_o(ry)}{I_o(rh)\cosh(ar) - mI_1(rh)\sinh(ar)} - 1\right] dp \qquad \text{(A-35)}$$

where $i = \sqrt{-1}$ and

$$F_2 = \frac{S_1^2}{2\pi i}\int_{\gamma-i\infty}^{\gamma+i\infty} \frac{e^{pt}}{(p^2+cp)}\left[\frac{I_o(rh)\cosh\frac{S_1}{S_2}h(y-h) + mI_1(rh)\sinh\frac{S_1}{S_2}r(y-h)}{I_o(rh)\cosh(ar) - mI_1(rh)\sinh(ar)} - 1\right] dp \qquad \text{(A-36)}$$

where

$$r = \frac{1}{S_1}(p^2 + cp)^{1/2}$$

To apply the theory of residues, the poles are at $p = 0$; $p = -c$; and at those values of $p = p_n$ that make

$$I_o rh \cosh ar - mI_1 rh \sinh ar = 0 \qquad \text{(A-37)}$$

The roots of Equation A-37 are all imaginary. Let $rh = i\bar{a}_n$ be the roots. Then

$$p_n = -\frac{c}{2} \pm \frac{1}{2}\sqrt{c^2 - 4\frac{\bar{a}_n^2 S_1^2}{h^2}} \qquad \text{(A-38)}$$

are the poles, and Equation A-37 becomes

$$\frac{J_o \bar{a}_n}{J_1 \bar{a}_n} = m \tan q\bar{a}_n \qquad \text{(A-39)}$$

where

$$q = -\frac{a}{h} = m \cdot \frac{\rho_2}{\rho_1} \cdot \frac{H - h}{h} \qquad \text{(A-40)}$$

Put

$$\frac{\bar{a}_n S}{h} = \omega_{on} \qquad \text{(A-41)}$$

and

$$c = 2\lambda_n \omega_{on} \qquad \text{(A-42)}$$

then

$$P_n = -\lambda_n \omega_{on} \pm i\omega_{on}\sqrt{1 - \gamma_n^2} \qquad \text{(A-43)}$$

3. The residues at $p = 0$ and $p = -c$ are zero, therefore

$$F_1(t) = S_1^2 \sum_{n=1}^{\infty} \frac{e^{p_n t}}{p_n^2 + cp_n} \cdot \frac{J_o(\bar{a}_n y/h)}{\frac{d}{dp}\left[I_o(rh)\cosh(ar) - mI_1(rh)\sinh(ar)\right]_{p = p_n}} \qquad \text{(A-44)}$$

$$F_2(t) =$$

$$S_1^2 \sum_{n=1}^{\infty} \frac{e^{p_n t}}{p_n^2 + cp_n} \cdot \frac{J_c(\bar{a}_n)\cos\left[\frac{S_1}{S_2} \cdot \frac{\bar{a}_n}{h}(y-h)\right] - mJ_1(\bar{a}_n)\sin\left[\frac{S_1}{S_2} \cdot \frac{\bar{a}_n}{h}(y-h)\right]}{\frac{d}{dp}\left[I_o(rh)\cosh(ar) - mI_1(rh)\sinh(ar)\right]_{p=p_n}} \quad \text{(A-45)}$$

Let

$$D = \frac{d}{dp}\left[I_o(rh)\cosh(ar) - mI_1(rh)\sinh(ar)\right]$$

$$= \frac{2p + c}{2S_1\sqrt{p^2 + cp}} \left\{ hI_1(rh)\cosh(ar) + aI_o(rh)\sinh(ar) \right.$$

$$\left. - mh\sinh(ar)\left[I_o(rh) - \frac{I_1(rh)}{rh}\right] - maI_1(rh)\cosh(ar) \right\}$$

for $p = p_n$ when $rh = i\bar{a}_n$

$$D = ih \frac{(2p_n + c)}{2S_1\sqrt{p_n^2 + cp_n}} \left\{ J_1(\bar{a}_n)\cos(q\bar{a}_n) + qJ_o(\bar{a}_n)\sin(q\bar{a}_n) \right.$$

$$\left. + m\sin(q\bar{a}_n)\left[J_o(\bar{a}_n) - \frac{J_1(\bar{a}_n)}{\bar{a}_n}\right] + mqJ_1(\bar{a}_n)\cos(q\bar{a}_n) \right\}$$

$$= \frac{ih(2p_n+c)}{2S_1\sqrt{p_n^2+cp_n}} \cdot \frac{J_1(a_n)}{\cos(qa_n)} \left[mq + m^2\sin^2 q\bar{a}_n + \cos^2 q\bar{a}_n \right.$$

$$\left. - \frac{m}{\bar{a}_n}\sin(q\bar{a}_n)\cos(q\bar{a}_n) \right]$$

$$+ \frac{ih(2p_n + c)}{2S_1\sqrt{p_n^2 + cp_n}} \cdot p_o(q,m,n) \quad \text{(A-46)}$$

where

$$p_o(q,m,n) = \frac{J_1(\bar{a}_n)}{\cos(q\bar{a}_n)}\left(mq + m^2 \sin^2 q\bar{a}_n + \cos^2 q\bar{a}_n - \frac{m}{\bar{a}_n}\sin q\bar{a}_n \cos q\bar{a}_n\right) \quad \text{(A-47)}$$

At $p_n = -\lambda_n\omega_{on} \pm i\omega_{on}\sqrt{1-\lambda_n^2}$

$$D = \pm i \frac{h}{s_1} p_o(q,m,n)\sqrt{1-\lambda_n^2}$$

Therefore

$$F_1(t) = S_1^2\left[\left\{\frac{e^{-\lambda_n\omega_{on}t}\, e^{i\omega_{on}\sqrt{1-\lambda_n^2}t}\, J_o(\bar{a}_n y/h)}{\frac{-S_1^2\bar{a}_n^2}{h^2}\left[i\frac{h}{s}p_o(q,m,n)\sqrt{1-\lambda_n^2}\right]} + \frac{e^{-\lambda_n\omega_{on}t}\, e^{i\omega_{on}\sqrt{1-\lambda_n^2}t}\, J_o(\bar{a}_n y/h)}{\frac{+S_1^2\bar{a}_n^2}{h^2}\left[i\frac{h}{s}p_o(q,m,n)\sqrt{1-\lambda_n^2}\right]}\right\}\right]$$

$$= S_1^2\left[\left[\frac{e^{-\lambda_n\omega_{on}t} J_o(\bar{a}_n y/h)}{-\omega_{on} i\bar{a}_n p_o(q,m,n)\sqrt{1-\lambda_n^2}}\left(e^{i\omega_{on}\sqrt{1-\lambda_n^2}t} - e^{-i\omega_{on}\sqrt{1-\lambda_n^2}t}\right)\right]\right]$$

$$= S_1^2\left[\left[\frac{e^{-\lambda_n\omega_{on}t} J_o(\bar{a}_n y/h)}{\bar{a}_n p_o(q,m,n)}\,\frac{2}{-\omega_{on}\sqrt{1-\lambda_n^2}}\sin\left(\omega_{on}\sqrt{1-\lambda_n^2}t\right)\right]\right] \quad \text{(A-48)}$$

Similarly,

$$F_2(t) = S_1^2 \left[\left[\frac{2mJ_1(\bar{a}_n) \sin\left(q\bar{a}_n \frac{H-y}{H-h}\right)}{\cos(q\bar{a}_n)\bar{a}_n p_o(q,m,n)} \right] \frac{e^{-\lambda_n \omega_{on} t}\left(\sin \omega_{on} \sqrt{1-\lambda_n^2 t}\right)}{-\omega_{on}\sqrt{1-\lambda_n^2}} \right] \quad \text{(A-49)}$$

Equations A-31 and A-32 then yield the solutions for $u_1(y,t)$ and $u_2(y,t)$ given in the main text.

AD-A073 010 IMPERIAL COLL OF SCIENCE AND TECHNOLOGY LONDON (ENGLA--ETC F/G 13/2
RESPONSE AND STABILITY OF EARTH DAMS DURING STRONG EARTHQUAKES.(U)
JUN 79 S K SARMA DA-ERO-75-G-010

UNCLASSIFIED WES-MP-GL-79-13 NL

2 OF 3
AD
A073010

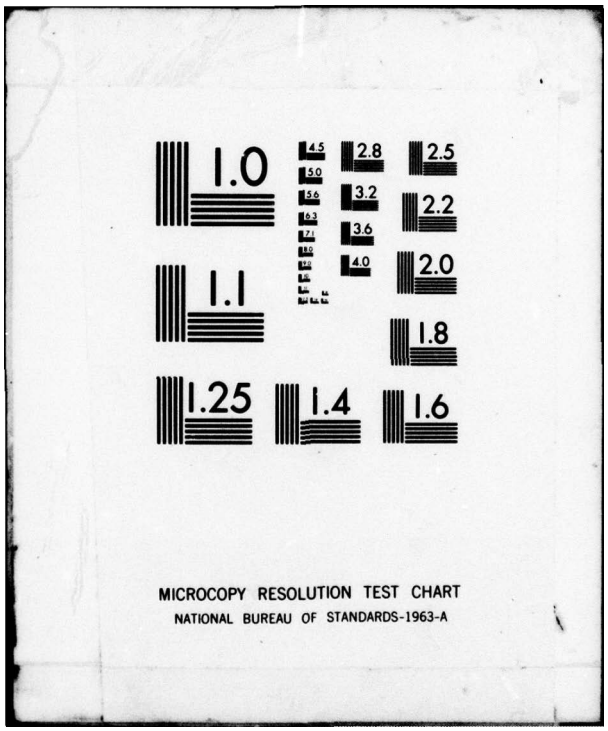
1.0
1.1
1.25
1.4
1.6
1.8
2.0
2.2
2.5
2.8
3.2
3.6
4.0
4.5
5.0
5.6
6.3
7.1
8.0
MICROCOPY RESOLUTION TEST CHART
NATIONAL BUREAU OF STANDARDS-1963-A

APPENDIX B:

SEISMIC COEFFICIENTS

1. For the one-parameter sliding wedge

$$\phi 1_n(\alpha) = \frac{\int_0^{\alpha h} y\phi_n \, dy}{\int_0^{\alpha h} y \, dy}$$

$$= \frac{\int_0^{\alpha h} y \, \frac{2J_o(a_n y/h)}{a_n p_o(q,m,n)} \, dy}{\alpha^2 \frac{h^2}{2}}$$

$$= \frac{4J_1(\alpha \bar{a}_n)}{\alpha \bar{a}_n^2 p_o(q,m,n)} \qquad \text{(B-1)}$$

2. For the four-parameter sliding wedge, no such simple form exists. In computing $\phi 4_n(\alpha)$, there are three possibilities, depending on the geometry of the sliding wedge.

Case 1: The entire sliding surface is in the dam: $\alpha \leq 1$.

Case 2: Part of the sliding surface is in the foundation, but the exit points are in the dam: $\alpha > 1$.

Case 3: Part of the sliding surface is in the foundation, and the lower exit point is in the foundation: $\alpha > 1$.

3. Sarma (1968) determined these seismic coefficients by computing the accelerations in the dam first and then numerically determining the seismic coefficient. But it is possible to formulate the seismic coefficients analytically for the three cases separately.

Case 1:

$$\phi 4_n(\alpha) = \frac{\int_0^{\alpha h} b(y)\phi_n \, dy}{\int_0^{\alpha h} b(y) \, dy}$$

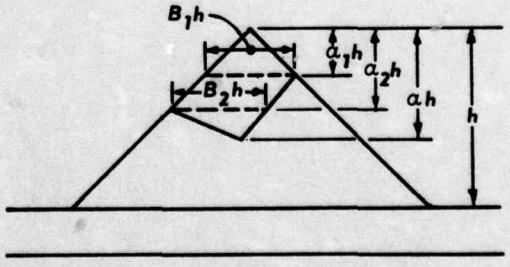

CASE 1

$$\text{Denominator} = \int_0^{\alpha h} b(y)\, dy$$

$$= \int_0^{\alpha_1 h} b_1(y)\, dy + \int_{\alpha_1 h}^{\alpha_2 h} b_2(y)\, dy + \int_{\alpha_2 h}^{\alpha h} b_3(y)\, dy$$

where

$$b_1(y) = \frac{B_1}{\alpha_1}\, y \; ; \quad b_2(y) = B_1 h + \frac{(B_2 - B_1)}{\alpha_2 - \alpha_1}\,(y - \alpha_1 h) \; ;$$

$$B_3(y) = \frac{B_2(\alpha h - y)}{(\alpha - \alpha_2)}$$

Therefore,

$$\text{Denominator} = \frac{h^2}{2}\left[B_1\alpha_2 + B_2(\alpha - \alpha_1)\right]$$

$$\text{Numerator} = \int_0^{\alpha_1 h} b_1(y)\phi_n\, dy + \int_{\alpha_1 h}^{\alpha_2 h} b_2(y)\phi_n\, dy + \int_{\alpha_2 h}^{\alpha h} b_3(y)\phi_n\, dy$$

$$= \frac{B_1}{\alpha_1}\int_0^{\alpha_1 h} y\phi_n\, dy + \frac{(\alpha_2 B_1 - \alpha_1 B_2)h}{(\alpha_2 - \alpha_1)} \int_{\alpha_1 h}^{\alpha_2 h} \phi_n\, dy + \frac{B_2 - B_1}{\alpha_2 - \alpha_1}\int_{\alpha_1 h}^{\alpha_2 h} y\phi_n\, dy$$

$$+ \frac{\alpha B_2 h}{\alpha - \alpha_2} \int_{\alpha_2 h}^{\alpha h} \phi_n\, dy - \frac{B_2}{(\alpha - \alpha_2)} \int_{\alpha_2 h}^{\alpha h} y\phi_n\, dy$$

$$= \frac{2h^2}{\bar{a}_n p_o(q,m,n)} \left\{ \frac{B_1}{\alpha_1} \cdot \frac{\alpha_1}{\bar{a}_n} J_1(\alpha_1 \bar{a}_n) - \frac{B_2}{(\alpha - \alpha_2)} \left[\frac{\alpha}{\bar{a}_n} J_1(\alpha\, \bar{a}_n) - \frac{\alpha_2}{\bar{a}_n} J_1(\alpha_2 \bar{a}_n) \right] \right.$$

$$\left. + \frac{B_2 - B_1}{\alpha_2 - \alpha_1} \left[\frac{\alpha_2}{\bar{a}_n} J_1(\alpha_2 \bar{a}_n) - \frac{\alpha_1}{\bar{a}_n} J_1(\alpha_1 \bar{a}_n) \right] \right\}$$

$$+ \frac{\alpha_2 B_1 - \alpha_1 B_2}{\alpha_2 - \alpha_1} \left[\text{BESINT } (\bar{a}_n, \alpha_2) - \text{BESINT } (\bar{a}_n, \alpha_1) \right]$$

$$+ \frac{\alpha B_2}{\alpha - \alpha_2} \left[\text{BESINT } (\bar{a}_{n1}\alpha) - \text{BESINT } (\bar{a}_n \alpha_2) \right]$$

where

$$\text{BESINT } (a_n, \alpha) = \int_0^{\alpha} J_o(a_n y)\, dy$$

Thus,

$$\phi 4_n(\alpha) = \text{Numerator/Denominator}$$

Case 2:

$$\phi 4_n(\alpha) = \frac{\int_0^h b(y)\phi_n\, dy + \int_h^{\alpha h} b(y)\psi_n\, dy}{\int_0^{\alpha h} b(y)\, dy}$$

$$\text{Denominator} = \frac{h^2}{2}\left[B_1\alpha_2 + B_2(\alpha - \alpha_1)\right]$$

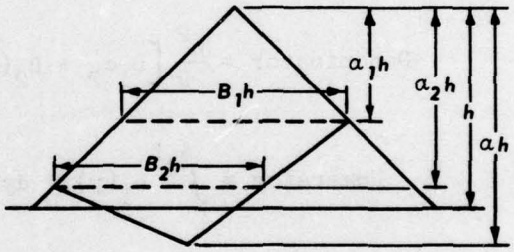

CASE 2

$$\text{Numerator} = \int_0^{\alpha_1 h} b_1(y)\phi_n\, dy + \int_{\alpha_1 h}^{\alpha_2 h} b_2(y)\phi_n\, dy + \int_{\alpha_2 h}^{h} b_3(y)\phi_n\, dy$$

$$+ \int_h^{\alpha h} b_3(y)_n\, dy = \frac{B_1}{\alpha_1}\int_0^{\alpha_1 h} y\phi_n\, dy + \frac{(\alpha_2 B_1 - \alpha_1 B_2)h}{\alpha_2 - \alpha_1} \int_{\alpha_1 h}^{\alpha_2 h} \phi_n\, dy$$

$$+ \frac{B_2 - B_1}{\alpha_2 - \alpha_1} \int_{\alpha_1 h}^{\alpha_2 h} y\phi_n\, dy + \frac{\alpha B_2 h}{\alpha - \alpha_2} \int_{\alpha_2 h}^{h} \phi_n\, dy - \frac{B_2}{(\alpha - \alpha_2)} \int_{\alpha_2 h}^{h} y\phi_n\, dy$$

$$+ \frac{B_2}{(\alpha - \alpha_2)} \int_h^{\alpha h} (\alpha h - y)\psi_n \, dy = \frac{2h^2}{\bar{a}_n p_o(q,m,n)} \left(\frac{B_1}{\alpha_1} \cdot \frac{\alpha_1}{\bar{a}_n} J_1(\alpha_1 \bar{a}_n) \right.$$

$$+ \frac{B_2 - B_1}{\alpha_2 - \alpha_1} \left[\frac{\alpha_2}{\bar{a}_n} J_1(\alpha_2 a_n) - \frac{\alpha_1}{\bar{a}_n} J_1(\alpha_1 \bar{a}_n) \right] - \frac{B_2}{(\alpha - \alpha_2)} \left[\frac{1}{\bar{a}_n} J_1(\bar{a}_n) \right.$$

$$\left. - \frac{\alpha_2}{\bar{a}_n} J_1(\alpha_2 \bar{a}_n) \right] + \frac{(\alpha_2 B_1 - \alpha_1 B_2)}{\alpha_2 - \alpha_1} \left[\text{BESINT}\,(\bar{a}_n, \alpha_2) - \text{BESINT}\,(\bar{a}_n, \alpha_1) \right]$$

$$+ \frac{\alpha B_2}{\alpha - \alpha_2} \left[\text{BESINT}\,(\bar{a}_n, 1) - \text{BESINT}\,(\bar{a}_n, \alpha_2) \right] + \frac{m J_1(\bar{a}_n)}{\cos(q\bar{a}_n)} \,,$$

$$\frac{B_2}{(\alpha - \alpha_2)} \left\{ \frac{(H/h - 1)^2}{q^2 \bar{a}_n^2} \left[\sin(qa_n) - \sin\left(qa_n \frac{H/h - \alpha}{H/h - 1} \right) \right] \right.$$

$$\left. \left. - \frac{(H/h - 1)(\alpha - 1)}{q\bar{a}_n} \cos qa_n \right\} \right)$$

Case 3:

$$\phi 4_n(\alpha) = \frac{\int_o^h b(y)\phi_n \, dy + \int_o^{\alpha h} b(y)\psi_n \, dy}{\int_o^{\alpha h} b(y) \, dy}$$

$$\text{Denominator} = \int_o^{\alpha_1 h} b_1(y) \, dy + \int_{\alpha_1 h}^{h} b_2(y) \, dy + \int_h^{\alpha h} b_3(y) \, dy$$

where

$$b_1(y) = \frac{B_1}{\alpha_1} y$$

$$b_2(y) = B_1 h + \frac{(B_2 - B_1)}{1 - \alpha_1}(y - \alpha_1 h) \text{ and}$$

$$b_3(y) = \frac{B_3(\alpha h - y)}{\alpha - 1}$$

$$\text{Denominator} = \frac{h^2}{2}\left[B_1 + B_2(1 - \alpha_1) + B_3(\alpha - 1)\right]$$

$$\text{Numerator} = \frac{B_1}{\alpha_1}\int_0^{\alpha_1 h} y\phi_n \, dy + \frac{B_2 - B_1}{1 - \alpha_1}\int_{\alpha_1 h}^{h} y\phi_n \, dy$$

$$+ \frac{(B_1 - \alpha_1 B_2)h}{1 - \alpha_1}\int_{\alpha_1 h}^{h} \phi_n \, dy$$

$$+ \frac{B_3}{\alpha - 1}\int_h^{\alpha h} (\alpha h - y)\psi_n \, dy$$

$$= \frac{2h^2}{\bar{a}_n p_o(q,m,n)}\left(\frac{B_1}{\alpha_1} \cdot \frac{\alpha_1}{\bar{a}_n} J_1(\alpha_1 \bar{a}_n) + \frac{B_2 - B_1}{1 - \alpha_1}\left[\frac{1}{\bar{a}_n} J_1(\bar{a}_n) - \frac{\alpha_1}{\bar{a}_n} J_1(\alpha_1 \bar{a}_n)\right]\right.$$

$$+ \frac{(B_1 - \alpha_1 B_2)}{(1 - \alpha_1)}\left[\text{BESINT}\,(\bar{a}_n, 1) - \text{BESINT}\,(\bar{a}_n, \alpha_1)\right]$$

$$\left. + \frac{mJ_1(\bar{a}_n)}{\cos q\bar{a}_n} \cdot \frac{B_3}{(\alpha - 1)}\left\{\frac{(H/h - 1)^2}{q^2 \bar{a}_n^2}\left[\sin\left(q\bar{a}_n\right) - \sin\left(q\bar{a}_n \frac{H/h - \alpha}{H/h - 1}\right)\right.\right.\right.$$

$$\left.\left.\left. - \frac{(H/h - 1)(\alpha - 1)}{q\bar{a}_n} \cos\left(q\bar{a}_n\right)\right]\right\}\right)$$

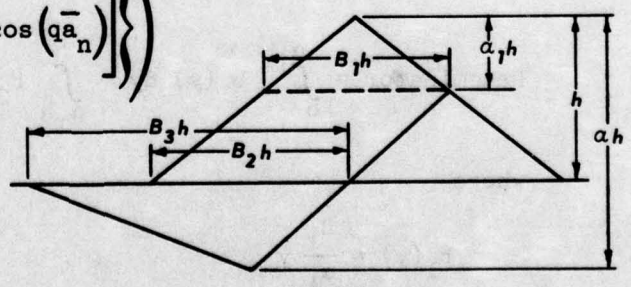

CASE 3

APPENDIX C:

ROOTS OF THE EQUATION

$$m \tan (q\bar{a}_n) = J_o(\bar{a}_n)/J_1(\bar{a}_n)$$

ROOTS OF EQUATION M.TAN(Q.AN)=JO(AN)/J1(AN)

****

M= 1.000

N	Q= .250	.500	.750	1.000	1.500	2.000
1	1.8774	1.4934	1.2238	1.0312	.7803	.6262
2	4.3444	3.6063	3.1241	2.7612	2.2156	1.8256
3	6.8703	5.7708	4.9329	4.2832	3.4266	2.8824
4	9.4152	7.8423	6.7356	5.8958	4.7003	3.8954
5	11.9457	9.9259	8.5349	7.4405	5.9713	4.9731
6	14.4523	12.0480	10.3019	9.0353	7.2055	6.0221
7	16.9515	14.1309	12.1211	10.5883	8.4874	7.0509
8	19.4631	16.2177	13.9030	12.1759	9.7281	8.1154
9	21.9868	18.3294	15.7036	13.7332	10.9907	9.1633
10	24.5081	20.4161	17.5025	15.3172	12.2530	10.1980
11	27.0183	22.5047	19.2890	16.8771	13.4981	11.2572
12	29.5235	24.6117	21.0967	18.4584	14.7684	12.3407
13	32.0352	26.7003	22.8796	28.0200	16.0154	13.3424
14	34.5547	28.7901	24.6856	21.5997	17.2758	14.3988
15	37.0732	30.8944	26.4740	23.1626	18.5360	15.4464
16	39.5845	32.9841	28.2716	24.7411	19.7849	16.4858
17	42.0921	35.0747	30.0692	26.3852	21.0508	17.5405
18	44.6041	37.1771	31.8591	27.8827	22.3005	18.5877
19	47.1218	39.2677	33.6619	29.4473	23.5597	19.6286
20	49.6390	41.3589	35.4492	31.0241	24.8190	20.6821

M= .500

N	Q= .125	.250	.375	.500	.750	1.000
1	2.2563	2.1032	1.9407	1.7727	1.4591	1.2109
2	5.1492	4.6135	3.9859	3.4996	2.9465	2.6526
3	7.9720	6.7769	6.0396	5.6739	5.1122	4.4157
4	10.6397	9.1594	8.6100	8.0771	6.5901	5.7817
5	13.1736	11.8779	11.0926	9.8089	8.5779	7.5670
6	15.7793	14.6492	13.0064	11.9487	10.3526	8.9194
7	18.5585	17.2027	15.2375	14.3616	12.0084	10.7126
8	21.4531	19.3642	17.8545	16.0986	14.0852	12.0594
9	24.3984	21.7250	20.1647	18.2293	15.5130	13.8564
10	27.3519	24.4396	22.0479	20.6448	17.6754	15.2000
11	30.2744	27.2133	24.4770	22.3841	19.1678	16.9992
12	33.1114	29.7715	27.0719	24.5112	21.1383	18.3406
13	35.7882	31.9362	29.1645	26.9282	22.9269	20.1418
14	38.3206	34.2913	31.1715	28.6689	24.5716	21.4821
15	40.9171	37.0047	33.7338	30.7936	26.6543	23.2843
16	43.6907	39.7788	36.2293	33.2120	28.0797	24.6234
17	46.5835	42.3391	38.1483	34.9530	30.2411	26.4261
18	49.5287	44.5038	40.3674	37.0763	31.7365	27.7644
19	52.4821	46.8576	42.9844	39.4948	33.7031	29.5684
20	55.4064	49.5701	45.3016	41.2369	35.4950	30.9058

M= 0

Q= 0
1 2.4048
2 5.5201
3 8.6538
4 11.7915
5 14.9309
6 18.0710
7 21.2163
8 24.3525
9 27.4933
10 30.6346
11 33.7762
12 36.9171
13 40.0584
14 43.1998
15 46.3412
16 49.4820
17 52.6241
18 55.7657
19 58.9070
20 62.0485

APPENDIX D:

ACCELERATION RECORDS OF FIVE EARTHQUAKES

In each of the following figures (D1-D9), a represents acceleration, velocity, displacement records, and energy flux plots; and b represents acceleration, velocity, and displacement spectra of strong motion records.

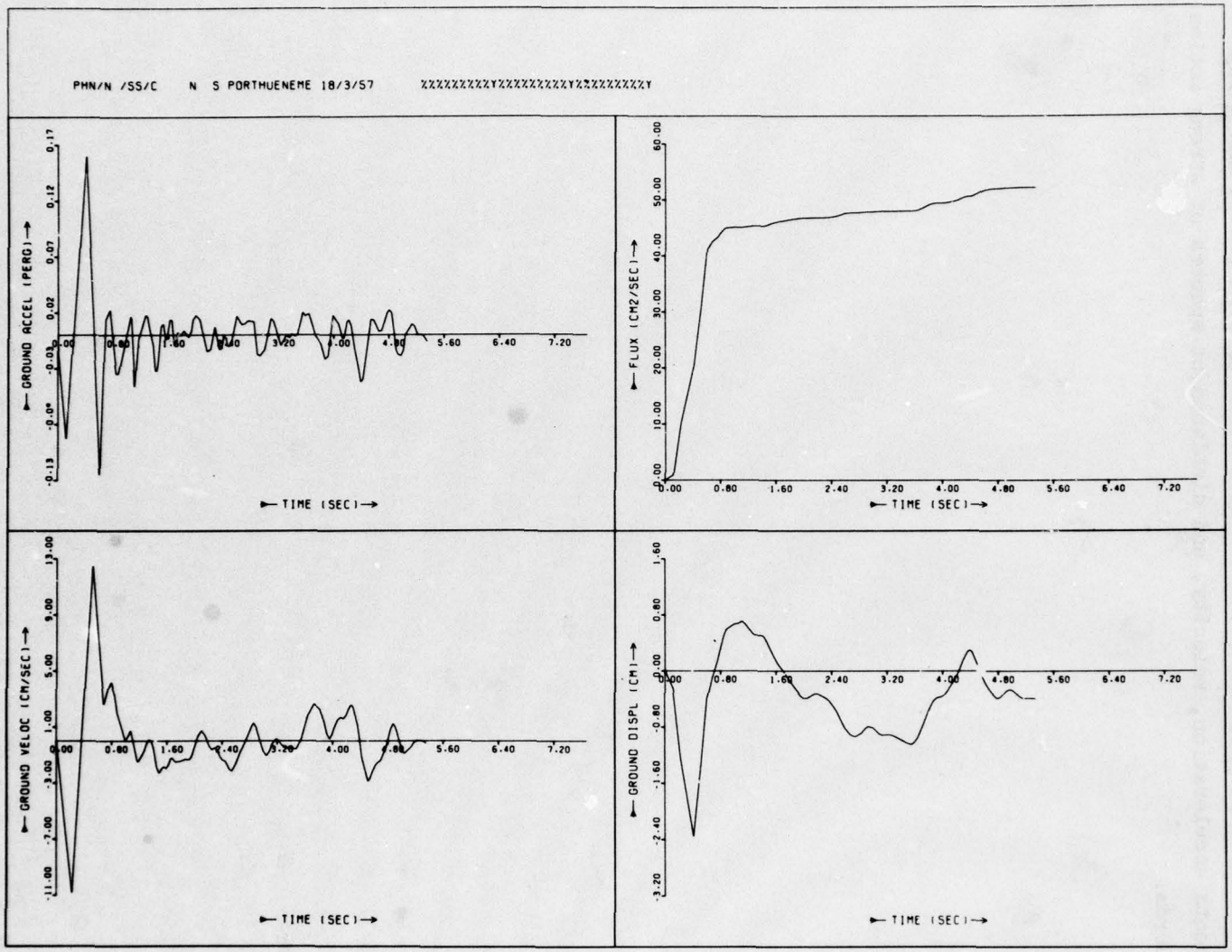
PHN/N /SS/C N S PORTHUENEME 18/3/57 XXXXXXXXXYXXXXXXXXXYXXXXXXXXX
GROUND ACCEL (PERG)
TIME (SEC)
FLUX (CM2/SEC)
TIME (SEC)
GROUND VELOC (CM/SEC)
TIME (SEC)
GROUND DISPL (CM)
TIME (SEC)

Figure D1a

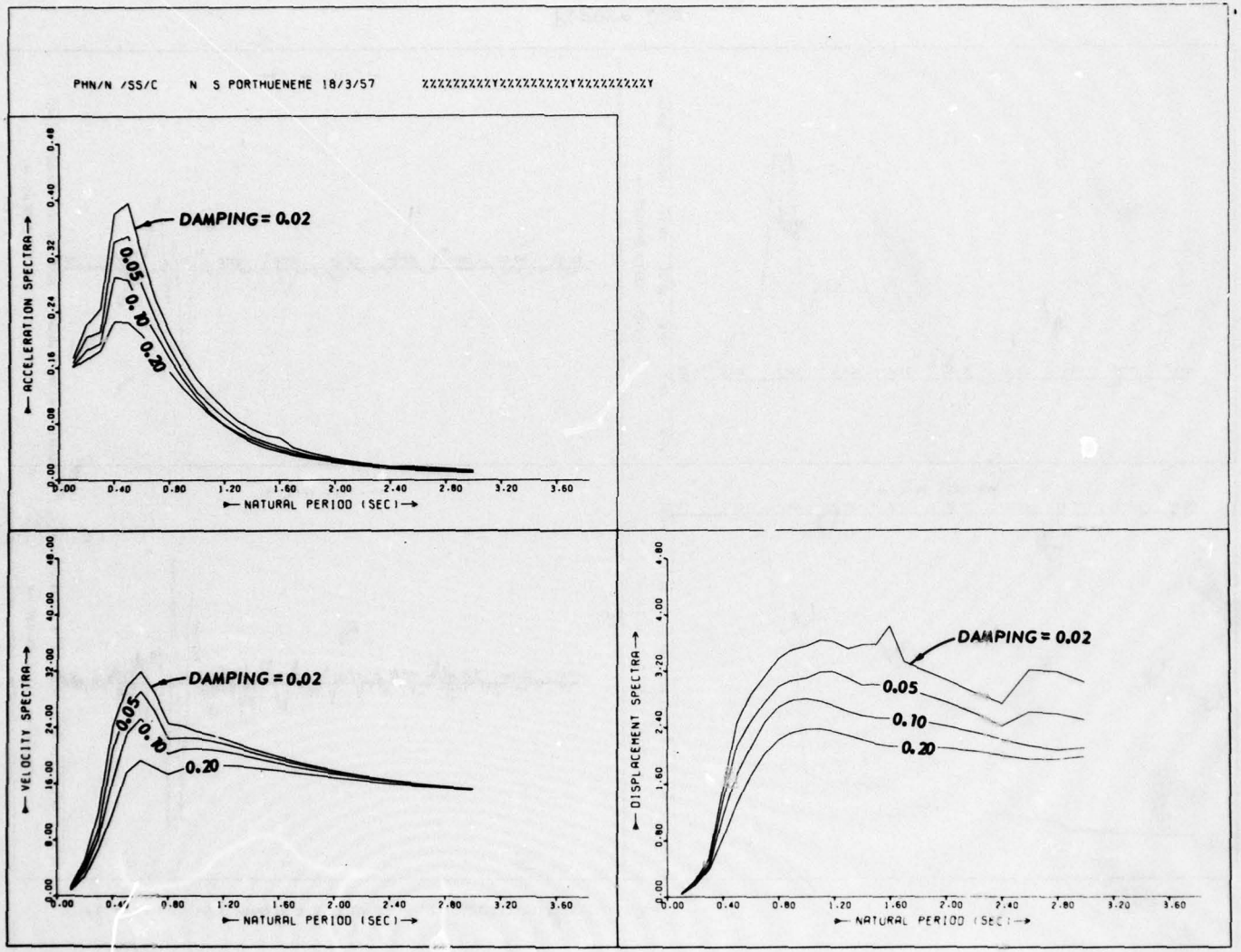
PHN/N /SS/C N S PORTHUENEME 18/3/57 XXXXXXXXXYXXXXXXXXXYXXXXXXXXX
ACCELERATION SPECTRA
DAMPING = 0.02
0.05
0.10
0.20
NATURAL PERIOD (SEC)
VELOCITY SPECTRA
DAMPING = 0.02
0.05
0.10
0.20
NATURAL PERIOD (SEC)
DISPLACEMENT SPECTRA
DAMPING = 0.02
0.05
0.10
0.20
NATURAL PERIOD (SEC)

Figure D1b

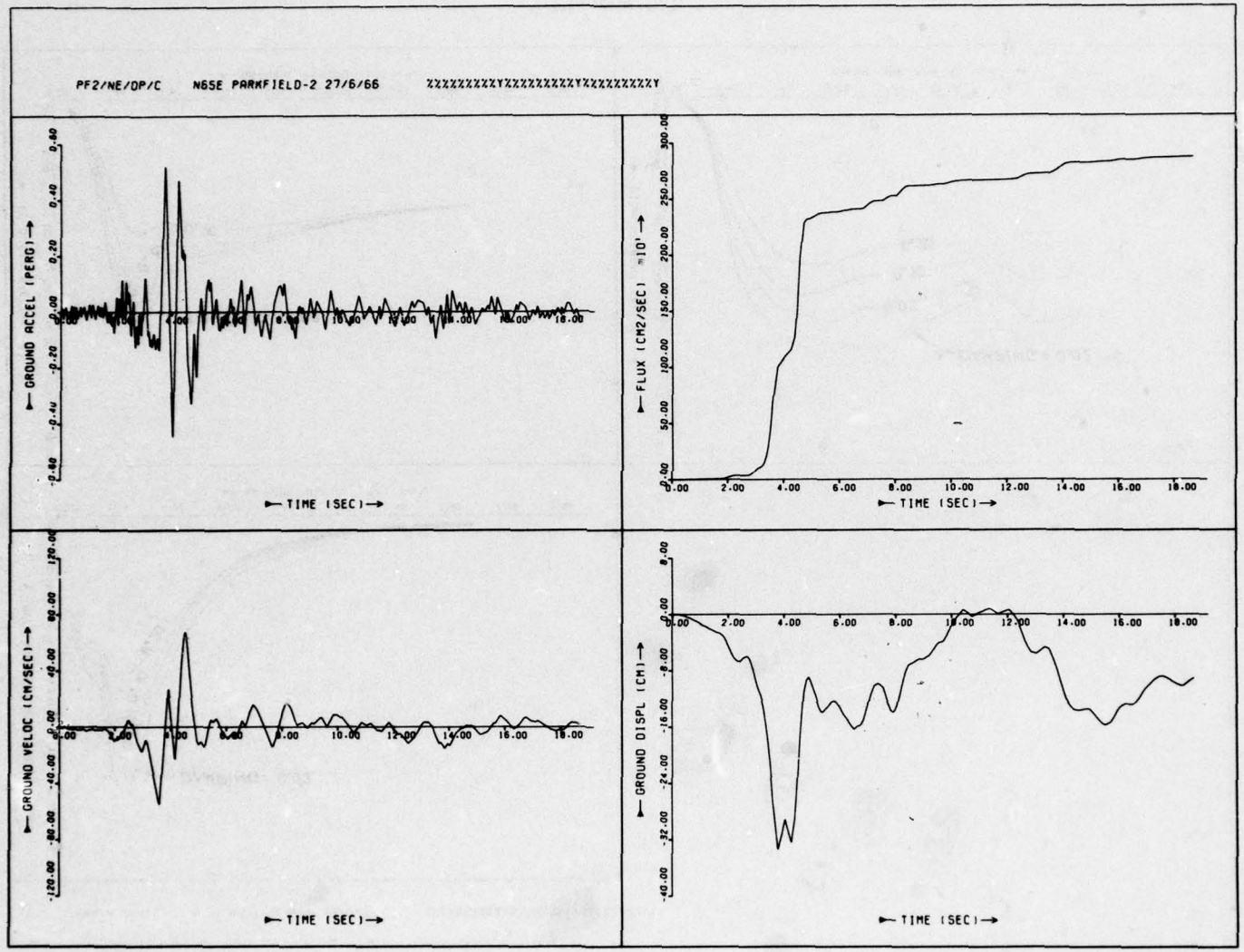
PF2/NE/OP/C N65E PARKFIELD-2 27/6/66
GROUND ACCEL (PERG)
TIME (SEC)
FLUX (CM2/SEC) *10¹
TIME (SEC)
GROUND VELOC (CM/SEC)
TIME (SEC)
GROUND DISPL (CM)
TIME (SEC)

Figure D2a

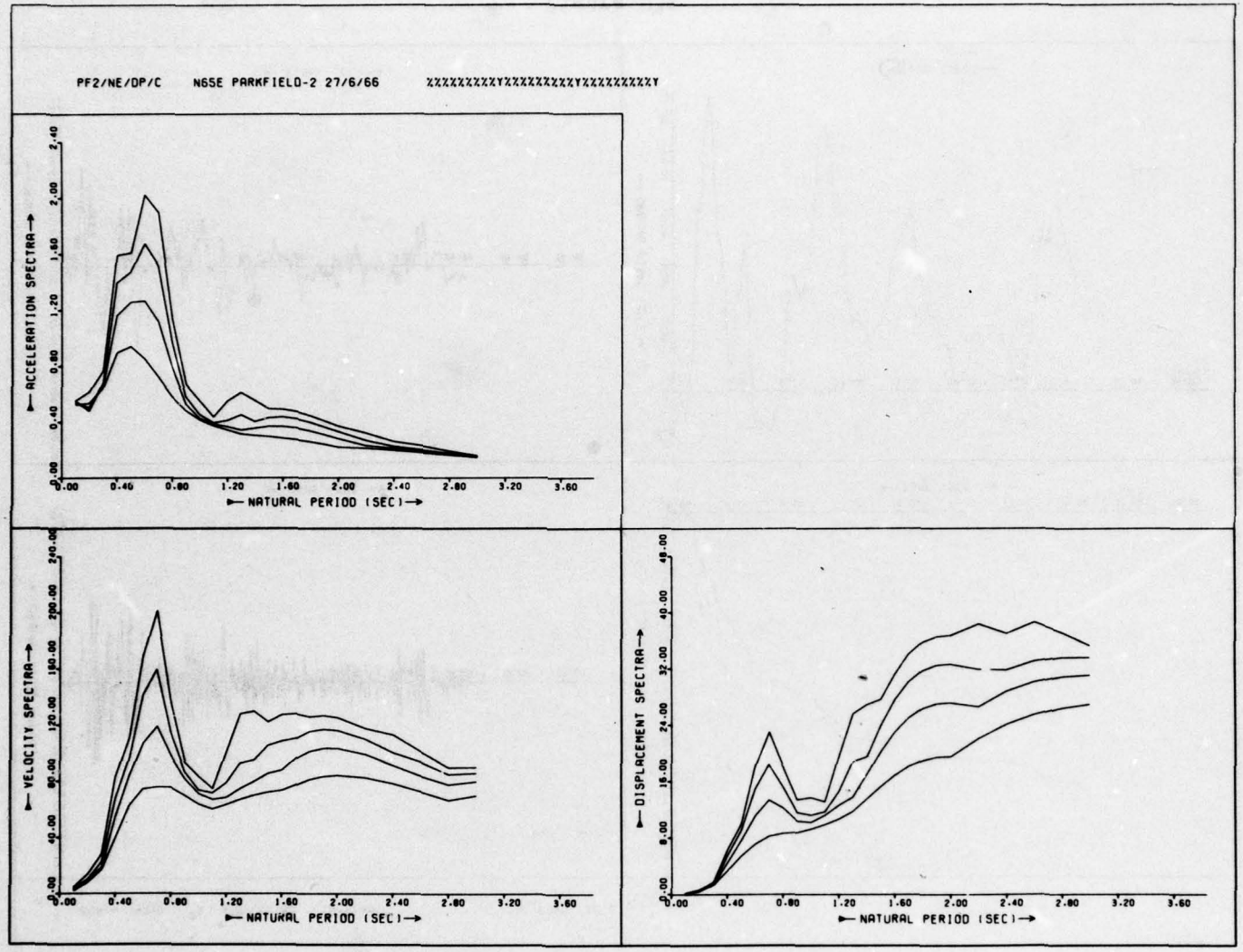
PF2/NE/DP/C N65E PARKFIELD-2 27/6/66 XXXXXXXXXYXXXXXXXXXYXXXXXXXXX
ACCELERATION SPECTRA
NATURAL PERIOD (SEC)
VELOCITY SPECTRA
NATURAL PERIOD (SEC)
DISPLACEMENT SPECTRA
NATURAL PERIOD (SEC)

Figure D2b

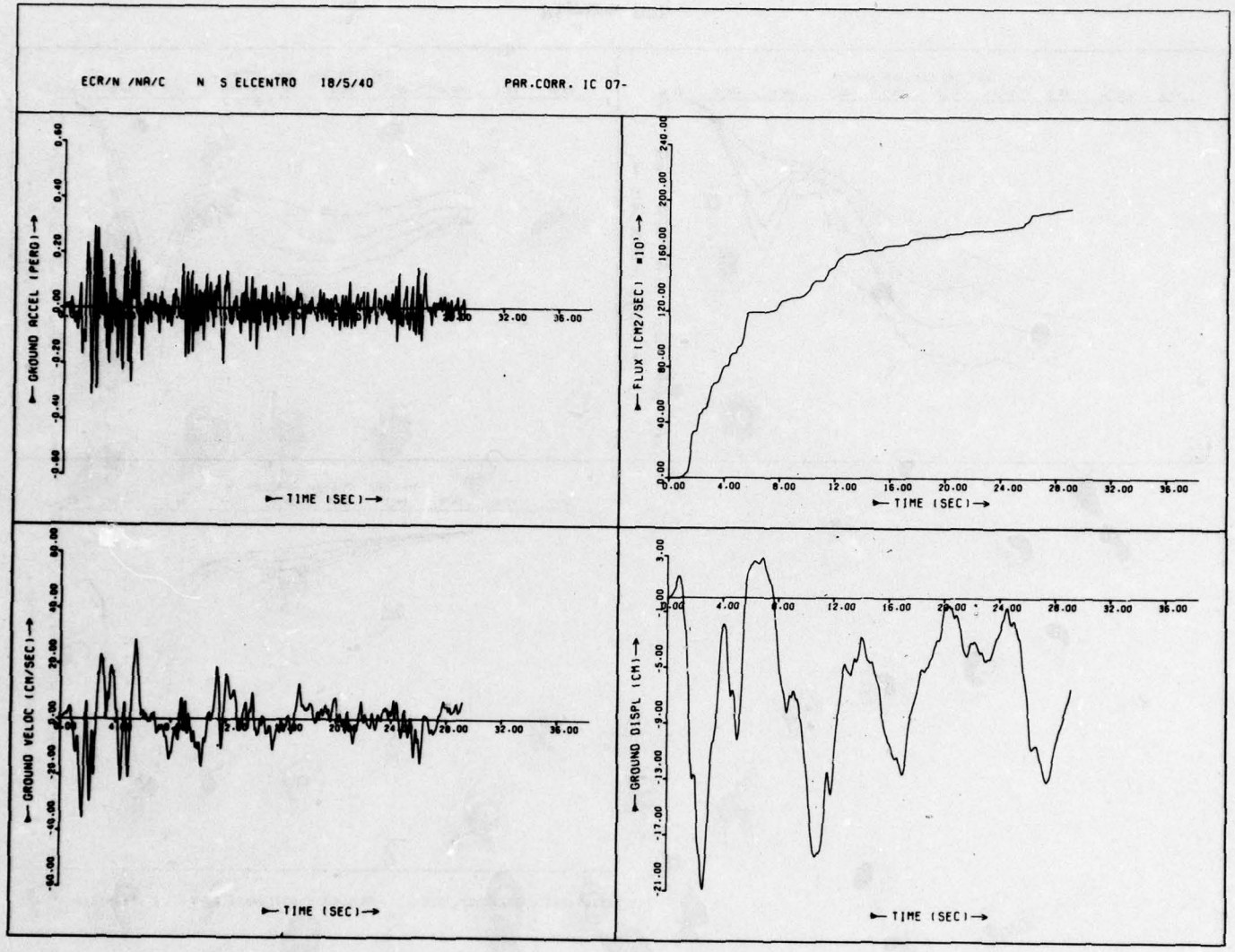
ECR/N /NA/C N S ELCENTRO 18/5/40 PAR.CORR. IC 07-
GROUND ACCEL (PERG)→
TIME (SEC)→
FLUX (CM2/SEC) *10'→
TIME (SEC)→
GROUND VELOC (CM/SEC)→
TIME (SEC)→
GROUND DISPL (CM)→
TIME (SEC)→

Figure D3a

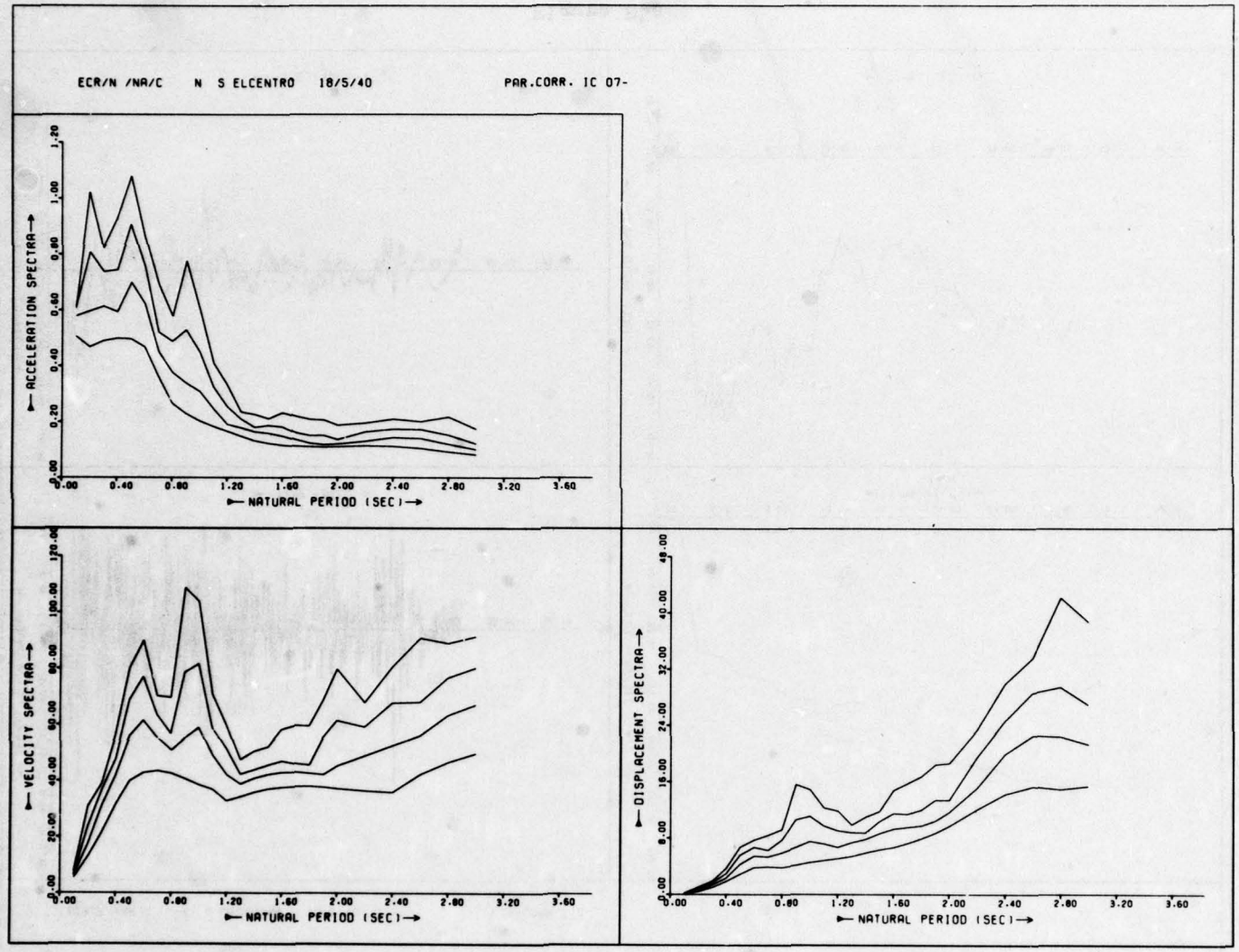
ECR/N /NA/C N S ELCENTRO 18/5/40 PAR.CORR. IC 07-
ACCELERATION SPECTRA
VELOCITY SPECTRA
DISPLACEMENT SPECTRA
NATURAL PERIOD (SEC)
0.00
0.40
0.80
1.20
1.60
2.00
2.40
2.80
3.20
3.60

Figure D3b

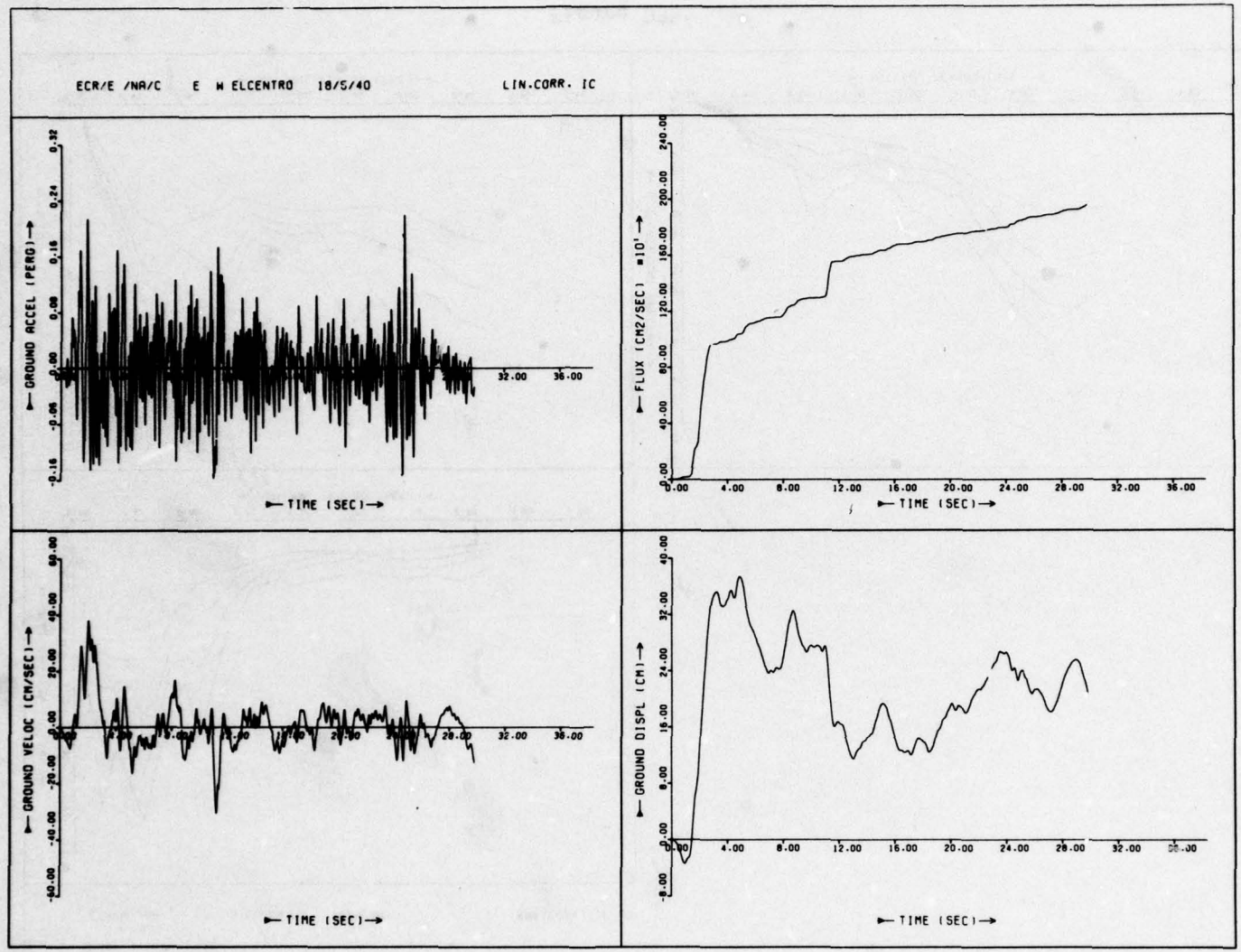
ECR/E /NA/C E W ELCENTRO 18/5/40 LIN.CORR. IC
GROUND ACCEL (PERG)
TIME (SEC)
FLUX (CM2/SEC) *10'
TIME (SEC)
GROUND VELOC (CM/SEC)
TIME (SEC)
GROUND DISPL (CM)
TIME (SEC)

Figure D4a

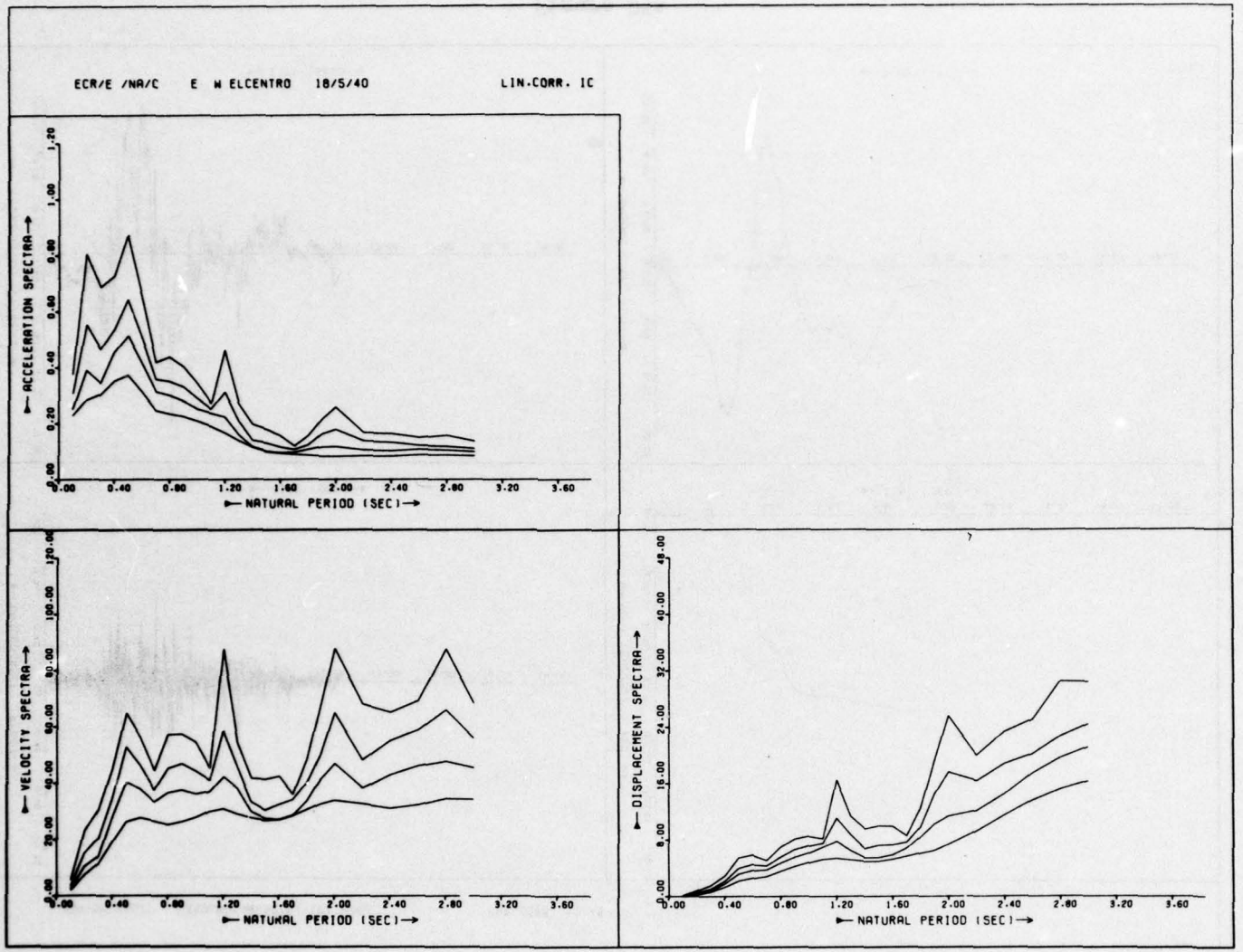
ECR/E /NA/C E W ELCENTRO 18/5/40 LIN.CORR. IC
ACCELERATION SPECTRA
NATURAL PERIOD (SEC)
VELOCITY SPECTRA
NATURAL PERIOD (SEC)
DISPLACEMENT SPECTRA
NATURAL PERIOD (SEC)

Figure D4b

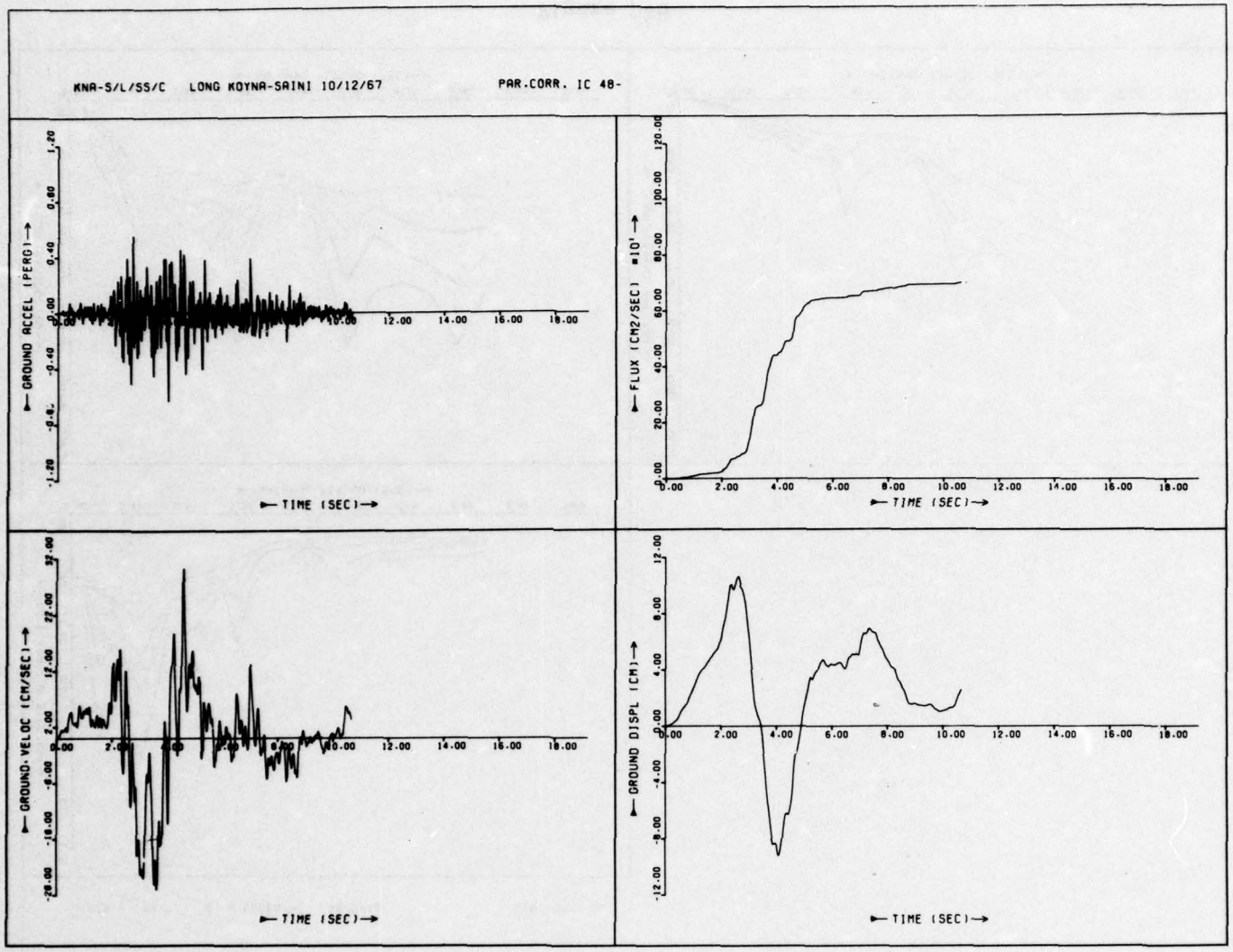
KNA-S/L/SS/C LONG KOYNA-SAINI 10/12/67 PAR.CORR. IC 48-
GROUND ACCEL (PERG)
TIME (SEC)
FLUX (CM2/SEC) *10'
TIME (SEC)
GROUND VELOC (CM/SEC)
TIME (SEC)
GROUND DISPL (CM)
TIME (SEC)

Figure D5a

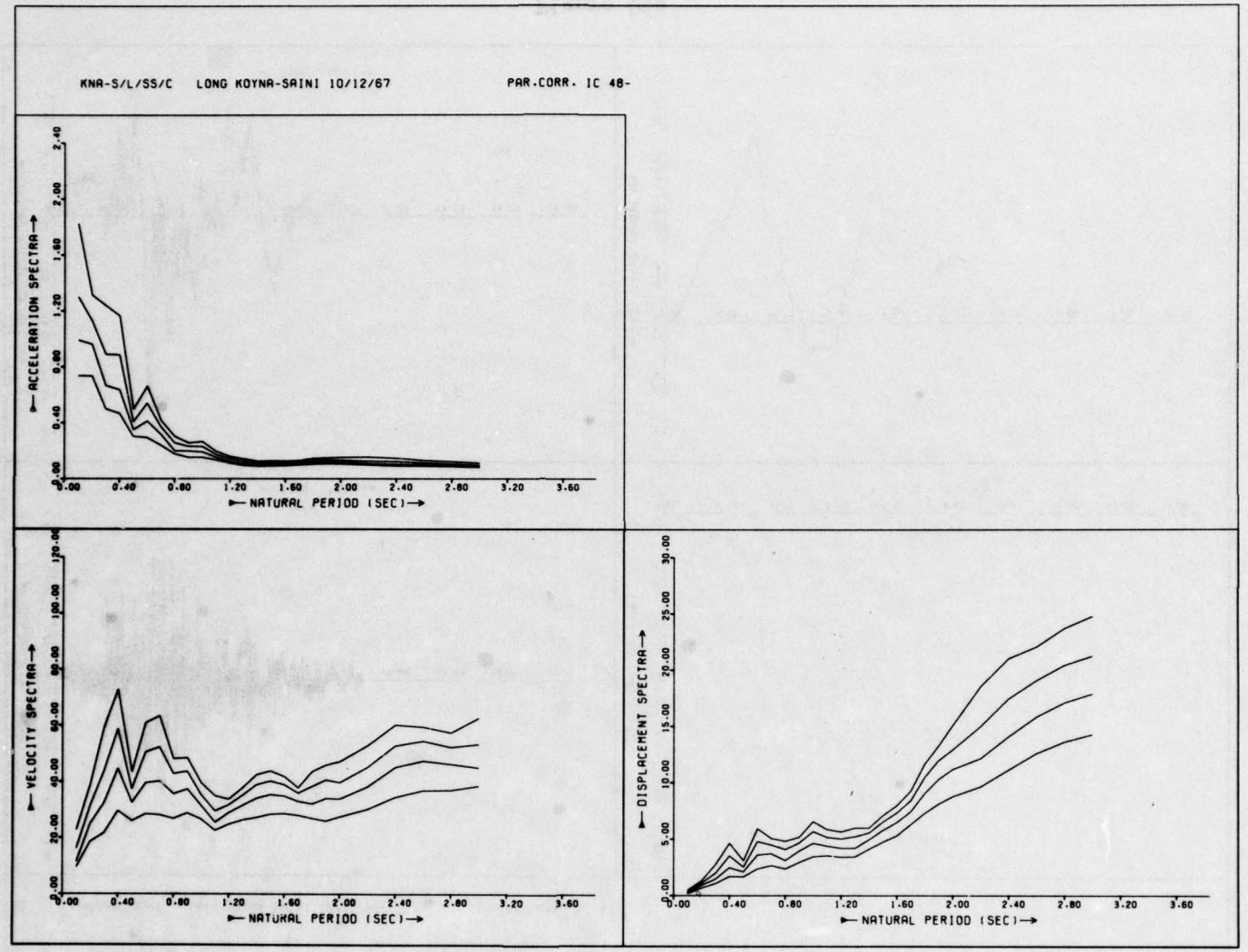
KNA-S/L/SS/C LONG KOYNA-SAINI 10/12/67
PAR.CORR. IC 48-
ACCELERATION SPECTRA
NATURAL PERIOD (SEC)
VELOCITY SPECTRA
NATURAL PERIOD (SEC)
DISPLACEMENT SPECTRA
NATURAL PERIOD (SEC)

Figure D5b

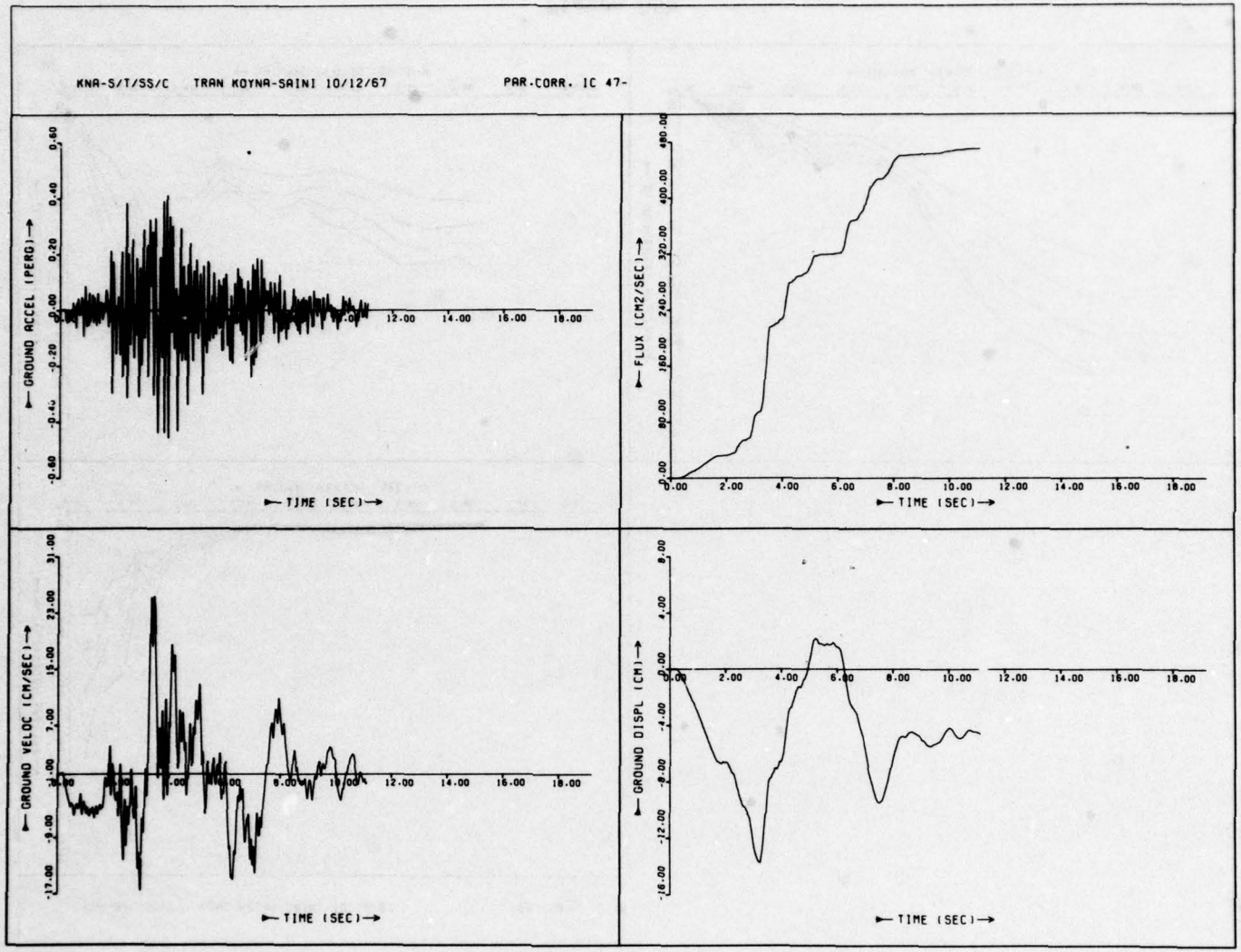
KNA-S/T/SS/C TRAN KOYNA-SAINI 10/12/67 PAR.CORR. IC 47-
GROUND ACCEL (PERG)
TIME (SEC)
FLUX (CM2/SEC)
TIME (SEC)
GROUND VELOC (CM/SEC)
TIME (SEC)
GROUND DISPL (CM)
TIME (SEC)

Figure D6a

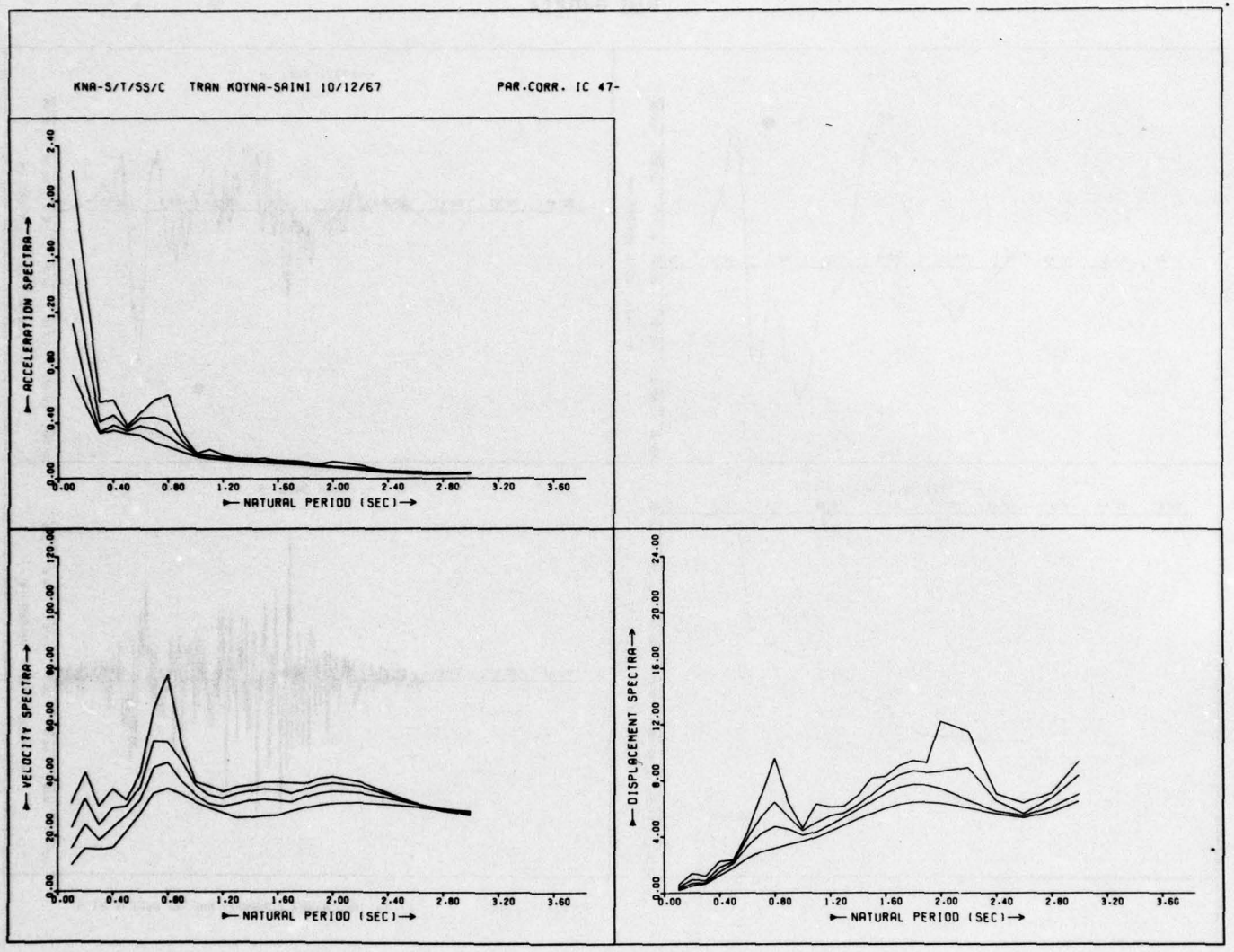
KNA-S/T/SS/C TRAN KOYNA-SAINI 10/12/67 PAR.CORR. IC 47-
ACCELERATION SPECTRA
NATURAL PERIOD (SEC)
VELOCITY SPECTRA
NATURAL PERIOD (SEC)
DISPLACEMENT SPECTRA
NATURAL PERIOD (SEC)

Figure D6b

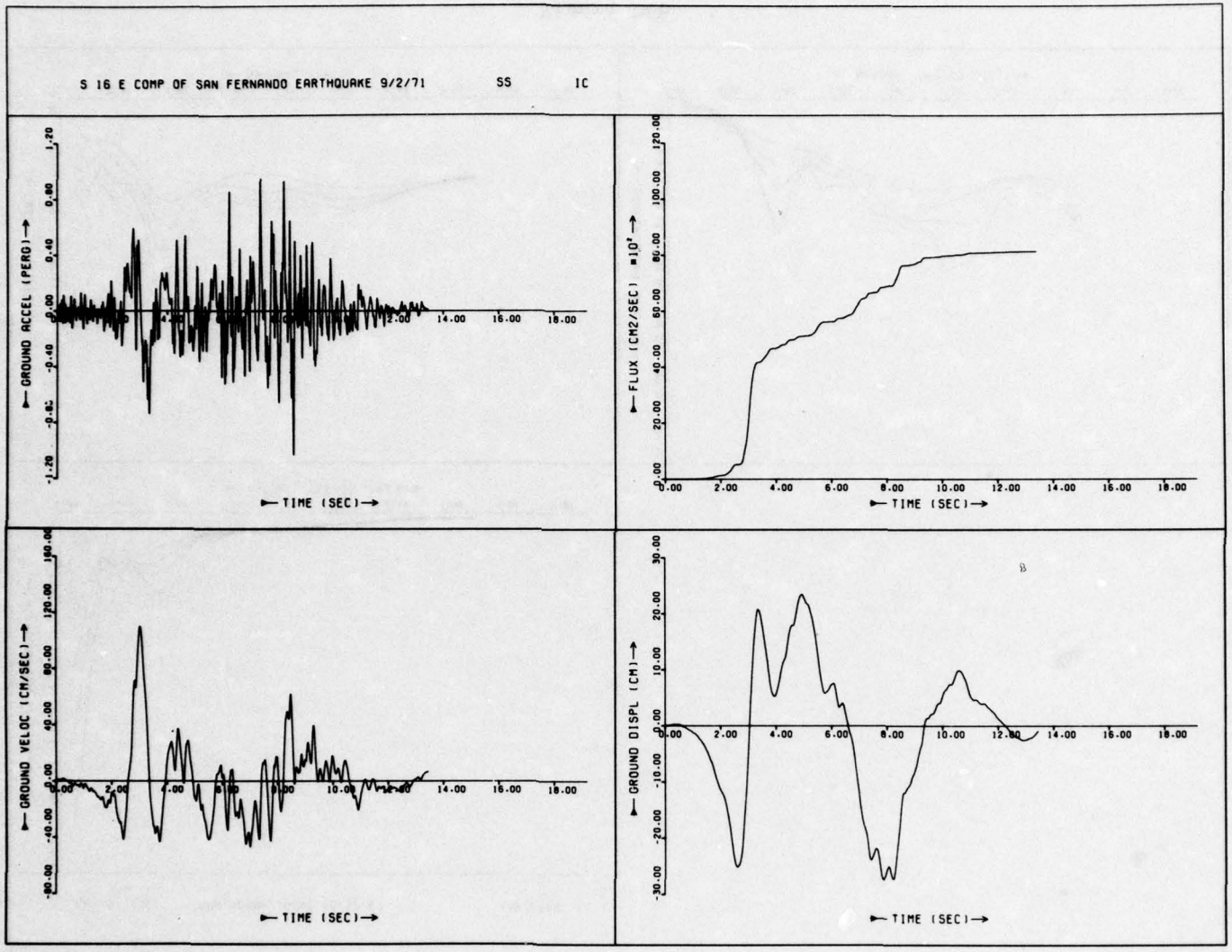
S 16 E COMP OF SAN FERNANDO EARTHQUAKE 9/2/71 SS IC
GROUND ACCEL (PERD)
TIME (SEC)
FLUX (CM2/SEC) *10⁴
TIME (SEC)
GROUND VELOC (CM/SEC)
TIME (SEC)
GROUND DISPL (CM)
TIME (SEC)

Figure D7a

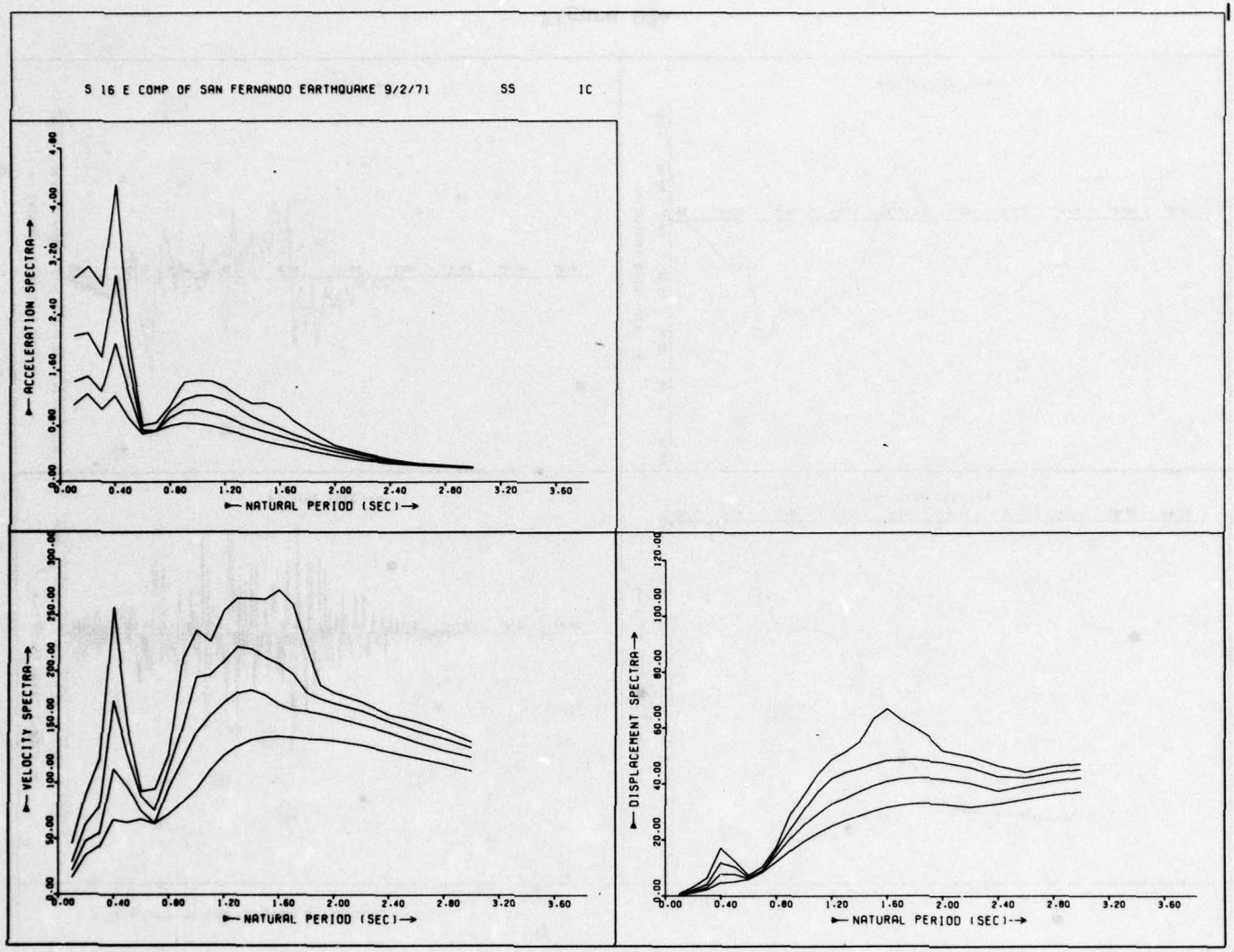
S 16 E COMP OF SAN FERNANDO EARTHQUAKE 9/2/71 SS IC
ACCELERATION SPECTRA
NATURAL PERIOD (SEC)
VELOCITY SPECTRA
NATURAL PERIOD (SEC)
DISPLACEMENT SPECTRA
NATURAL PERIOD (SEC)

Figure D7b

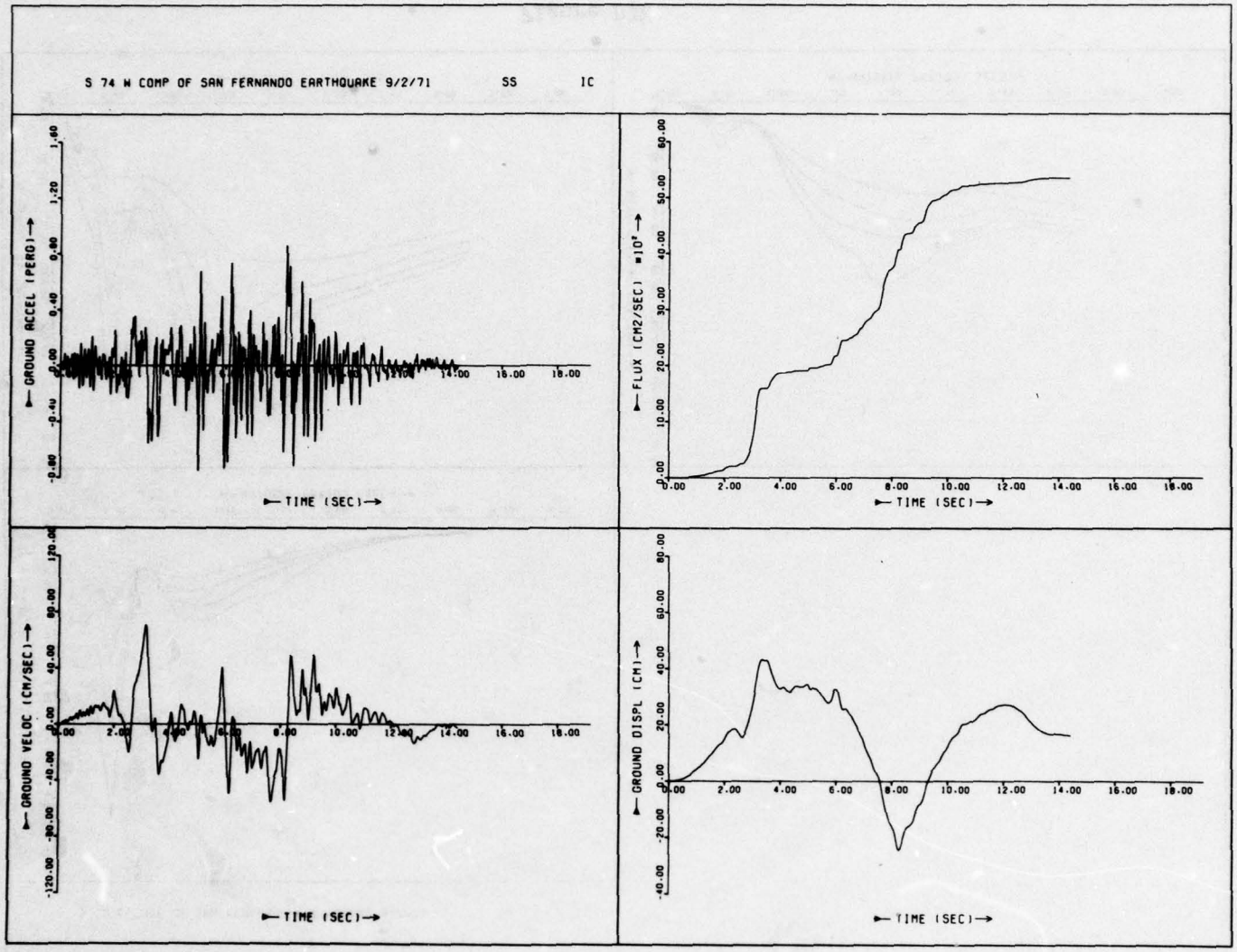
S 74 W COMP OF SAN FERNANDO EARTHQUAKE 9/2/71 SS IC
GROUND ACCEL (PERO)
TIME (SEC)
FLUX (CM2/SEC) *10**7
TIME (SEC)
GROUND VELOC (CM/SEC)
TIME (SEC)
GROUND DISPL (CM)
TIME (SEC)

Figure D8a

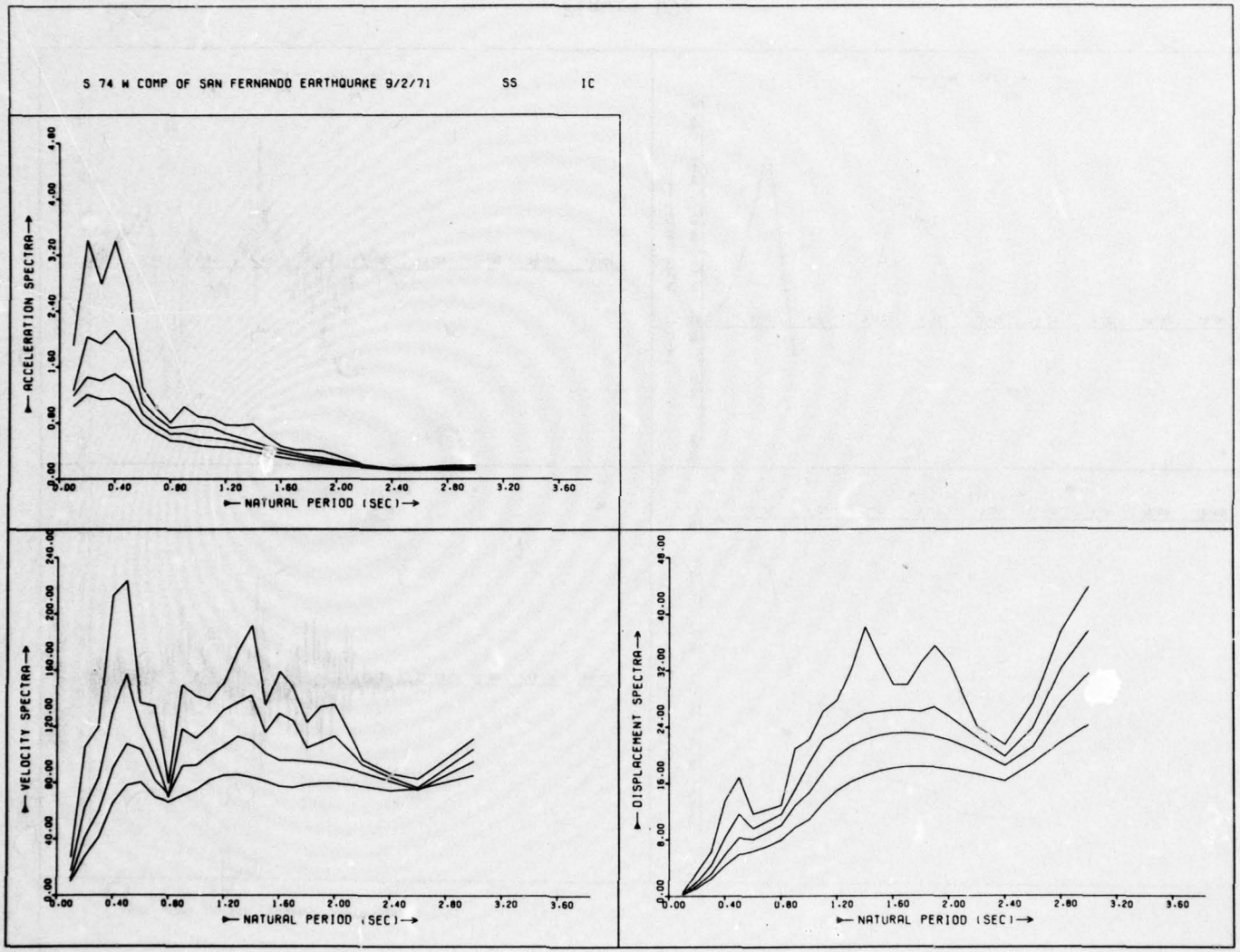
S 74 W COMP OF SAN FERNANDO EARTHQUAKE 9/2/71 SS IC
ACCELERATION SPECTRA
VELOCITY SPECTRA
DISPLACEMENT SPECTRA
NATURAL PERIOD (SEC)
0.00
0.40
0.80
1.20
1.60
2.00
2.40
2.80
3.20
3.60

Figure D8b

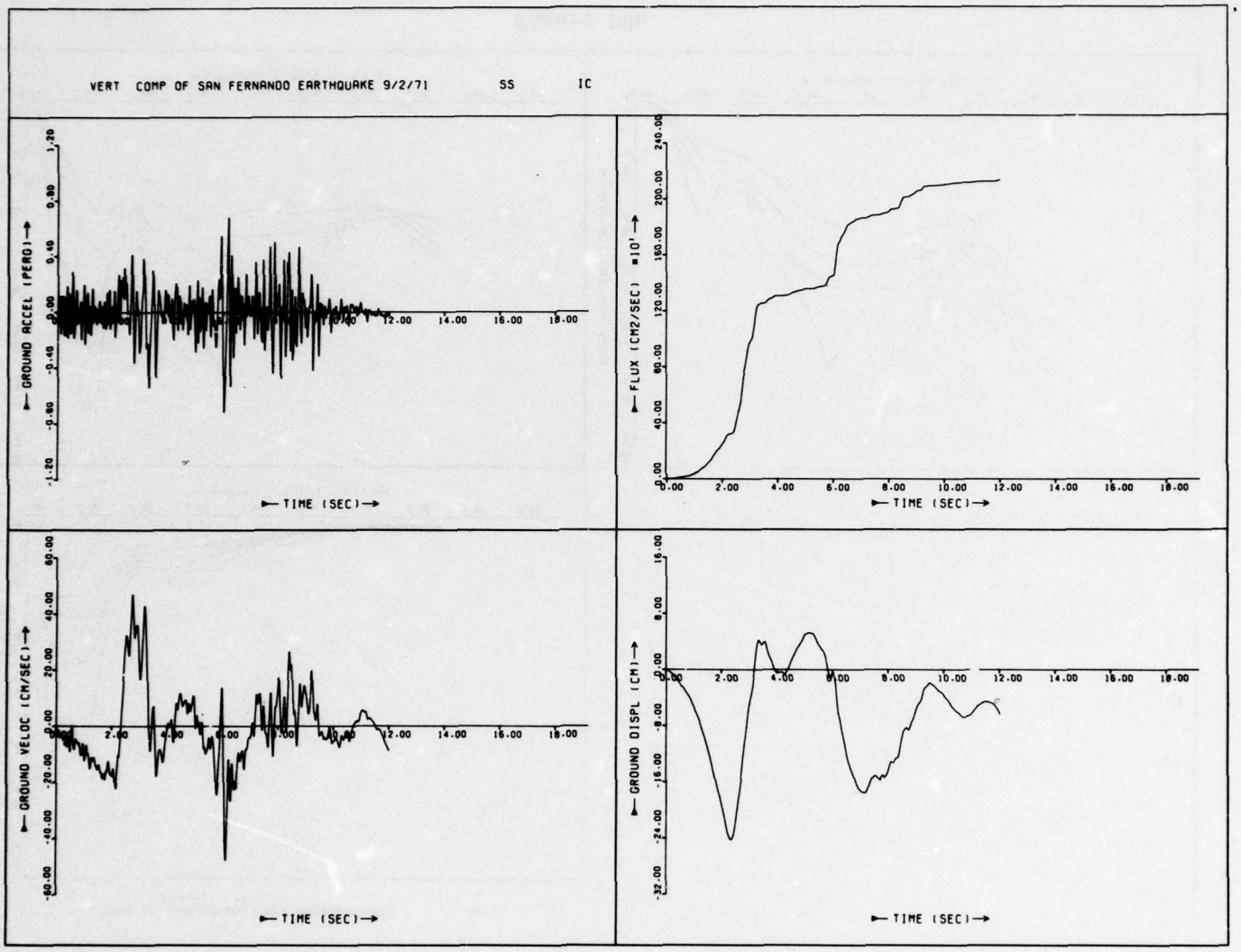
VERT COMP OF SAN FERNANDO EARTHQUAKE 9/2/71 SS IC
GROUND ACCEL (PERG)
TIME (SEC)
FLUX (CM2/SEC) =10'
TIME (SEC)
GROUND VELOC (CM/SEC)
TIME (SEC)
GROUND DISPL (CM)
TIME (SEC)

Figure D9a

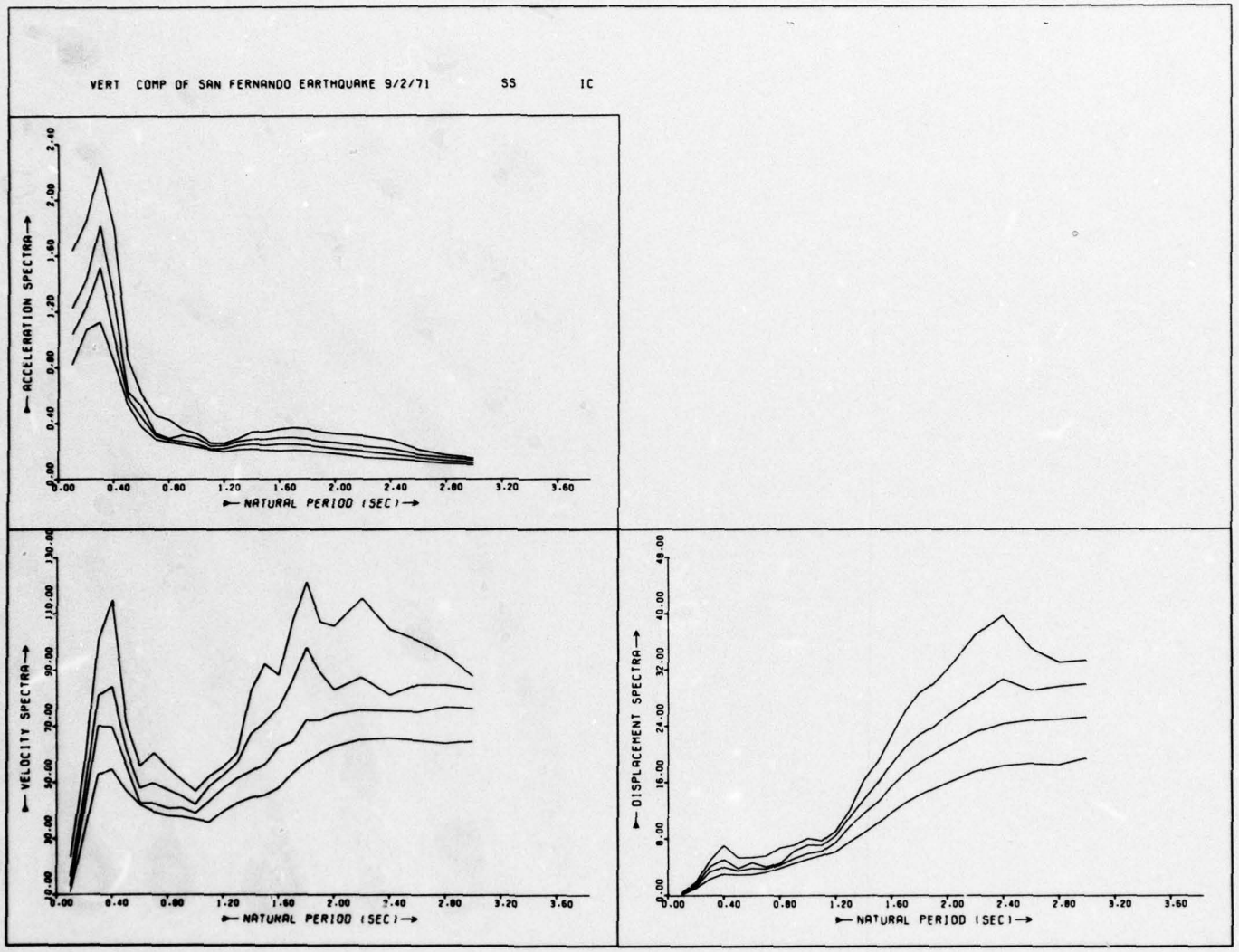
VERT COMP OF SAN FERNANDO EARTHQUAKE 9/2/71 SS IC
ACCELERATION SPECTRA
NATURAL PERIOD (SEC)
VELOCITY SPECTRA
NATURAL PERIOD (SEC)
DISPLACEMENT SPECTRA
NATURAL PERIOD (SEC)

Figure D9b

APPENDIX E:

SEISMIC COEFFICIENTS AND POINT ACCELERATION SPECTRA

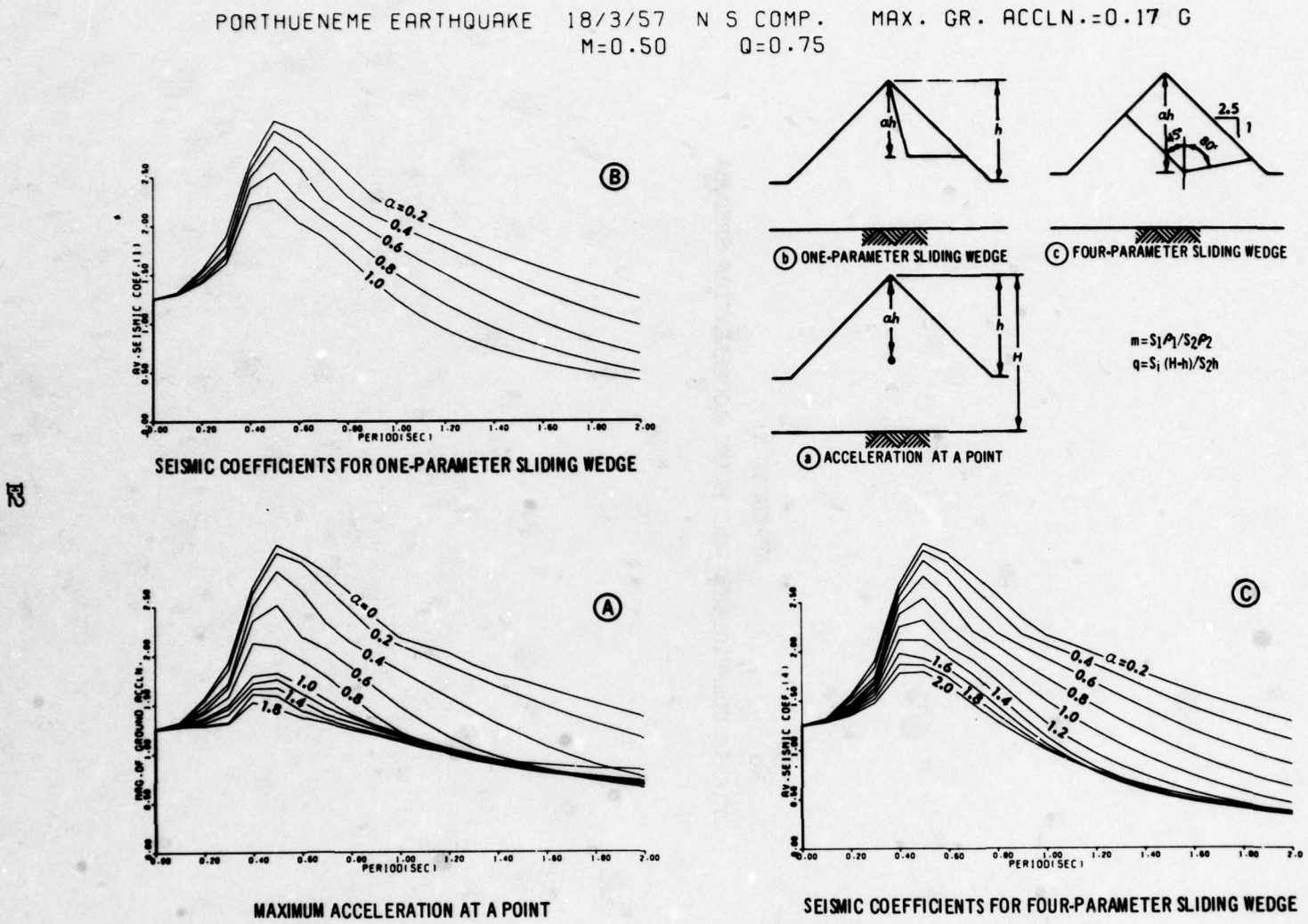

Figure E1. Explanations for Figures E2 through E127

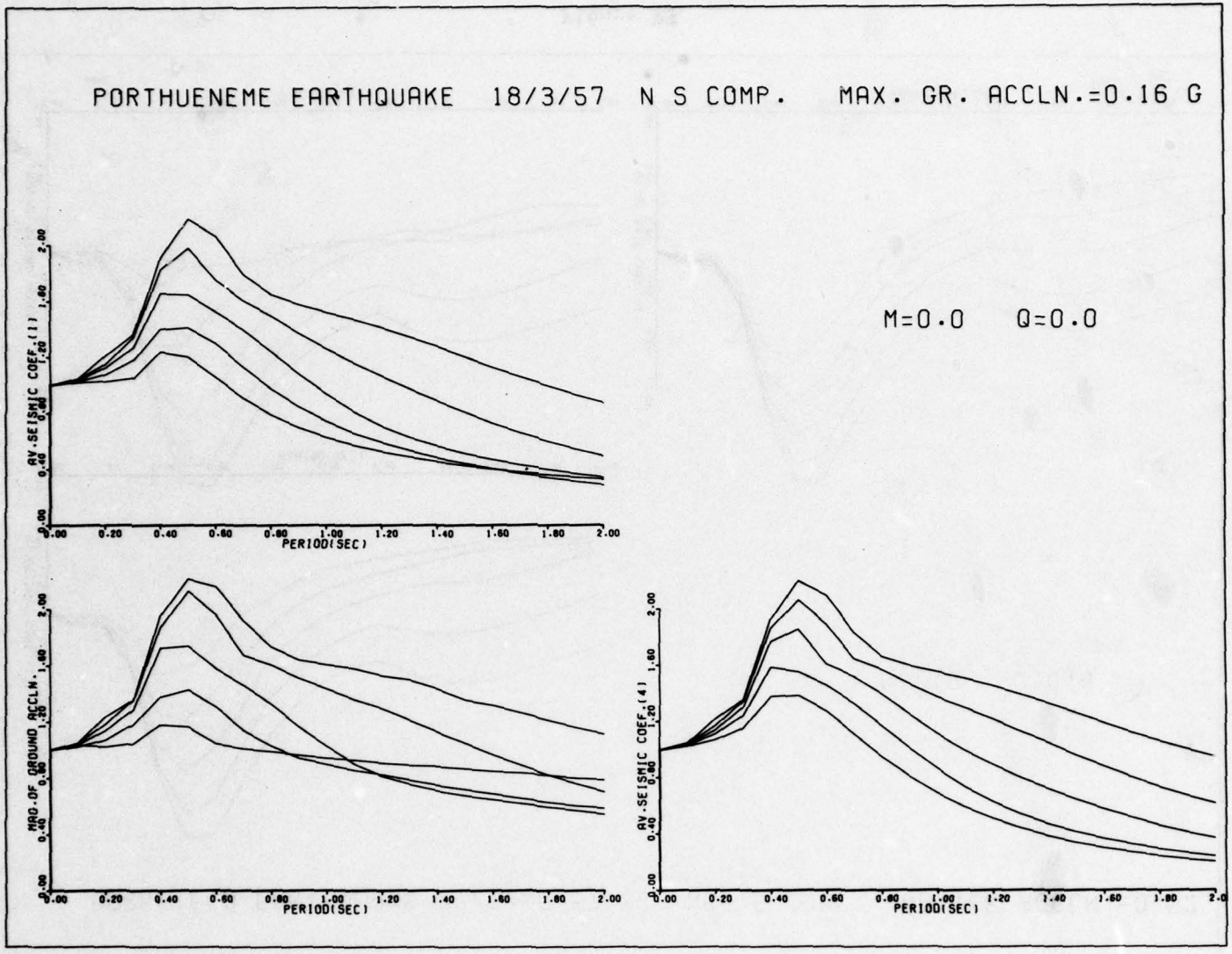
PORTHUENEME EARTHQUAKE 18/3/57 N S COMP. MAX. GR. ACCLN.=0.16 G
M=0.0 Q=0.0
AV.SEISMIC COEF.(1)
PERIOD(SEC)
MAG.OF GROUND ACCLN.
PERIOD(SEC)
AV.SEISMIC COEF.(4)
PERIOD(SEC)

Figure E2

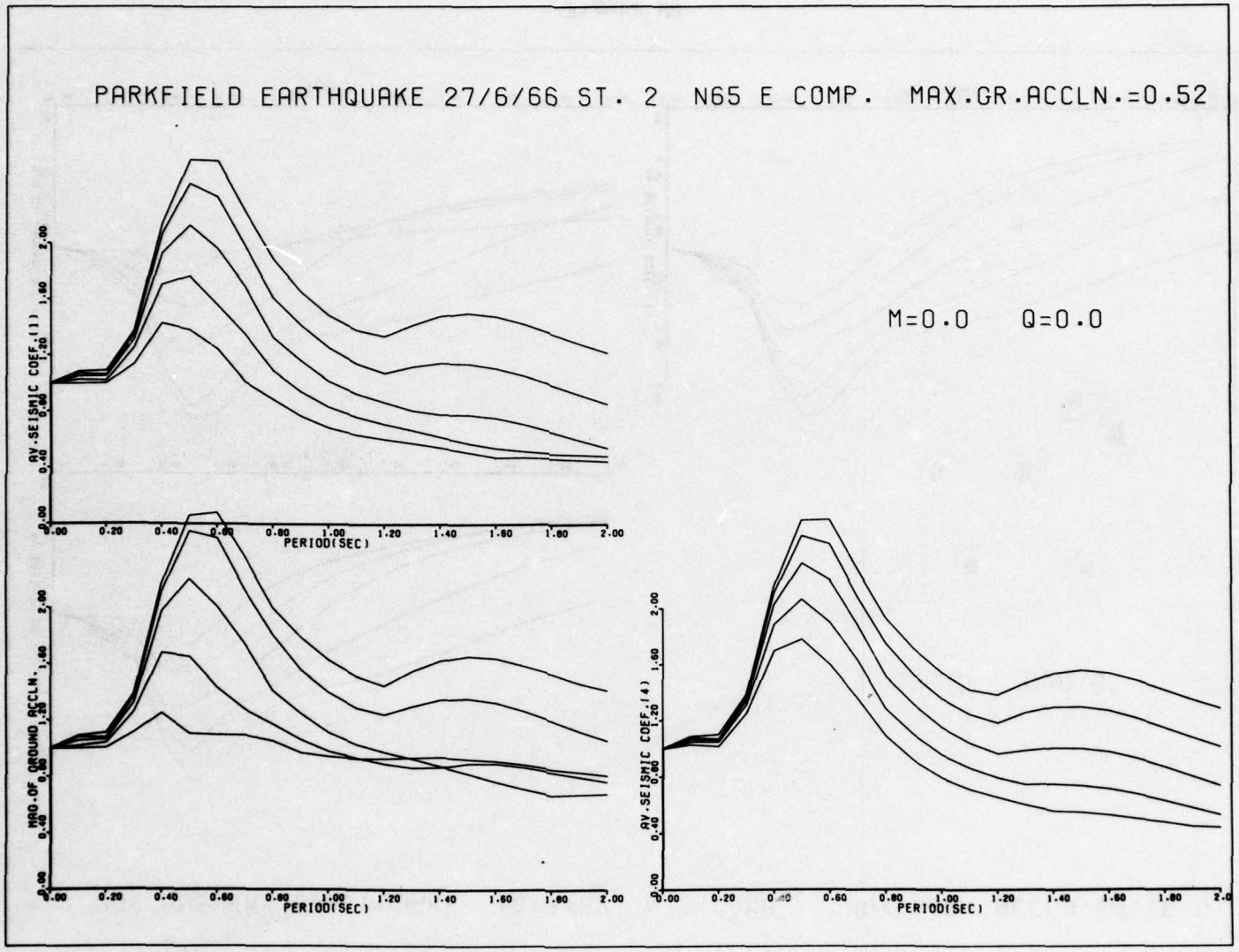
PARKFIELD EARTHQUAKE 27/6/66 ST. 2 N65 E COMP. MAX.GR.ACCLN.=0.52
M=0.0 Q=0.0
AV.SEISMIC COEF.(1)
MAG.OF GROUND ACCLN.
AV.SEISMIC COEF.(4)
PERIOD(SEC)
0.00
0.20
0.40
0.60
0.80
1.00
1.20
1.40
1.60
1.80
2.00

Figure E3

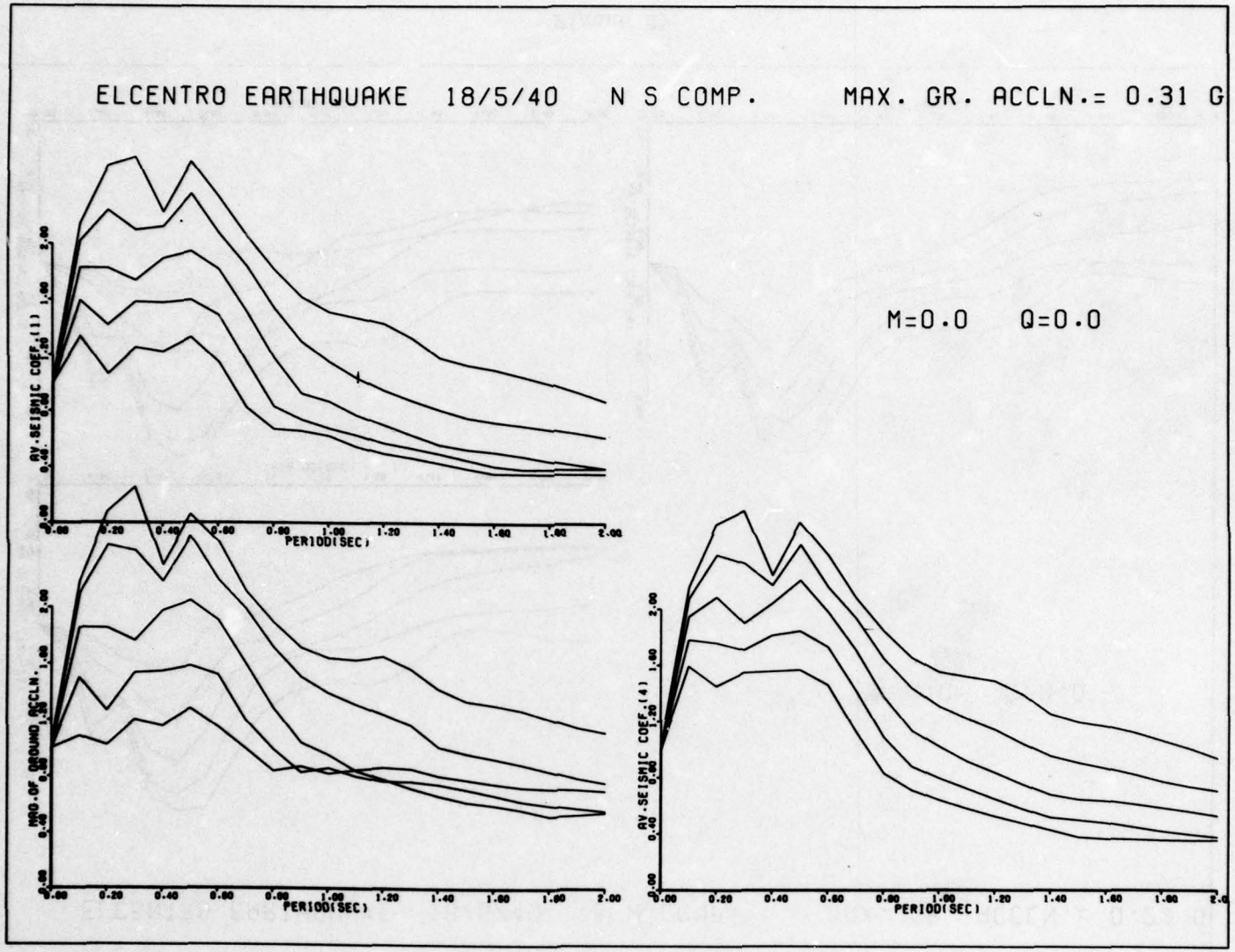
ELCENTRO EARTHQUAKE 18/5/40 N S COMP.
MAX. GR. ACCLN.= 0.31 G
M=0.0 Q=0.0
AV.SEISMIC COEF.(1)
PERIOD(SEC)
MAX.OF GROUND ACCLN.
PERIOD(SEC)
AV.SEISMIC COEF.(4)
PERIOD(SEC)

Figure E4

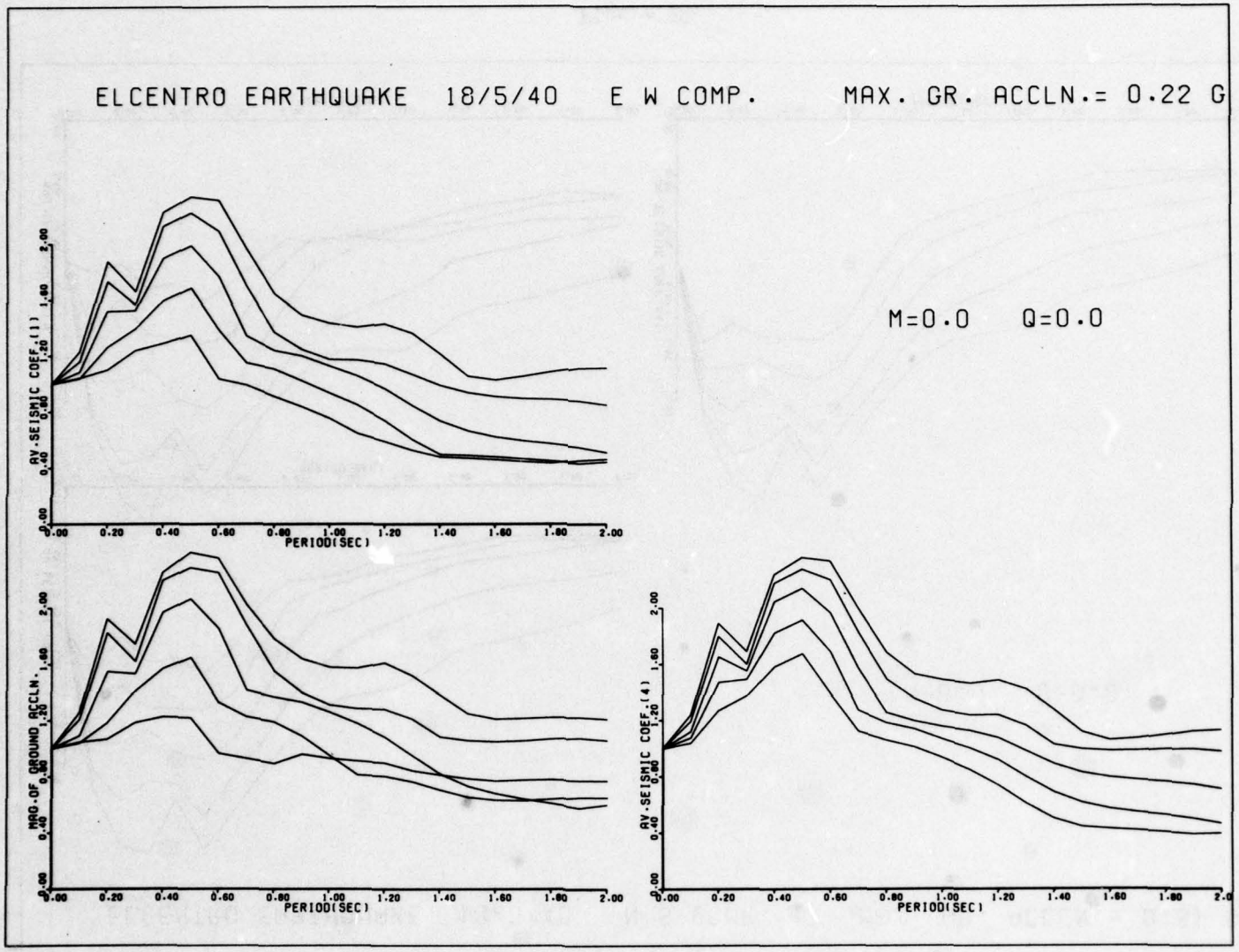
ELCENTRO EARTHQUAKE 18/5/40 E W COMP.
MAX. GR. ACCLN.= 0.22 G
M=0.0 Q=0.0
AV.SEISMIC COEF.(1)
PERIOD(SEC)
NRO.OF GROUND ACCLN.
PERIOD(SEC)
AV.SEISMIC COEF.(4)
PERIOD(SEC)

Figure E5

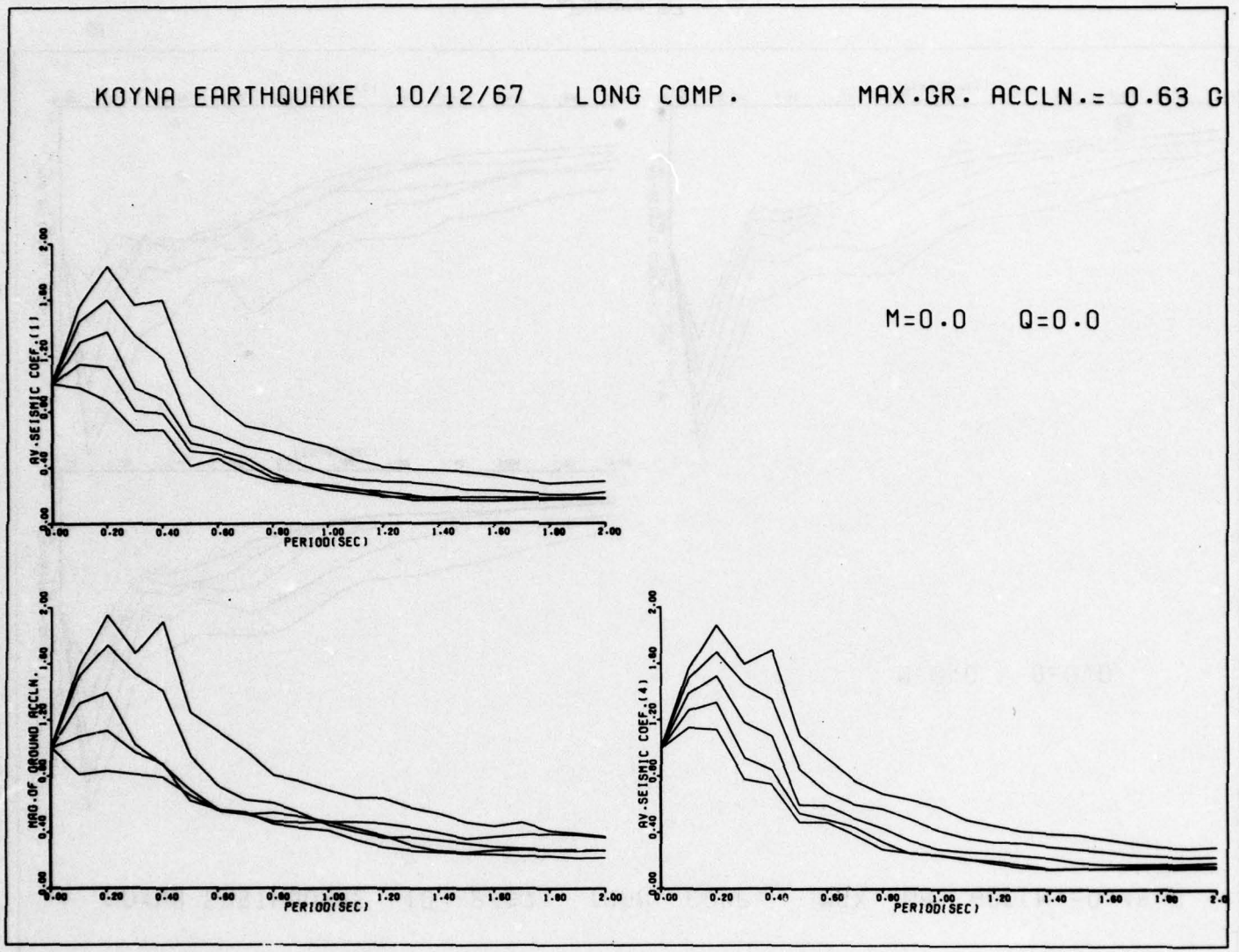
KOYNA EARTHQUAKE 10/12/67 LONG COMP.
MAX.GR. ACCLN.= 0.63 G
M=0.0 Q=0.0
AV.SEISMIC COEF.(1)
PERIOD(SEC)
NRO.OF GROUND ACCLN.
PERIOD(SEC)
AV.SEISMIC COEF.(4)
PERIOD(SEC)

Figure E6

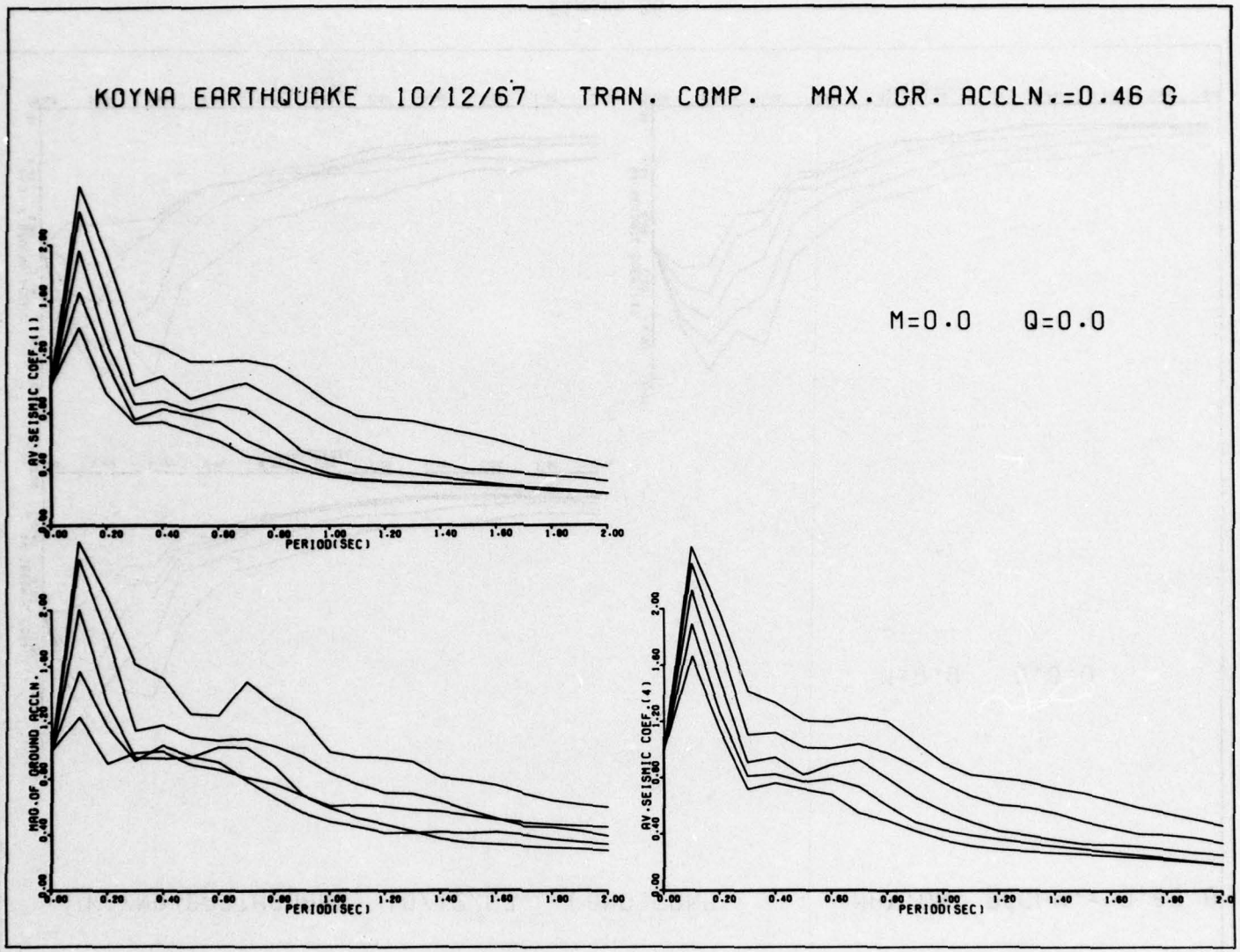
KOYNA EARTHQUAKE 10/12/67 TRAN. COMP. MAX. GR. ACCLN.=0.46 G
M=0.0 Q=0.0
AV.SEISMIC COEF.(1)
MAG.OF GROUND ACCLN.
AV.SEISMIC COEF.(4)
PERIOD(SEC)
PERIOD(SEC)
PERIOD(SEC)

Figure E7

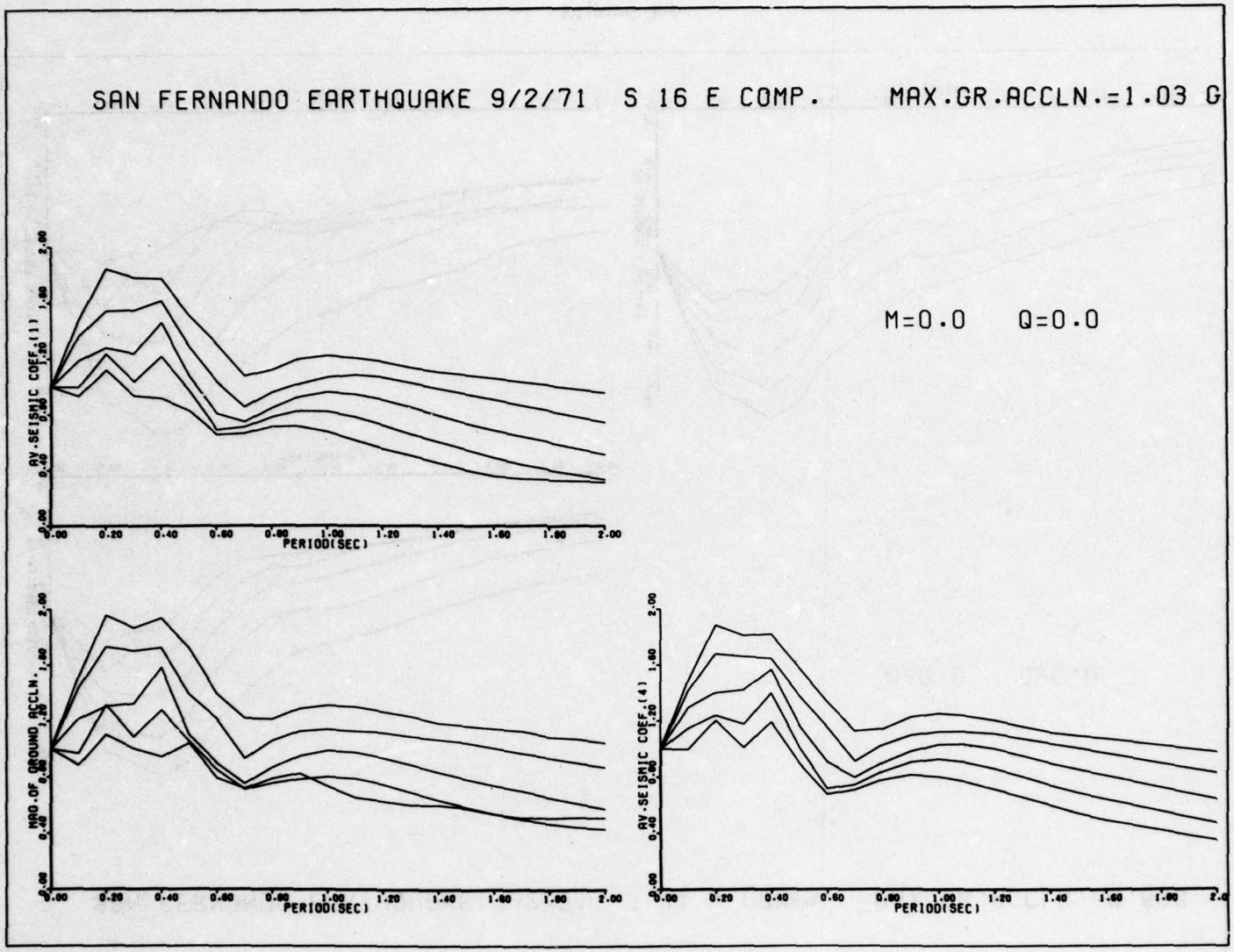
SAN FERNANDO EARTHQUAKE 9/2/71 S 16 E COMP. MAX.GR.ACCLN.=1.03 G
M=0.0 Q=0.0
AV.SEISMIC COEF.(1)
PERIOD(SEC)
NAG.OF GROUND ACCLN.
PERIOD(SEC)
AV.SEISMIC COEF.(4)
PERIOD(SEC)

Figure E8

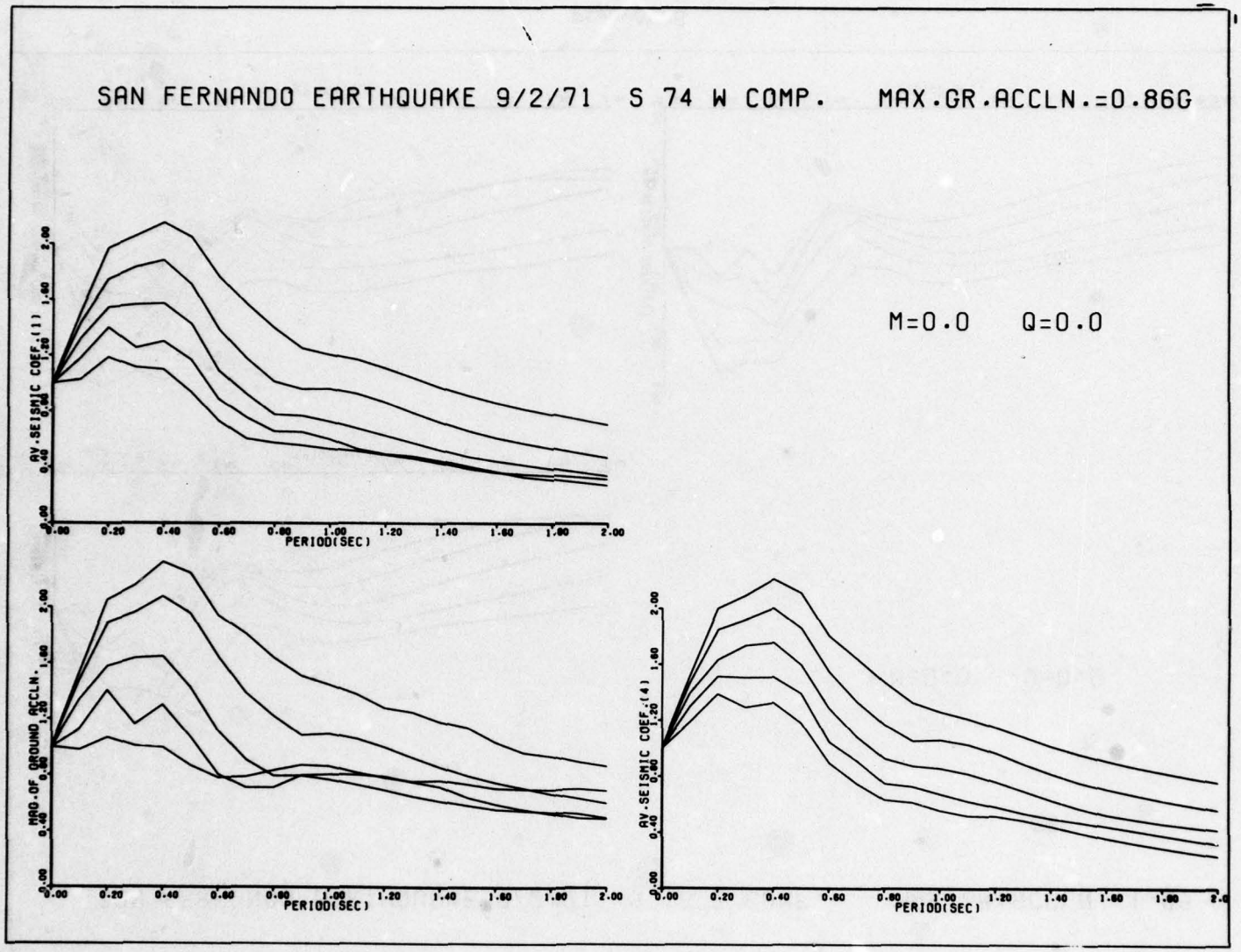
SAN FERNANDO EARTHQUAKE 9/2/71 S 74 W COMP. MAX.GR.ACCLN.=0.86G
M=0.0 Q=0.0
AV.SEISMIC COEF.(1)
PERIOD(SEC)
MAG.OF GROUND ACCLN.
PERIOD(SEC)
AV.SEISMIC COEF.(4)
PERIOD(SEC)

Figure E9

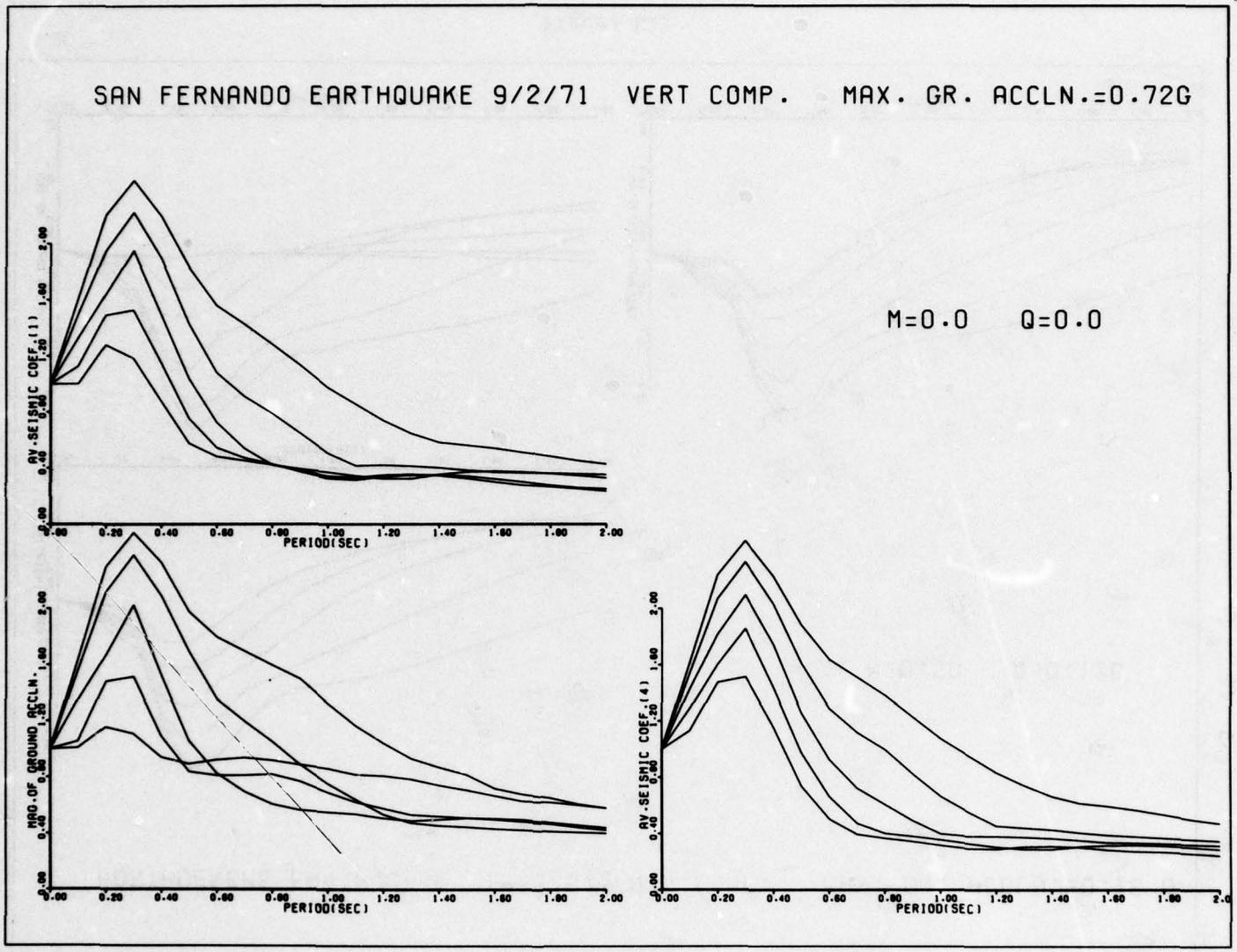
SAN FERNANDO EARTHQUAKE 9/2/71 VERT COMP. MAX. GR. ACCLN.=0.72G
M=0.0 Q=0.0
AV.SEISMIC COEF.(1)
MAG.OF GROUND ACCLN.
AV.SEISMIC COEF.(4)
PERIOD(SEC)

Figure E10

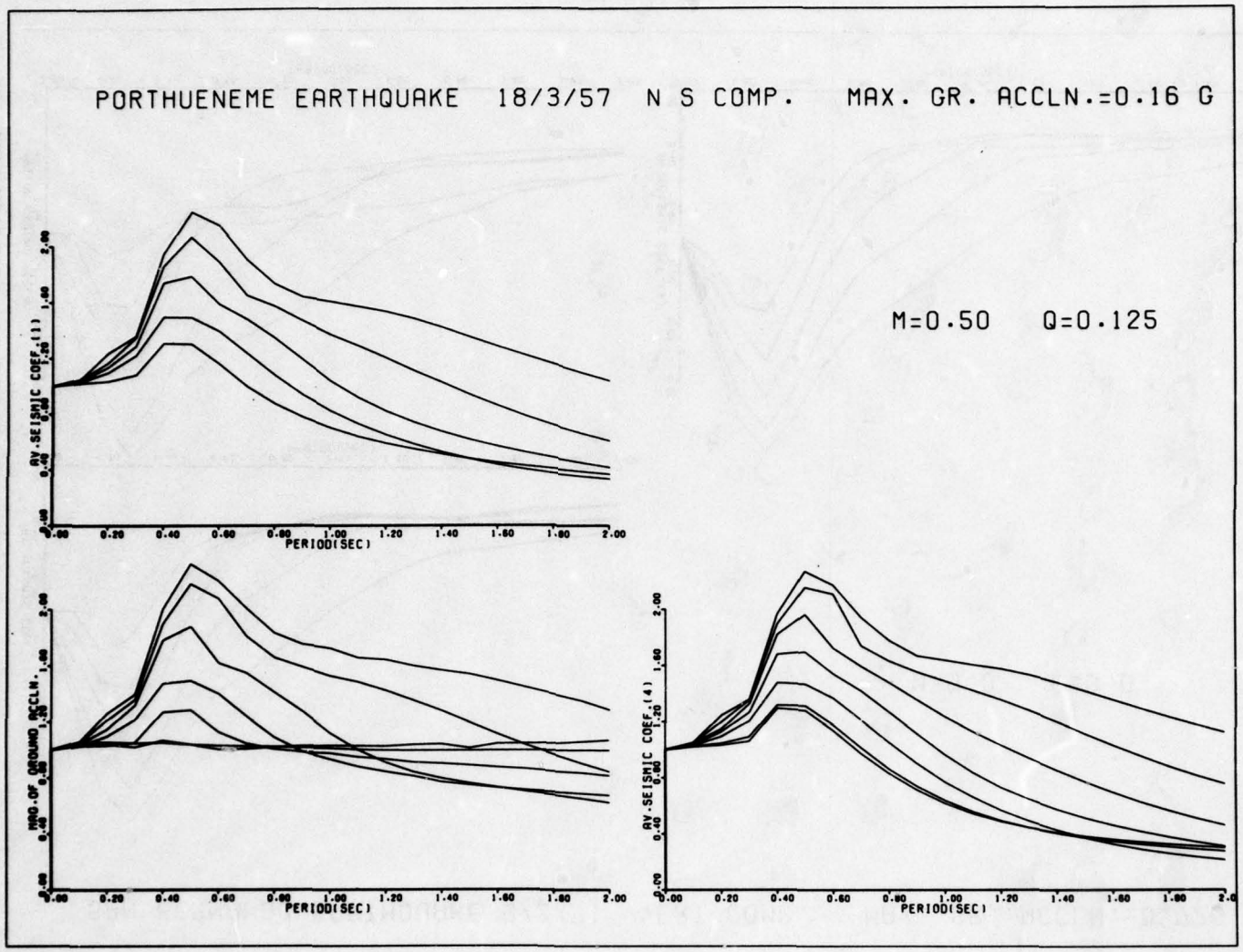
PORTHUENEME EARTHQUAKE 18/3/57 N S COMP. MAX. GR. ACCLN.=0.16 G
M=0.50 Q=0.125
AV.SEISMIC COEF.(1)
PERIOD(SEC)
NRO.OF GROUND ACCLN.
PERIOD(SEC)
AV.SEISMIC COEF.(4)
PERIOD(SEC)

Figure E11

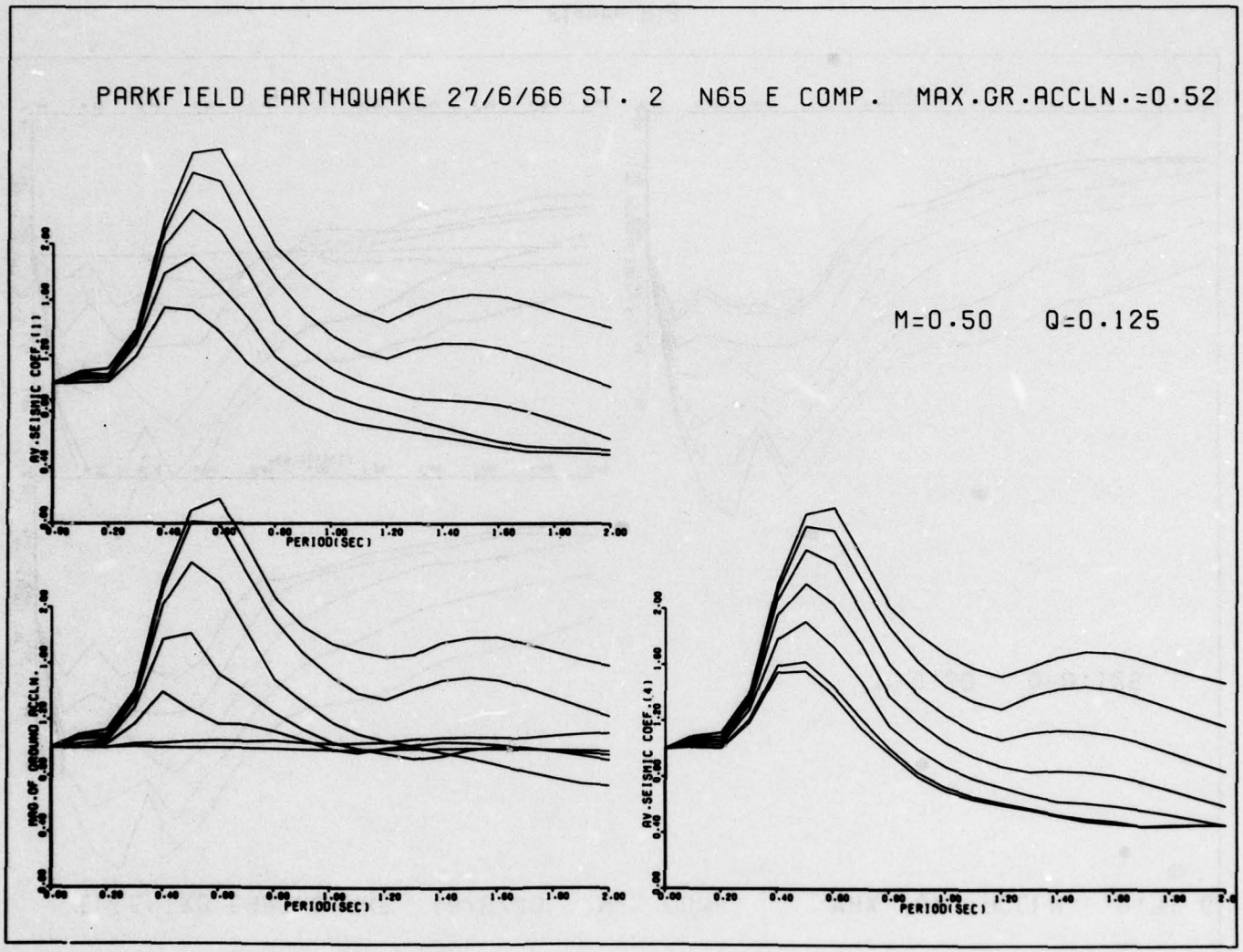
PARKFIELD EARTHQUAKE 27/6/66 ST. 2 N65 E COMP. MAX.GR.ACCLN.=0.52
M=0.50 Q=0.125
AV.SEISMIC COEF.(1)
PERIOD(SEC)
AV.SEISMIC COEF.(4)
PERIOD(SEC)
PERIOD(SEC)

Figure E12

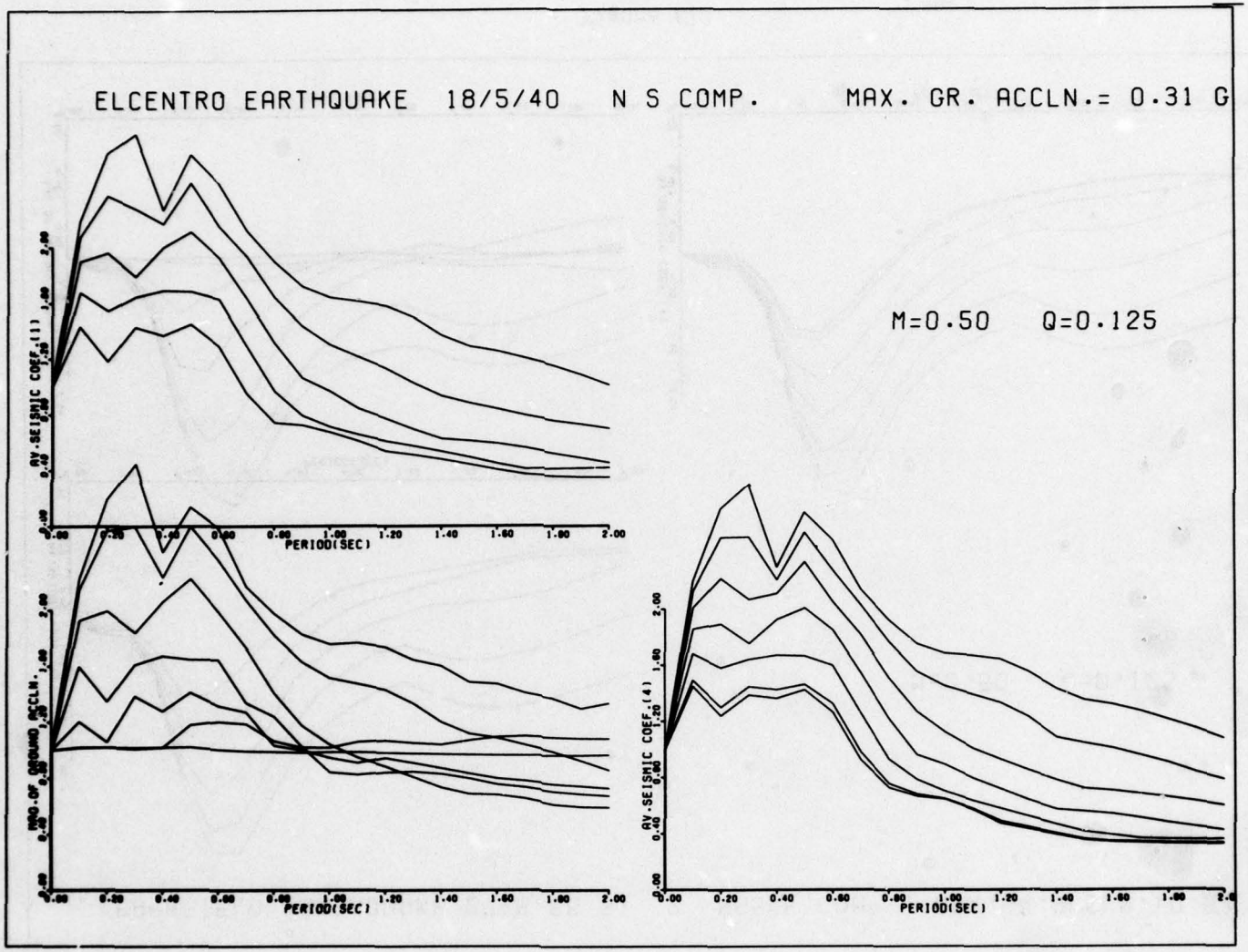
ELCENTRO EARTHQUAKE 18/5/40 N S COMP.
MAX. GR. ACCLN.= 0.31 G
M=0.50 Q=0.125
AV.SEISMIC COEF.(1)
PERIOD(SEC)
AV.SEISMIC COEF.(4)
PERIOD(SEC)
PERIOD(SEC)

Figure E13

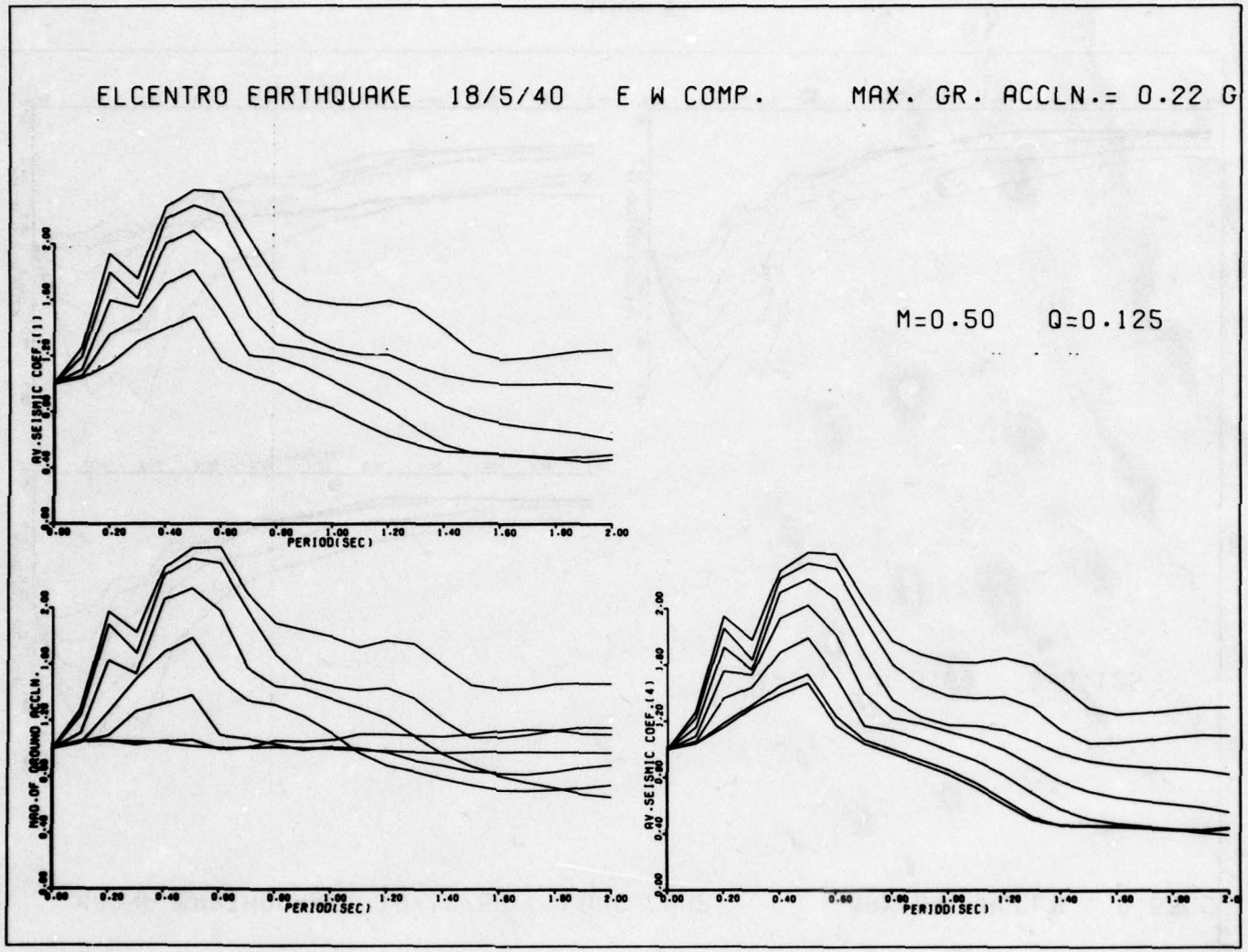
ELCENTRO EARTHQUAKE 18/5/40 E W COMP.
MAX. GR. ACCLN.= 0.22 G
M=0.50 Q=0.125
AV.SEISMIC COEF.(1)
NRO.OF GROUND ACCLN.
AV.SEISMIC COEF.(4)
PERIOD(SEC)

Figure E14

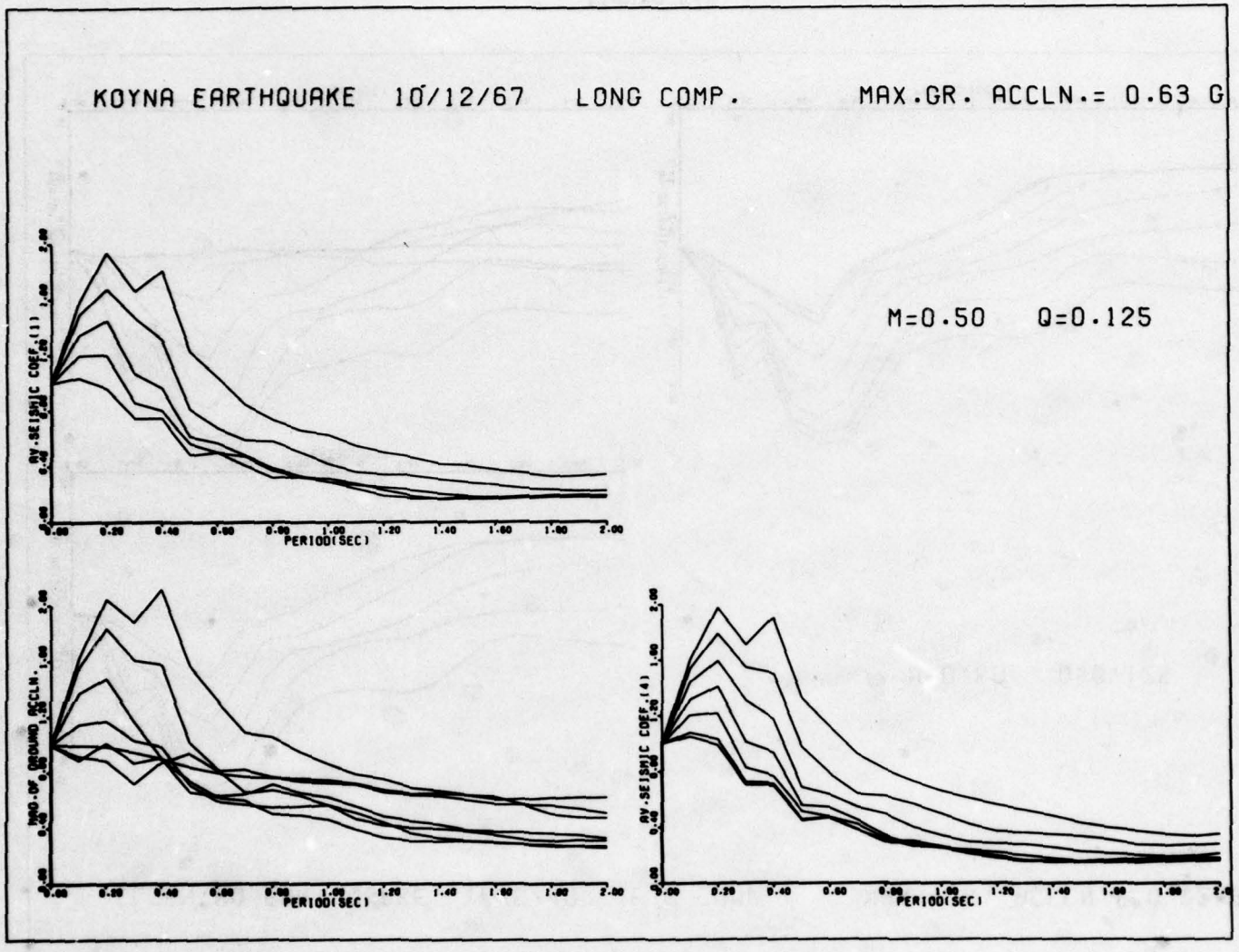
KOYNA EARTHQUAKE 10/12/67 LONG COMP.
MAX.GR. ACCLN.= 0.63 G
M=0.50 Q=0.125
AV.SEISMIC COEF.(1)
PERIOD(SEC)
AV.SEISMIC COEF.(4)
PERIOD(SEC)
PERIOD(SEC)

Figure E15

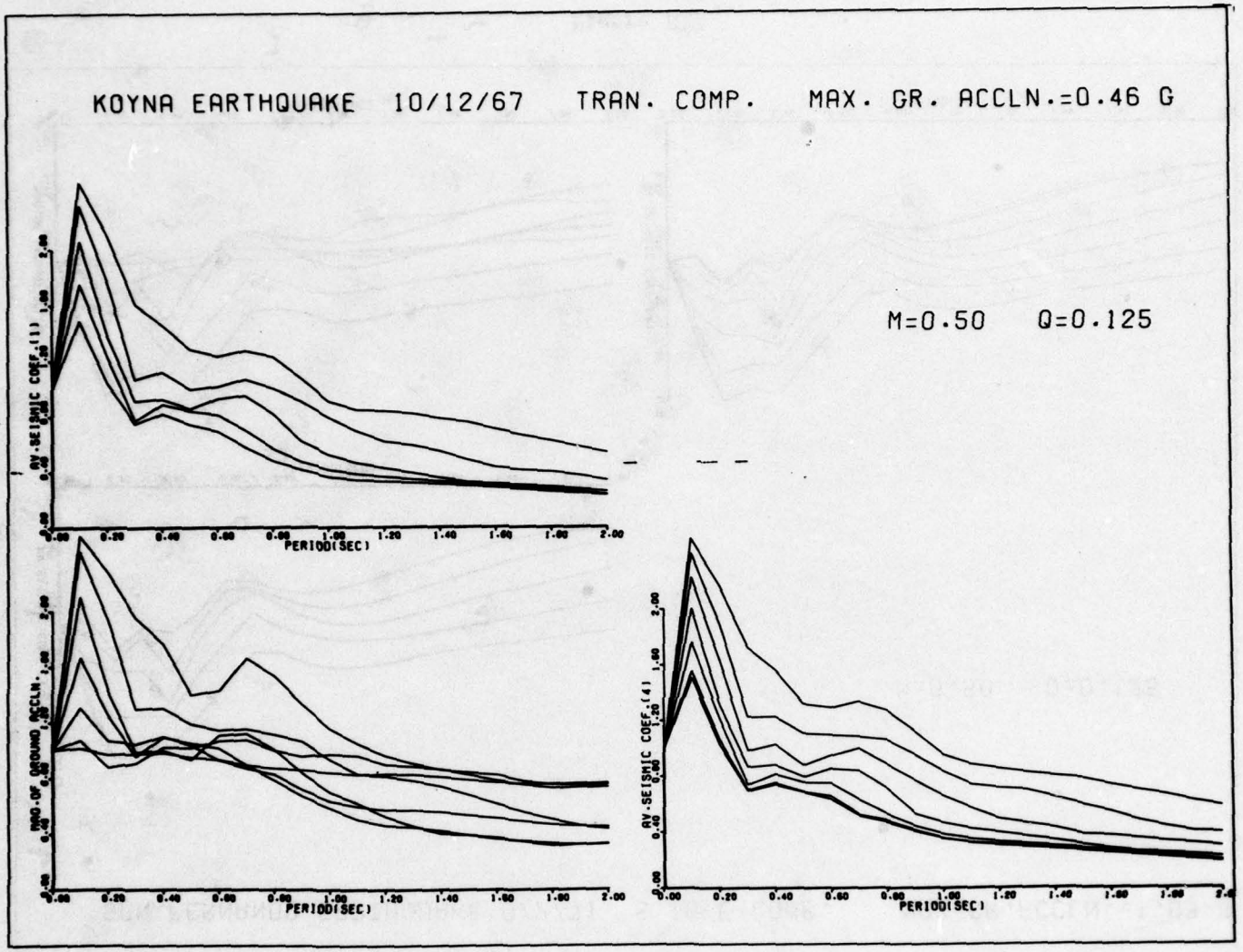
KOYNA EARTHQUAKE 10/12/67 TRAN. COMP. MAX. GR. ACCLN.=0.46 G
M=0.50 Q=0.125
AV.SEISMIC COEF.(I)
PERIOD(SEC)
PERIOD(SEC)
AV.SEISMIC COEF.(4)
PERIOD(SEC)

Figure E16

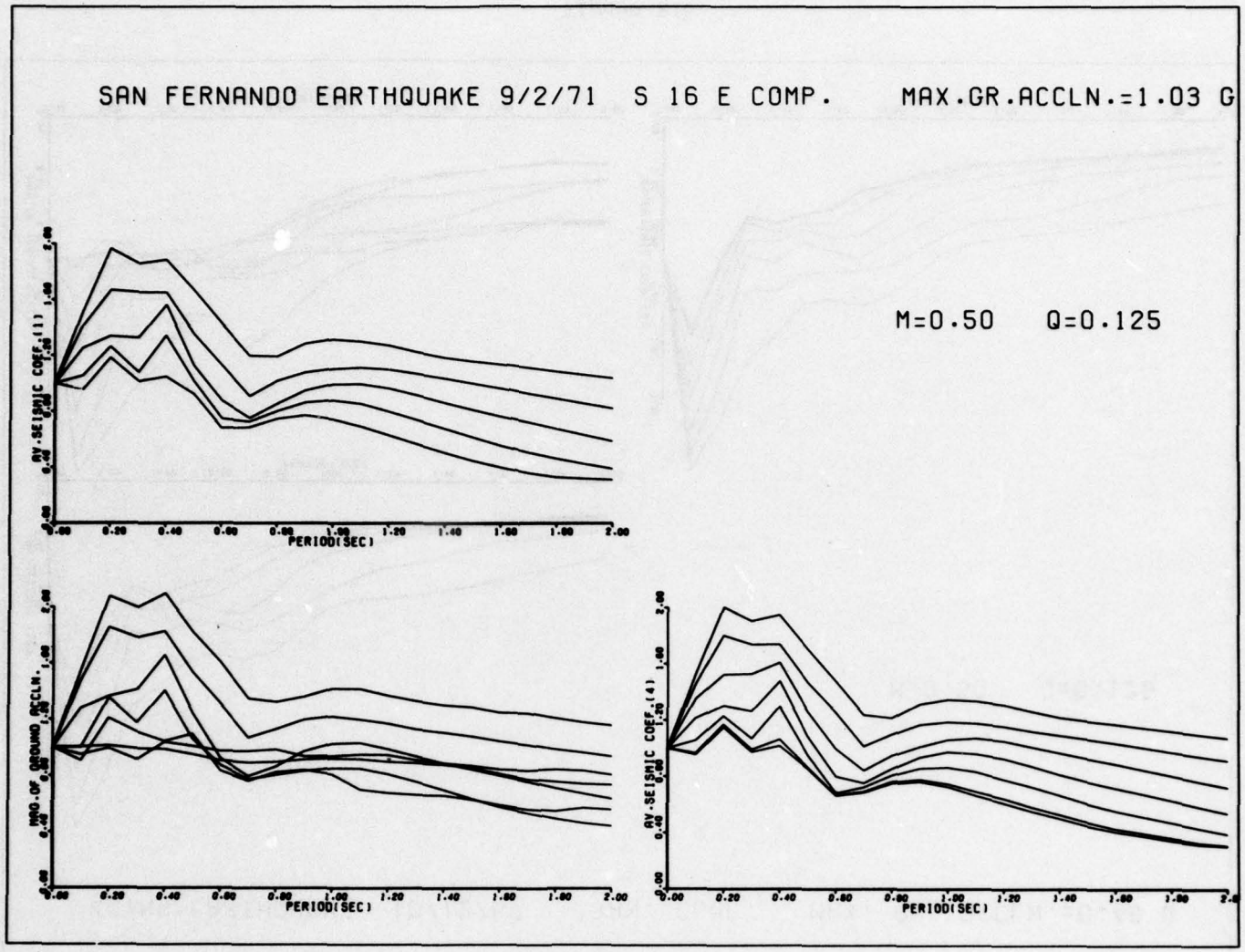
SAN FERNANDO EARTHQUAKE 9/2/71 S 16 E COMP. MAX.GR.ACCLN.=1.03 G
M=0.50 Q=0.125
AV.SEISMIC COEF.(1)
PERIOD(SEC)
RMO.OF GROUND ACCLN.
PERIOD(SEC)
AV.SEISMIC COEF.(4)
PERIOD(SEC)

Figure E17

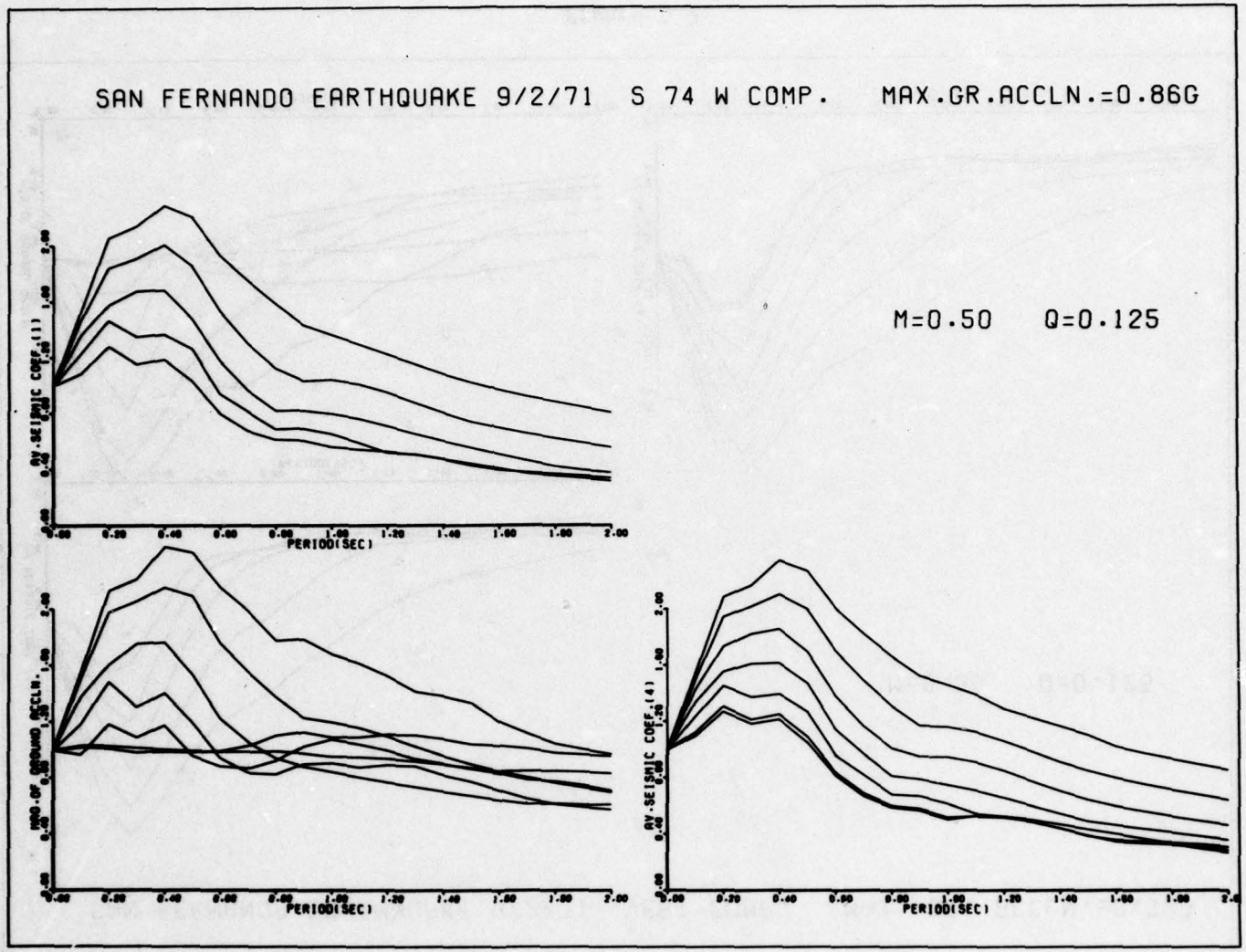
SAN FERNANDO EARTHQUAKE 9/2/71 S 74 W COMP. MAX.GR.ACCLN.=0.86G
M=0.50 Q=0.125
AV.SEISMIC COEF.(1)
PERIOD(SEC)
RMO-OF GROUND ACCLN.
PERIOD(SEC)
AV.SEISMIC COEF.(4)
PERIOD(SEC)

Figure E18

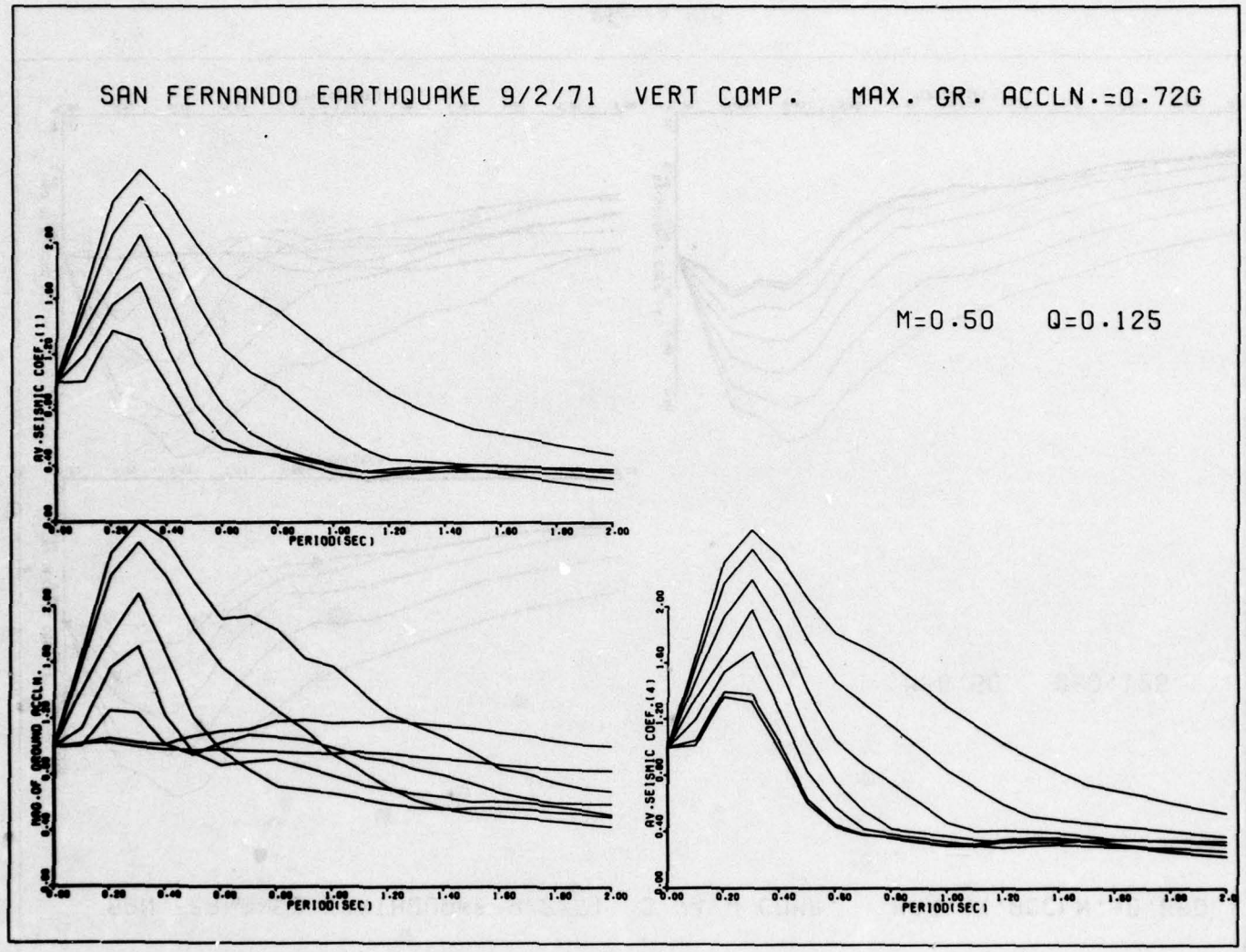
SAN FERNANDO EARTHQUAKE 9/2/71 VERT COMP. MAX. GR. ACCLN.=0.72G
M=0.50 Q=0.125
AV.SEISMIC COEF.(1)
AV.SEISMIC COEF.(4)
PERIOD(SEC)

Figure E19

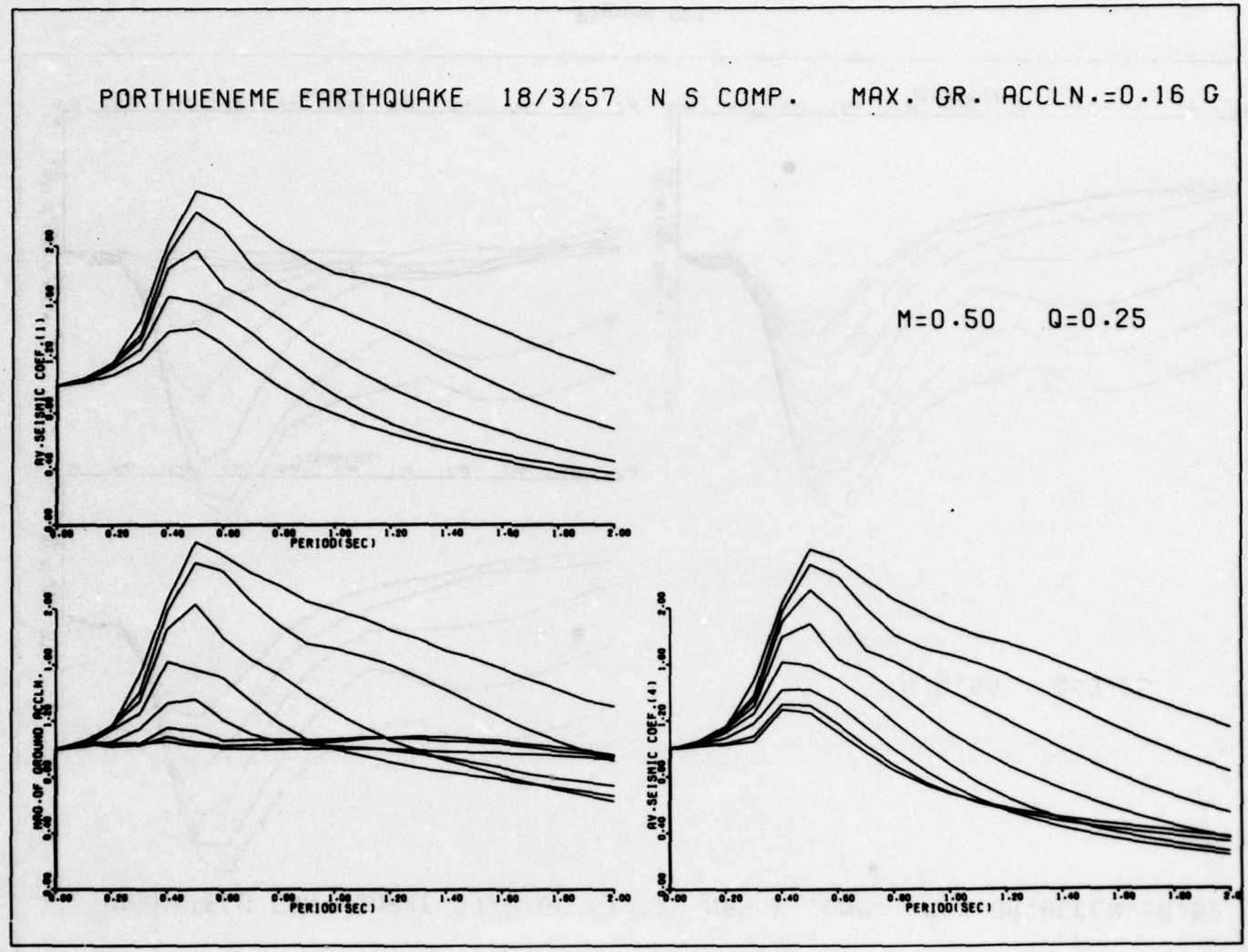
PORTHUENEME EARTHQUAKE 18/3/57 N S COMP. MAX. GR. ACCLN.=0.16 G
M=0.50 Q=0.25
AV.SEISMIC COEF.(1)
PERIOD(SEC)
RMO.OF GROUND ACCLN.
PERIOD(SEC)
AV.SEISMIC COEF.(4)
PERIOD(SEC)

Figure E20

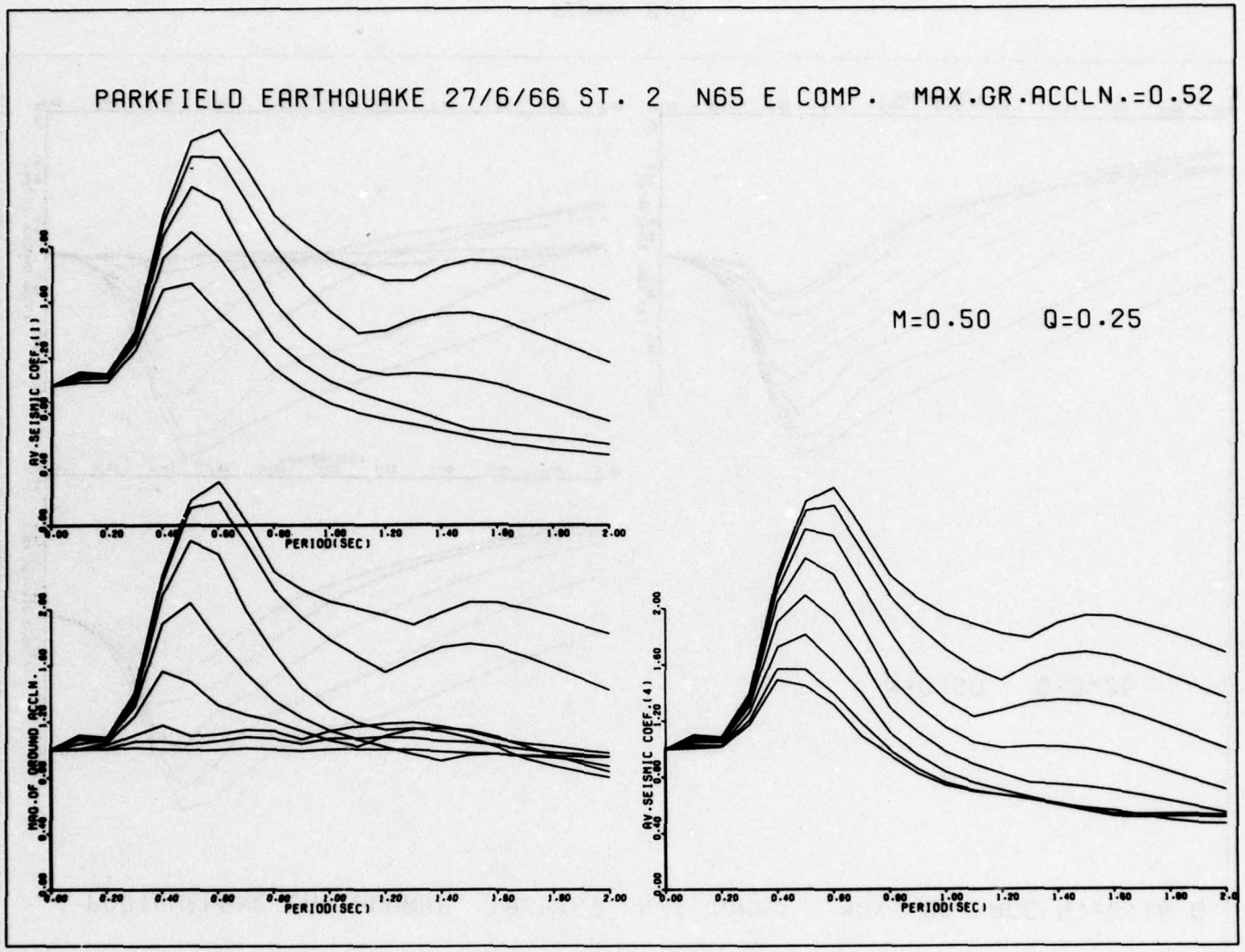
PARKFIELD EARTHQUAKE 27/6/66 ST. 2 N65 E COMP. MAX.GR.ACCLN.=0.52
M=0.50 Q=0.25
AV.SEISMIC COEF.(I)
NOO.OF GROUND ACCLN.
AV.SEISMIC COEF.(4)
PERIOD(SEC)
PERIOD(SEC)
PERIOD(SEC)

Figure E21

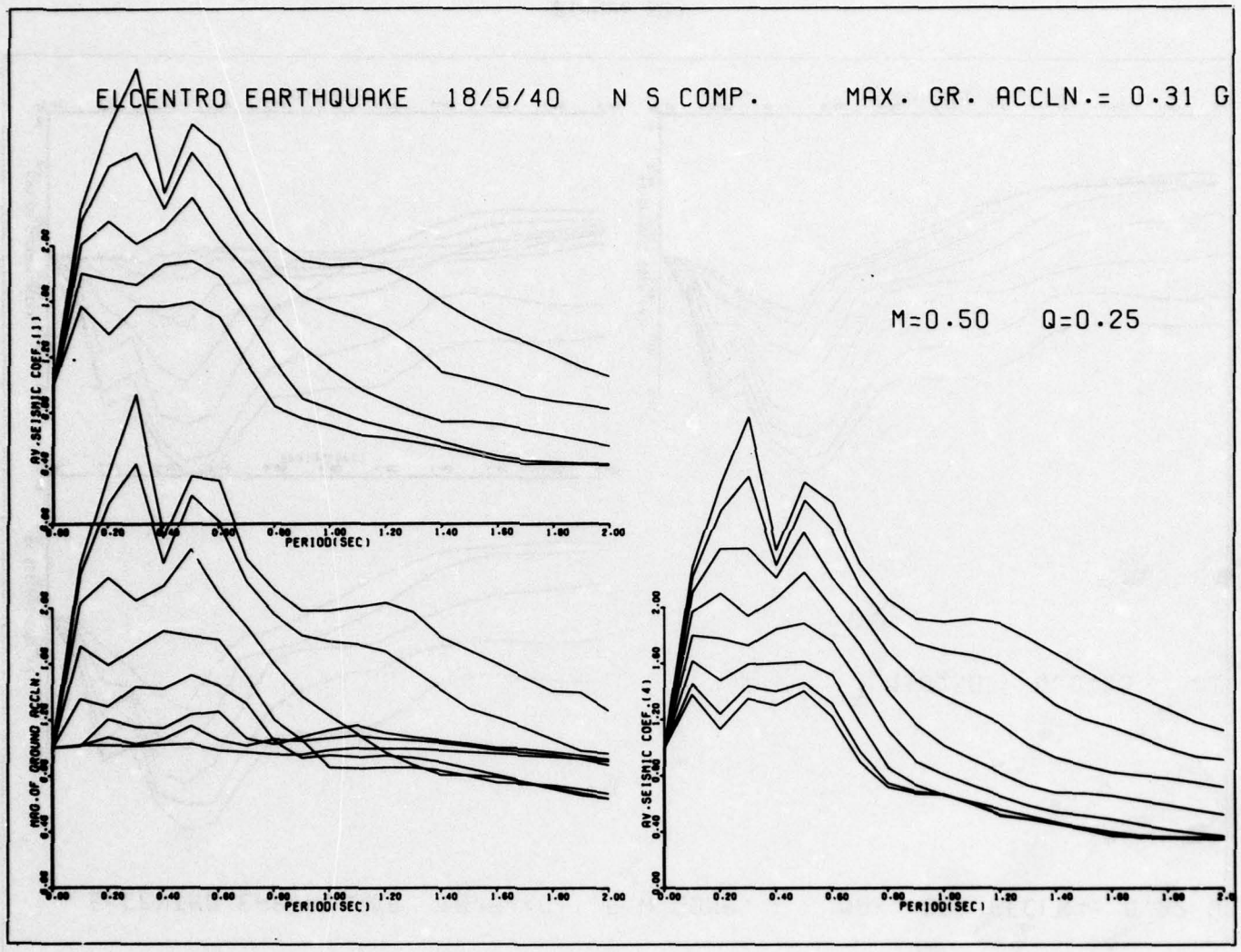
ELCENTRO EARTHQUAKE 18/5/40 N S COMP.
MAX. GR. ACCLN.= 0.31 G
M=0.50 Q=0.25
AV.SEISMIC COEF.(1)
AV.SEISMIC COEF.(4)
NRO.OF GROUND ACCLN.
PERIOD(SEC)

Figure E22

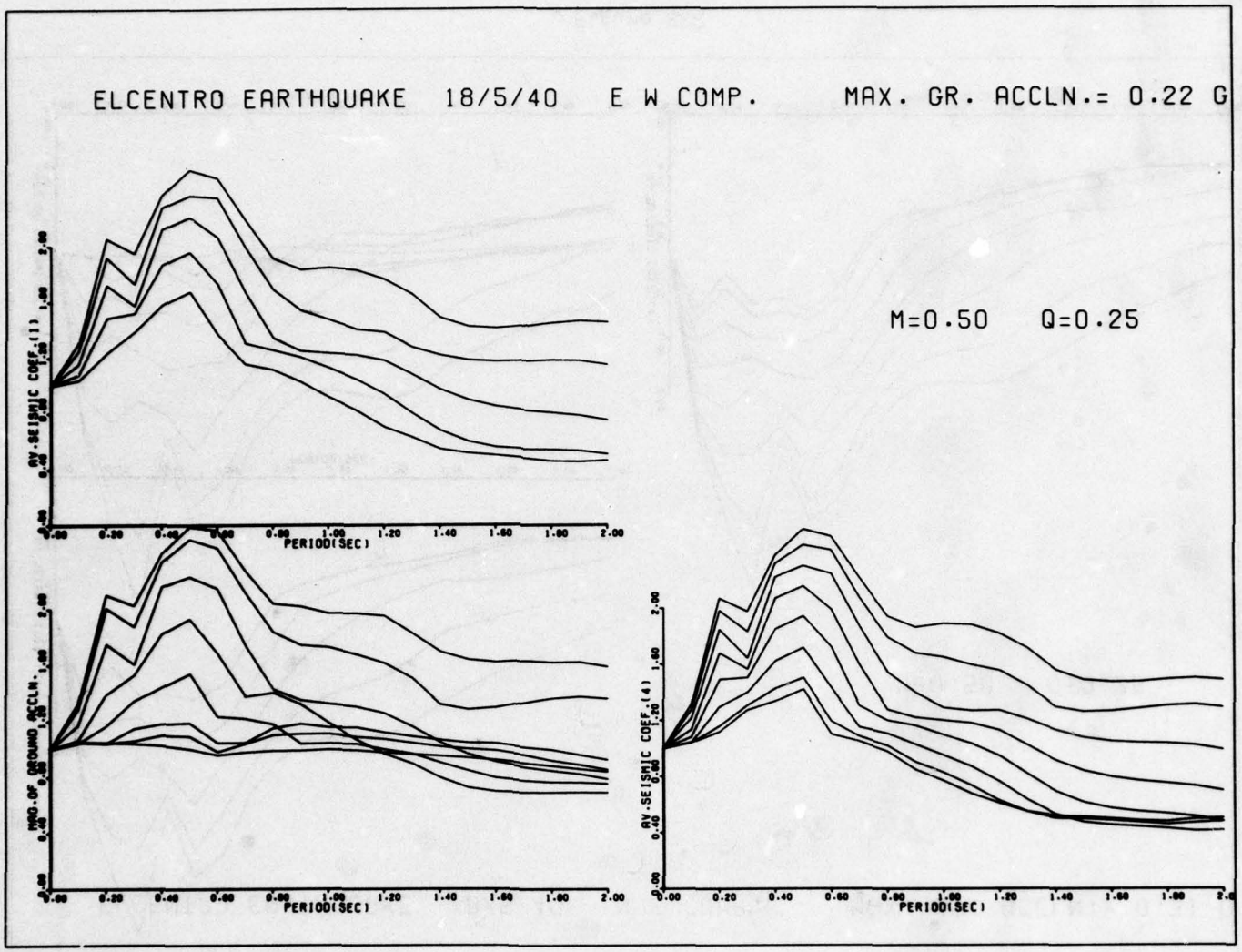
ELCENTRO EARTHQUAKE 18/5/40 E W COMP. MAX. GR. ACCLN.= 0.22 G
M=0.50 Q=0.25
AV.SEISMIC COEF.(1)
PERIOD(SEC)
PROD.OF GROUND ACCLN.
PERIOD(SEC)
AV.SEISMIC COEF.(4)
PERIOD(SEC)

Figure E23

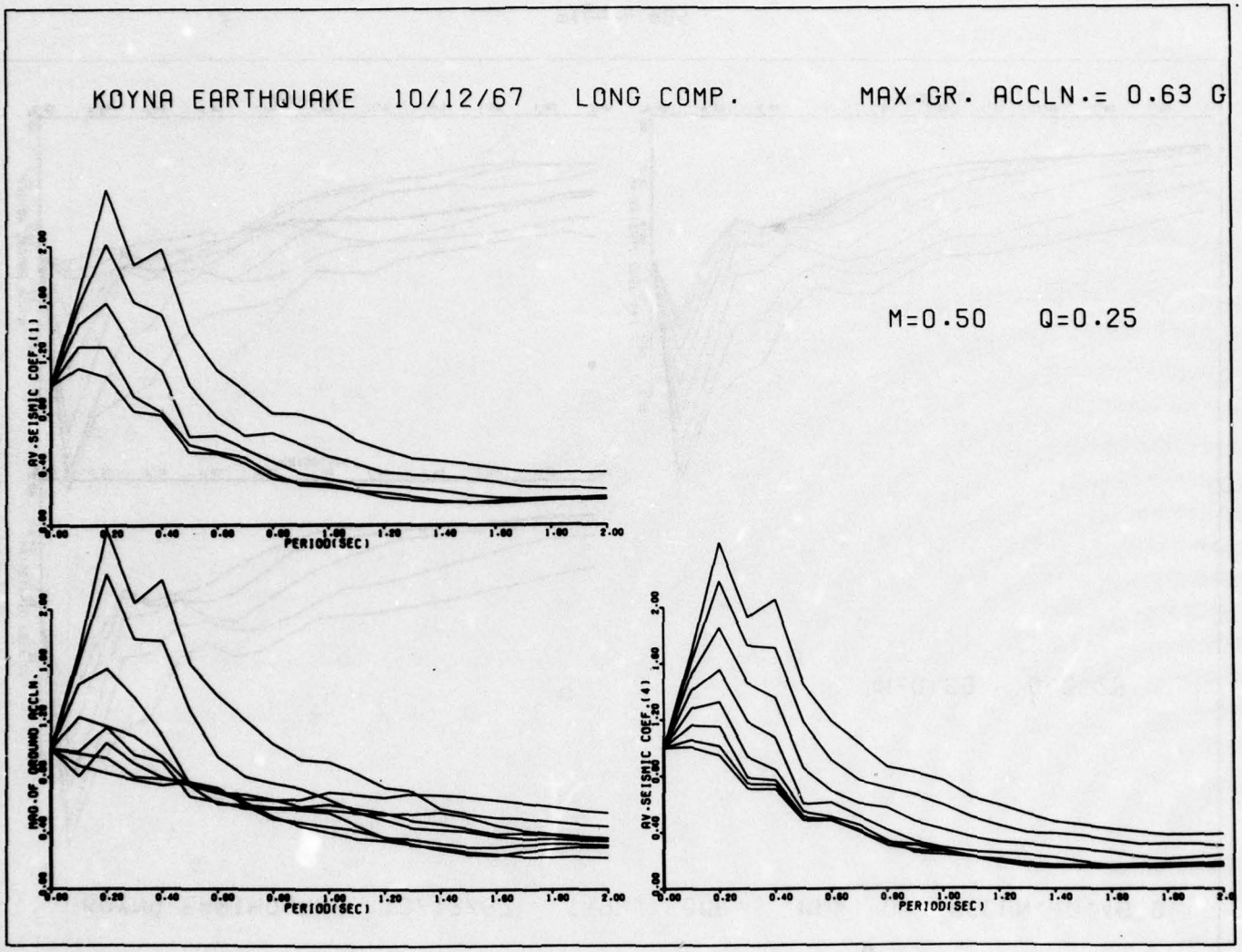
KOYNA EARTHQUAKE 10/12/67 LONG COMP.
MAX.GR. ACCLN.= 0.63 G
M=0.50 Q=0.25
AV.SEISMIC COEF.(1)
AV.SEISMIC COEF.(4)
PERIOD(SEC)

Figure E24

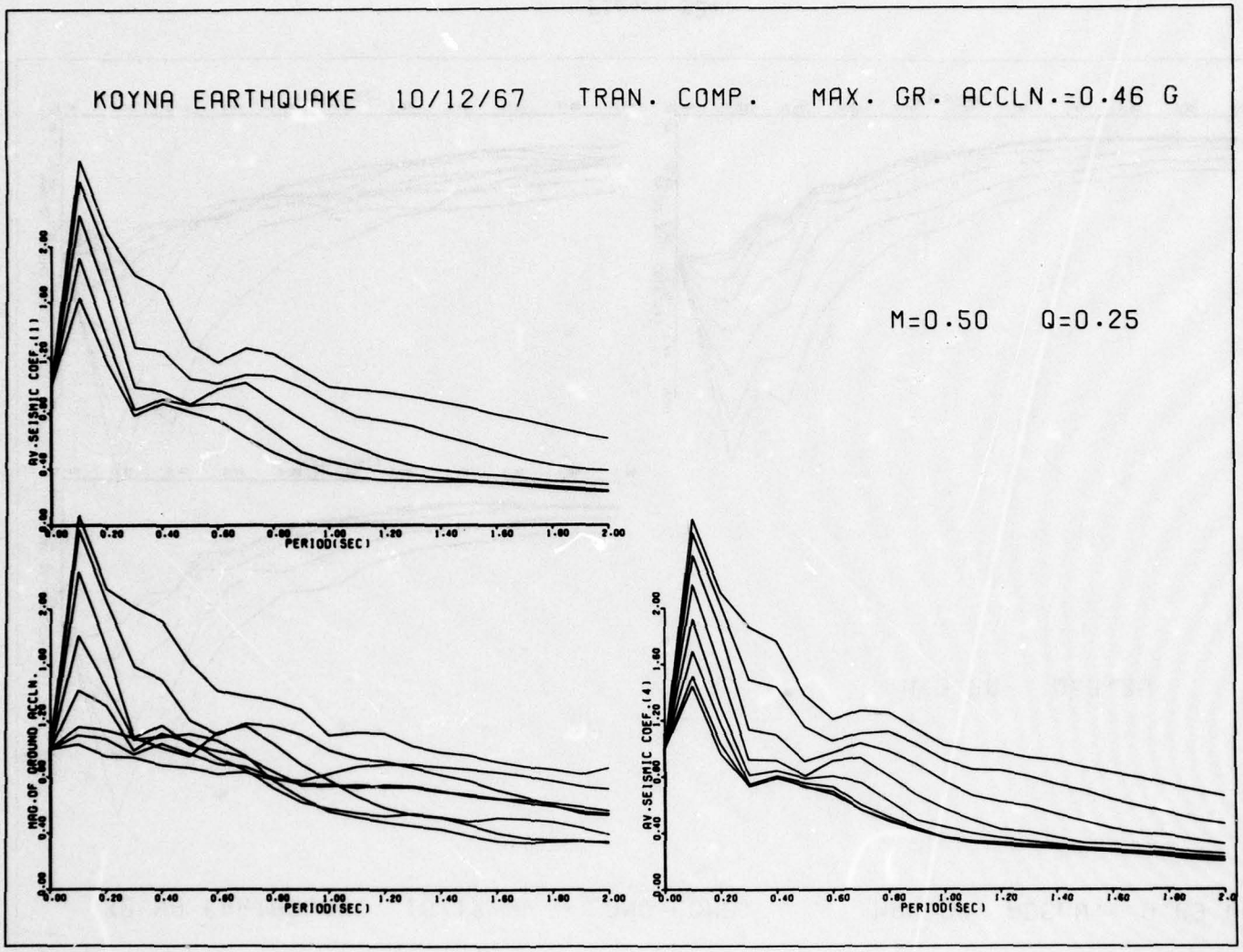
KOYNA EARTHQUAKE 10/12/67 TRAN. COMP. MAX. GR. ACCLN.=0.46 G
M=0.50 Q=0.25
AV.SEISMIC COEF.(1)
NRO. OF GROUND ACCLN.
AV.SEISMIC COEF.(4)
PERIOD(SEC)

Figure E25

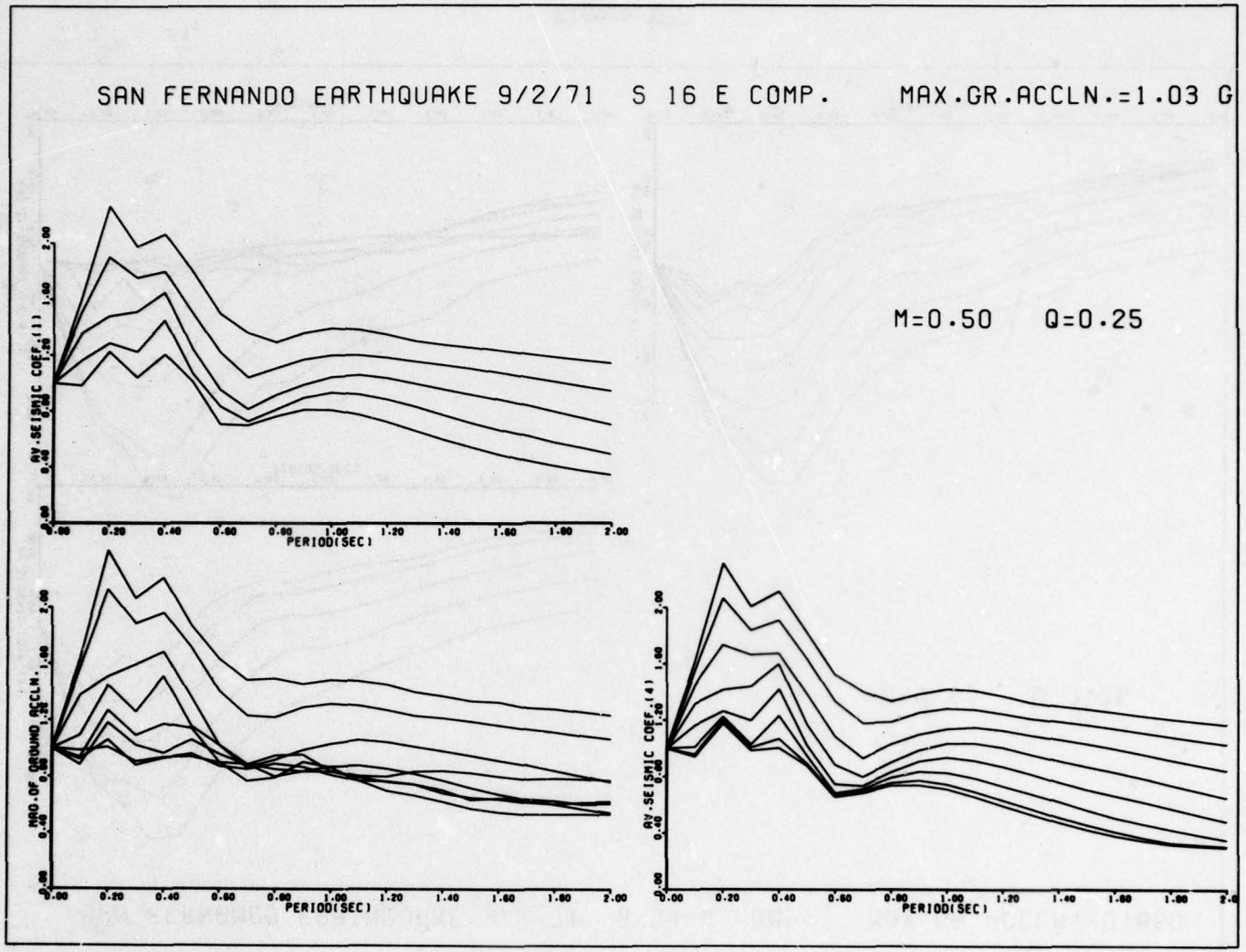
SAN FERNANDO EARTHQUAKE 9/2/71 S 16 E COMP. MAX.GR.ACCLN.=1.03 G
M=0.50 Q=0.25
AV.SEISMIC COEF.(1)
MAG.OF GROUND ACCLN.
AV.SEISMIC COEF.(4)
PERIOD(SEC)

Figure E26

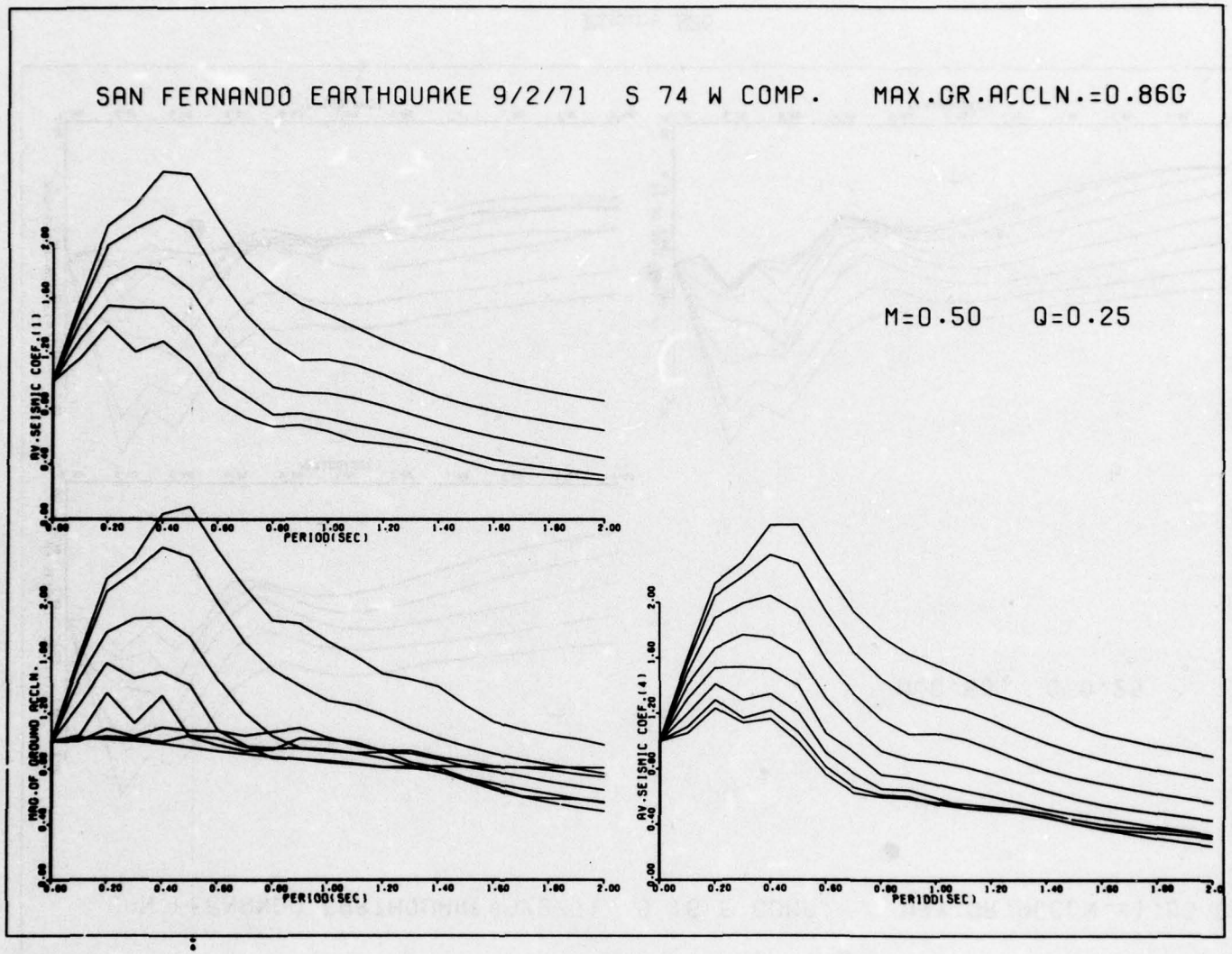
SAN FERNANDO EARTHQUAKE 9/2/71 S 74 W COMP. MAX.GR.ACCLN.=0.86G
M=0.50 Q=0.25
AV.SEISMIC COEF.(1)
PERIOD(SEC)
RNO.OF GROUND ACCLN.
PERIOD(SEC)
AV.SEISMIC COEF.(4)
PERIOD(SEC)

Figure E27

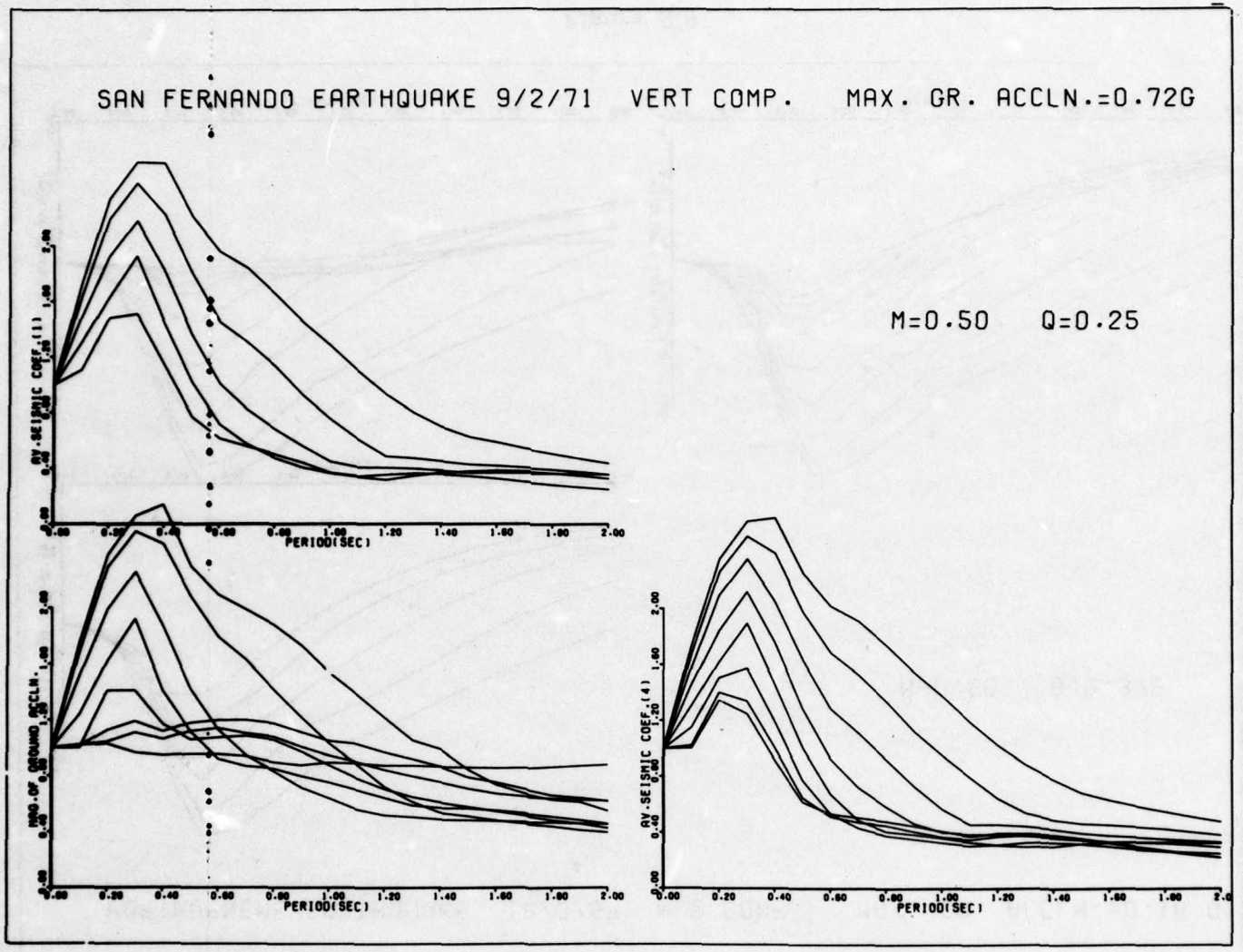
SAN FERNANDO EARTHQUAKE 9/2/71 VERT COMP. MAX. GR. ACCLN.=0.72G
M=0.50 Q=0.25
AV.SEISMIC COEF.(1)
PERIOD(SEC)
MAG.OF GROUND ACCLN.
PERIOD(SEC)
AV.SEISMIC COEF.(4)
PERIOD(SEC)

Figure E28

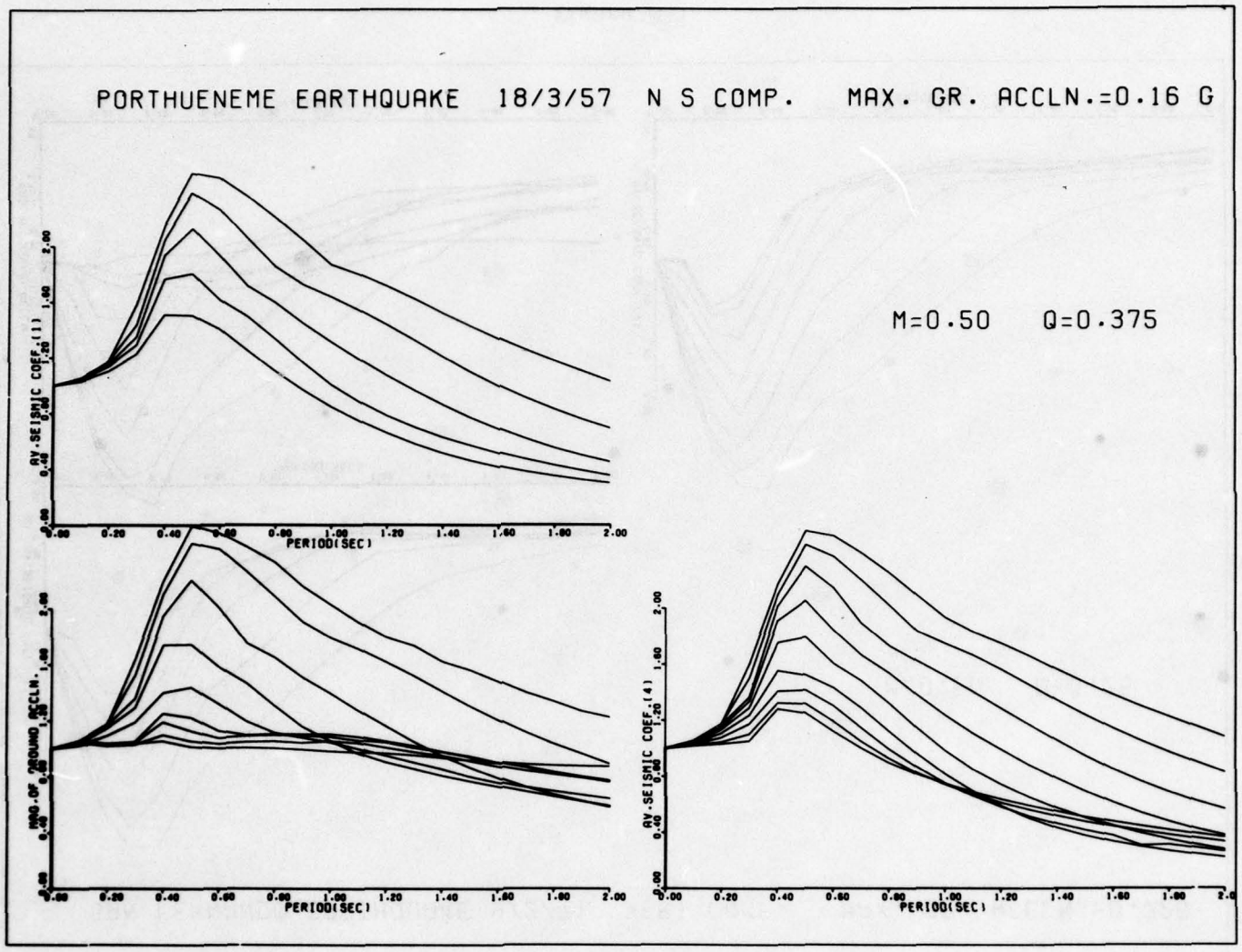
PORTHUENEME EARTHQUAKE 18/3/57 N S COMP. MAX. GR. ACCLN.=0.16 G
M=0.50 Q=0.375
AV.SEISMIC COEFF.(1)
PERIOD(SEC)
RMS OF GROUND ACCLN.
PERIOD(SEC)
AV.SEISMIC COEFF.(4)
PERIOD(SEC)

Figure E29

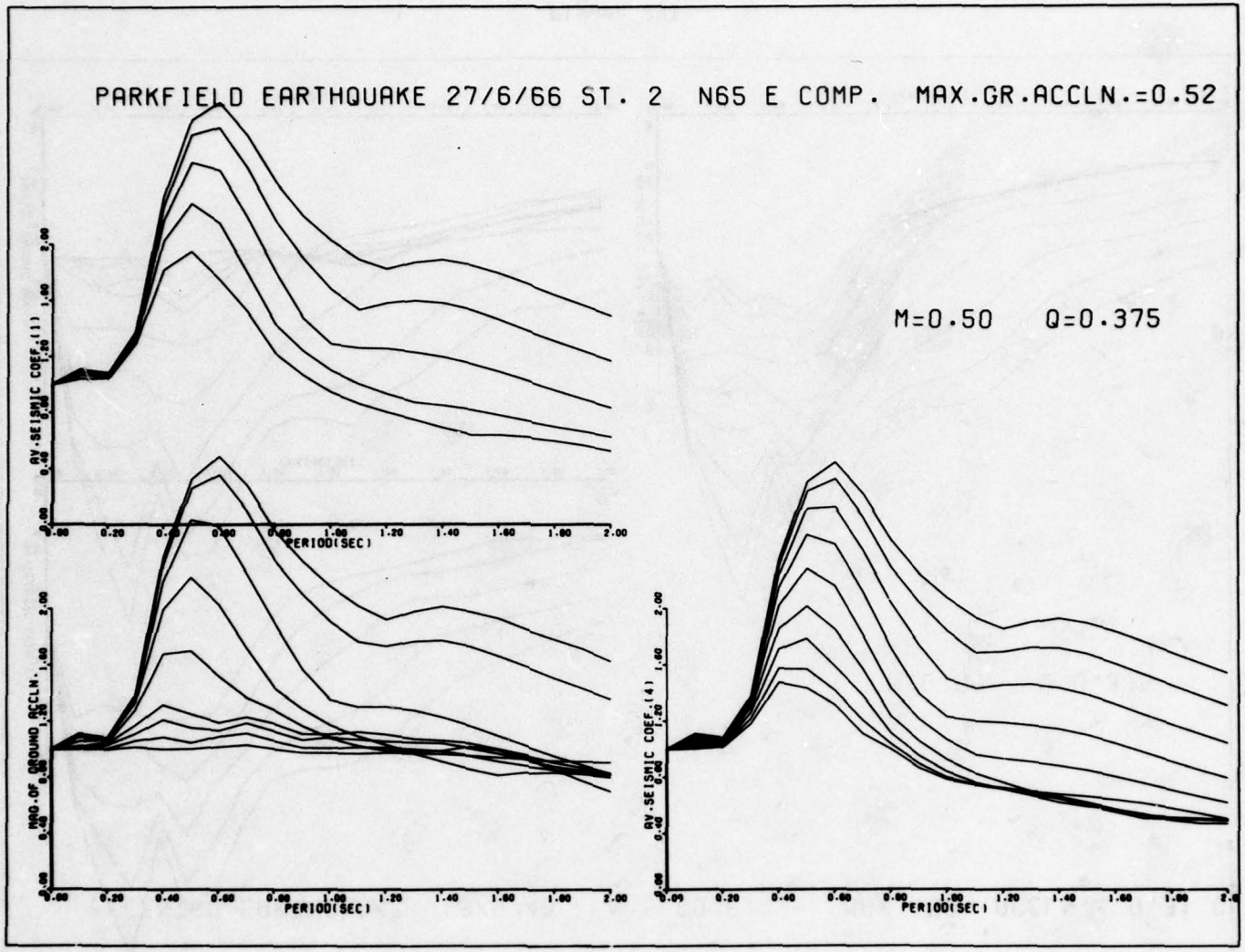
PARKFIELD EARTHQUAKE 27/6/66 ST. 2 N65 E COMP. MAX.GR.ACCLN.=0.52
M=0.50 Q=0.375
AV.SEISMIC COEF.(1)
MAG.OF GROUND ACCLN.
AV.SEISMIC COEF.(4)
PERIOD(SEC)

Figure E30

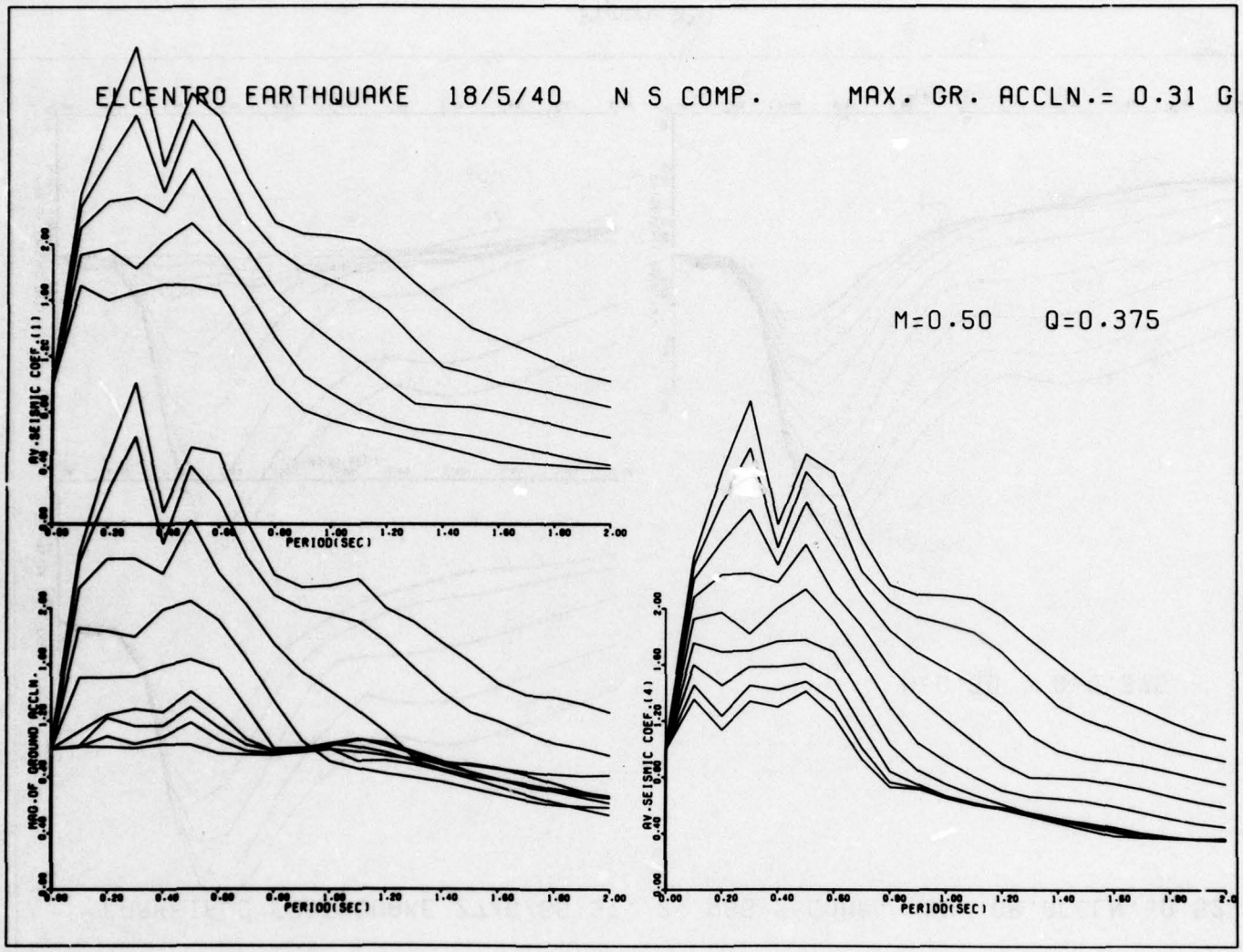
ELCENTRO EARTHQUAKE 18/5/40 N S COMP.
MAX. GR. ACCLN.= 0.31 G
M=0.50 Q=0.375
AV.SEISMIC COEF.(1)
NO.OF GROUND ACCLN.
AV.SEISMIC COEF.(4)
PERIOD(SEC)

Figure E31

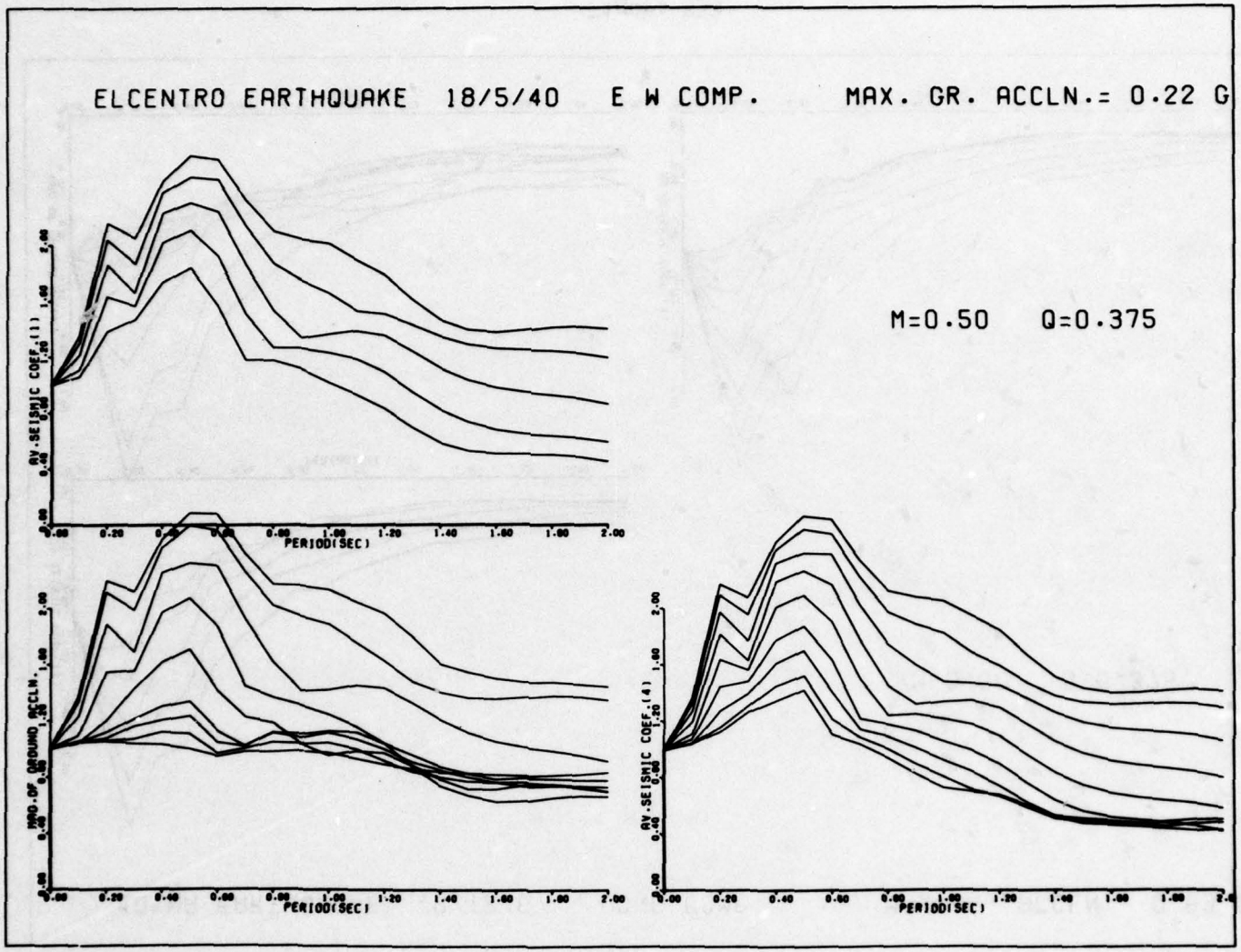
ELCENTRO EARTHQUAKE 18/5/40 E W COMP.
MAX. GR. ACCLN.= 0.22 G
M=0.50 Q=0.375
AV.SEISMIC COEF.(I)
PERIOD(SEC)
PERIOD(SEC)
AV.SEISMIC COEF.(A)
PERIOD(SEC)

Figure E32

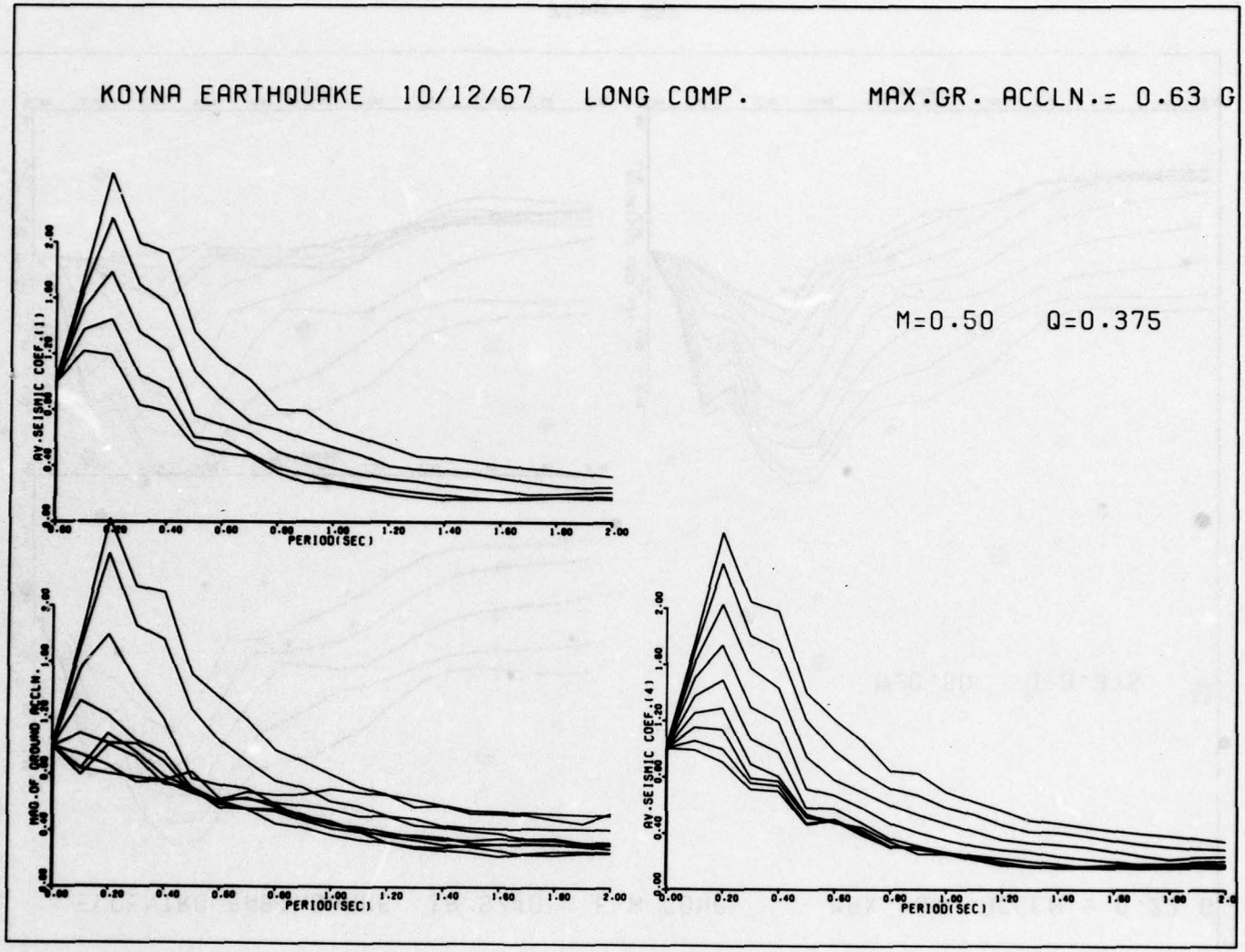
KOYNA EARTHQUAKE 10/12/67 LONG COMP.
MAX.GR. ACCLN.= 0.63 G
M=0.50 Q=0.375
AV.SEISMIC COEF.(1)
PERIOD(SEC)
AV.SEISMIC COEF.(4)
PERIOD(SEC)
PERIOD(SEC)

Figure E33

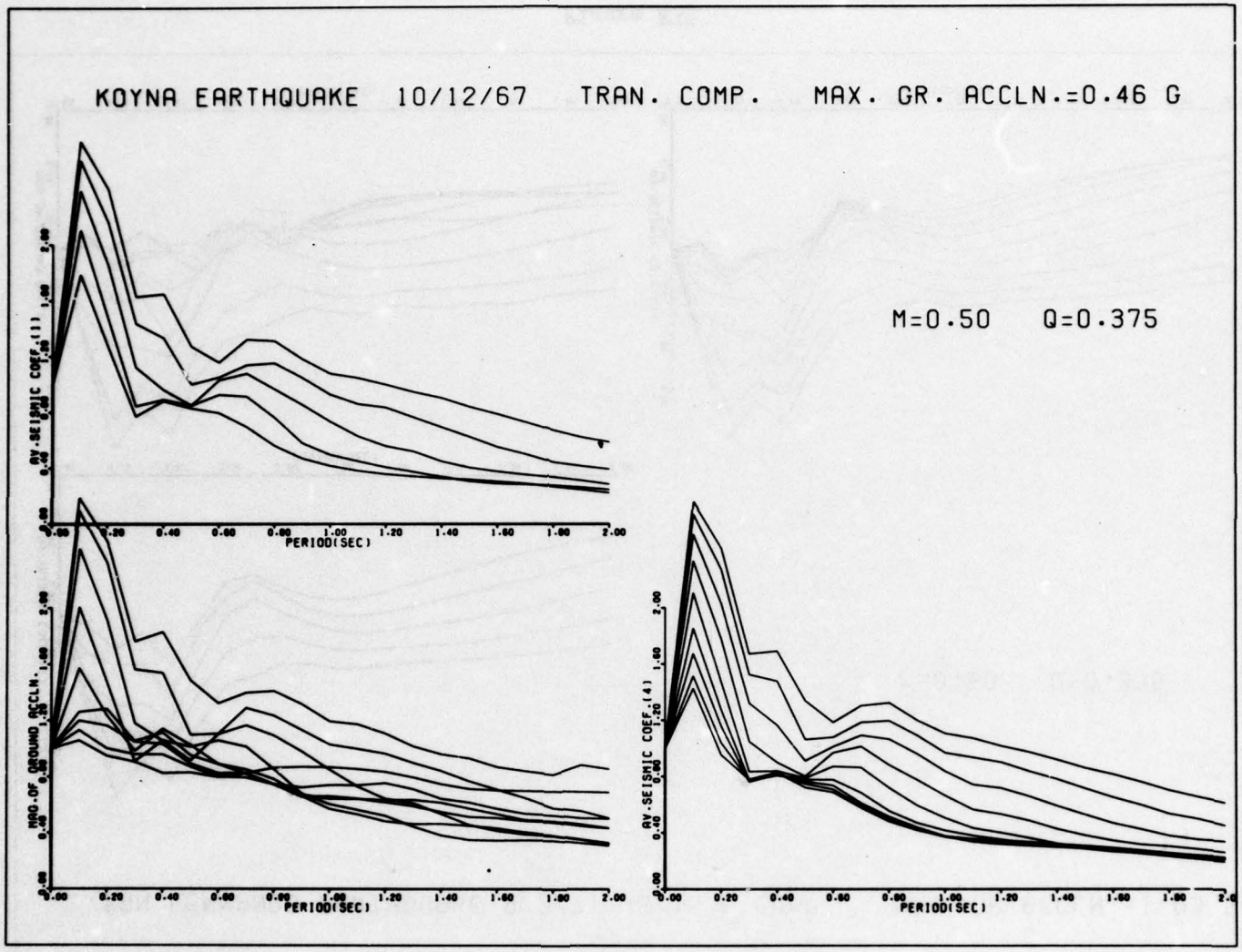
KOYNA EARTHQUAKE 10/12/67 TRAN. COMP. MAX. GR. ACCLN.=0.46 G
M=0.50 Q=0.375
AV.SEISMIC COEF.(1)
AV.SEISMIC COEF.(4)
RAD.OF GROUND ACCLN.
PERIOD(SEC)

Figure E34

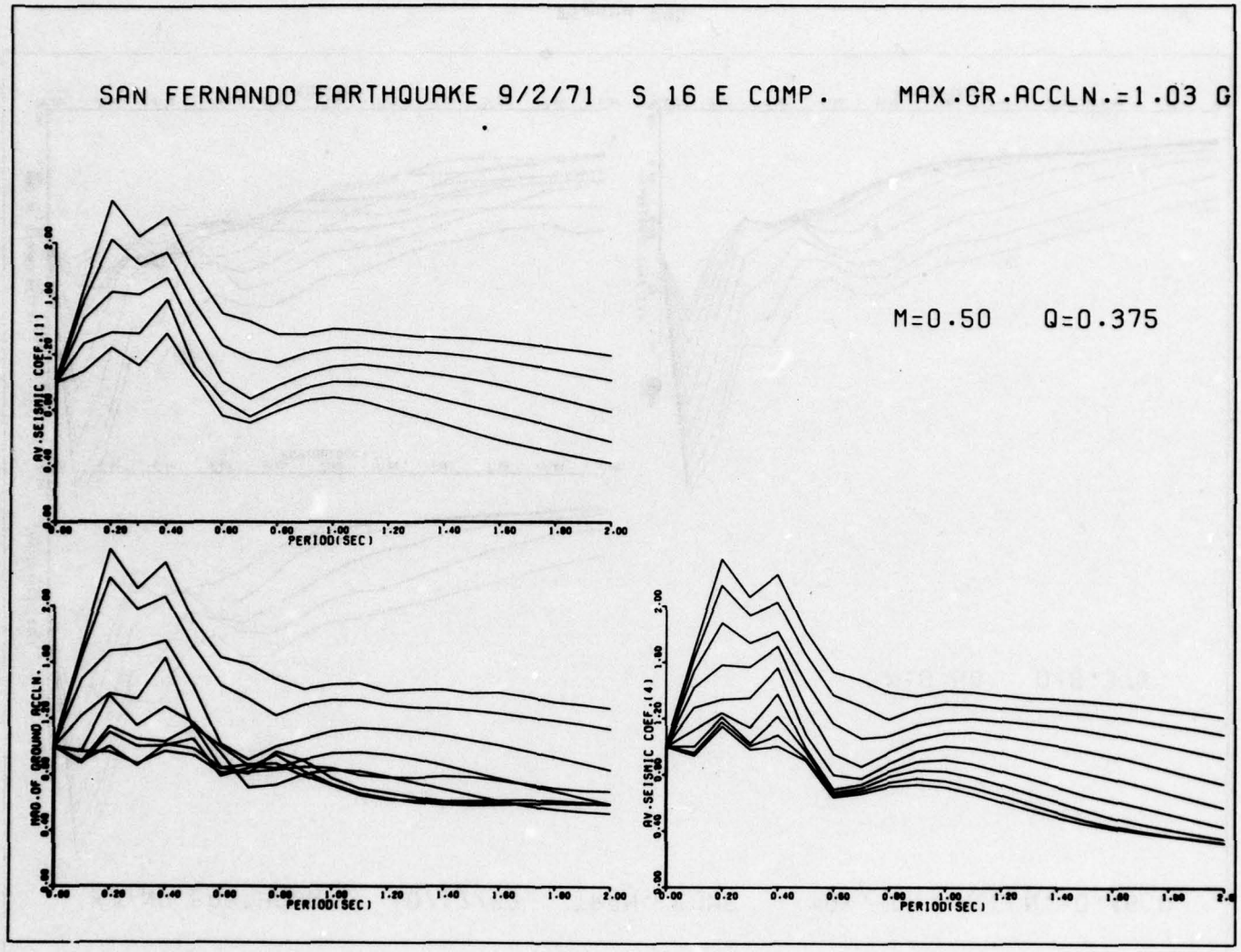
SAN FERNANDO EARTHQUAKE 9/2/71 S 16 E COMP. MAX.GR.ACCLN.=1.03 G
M=0.50 Q=0.375
AV-SEISMIC COEF.(1)
PERIOD(SEC)
RAD-OF GROUND ACCLN.
PERIOD(SEC)
AV-SEISMIC COEF.(4)
PERIOD(SEC)

Figure E35

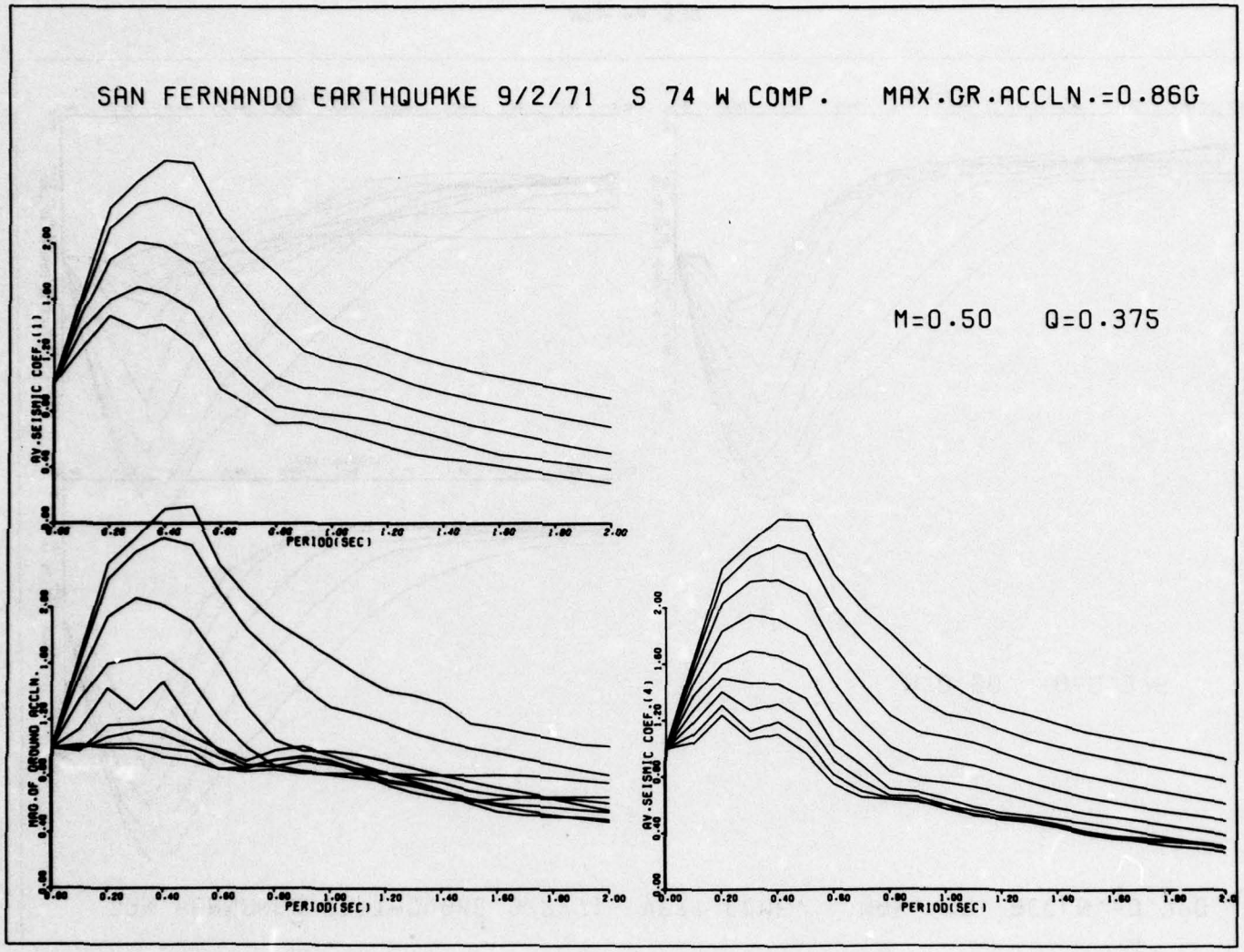
SAN FERNANDO EARTHQUAKE 9/2/71 S 74 W COMP. MAX.GR.ACCLN.=0.86G
M=0.50 Q=0.375
AV.SEISMIC COEF.(1)
MAG.OF GROUND ACCLN.
AV.SEISMIC COEF.(4)
PERIOD(SEC)

Figure E36

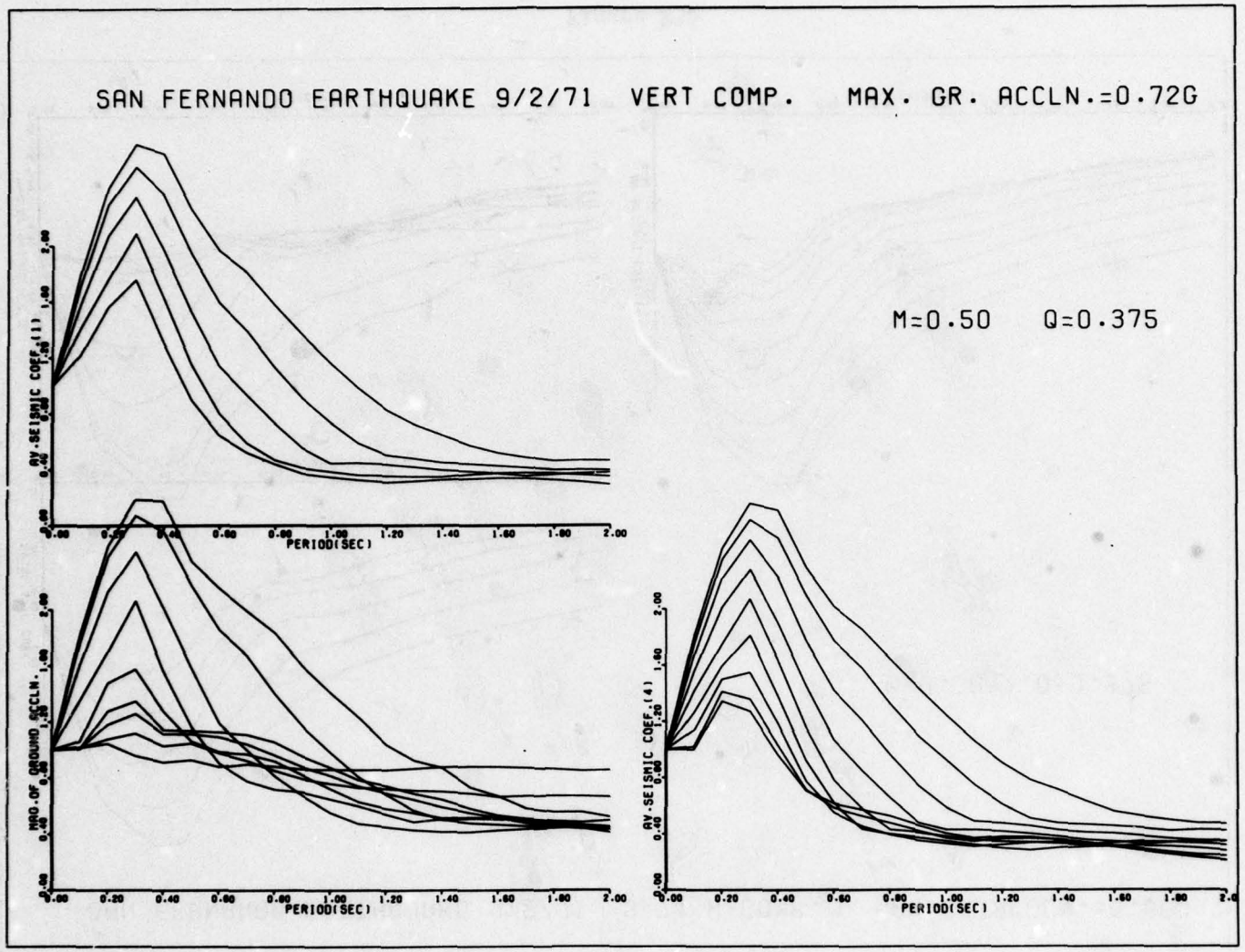
SAN FERNANDO EARTHQUAKE 9/2/71 VERT COMP. MAX. GR. ACCLN.=0.72G
M=0.50 Q=0.375
AV.SEISMIC COEF.(1)
PERIOD(SEC)
MAG.OF GROUND ACCLN.
PERIOD(SEC)
AV.SEISMIC COEF.(4)
PERIOD(SEC)

Figure E37

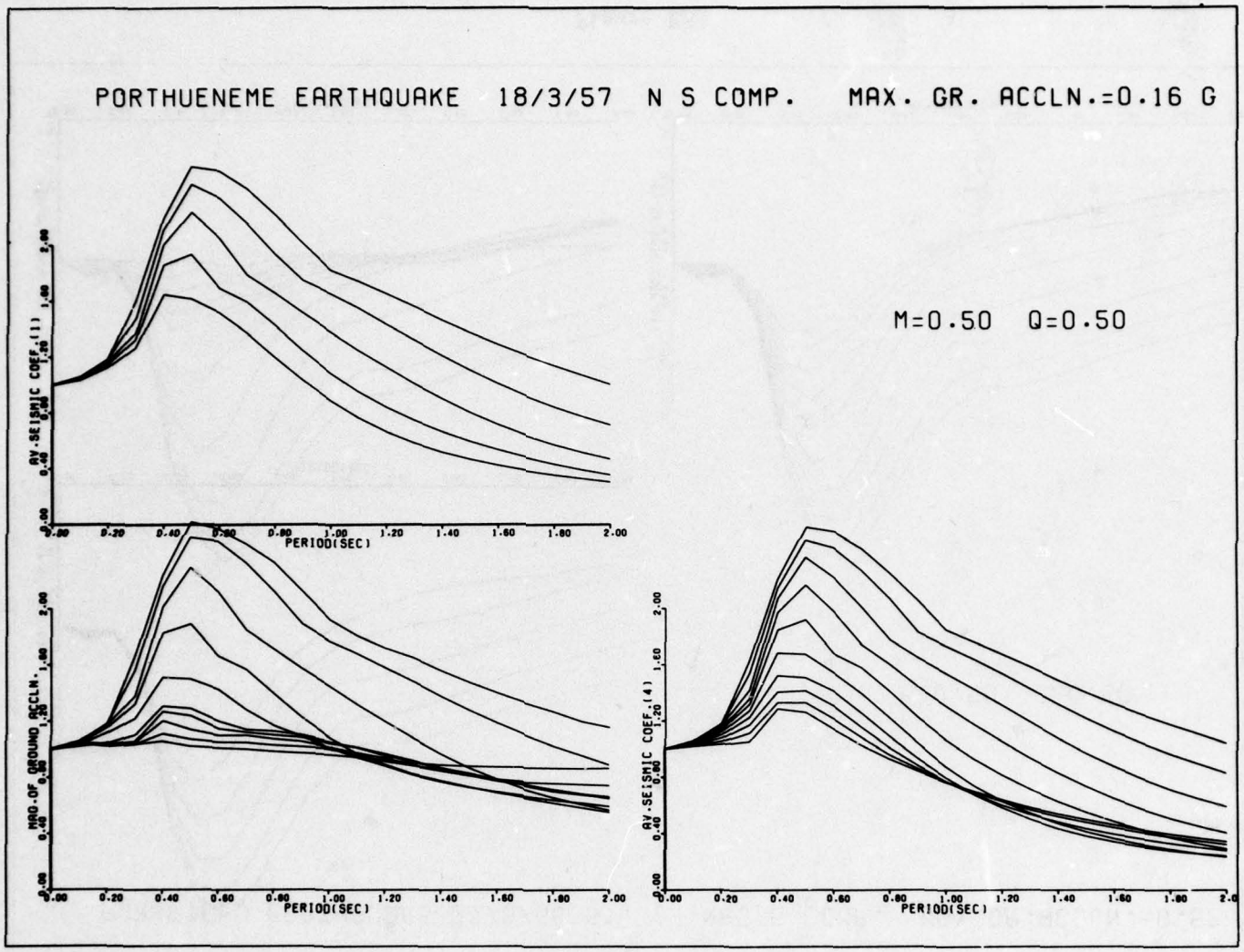
PORTHUENEME EARTHQUAKE 18/3/57 N S COMP. MAX. GR. ACCLN.=0.16 G
M=0.50 Q=0.50
AV.SEISMIC COEF.(1)
PERIOD(SEC)
MAG-OF GROUND ACCLN.
PERIOD(SEC)
AV.SEISMIC COEF.(4)
PERIOD(SEC)

Figure E38

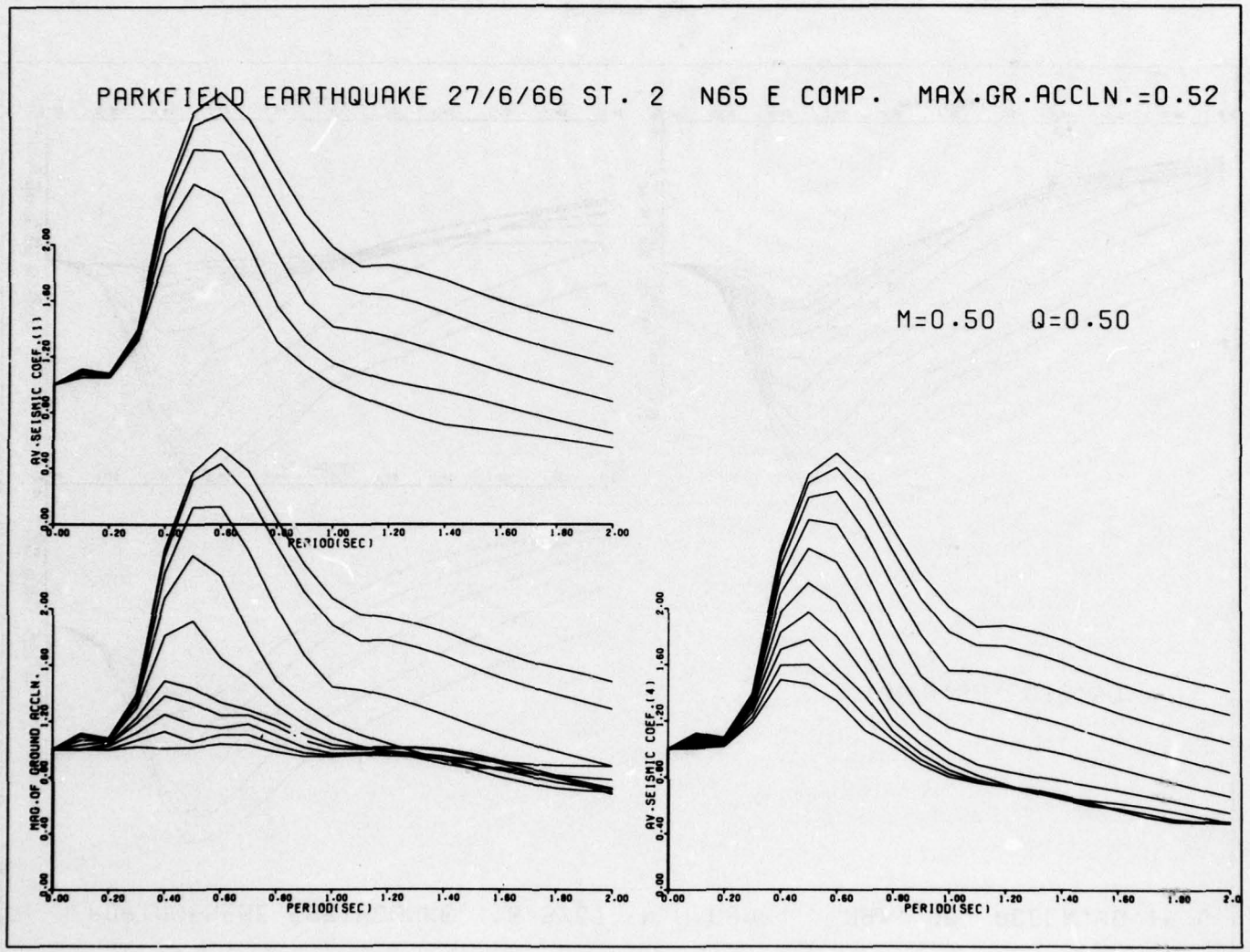
PARKFIELD EARTHQUAKE 27/6/66 ST. 2 N65 E COMP. MAX.GR.ACCLN.=0.52
M=0.50 Q=0.50
AV.SEISMIC COEF.(1)
MAG.OF GROUND ACCLN.
AV.SEISMIC COEF.(4)
PERIOD(SEC)
0.00
0.20
0.40
0.60
0.80
1.00
1.20
1.40
1.60
1.80
2.00

Figure E39

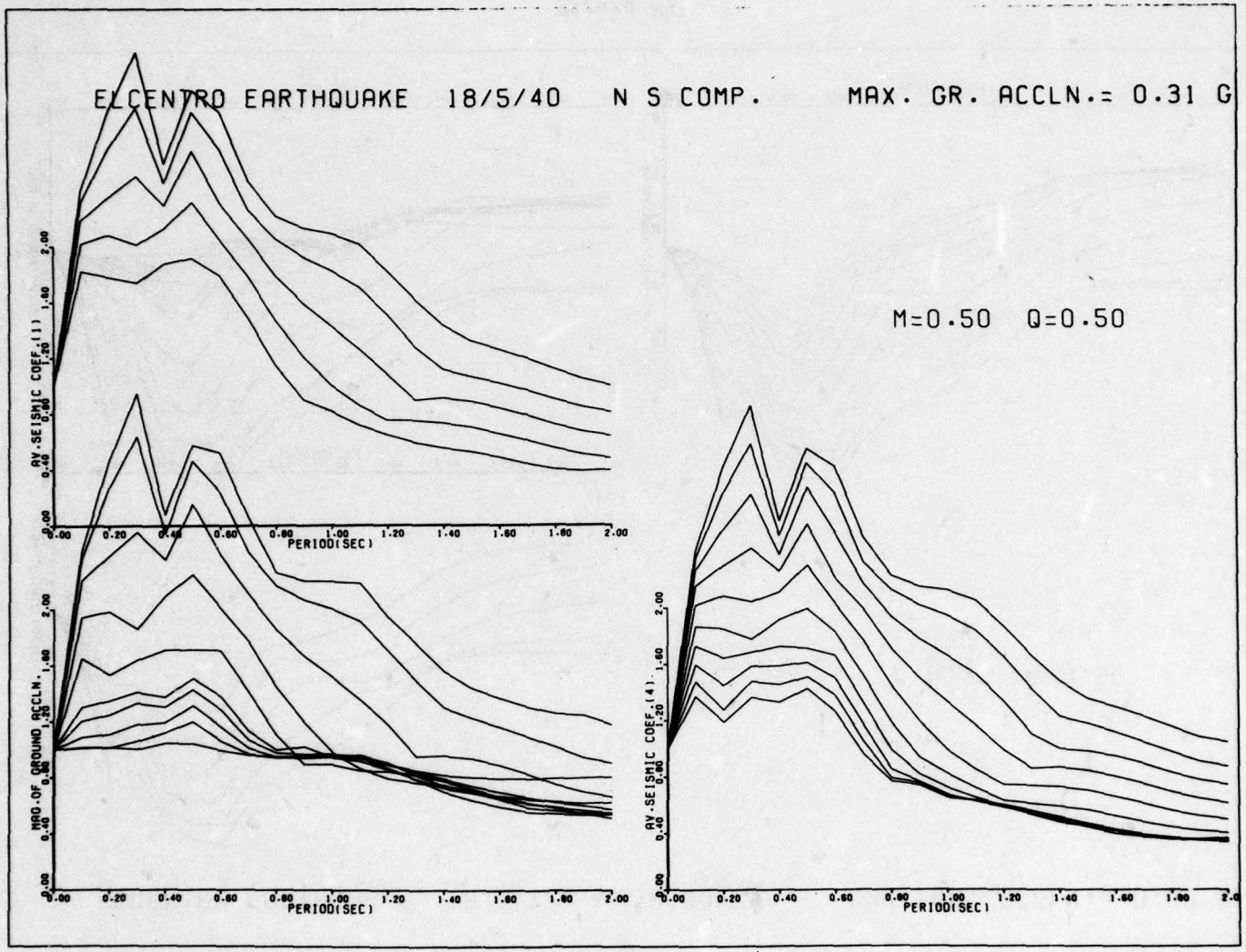
ELCENTRO EARTHQUAKE 18/5/40 N S COMP.
MAX. GR. ACCLN.= 0.31 G
M=0.50 Q=0.50
AV.SEISMIC COEF.(1)
MAG.OF GROUND ACCLN.
AV.SEISMIC COEF.(4)
PERIOD(SEC)

Figure E40

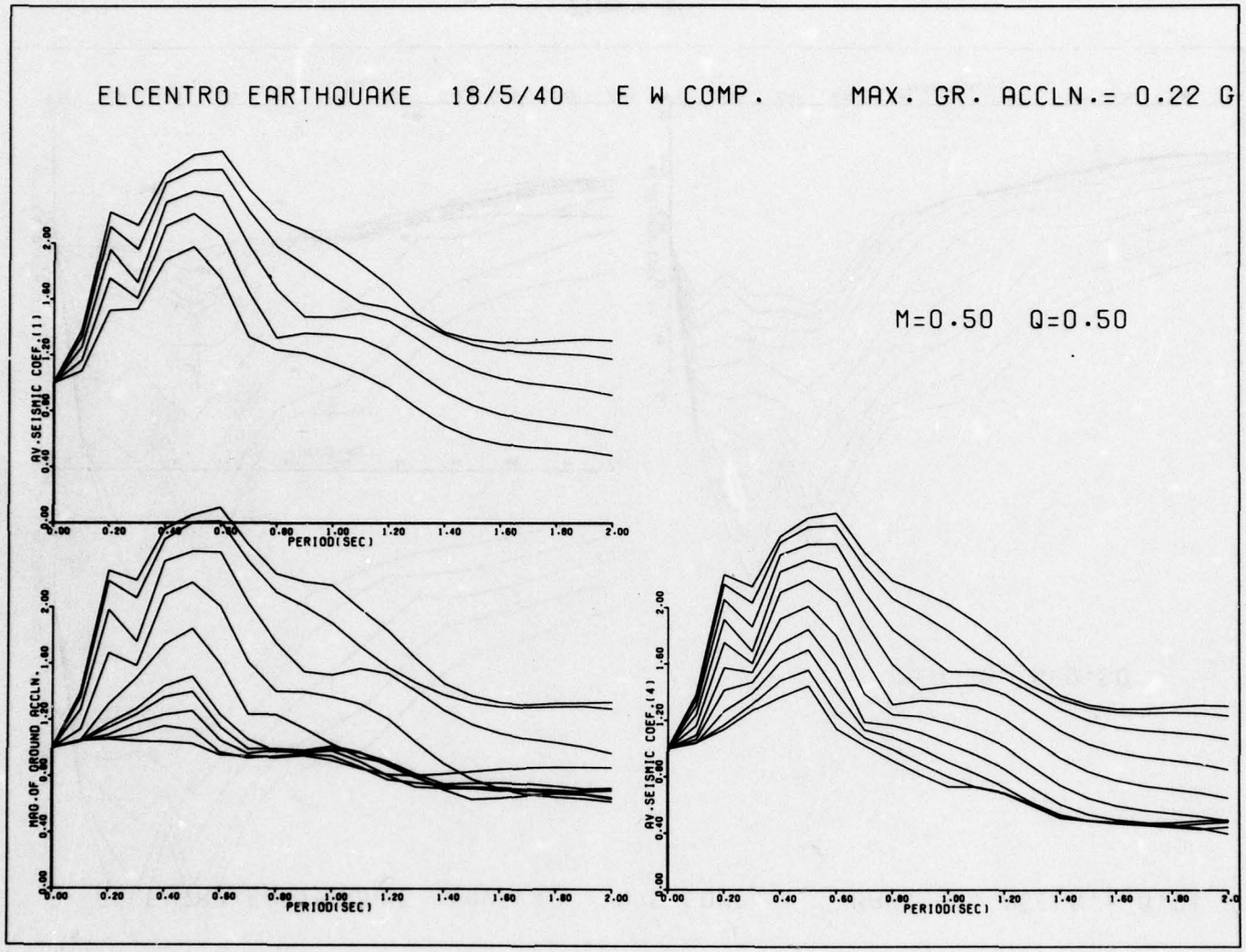
ELCENTRO EARTHQUAKE 18/5/40 E W COMP.
MAX. GR. ACCLN.= 0.22 G
M=0.50 Q=0.50
AV.SEISMIC COEF.(1)
MAG.OF GROUND ACCLN.
AV.SEISMIC COEF.(4)
PERIOD(SEC)
0.00
0.20
0.40
0.60
0.80
1.00
1.20
1.40
1.60
1.80
2.00

Figure E41

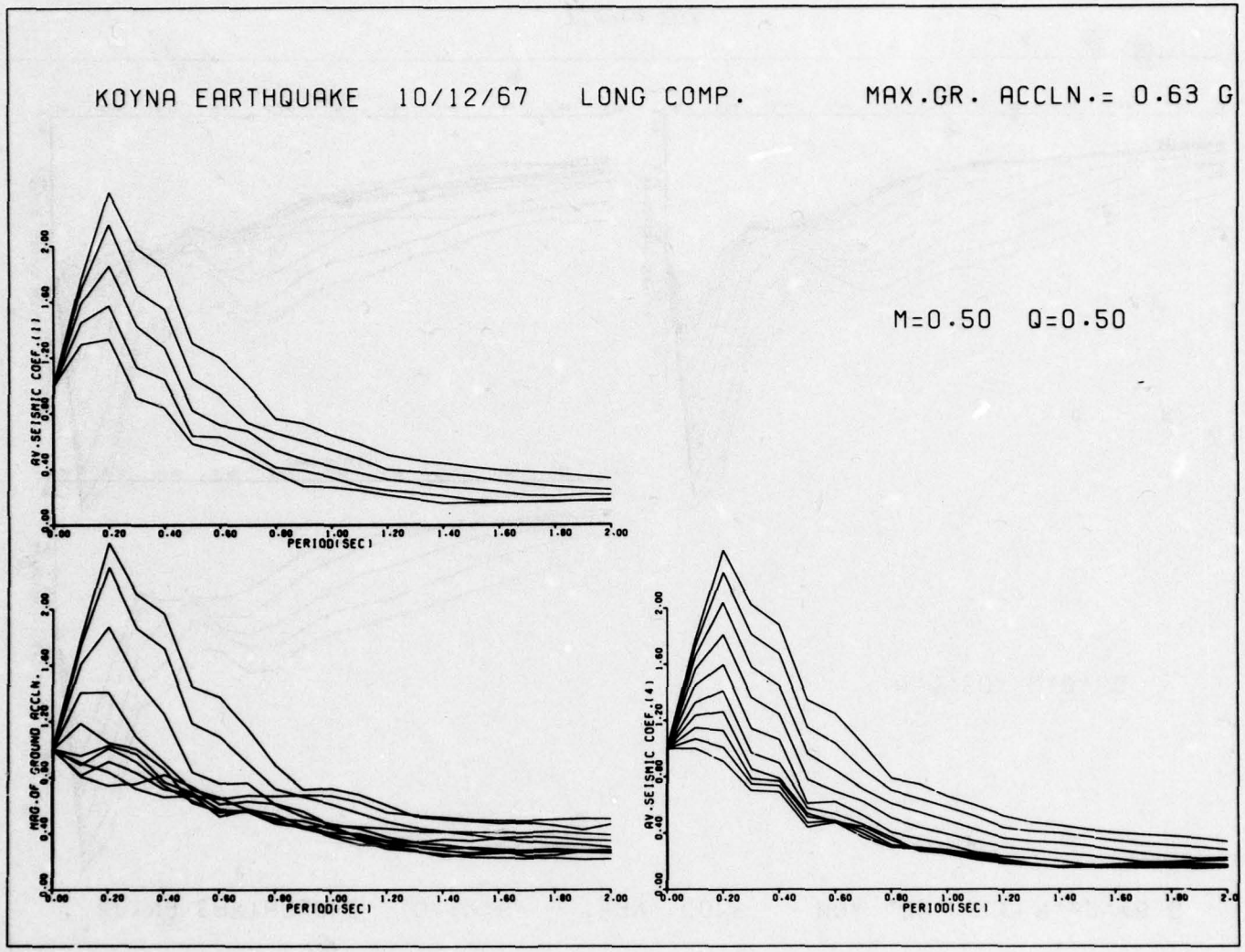
KOYNA EARTHQUAKE 10/12/67 LONG COMP.
MAX.GR. ACCLN.= 0.63 G
M=0.50 Q=0.50
AV.SEISMIC COEF.(1)
PERIOD(SEC)
MAG-OF GROUND ACCLN.
PERIOD(SEC)
AV.SEISMIC COEF.(4)
PERIOD(SEC)

Figure E42

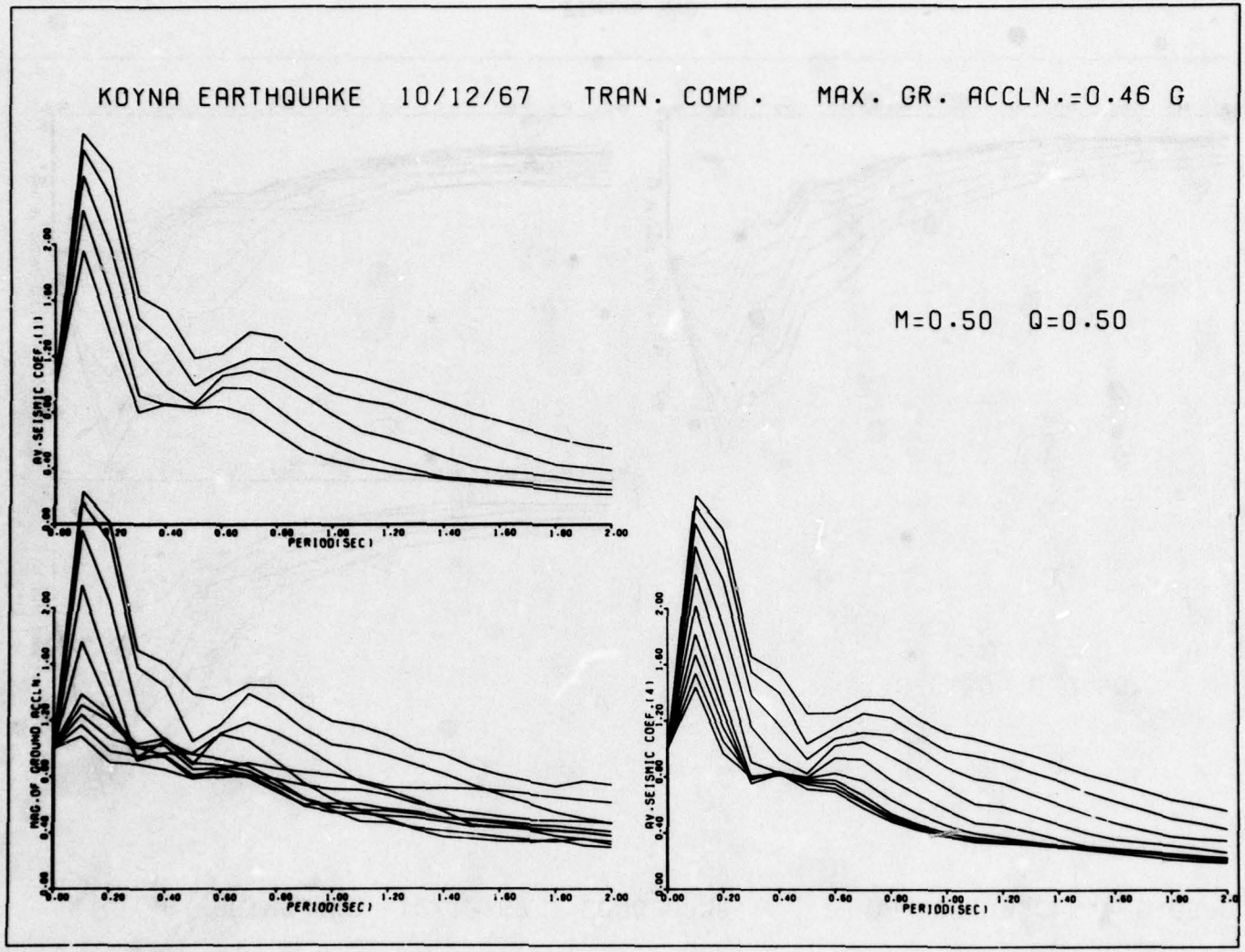
KOYNA EARTHQUAKE 10/12/67 TRAN. COMP. MAX. GR. ACCLN.=0.46 G
M=0.50 Q=0.50
AV.SEISMIC COEF.(1)
MAG.OF GROUND ACCLN.
AV.SEISMIC COEF.(4)
PERIOD(SEC)

Figure E43

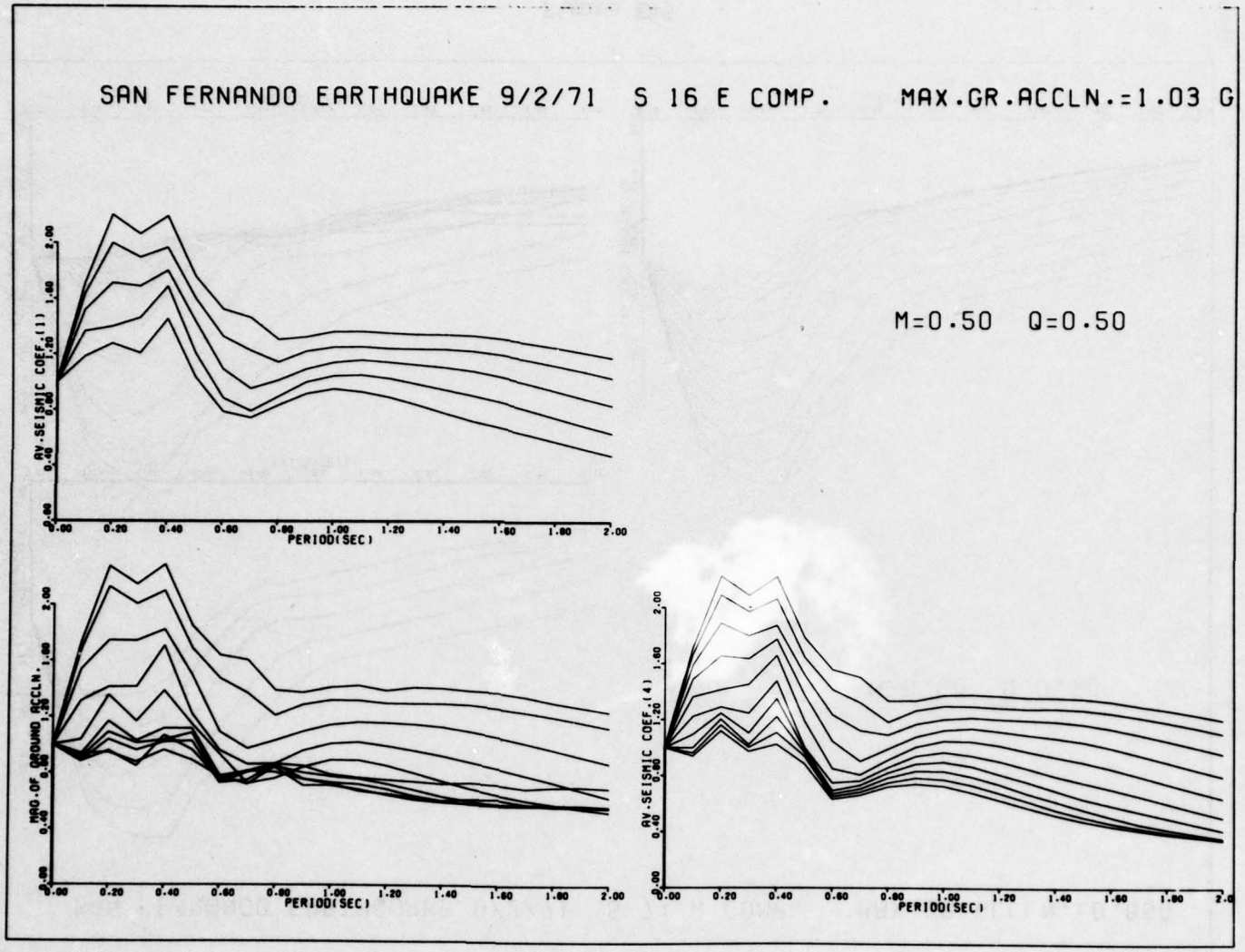
SAN FERNANDO EARTHQUAKE 9/2/71 S 16 E COMP. MAX.GR.ACCLN.=1.03 G
M=0.50 Q=0.50
AV.SEISMIC COEF.(1)
PERIOD(SEC)
MAG.OF GROUND ACCLN.
PERIOD(SEC)
AV.SEISMIC COEF.(4)
PERIOD(SEC)

Figure E44

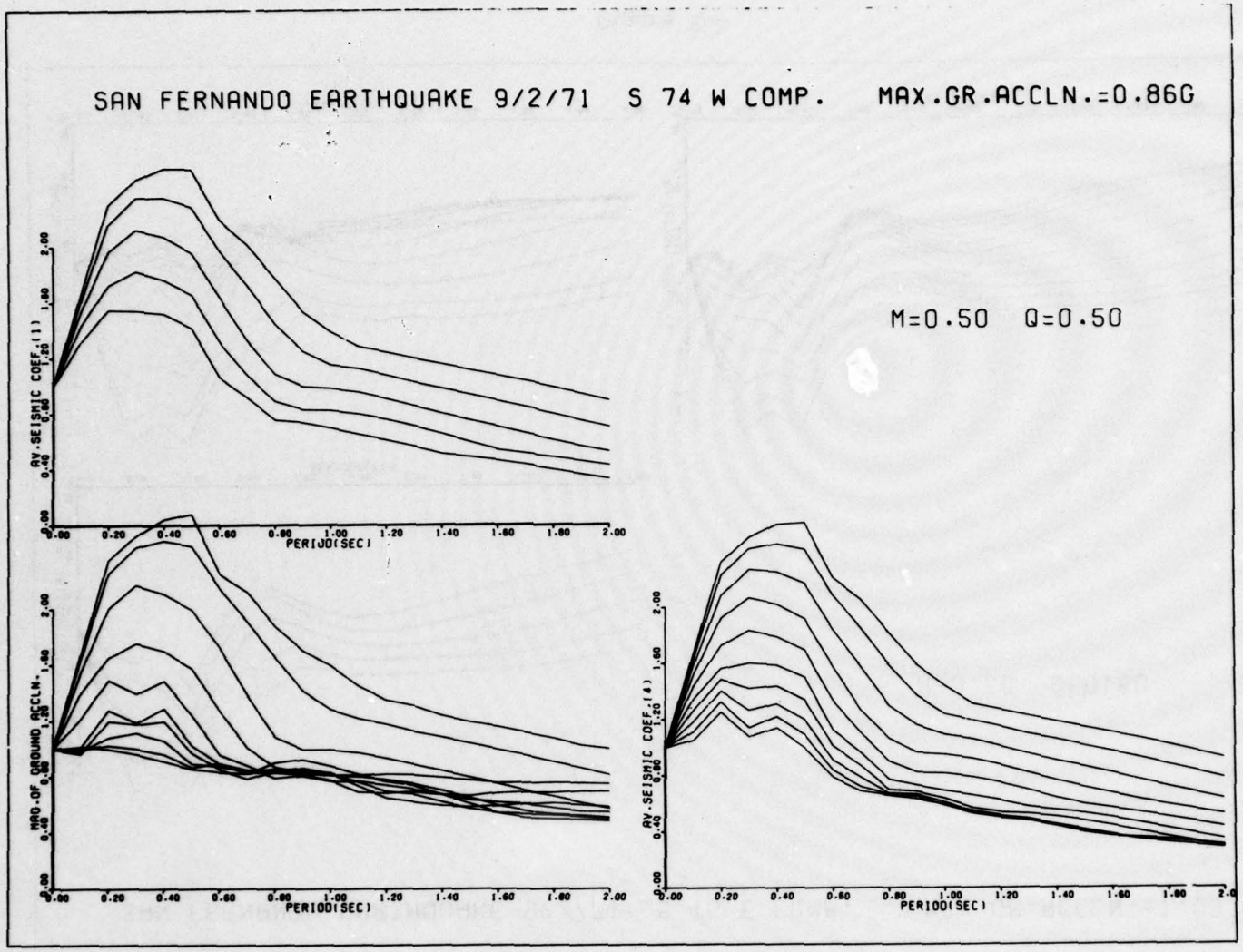
SAN FERNANDO EARTHQUAKE 9/2/71 S 74 W COMP. MAX.GR.ACCLN.=0.86G
M=0.50 Q=0.50
AV.SEISMIC COEF.(1)
PERIOD(SEC)
MAG.OF GROUND ACCLN.
PERIOD(SEC)
AV.SEISMIC COEF.(4)
PERIOD(SEC)

Figure E45

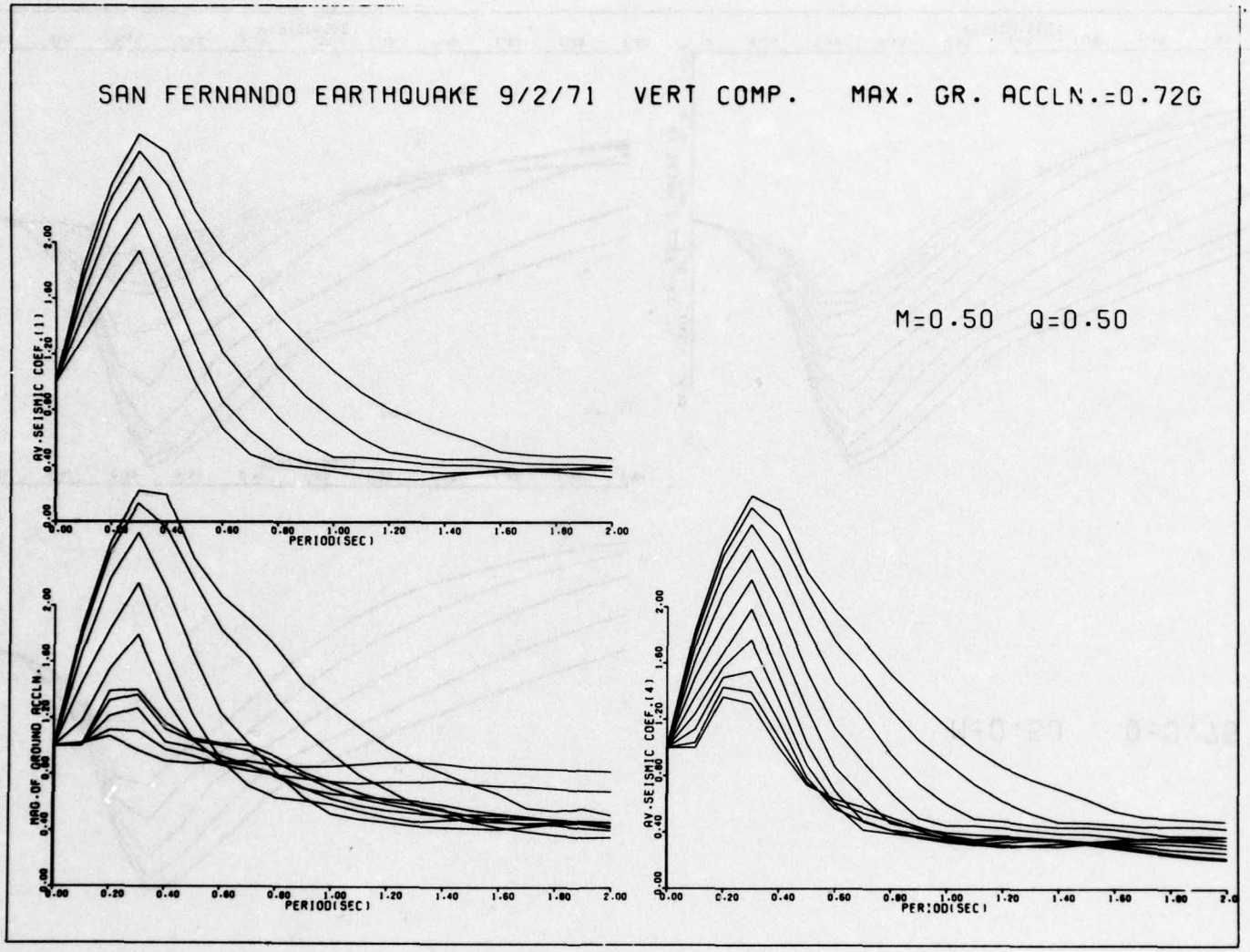
SAN FERNANDO EARTHQUAKE 9/2/71 VERT COMP. MAX. GR. ACCLN.=0.72G
M=0.50 Q=0.50
AV.SEISMIC COEF.(1)
PERIOD(SEC)
MAG.OF GROUND ACCLN.
PERIOD(SEC)
AV.SEISMIC COEF.(4)
PERIOD(SEC)

Figure E46

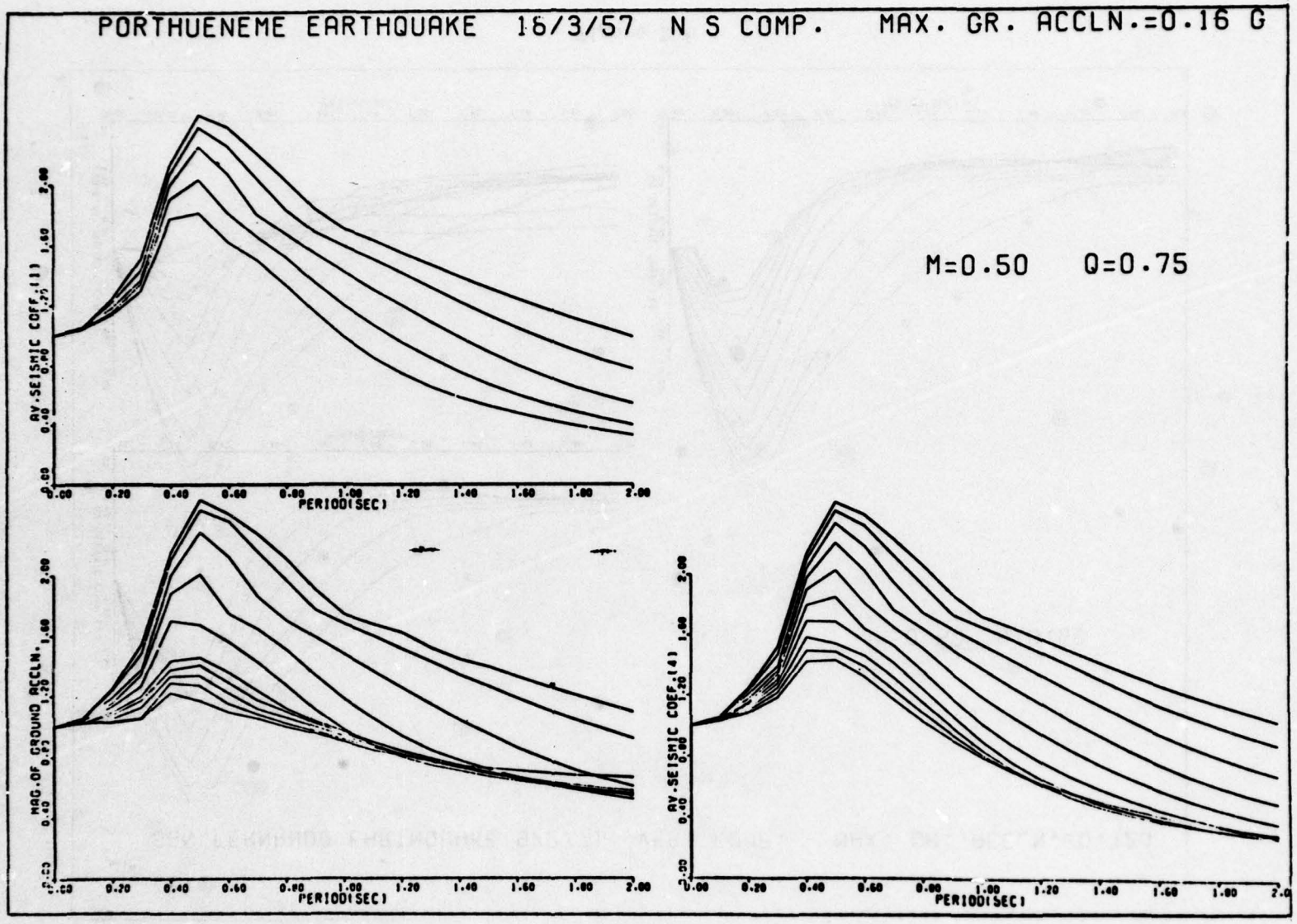
PORTHUENEME EARTHQUAKE 16/3/57 N S COMP. MAX. GR. ACCLN.=0.16 G
M=0.50 Q=0.75
AV.SEISMIC COEF.(I)
MAG.OF GROUND ACCLN.
AV.SEISMIC COEF.(A)
PERIOD(SEC)

Figure E47

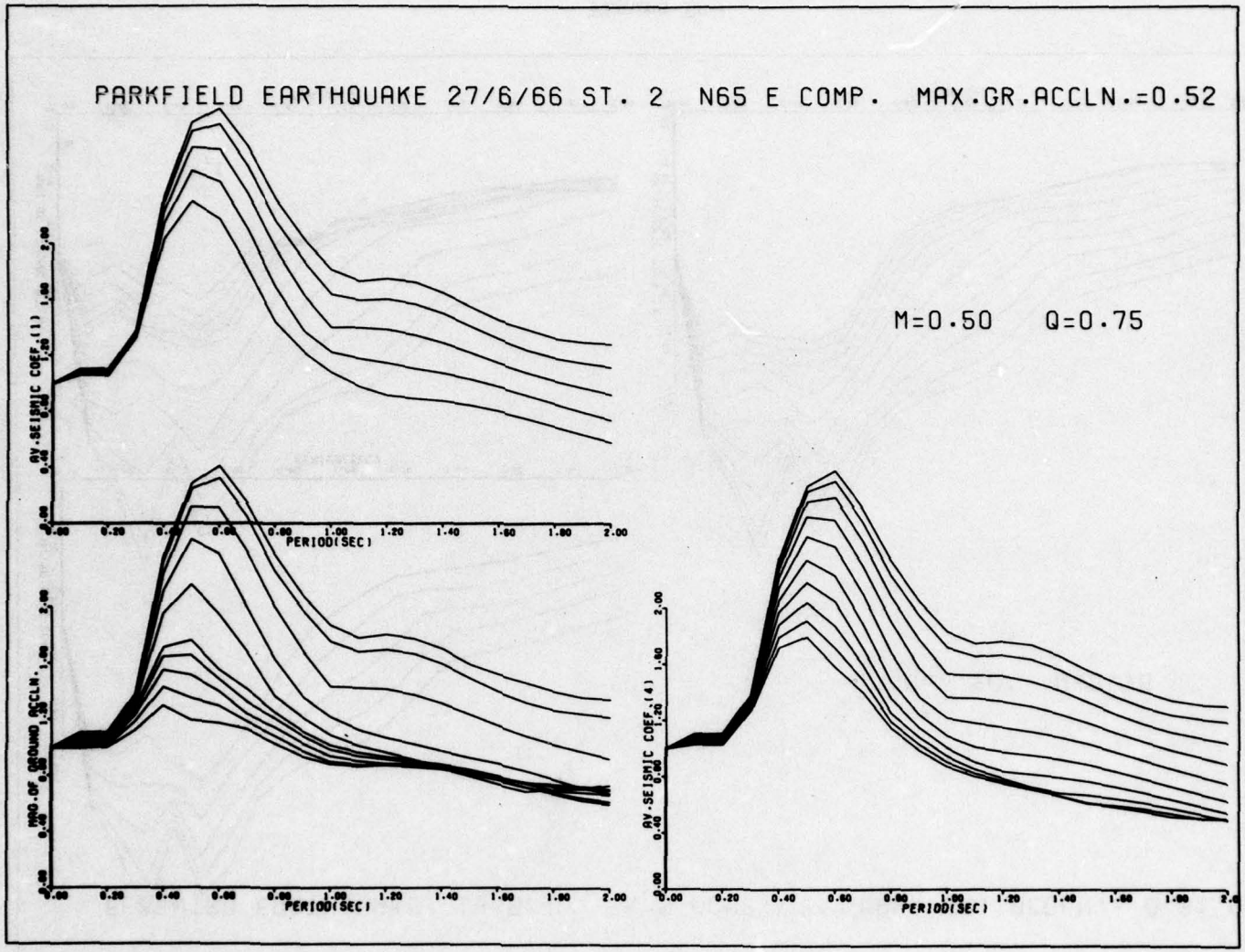
PARKFIELD EARTHQUAKE 27/6/66 ST. 2 N65 E COMP. MAX.GR.ACCLN.=0.52
M=0.50 Q=0.75
AV.SEISMIC COEF.(1)
PERIOD(SEC)
RAD.OF GROUND ACCLN.
PERIOD(SEC)
AV.SEISMIC COEF.(4)
PERIOD(SEC)

Figure E48

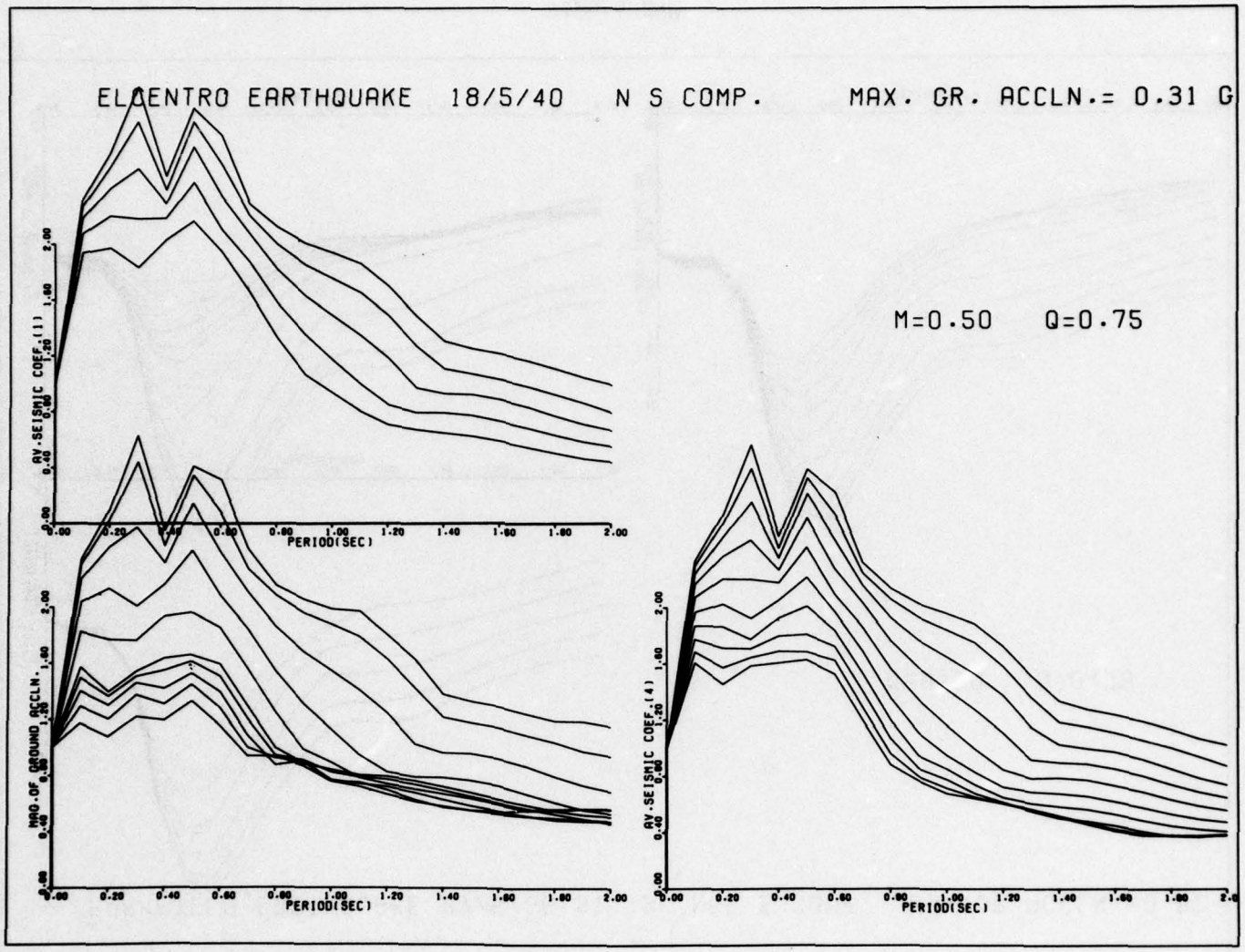
ELCENTRO EARTHQUAKE 18/5/40 N S COMP.
MAX. GR. ACCLN.= 0.31 G
M=0.50 Q=0.75
AV.SEISMIC COEF.(1)
PERIOD(SEC)
AV.SEISMIC COEF.(4)
PERIOD(SEC)
NRO.OF GROUND ACCLN.
PERIOD(SEC)

Figure E49

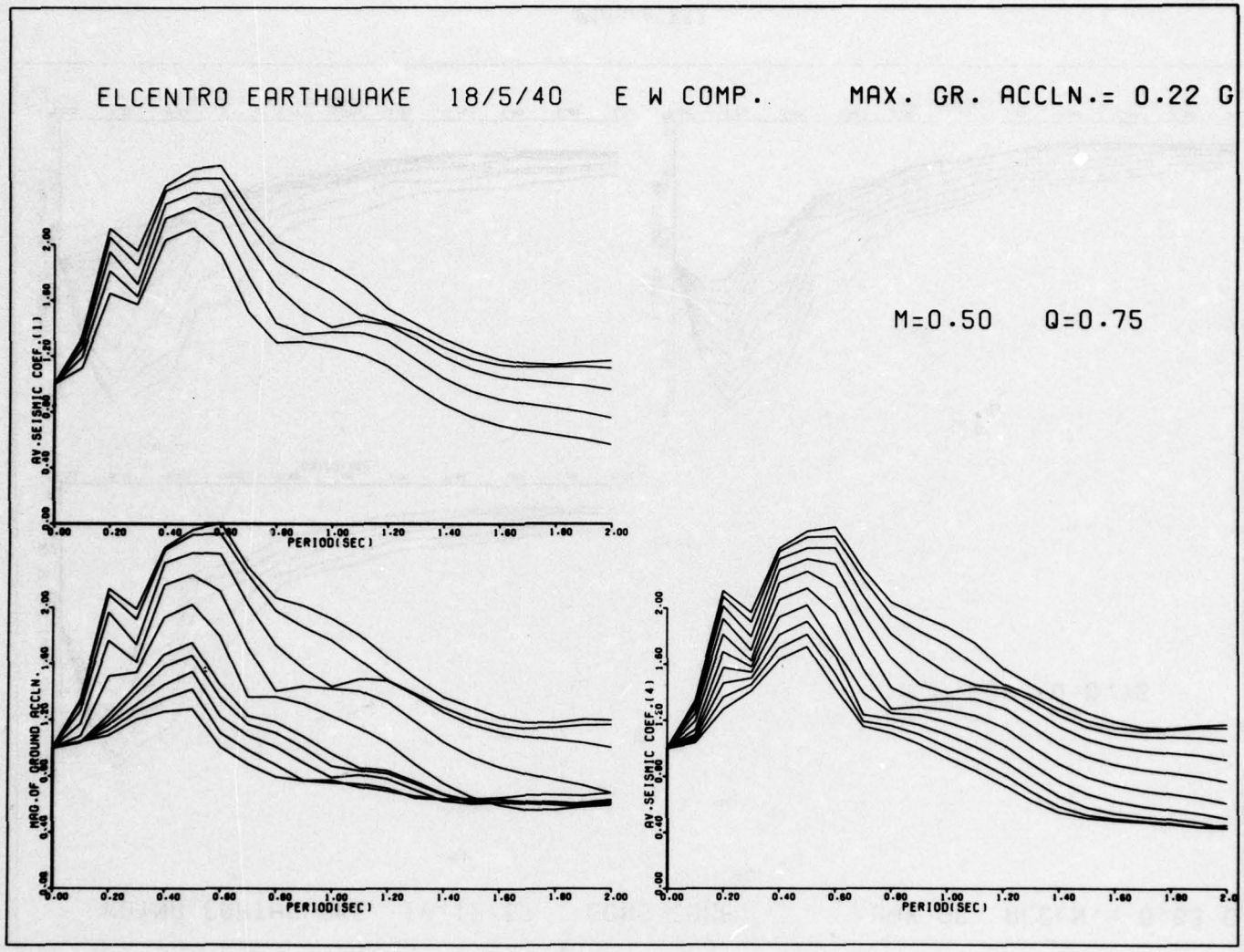
ELCENTRO EARTHQUAKE 18/5/40 E W COMP.
MAX. GR. ACCLN.= 0.22 G
M=0.50 Q=0.75
AV.SEISMIC COEF.(1)
PERIOD(SEC)
NRO.OF GROUND ACCLN.
PERIOD(SEC)
AV.SEISMIC COEF.(4)
PERIOD(SEC)

Figure E50

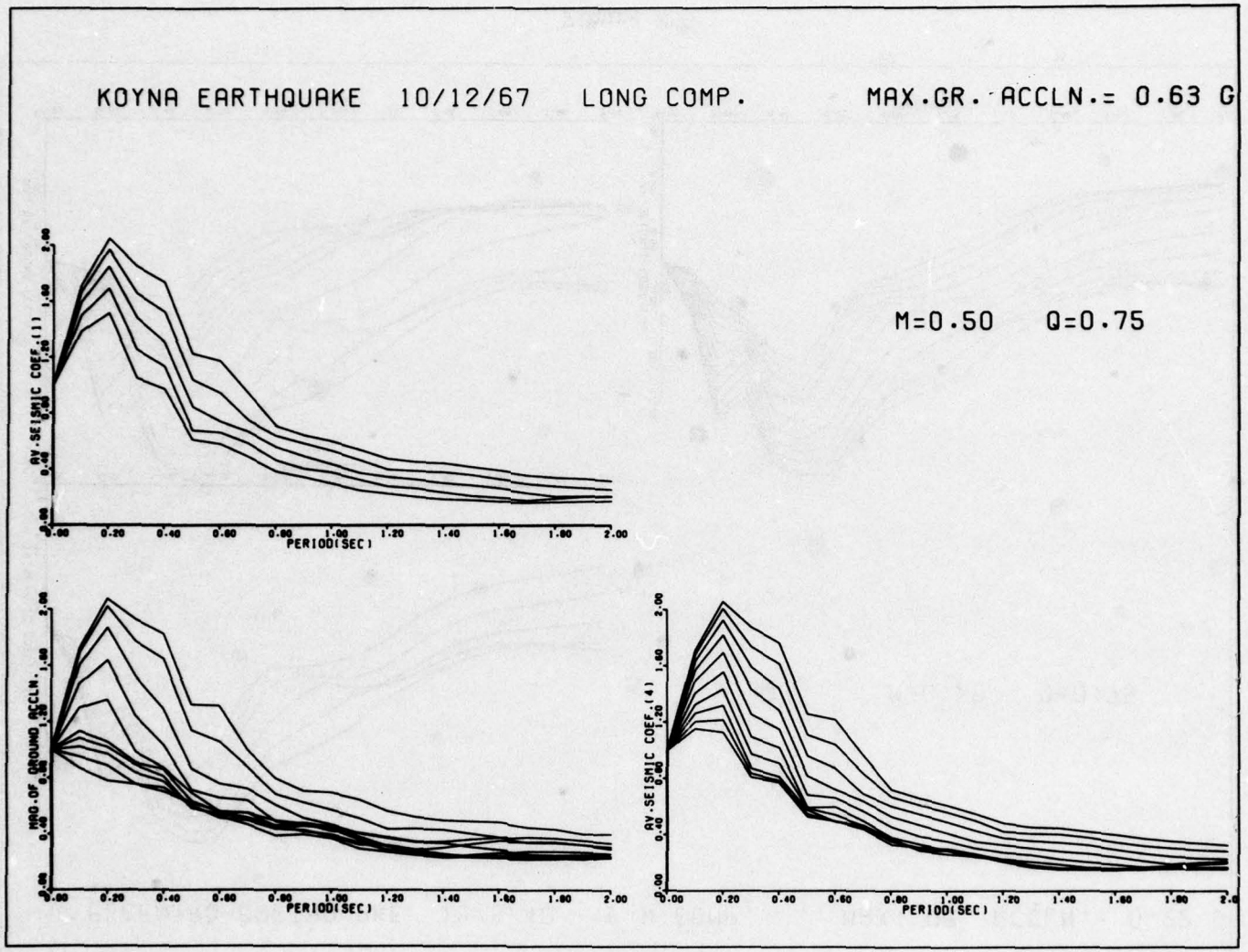
KOYNA EARTHQUAKE 10/12/67 LONG COMP.
MAX.GR. ACCLN.= 0.63 G
M=0.50 Q=0.75
AV.SEISMIC COEF.(1)
PERIOD(SEC)
MAG.OF GROUND ACCLN.
PERIOD(SEC)
AV.SEISMIC COEF.(4)
PERIOD(SEC)

Figure E51

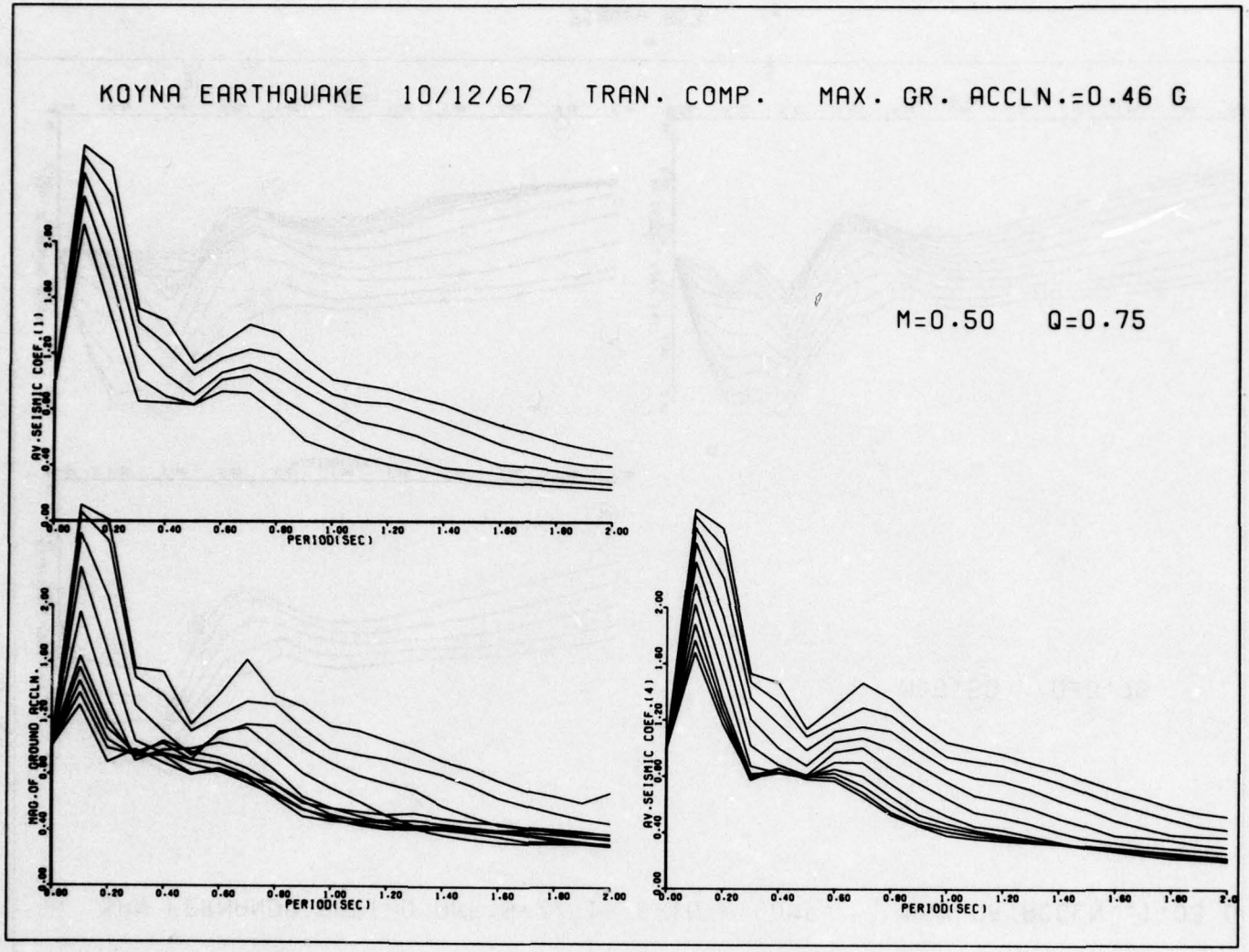
KOYNA EARTHQUAKE 10/12/67 TRAN. COMP. MAX. GR. ACCLN.=0.46 G
M=0.50 Q=0.75
AV.SEISMIC COEF.(1)
NRO.OF GROUND ACCLN.
AV.SEISMIC COEF.(4)
PERIOD(SEC)

Figure E52

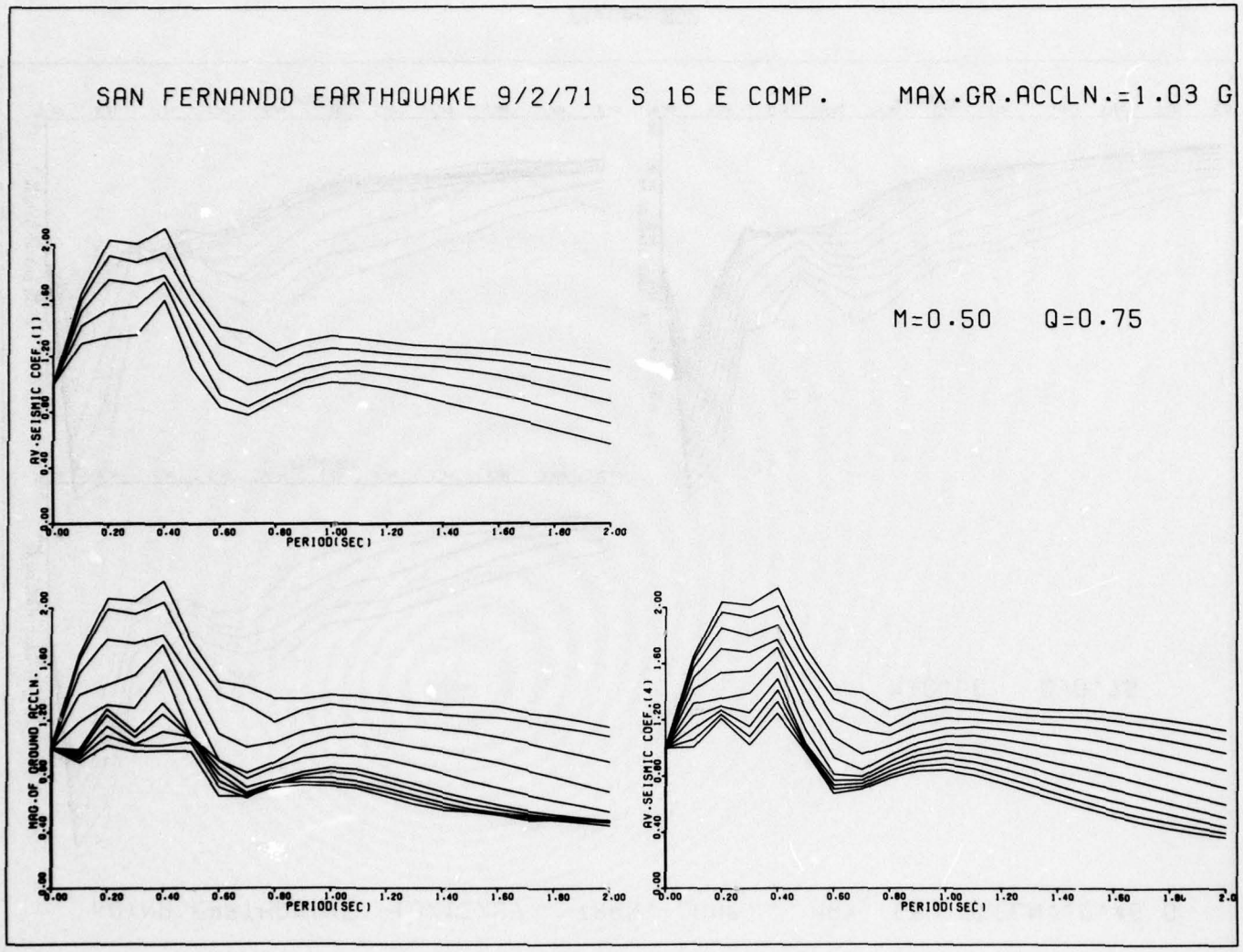
SAN FERNANDO EARTHQUAKE 9/2/71 S 16 E COMP.
MAX.GR.ACCLN.=1.03 G
M=0.50 Q=0.75
AV.SEISMIC COEF.(1)
MAG.OF GROUND ACCLN.
AV.SEISMIC COEF.(4)
PERIOD(SEC)
PERIOD(SEC)
PERIOD(SEC)

Figure E53

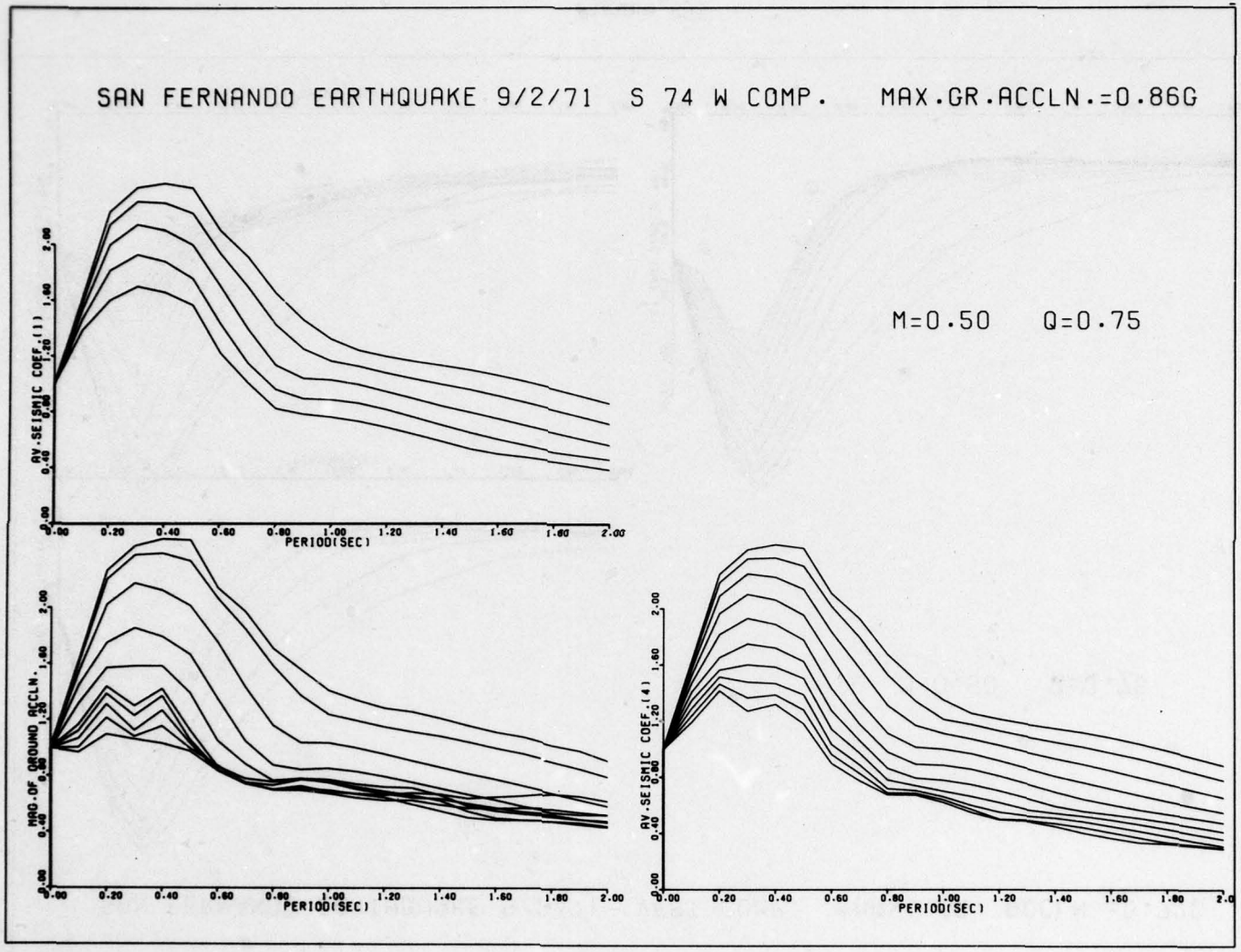
SAN FERNANDO EARTHQUAKE 9/2/71 S 74 W COMP. MAX.GR.ACCLN.=0.86G
M=0.50 Q=0.75
AV.SEISMIC COEF.(1)
PERIOD(SEC)
MAG.OF GROUND ACCLN.
PERIOD(SEC)
AV.SEISMIC COEF.(4)
PERIOD(SEC)

Figure E54

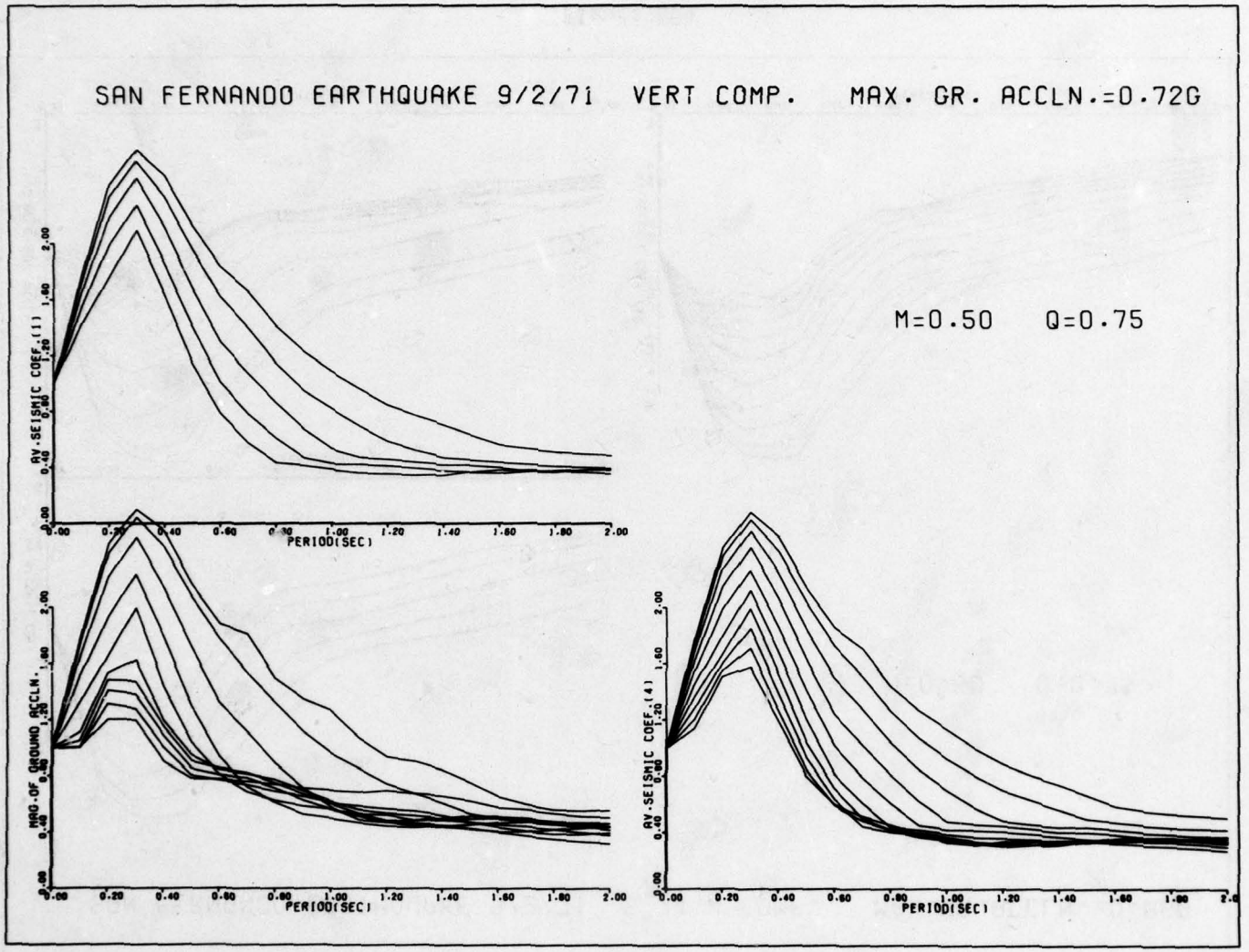
SAN FERNANDO EARTHQUAKE 9/2/71 VERT COMP. MAX. GR. ACCLN.=0.72G
M=0.50 Q=0.75
AV.SEISMIC COEF.(1)
AV.SEISMIC COEF.(4)
PERIOD(SEC)

Figure E55

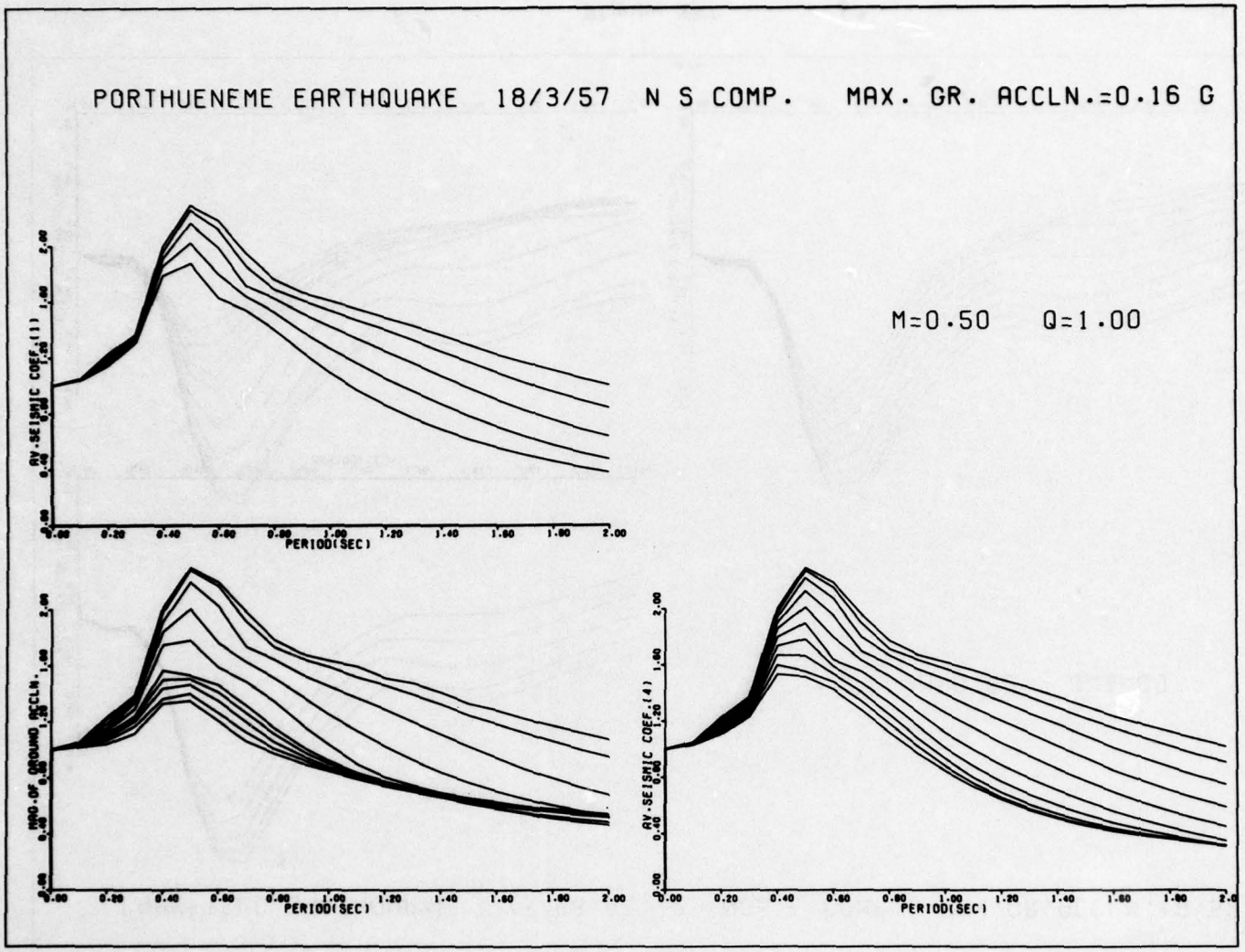
PORTHUENEME EARTHQUAKE 18/3/57 N S COMP. MAX. GR. ACCLN.=0.16 G
M=0.50 Q=1.00
AV.SEISMIC COEF.(1)
PERIOD(SEC)
RMS-OF GROUND ACCLN.
PERIOD(SEC)
AV.SEISMIC COEF.(4)
PERIOD(SEC)

Figure E56

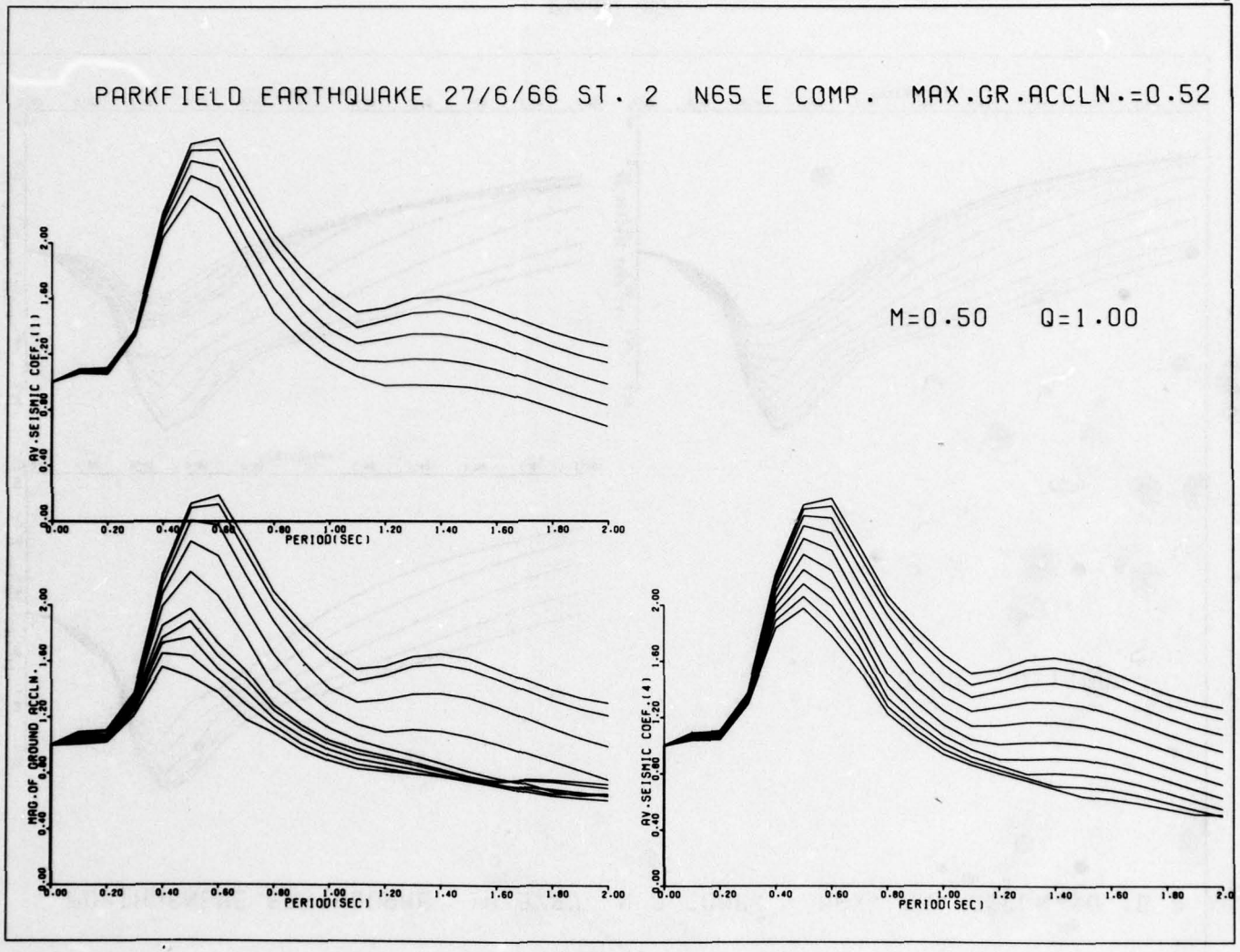
PARKFIELD EARTHQUAKE 27/6/66 ST. 2 N65 E COMP. MAX.GR.ACCLN.=0.52
M=0.50 Q=1.00
AV.SEISMIC COEF.(1)
MAG.OF GROUND ACCLN.
AV.SEISMIC COEF.(4)
PERIOD(SEC)
0.00
0.20
0.40
0.60
0.80
1.00
1.20
1.40
1.60
1.80
2.00

Figure E57

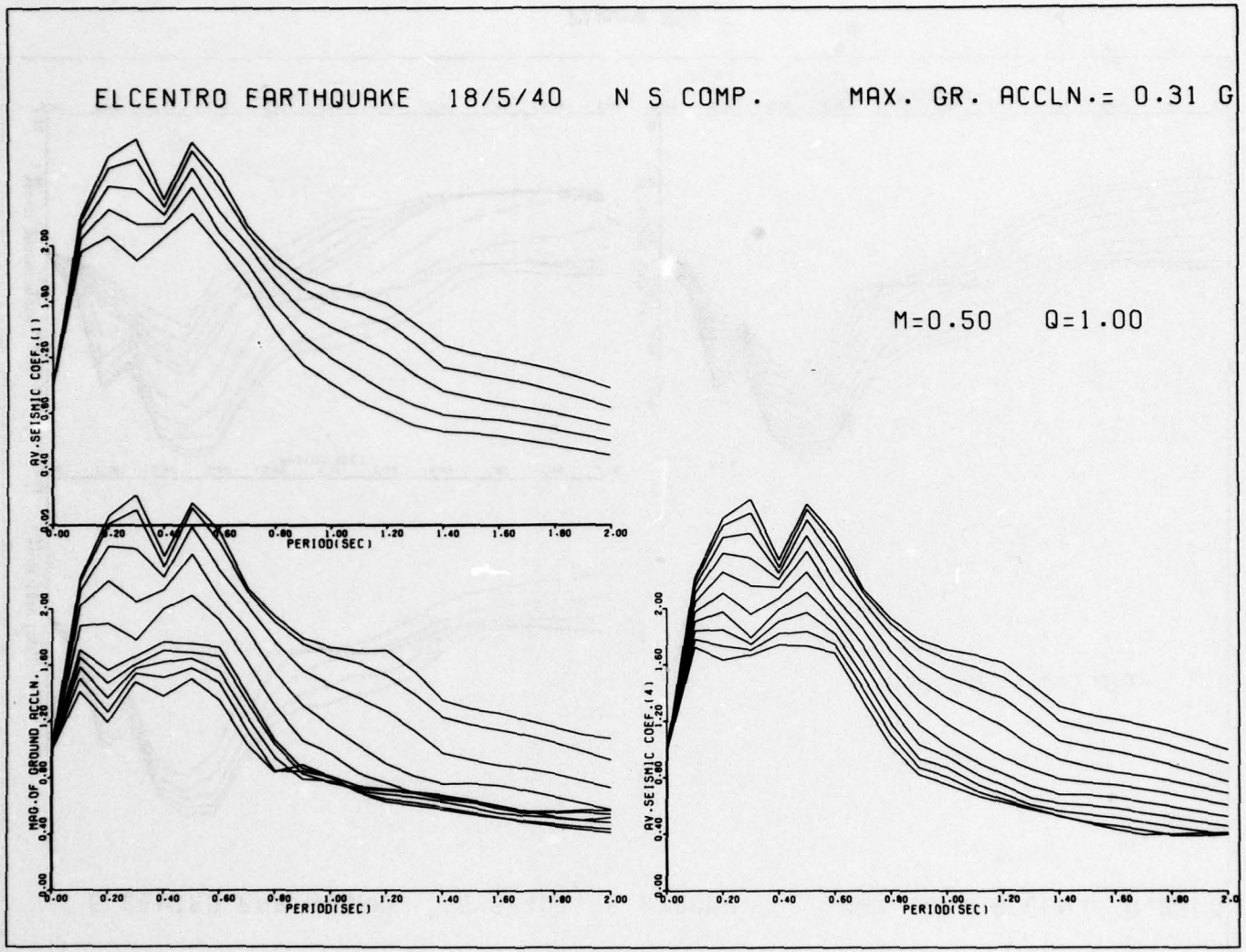
ELCENTRO EARTHQUAKE 18/5/40 N S COMP.
MAX. GR. ACCLN.= 0.31 G
M=0.50 Q=1.00
AV.SEISMIC COEF.(1)
PERIOD(SEC)
MAG.OF GROUND ACCLN.
PERIOD(SEC)
AV.SEISMIC COEF.(4)
PERIOD(SEC)

Figure E58

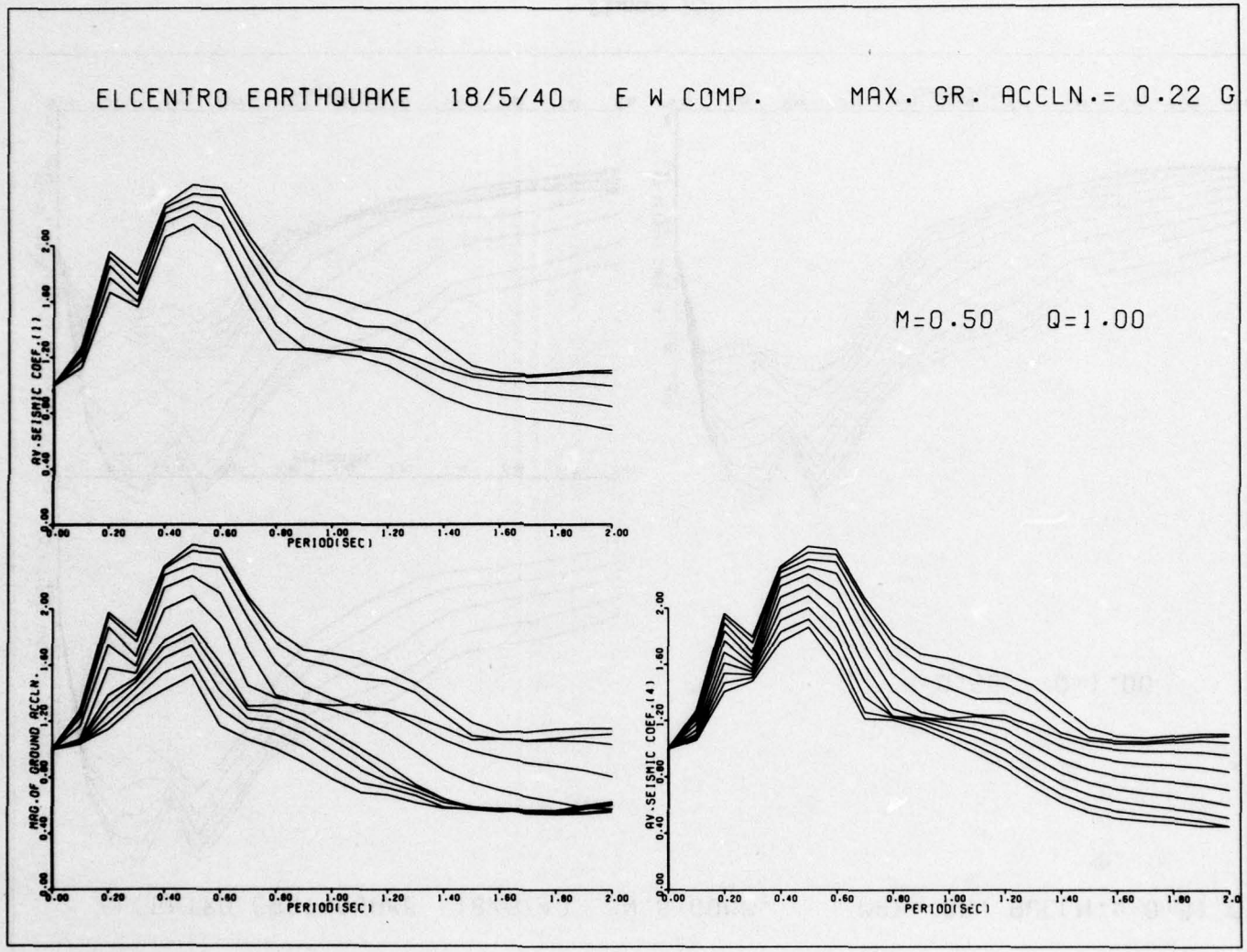
ELCENTRO EARTHQUAKE 18/5/40 E W COMP.
MAX. GR. ACCLN.= 0.22 G
M=0.50 Q=1.00
AV.SEISMIC COEF.(1)
MAG.OF GROUND ACCLN.
AV.SEISMIC COEF.(4)
PERIOD(SEC)
0.00
0.20
0.40
0.60
0.80
1.00
1.20
1.40
1.60
1.80
2.00

Figure E59

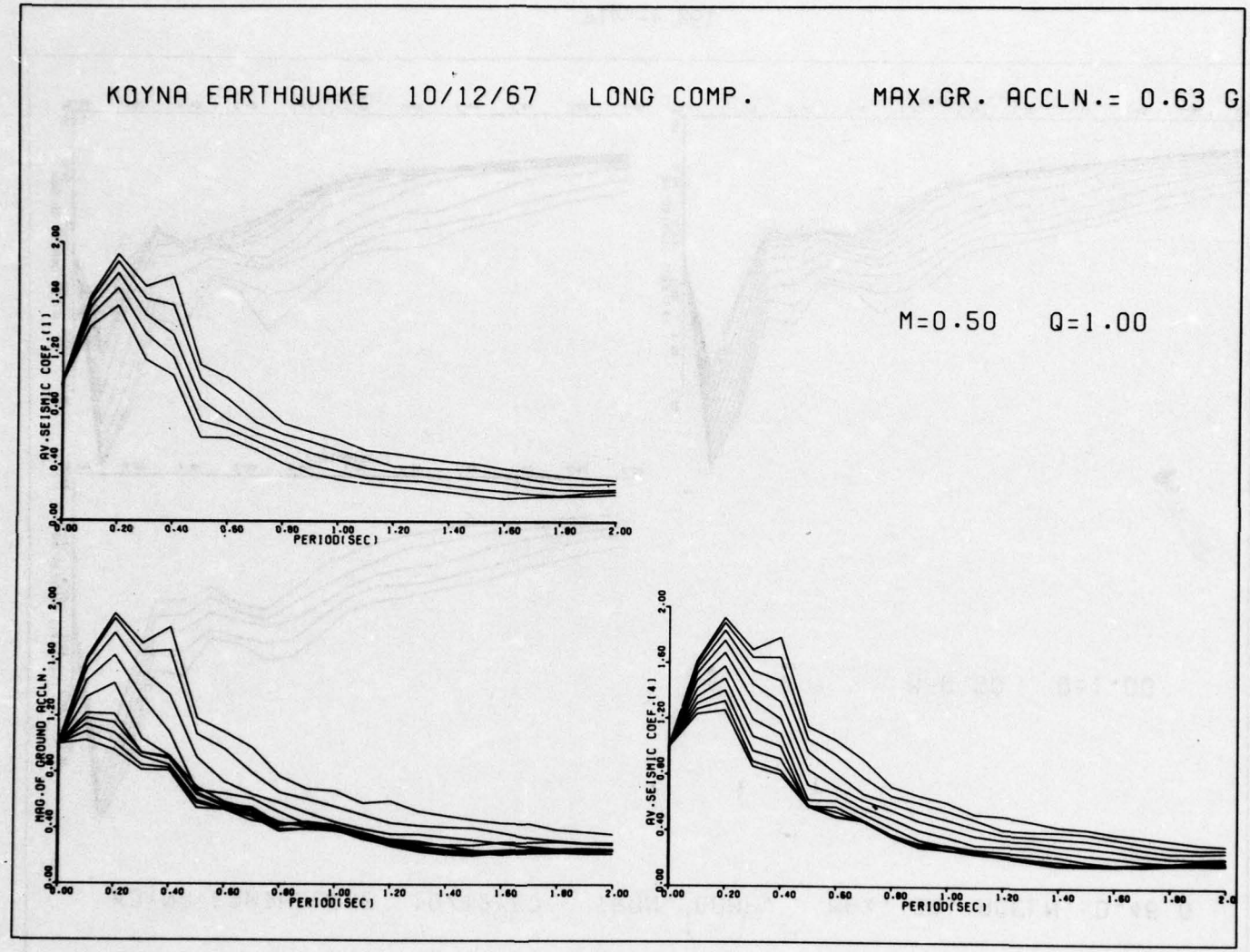
KOYNA EARTHQUAKE 10/12/67 LONG COMP.
MAX.GR. ACCLN.= 0.63 G
M=0.50 Q=1.00
AV.SEISMIC COEF.(1)
MAG.OF GROUND ACCLN.
AV.SEISMIC COEF.(4)
PERIOD(SEC)

Figure E60

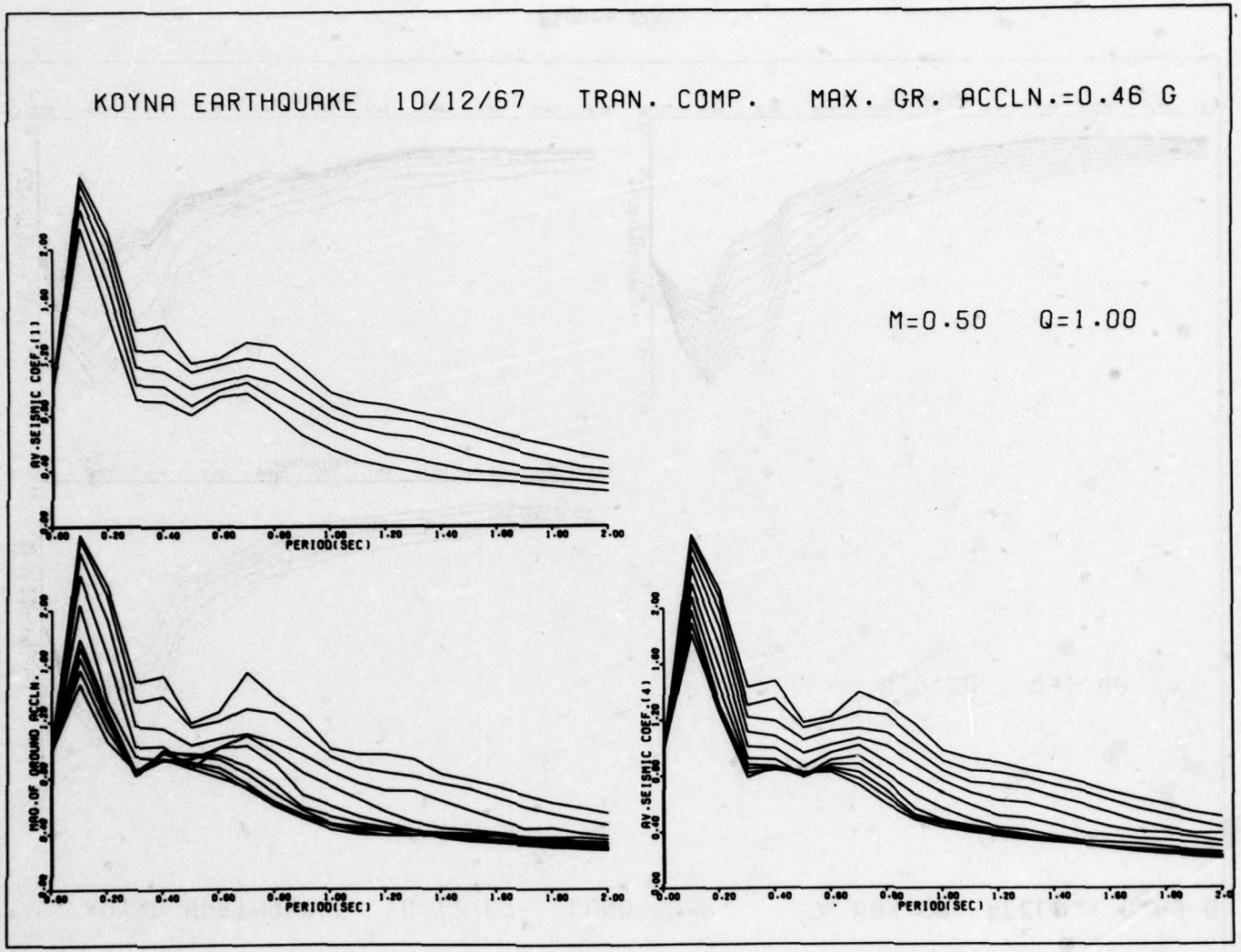
KOYNA EARTHQUAKE 10/12/67 TRAN. COMP. MAX. GR. ACCLN.=0.46 G
M=0.50 Q=1.00
AV.SEISMIC COEF.(1)
PERIOD(SEC)
NRD.OF GROUND ACCLN.
PERIOD(SEC)
AV.SEISMIC COEF.(4)
PERIOD(SEC)

Figure E61

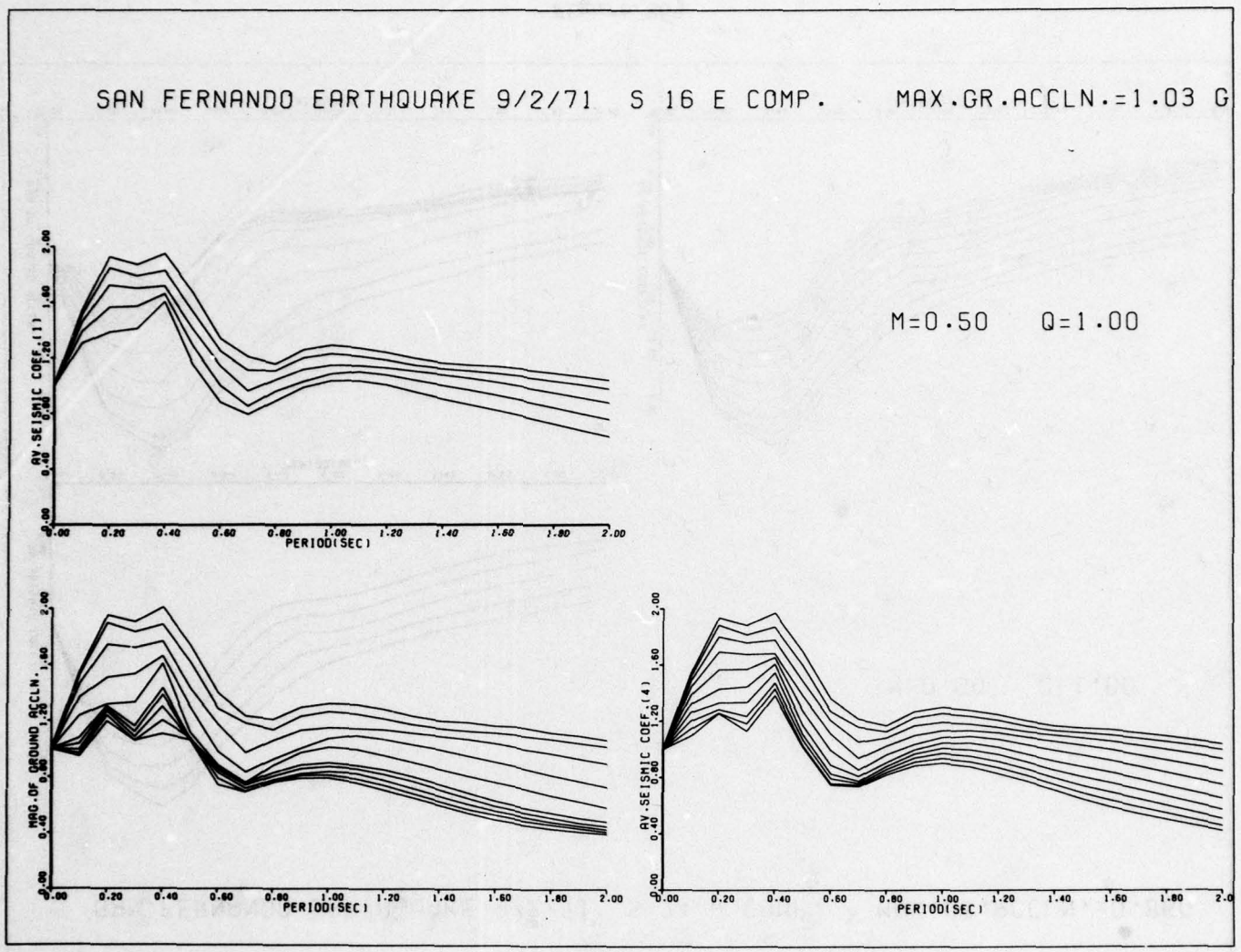
SAN FERNANDO EARTHQUAKE 9/2/71 S 16 E COMP.
MAX.GR.ACCLN.=1.03 G
M=0.50 Q=1.00
AV.SEISMIC COEF.(1)
MAG.OF GROUND ACCLN.
AV.SEISMIC COEF.(4)
PERIOD(SEC)

Figure E62

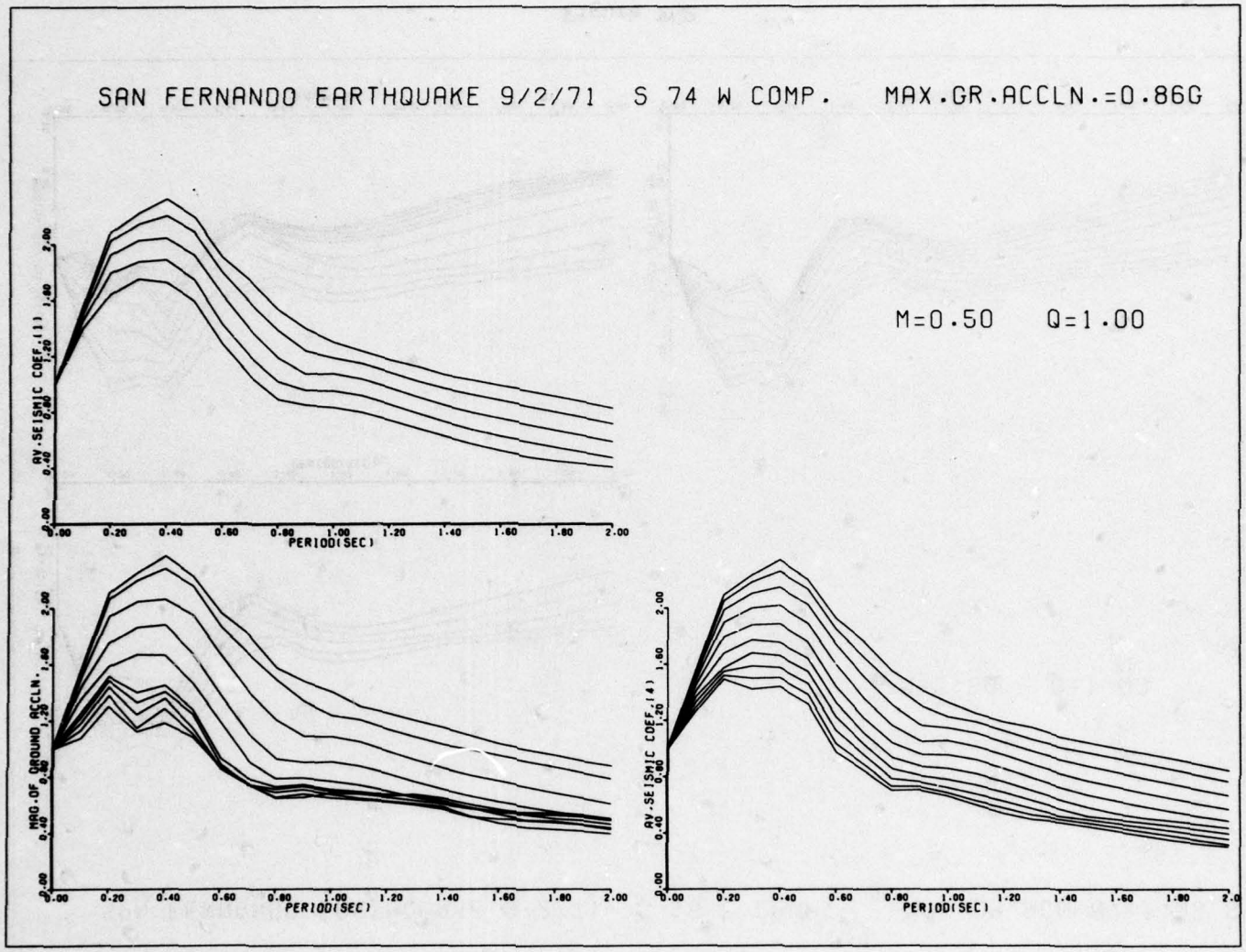
SAN FERNANDO EARTHQUAKE 9/2/71 S 74 W COMP. MAX.GR.ACCLN.=0.86G
M=0.50 Q=1.00
AV.SEISMIC COEF.(1)
MAG.OF GROUND ACCLN.
AV.SEISMIC COEF.(4)
PERIOD(SEC)
0.00
0.20
0.40
0.60
0.80
1.00
1.20
1.40
1.60
1.80
2.00

Figure E63

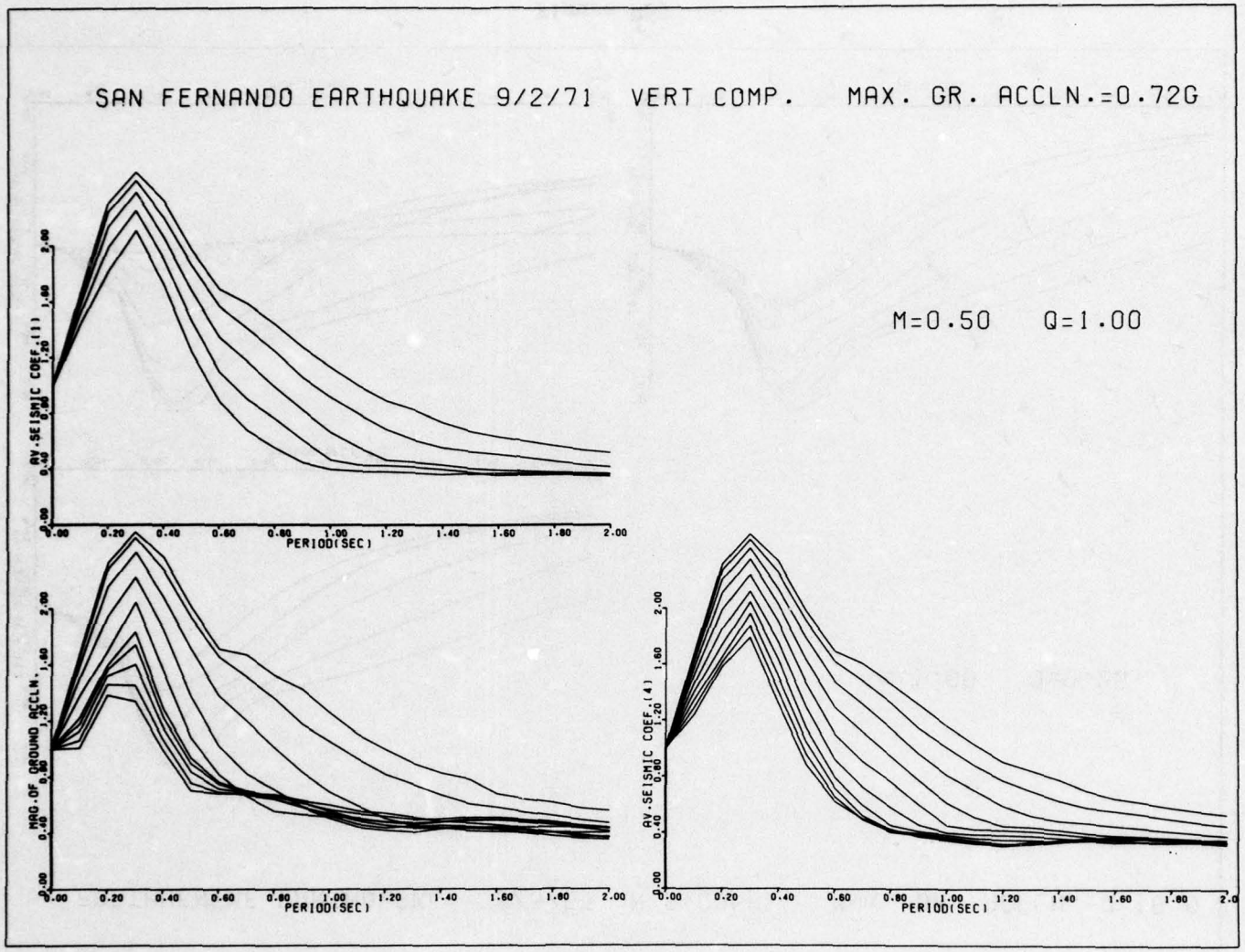
SAN FERNANDO EARTHQUAKE 9/2/71 VERT COMP. MAX. GR. ACCLN.=0.72G
M=0.50 Q=1.00
AV.SEISMIC COEF.(1)
MAG.OF GROUND ACCLN.
AV.SEISMIC COEF.(4)
PERIOD(SEC)

Figure E64

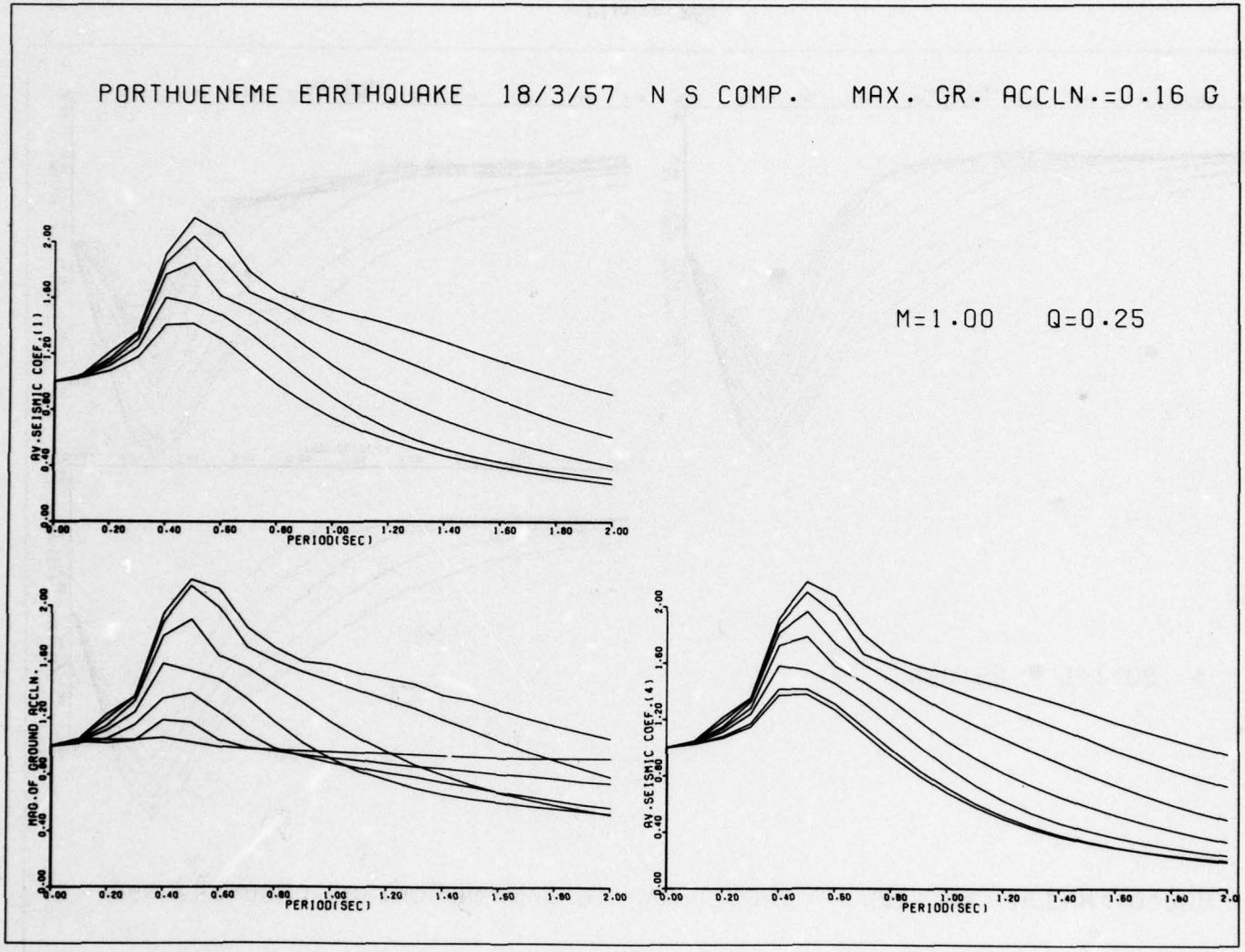
PORTHUENEME EARTHQUAKE 18/3/57 N S COMP. MAX. GR. ACCLN.=0.16 G
M=1.00 Q=0.25
AV.SEISMIC COEF.(1)
PERIOD(SEC)
MAG.OF GROUND ACCLN.
PERIOD(SEC)
AV.SEISMIC COEF.(4)
PERIOD(SEC)

Figure E65

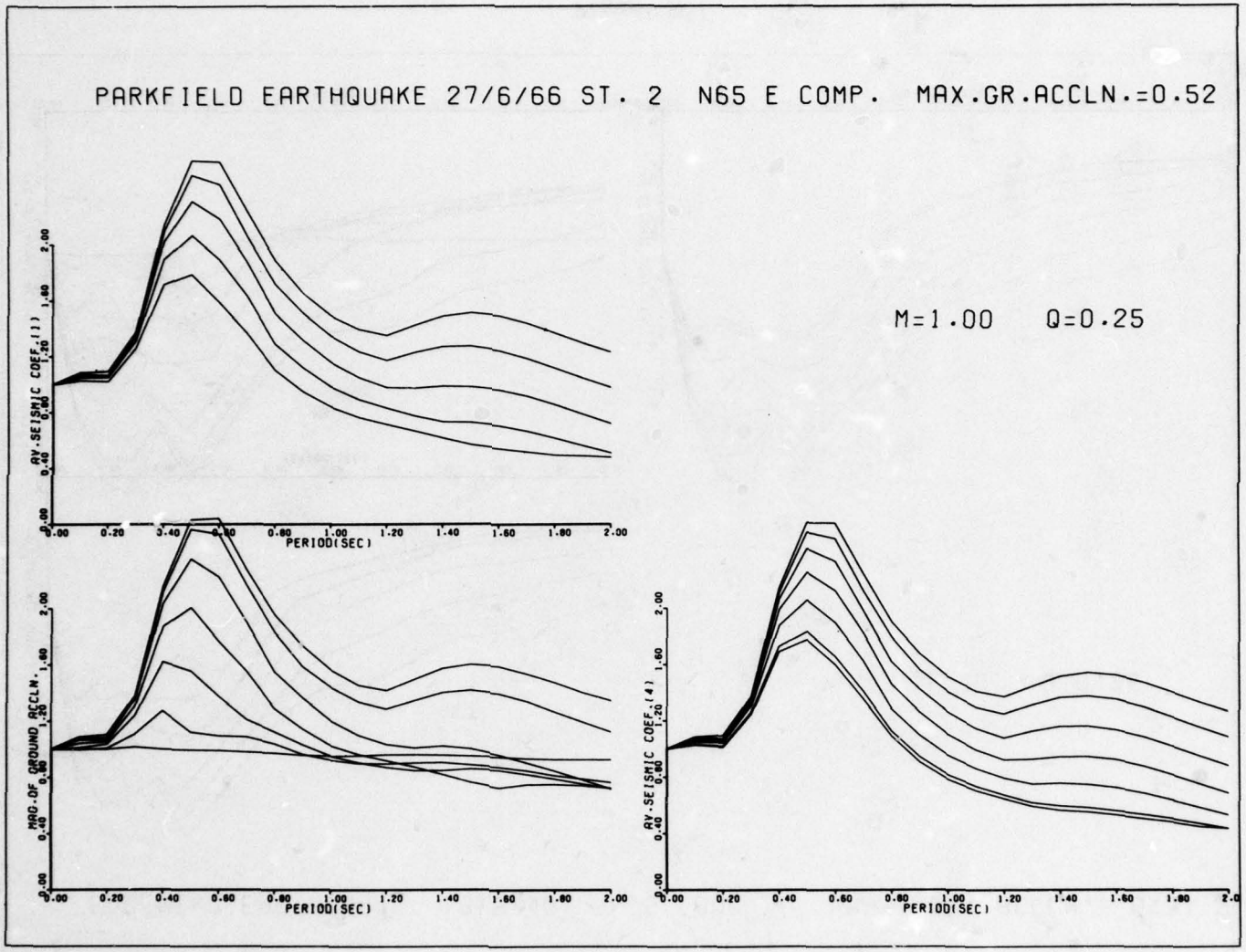
PARKFIELD EARTHQUAKE 27/6/66 ST. 2 N65 E COMP. MAX.GR.ACCLN.=0.52
M=1.00 Q=0.25
AV.SEISMIC COEF.(1)
MAG.OF GROUND ACCLN.
AV.SEISMIC COEF.(4)
PERIOD(SEC)
PERIOD(SEC)
PERIOD(SEC)

Figure E66

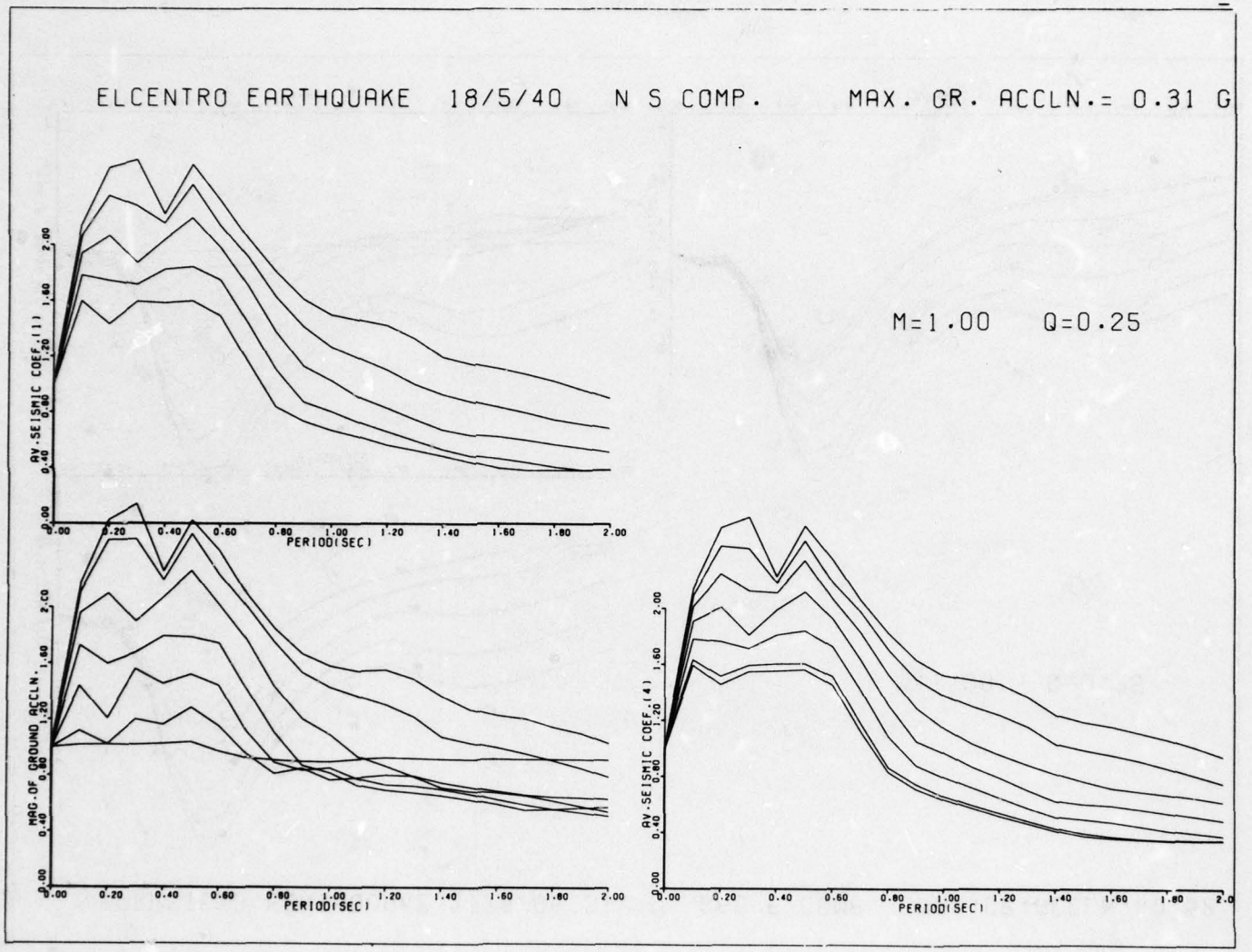
ELCENTRO EARTHQUAKE 18/5/40 N S COMP.
MAX. GR. ACCLN.= 0.31 G
M=1.00 Q=0.25
AV.SEISMIC COEF.(1)
MAG.OF GROUND ACCLN.
AV.SEISMIC COEF.(4)
PERIOD(SEC)

Figure E67

AD-A073 010 IMPERIAL COLL OF SCIENCE AND TECHNOLOGY LONDON (ENGLA--ETC F/G 13/2
RESPONSE AND STABILITY OF EARTH DAMS DURING STRONG EARTHQUAKES.(U)
JUN 79 S K SARMA DA-ERO-75-G-010

UNCLASSIFIED WES-MP-GL-79-13 NL

3 OF 3
AD
A073010

END
DATE
FILMED
10-79
DDC

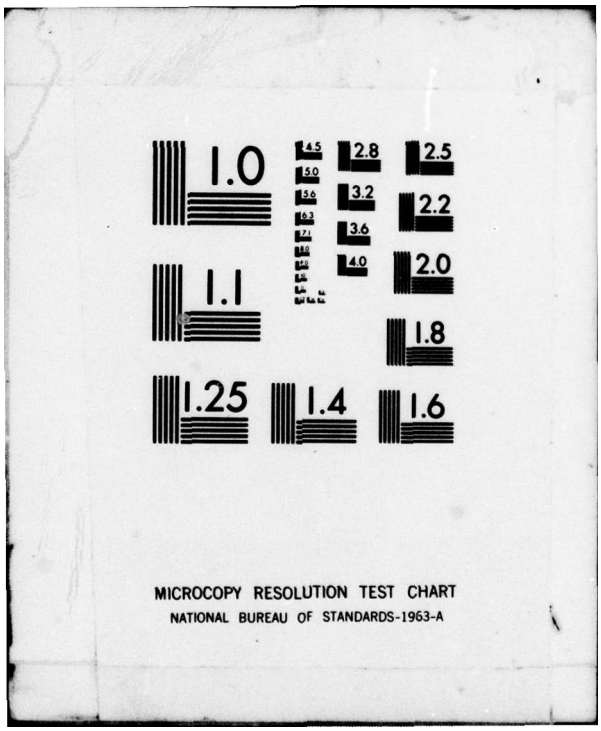
1.0
1.1
1.25
4.5
5.0
5.6
6.3
7.1
2.8
3.2
3.6
4.0
2.5
2.2
2.0
1.8
1.4
1.6
MICROCOPY RESOLUTION TEST CHART
NATIONAL BUREAU OF STANDARDS-1963-A

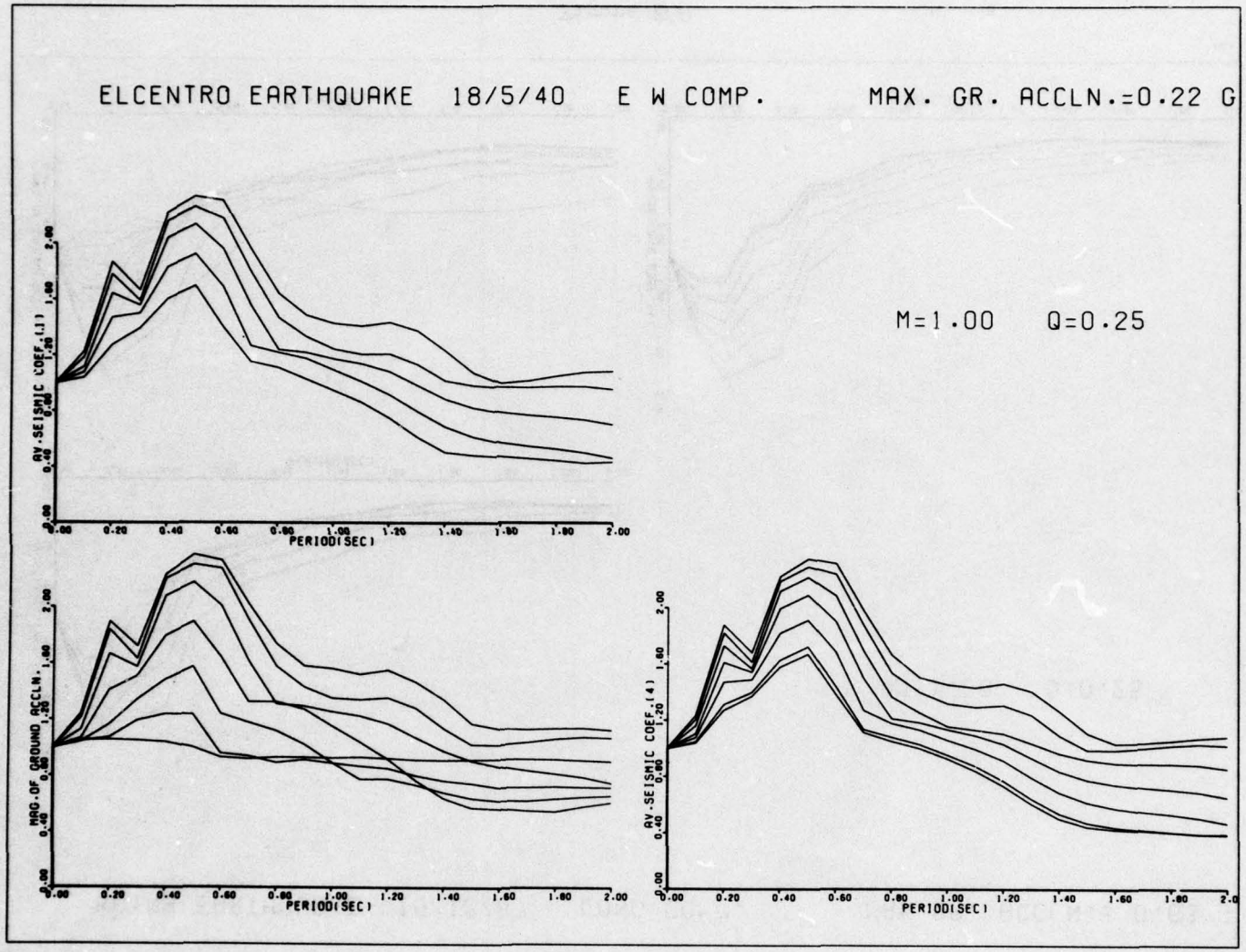
ELCENTRO EARTHQUAKE 18/5/40 E W COMP.
MAX. GR. ACCLN.=0.22 G
M=1.00 Q=0.25
AV.SEISMIC COEF.(3)
MAG.OF GROUND ACCLN.
AV.SEISMIC COEF.(4)
PERIOD(SEC)

Figure E68

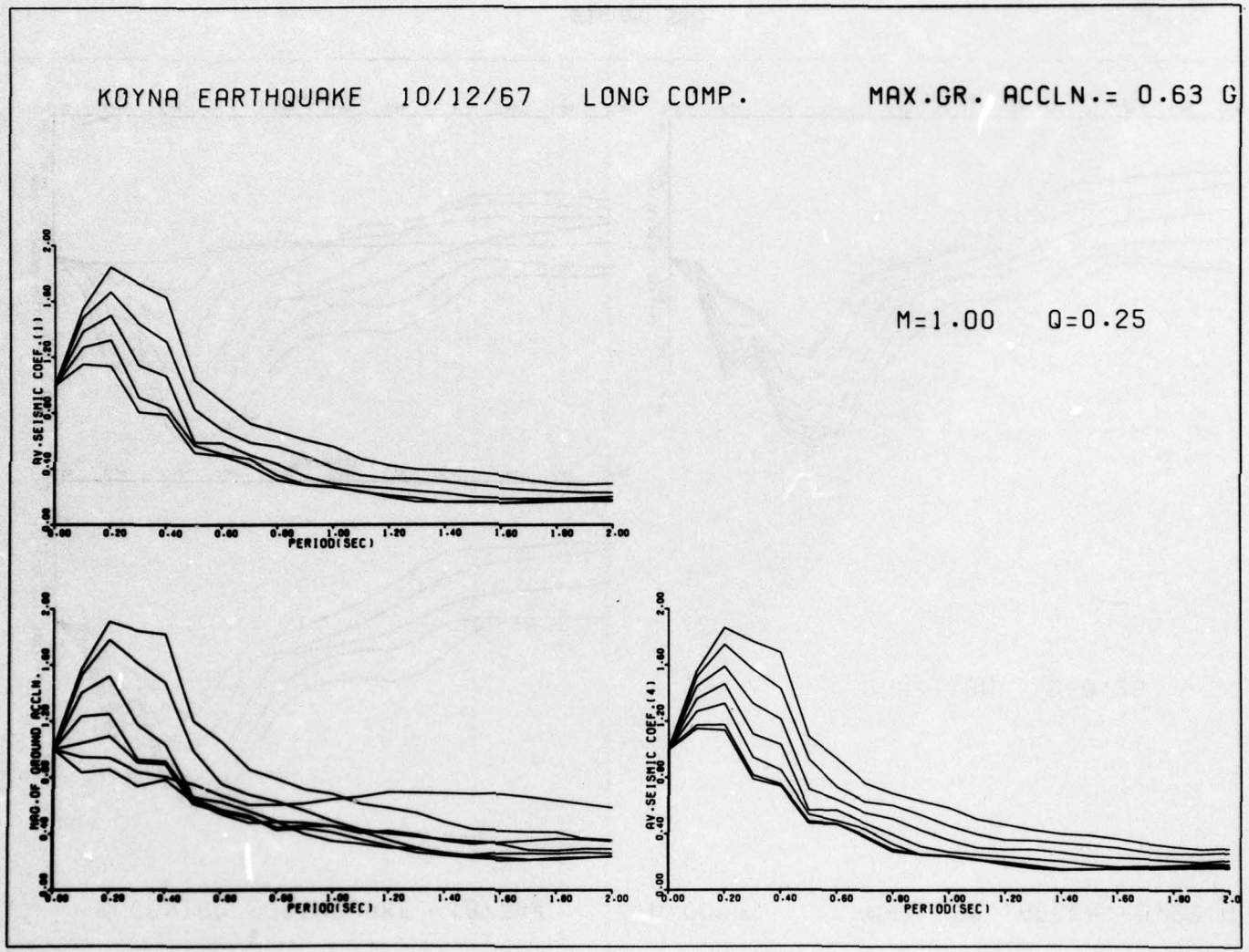
KOYNA EARTHQUAKE 10/12/67 LONG COMP.
MAX.GR. ACCLN.= 0.63 G
M=1.00 Q=0.25
AV.SEISMIC COEF.(1)
AV.SEISMIC COEF.(4)
PERIOD(SEC)

Figure E69

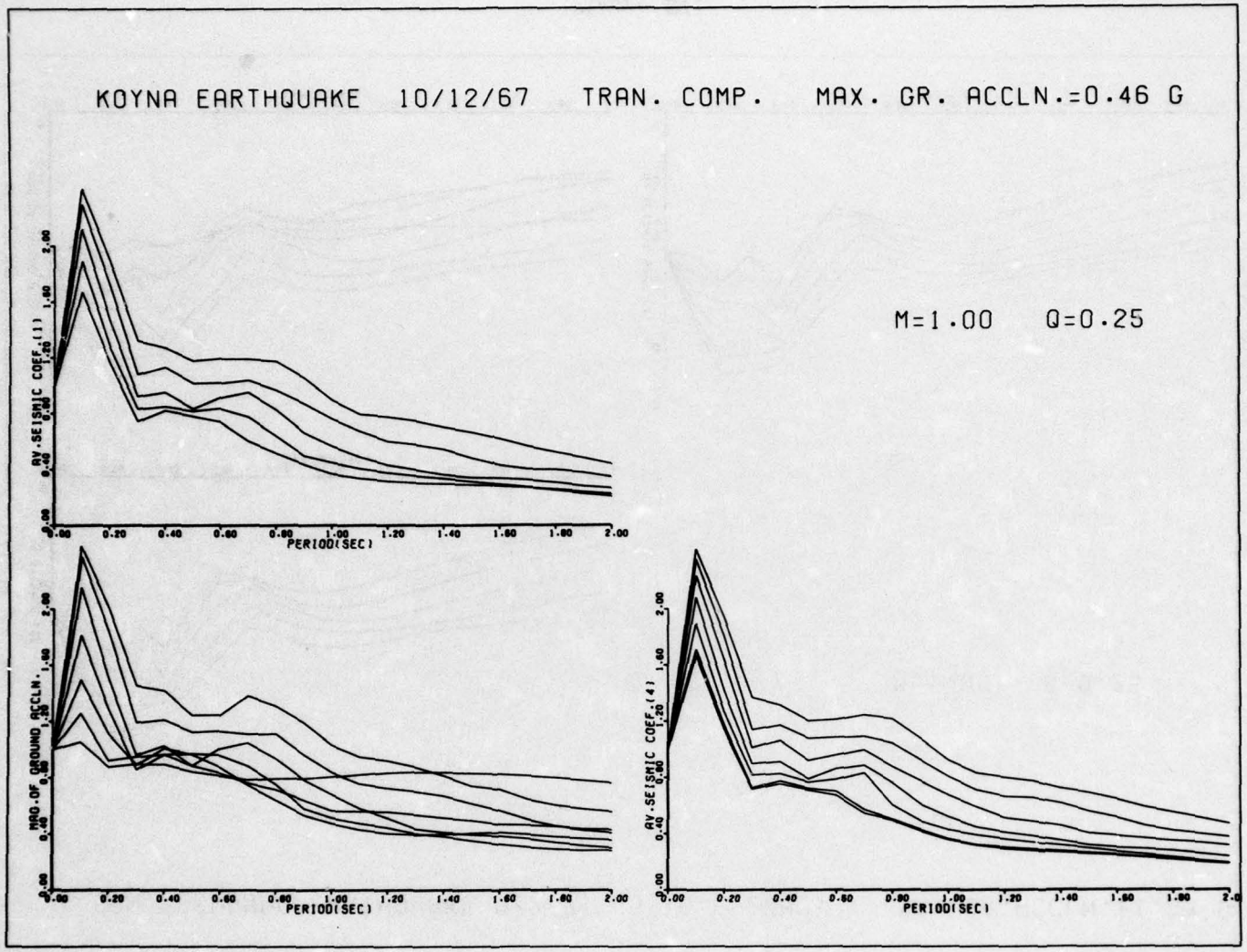
KOYNA EARTHQUAKE 10/12/67 TRAN. COMP. MAX. GR. ACCLN.=0.46 G
M=1.00 Q=0.25
AV.SEISMIC COEF.(1)
PERIOD(SEC)
PERIOD(SEC)
AV.SEISMIC COEF.(4)
PERIOD(SEC)

Figure E70

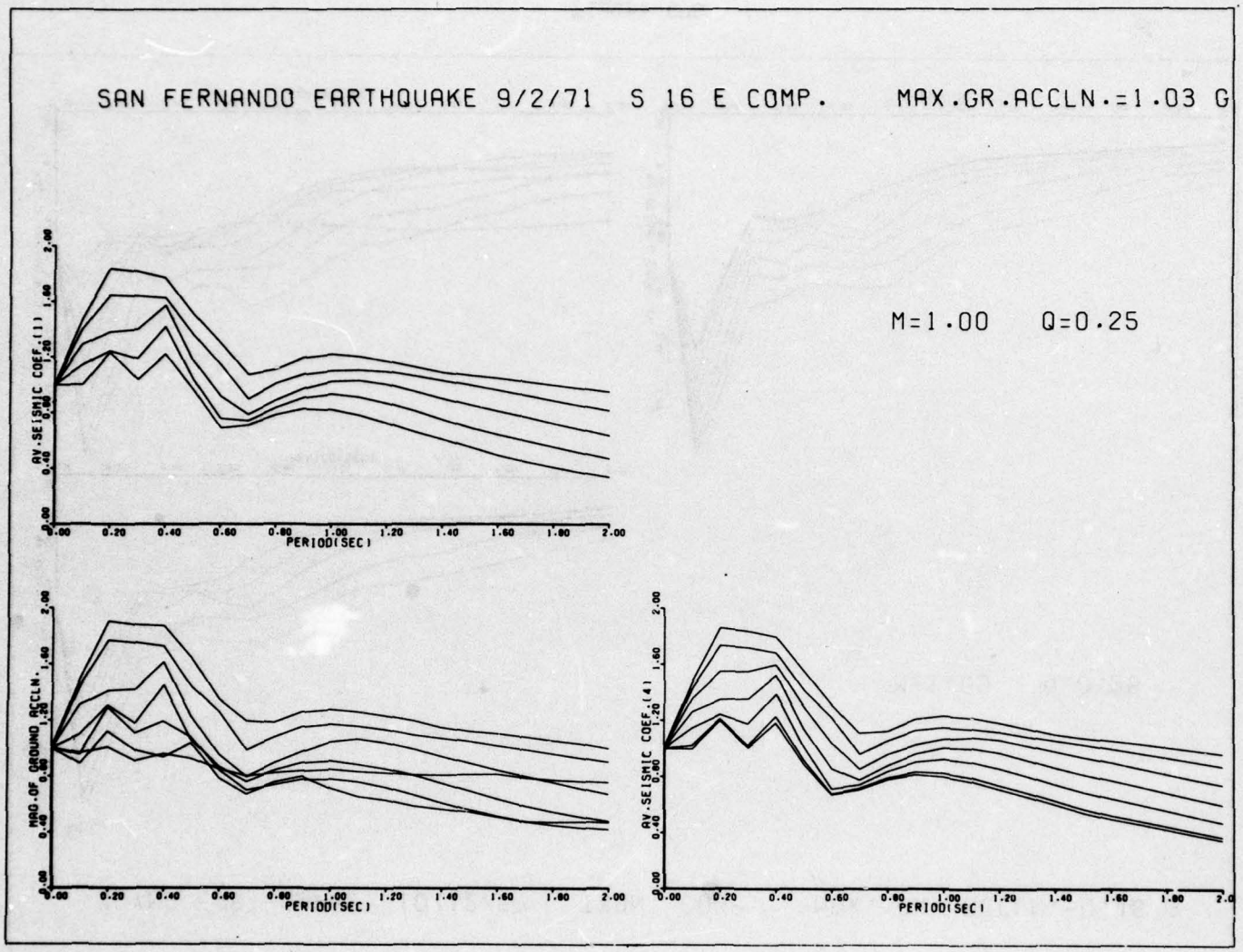
SAN FERNANDO EARTHQUAKE 9/2/71 S 16 E COMP. MAX.GR.ACCLN.=1.03 G
M=1.00 Q=0.25
AV.SEISMIC COEF.(1)
MAG.OF GROUND ACCLN.
AV.SEISMIC COEF.(4)
PERIOD(SEC)
0.00
0.20
0.40
0.60
0.80
1.00
1.20
1.40
1.60
1.80
2.00

Figure E71

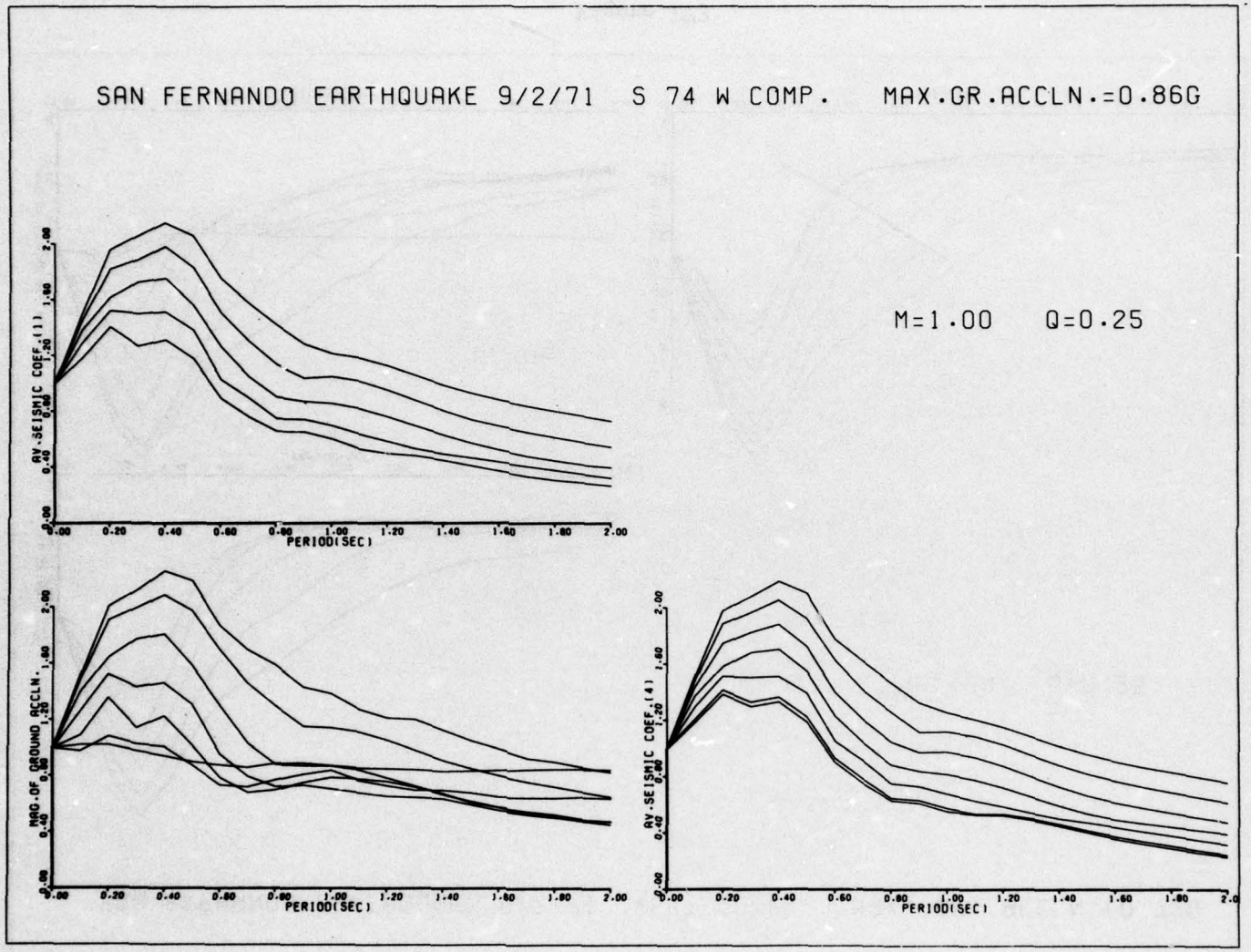
SAN FERNANDO EARTHQUAKE 9/2/71 S 74 W COMP. MAX.GR.ACCLN.=0.86G
M=1.00 Q=0.25
AV.SEISMIC COEF.(1)
AV.SEISMIC COEF.(4)
MAG.OF GROUND ACCLN.
PERIOD(SEC)
0.00
0.20
0.40
0.60
0.80
1.00
1.20
1.40
1.60
1.80
2.00

Figure E72

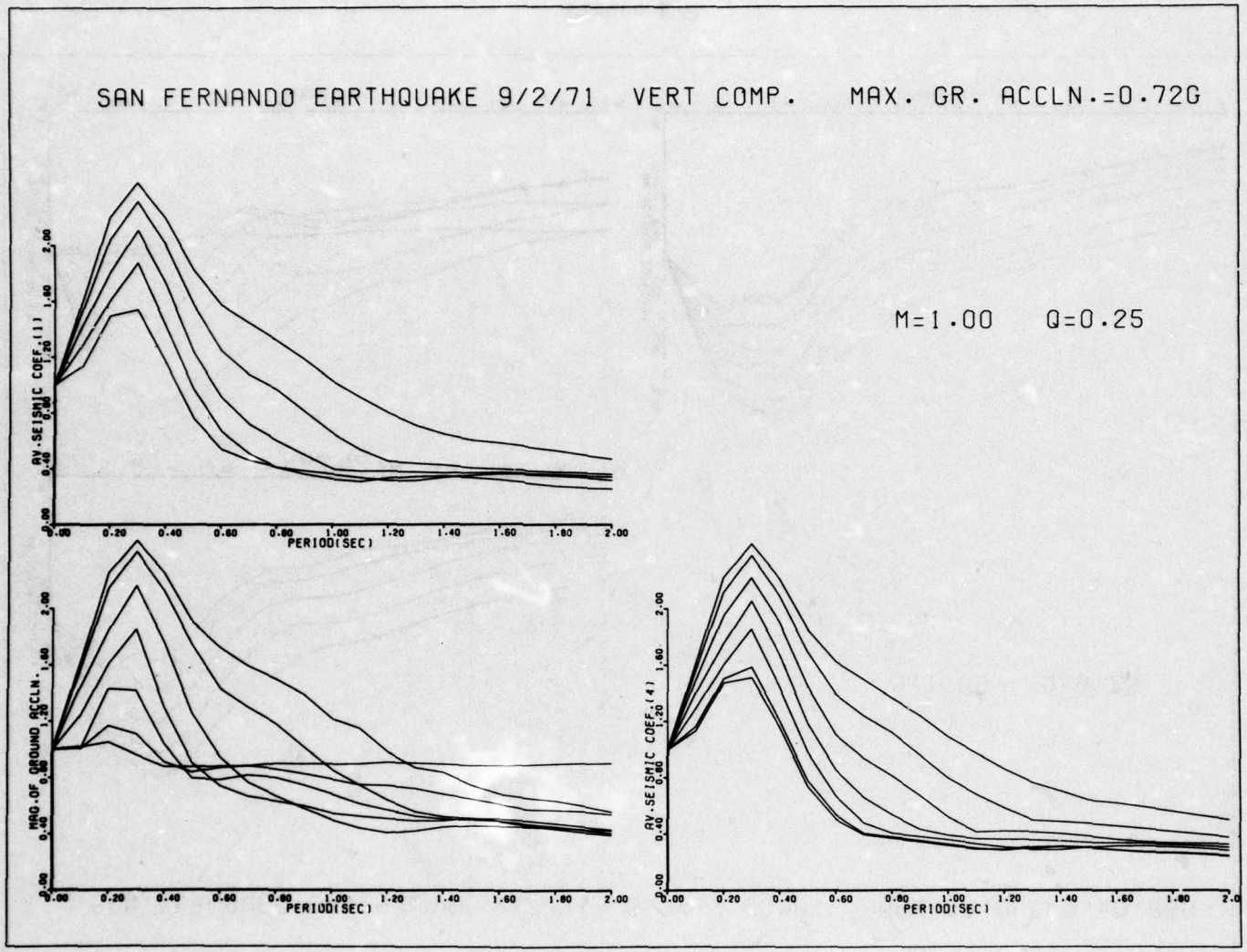
SAN FERNANDO EARTHQUAKE 9/2/71 VERT COMP. MAX. GR. ACCLN.=0.72G
M=1.00 Q=0.25
AV.SEISMIC COEF.(1)
MAG.OF GROUND ACCLN.
AV.SEISMIC COEF.(4)
PERIOD(SEC)
0.00
0.20
0.40
0.60
0.80
1.00
1.20
1.40
1.60
1.80
2.00

Figure E73

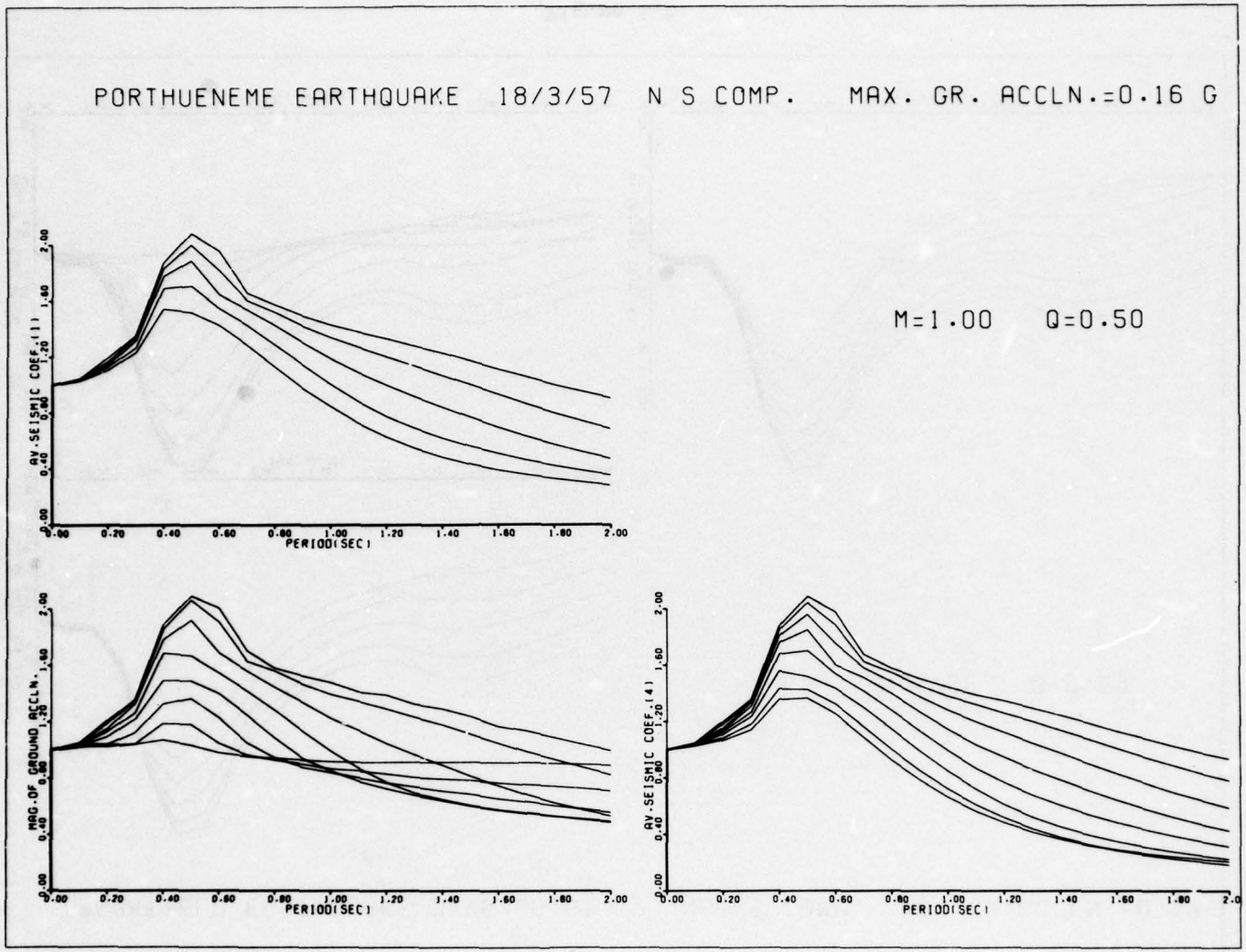
PORTHUENEME EARTHQUAKE 18/3/57 N S COMP. MAX. GR. ACCLN.=0.16 G
M=1.00 Q=0.50
AV.SEISMIC COEF.(1)
MAG.OF GROUND ACCLN.
AV.SEISMIC COEF.(4)
PERIOD(SEC)

Figure E74

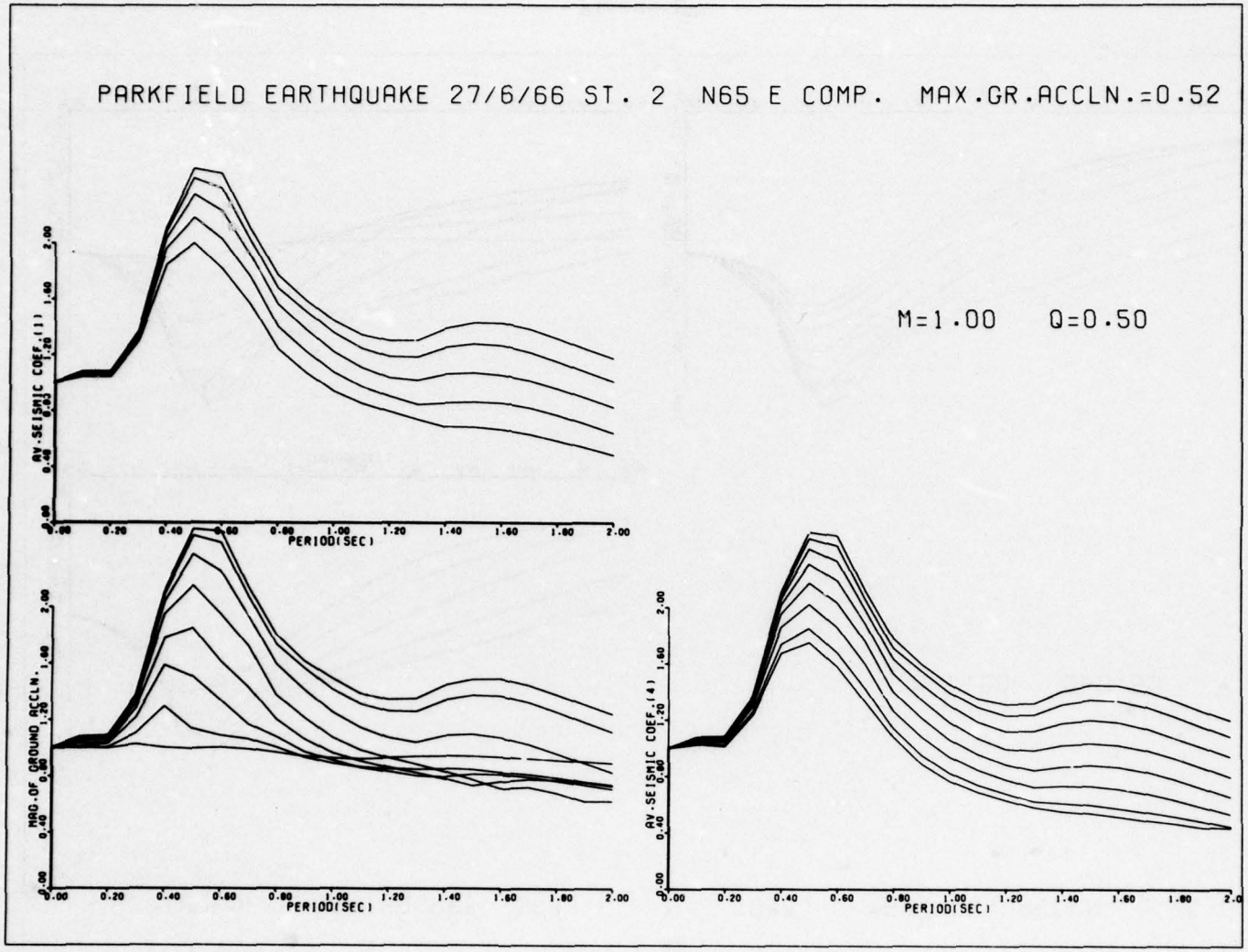
PARKFIELD EARTHQUAKE 27/6/66 ST. 2 N65 E COMP. MAX.GR.ACCLN.=0.52
M=1.00 Q=0.50
AV.SEISMIC COEF.(1)
PERIOD(SEC)
MAG.OF GROUND ACCLN.
PERIOD(SEC)
AV.SEISMIC COEF.(4)
PERIOD(SEC)

Figure E75

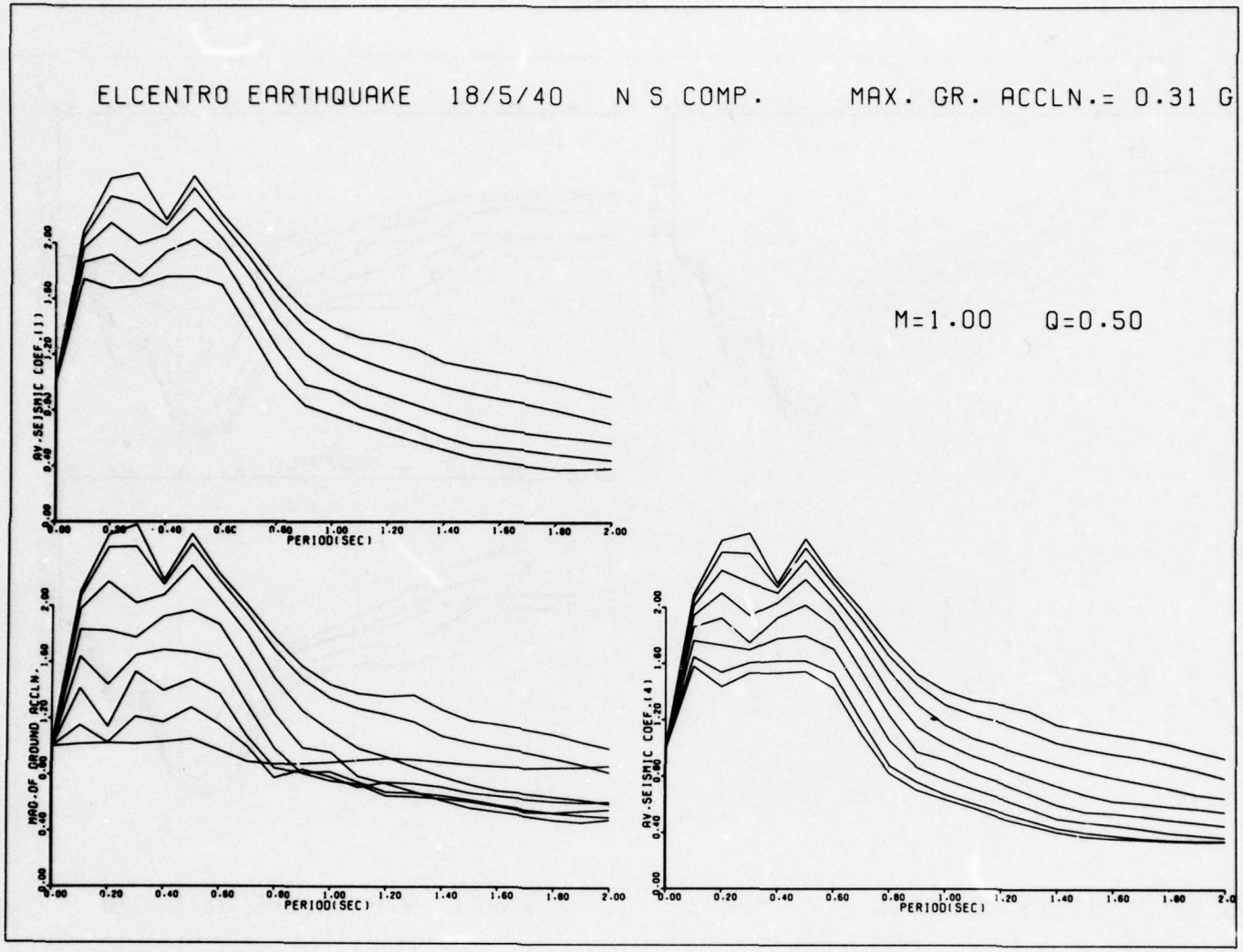
ELCENTRO EARTHQUAKE 18/5/40 N S COMP. MAX. GR. ACCLN.= 0.31 G
M=1.00 Q=0.50
AV.SEISMIC COEF.(I)
MOD.OF GROUND ACCLN.
AV.SEISMIC COEF.(4)
PERIOD(SEC)
PERIOD(SEC)
PERIOD(SEC)

Figure E76

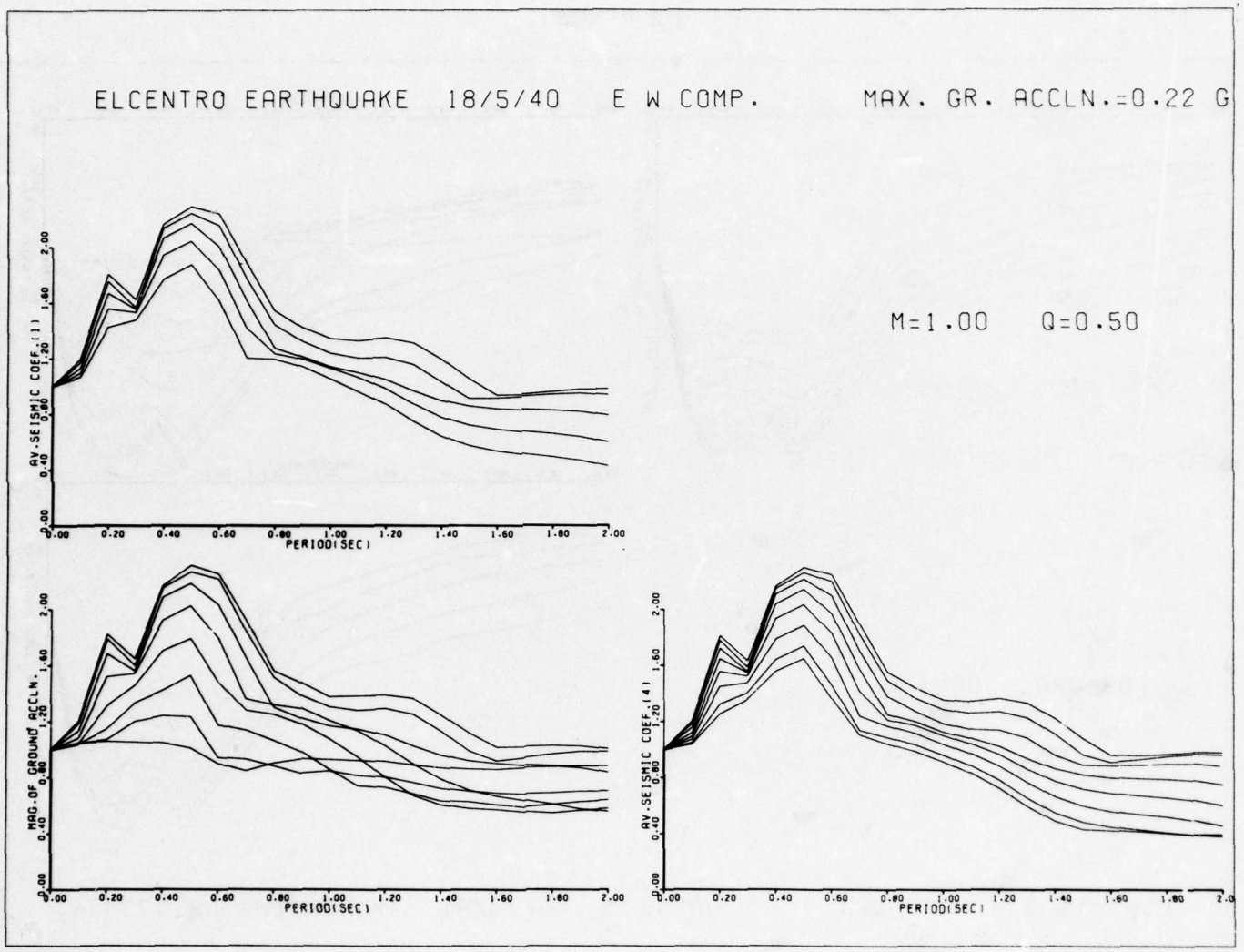
ELCENTRO EARTHQUAKE 18/5/40 E W COMP.
MAX. GR. ACCLN.=0.22 G
M=1.00 Q=0.50
AV.SEISMIC COEF.(1)
MAG.OF GROUND ACCLN.
AV.SEISMIC COEF.(4)
PERIOD(SEC)
0.00
0.20
0.40
0.60
0.80
1.00
1.20
1.40
1.60
1.80
2.00

Figure E77

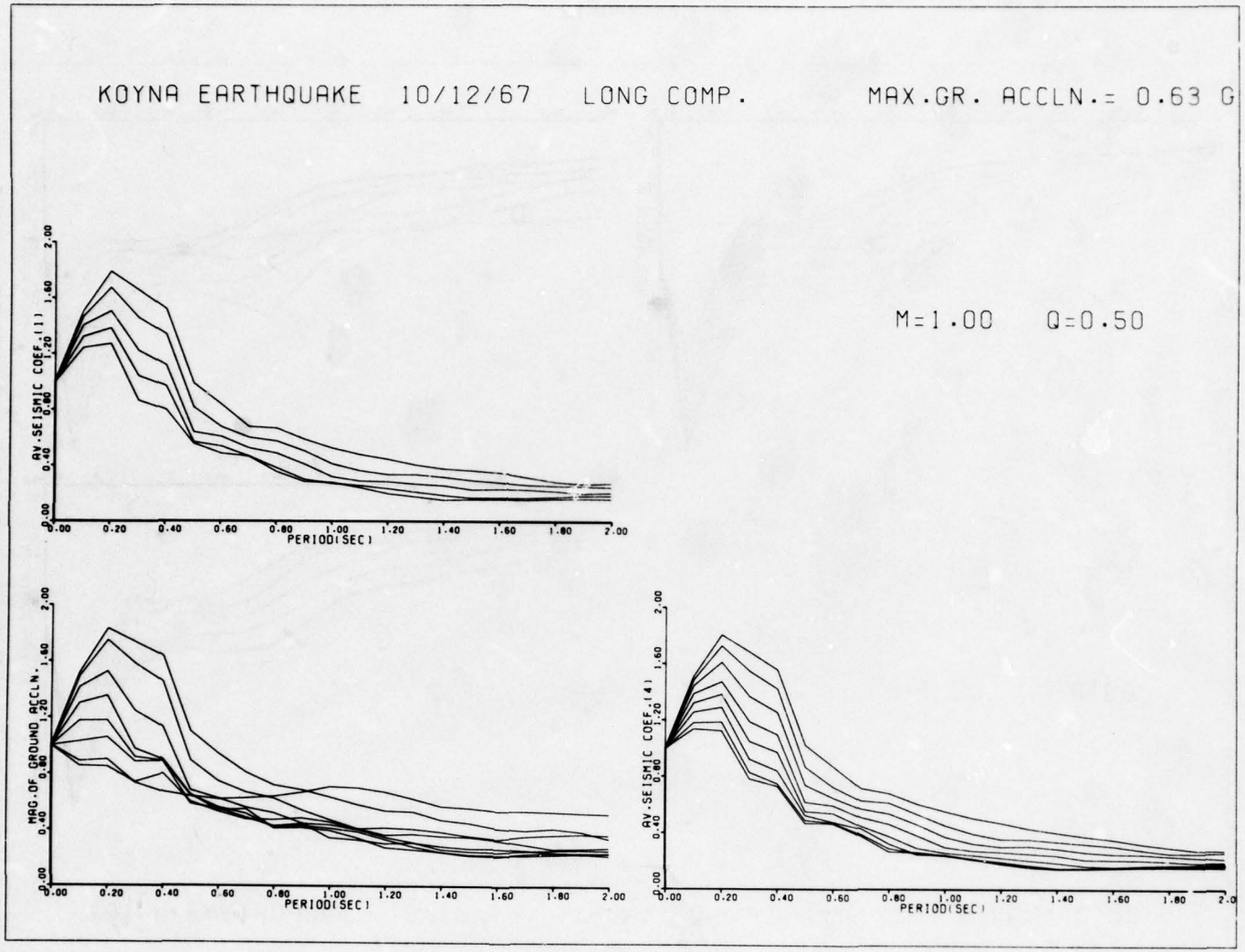
KOYNA EARTHQUAKE 10/12/67 LONG COMP.
MAX.GR. ACCLN.= 0.63 G
M=1.00 Q=0.50
AV.SEISMIC COEF.(1)
MAG.OF GROUND ACCLN.
AV.SEISMIC COEF.(4)
PERIOD(SEC)

Figure E78

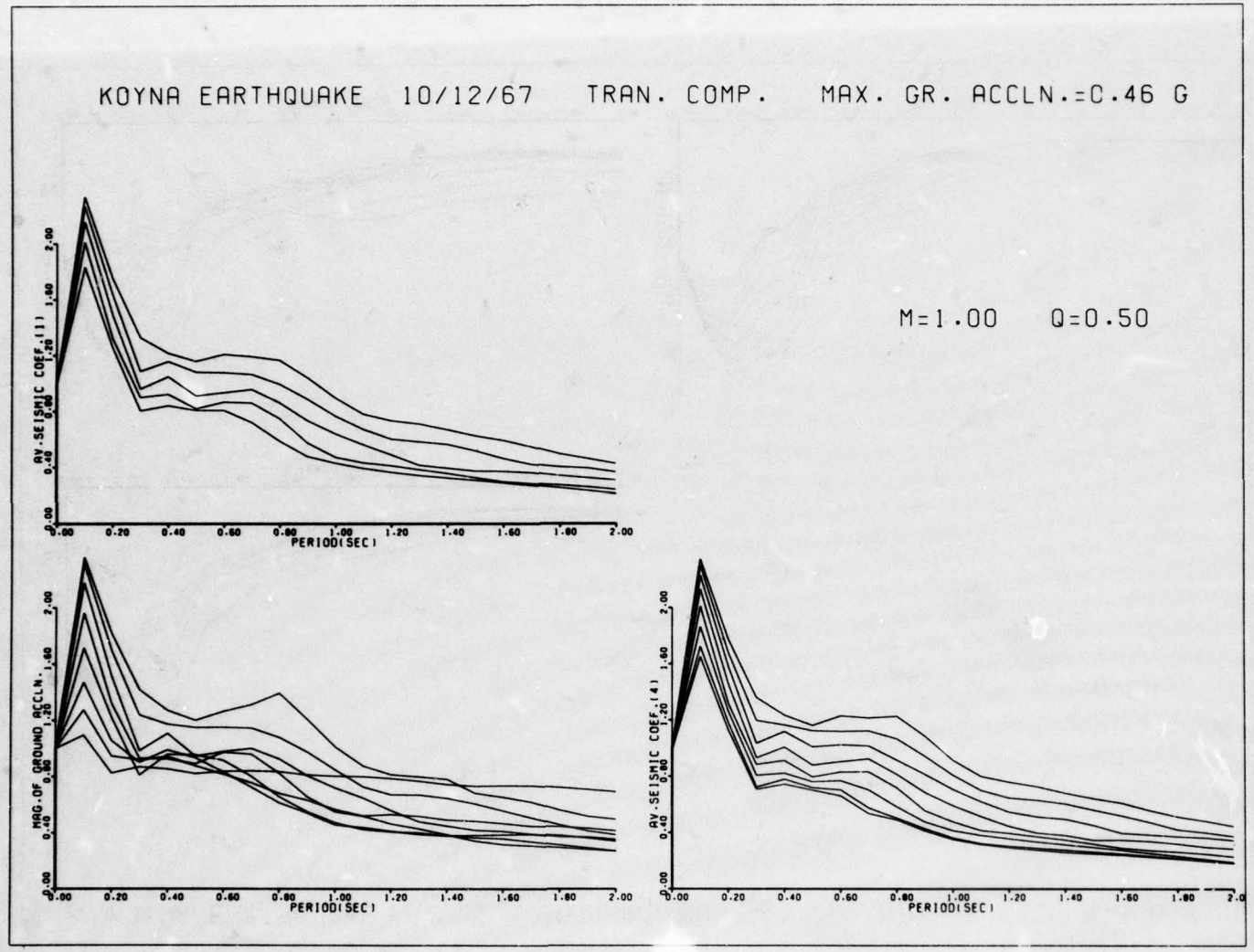
KOYNA EARTHQUAKE 10/12/67 TRAN. COMP. MAX. GR. ACCLN.=0.46 G
M=1.00 Q=0.50
AV.SEISMIC COEF.(1)
MAG.OF GROUND ACCLN.
AV.SEISMIC COEF.(4)
PERIOD(SEC)

Figure E79

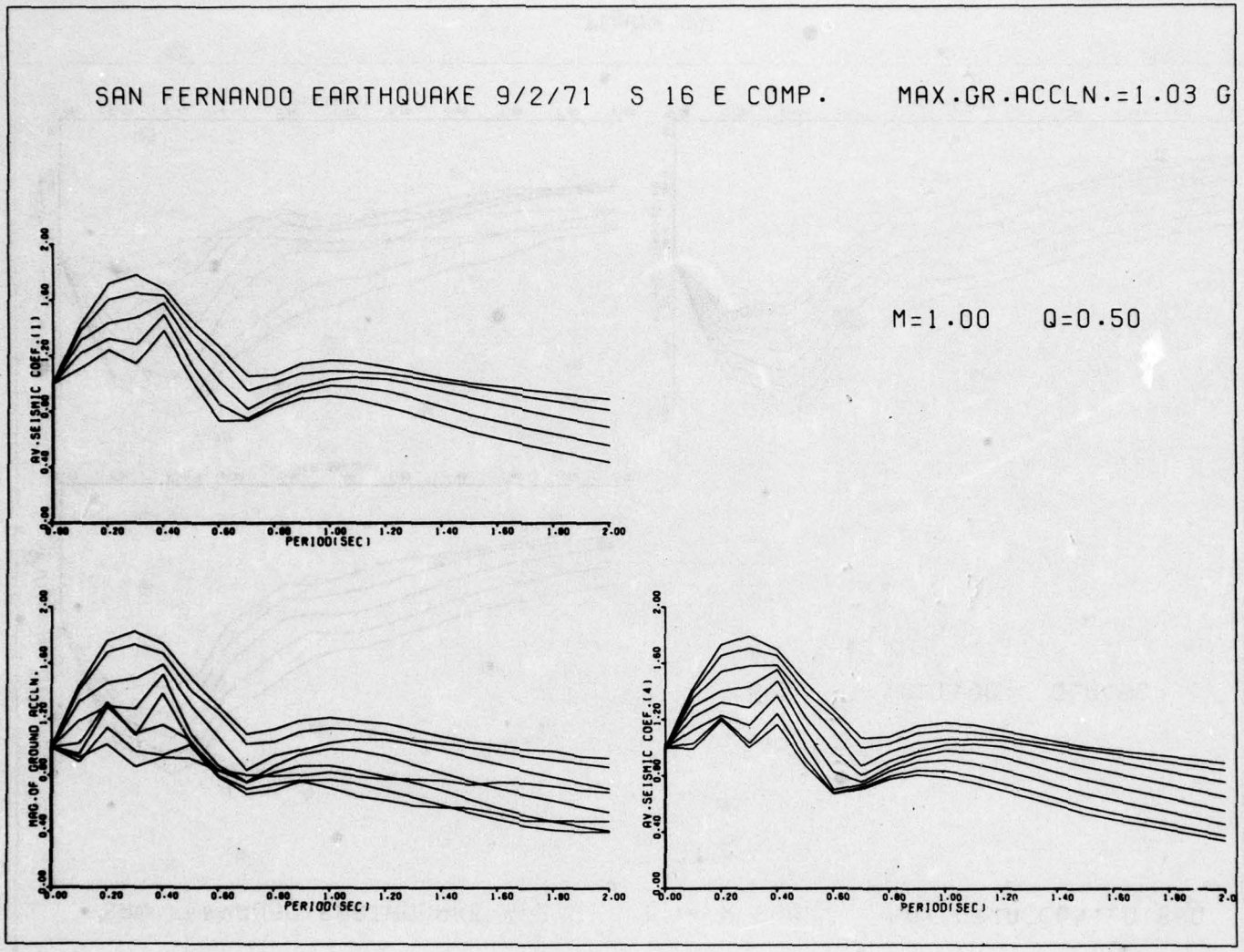
SAN FERNANDO EARTHQUAKE 9/2/71 S 16 E COMP. MAX.GR.ACCLN.=1.03 G
M=1.00 Q=0.50
AV.SEISMIC COEF.(1)
AV.SEISMIC COEF.(4)
PERIOD(SEC)

Figure E80

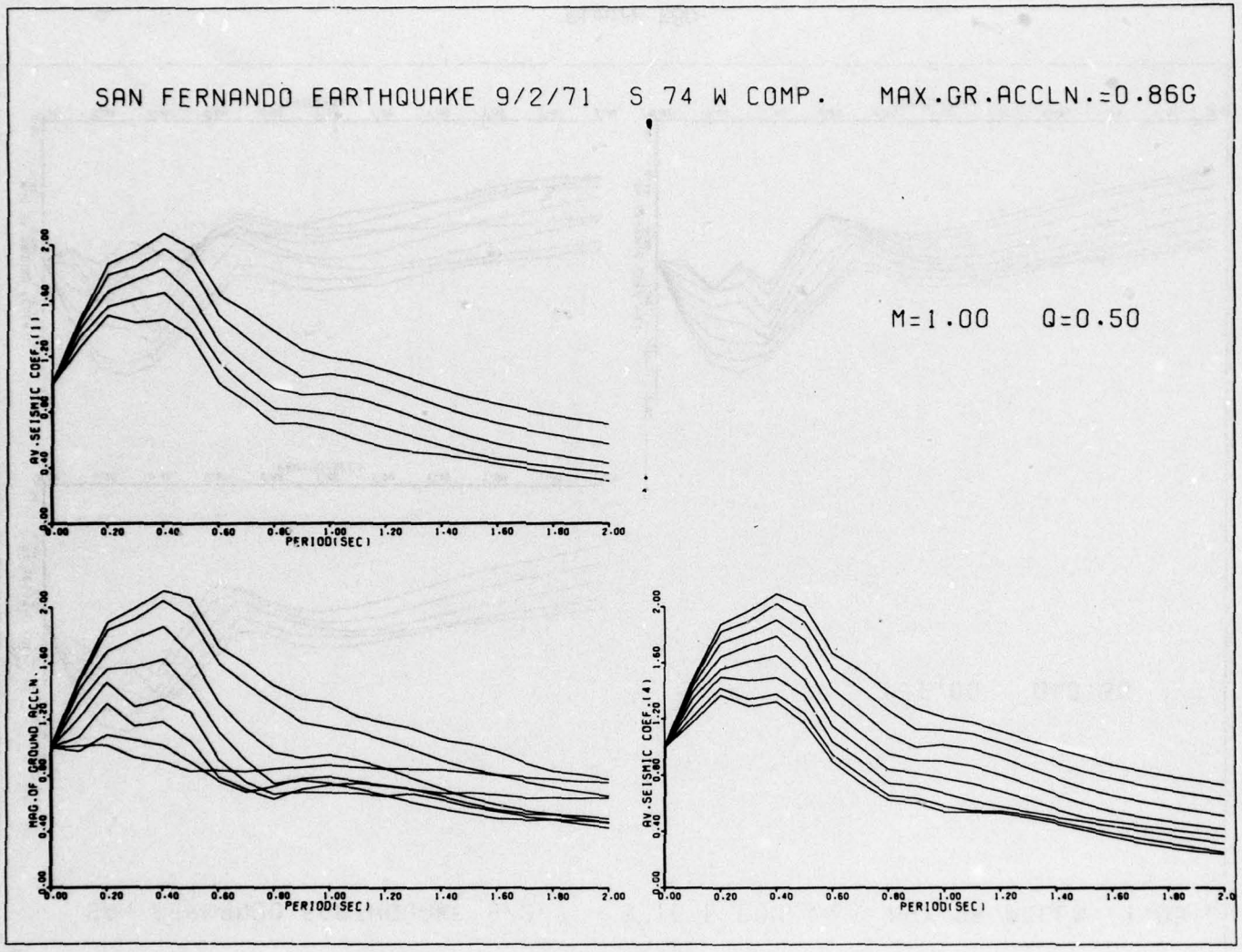
SAN FERNANDO EARTHQUAKE 9/2/71 S 74 W COMP. MAX.GR.ACCLN.=0.86G
M=1.00 Q=0.50
AV.SEISMIC COEF.(1)
MAG.OF GROUND ACCLN.
AV.SEISMIC COEF.(4)
PERIOD(SEC)

Figure E81

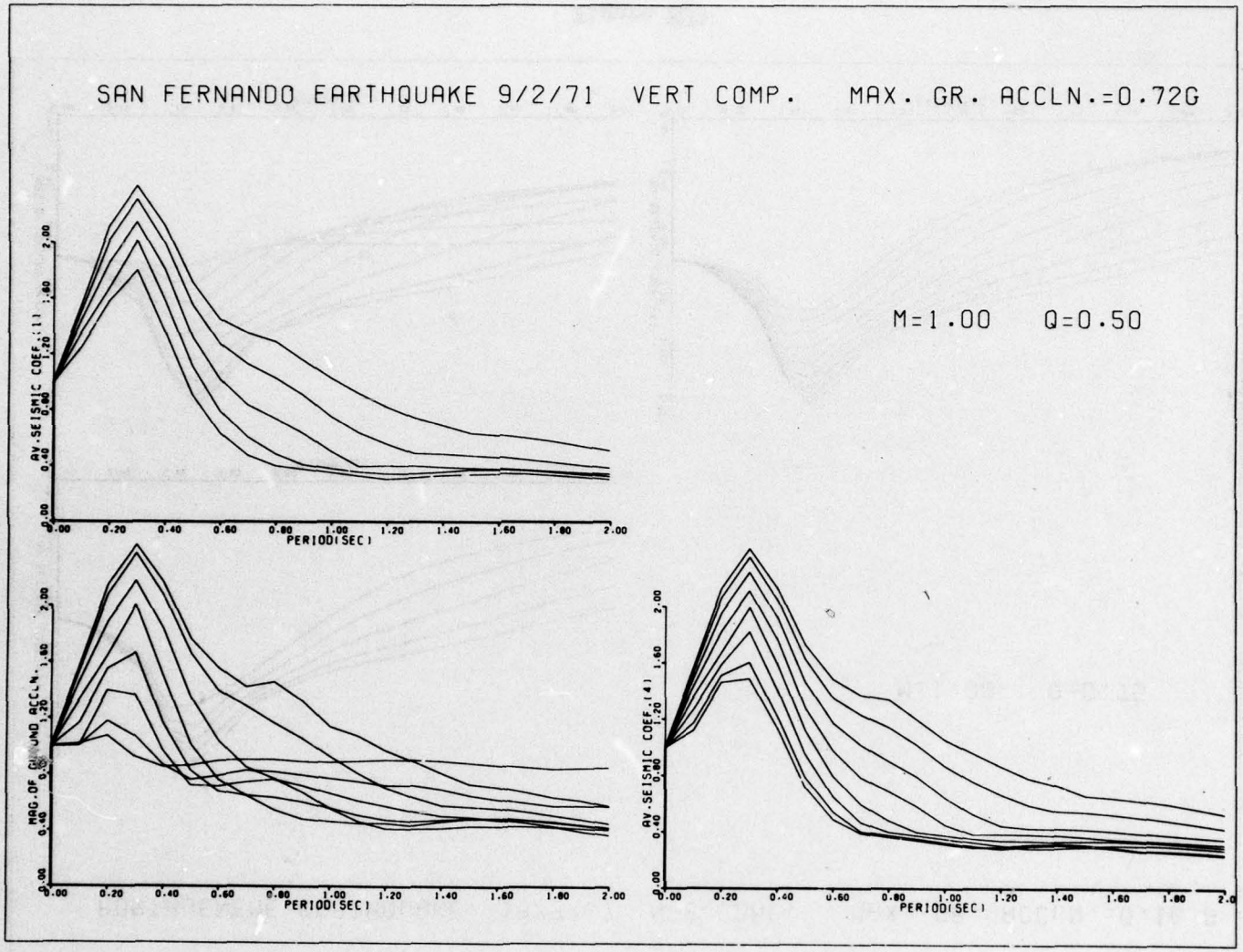
SAN FERNANDO EARTHQUAKE 9/2/71 VERT COMP. MAX. GR. ACCLN.=0.72G
M=1.00 Q=0.50
AV.SEISMIC COEF.(1)
MAG.OF GROUND ACCLN.
AV.SEISMIC COEF.(4)
PERIOD(SEC)

Figure E82

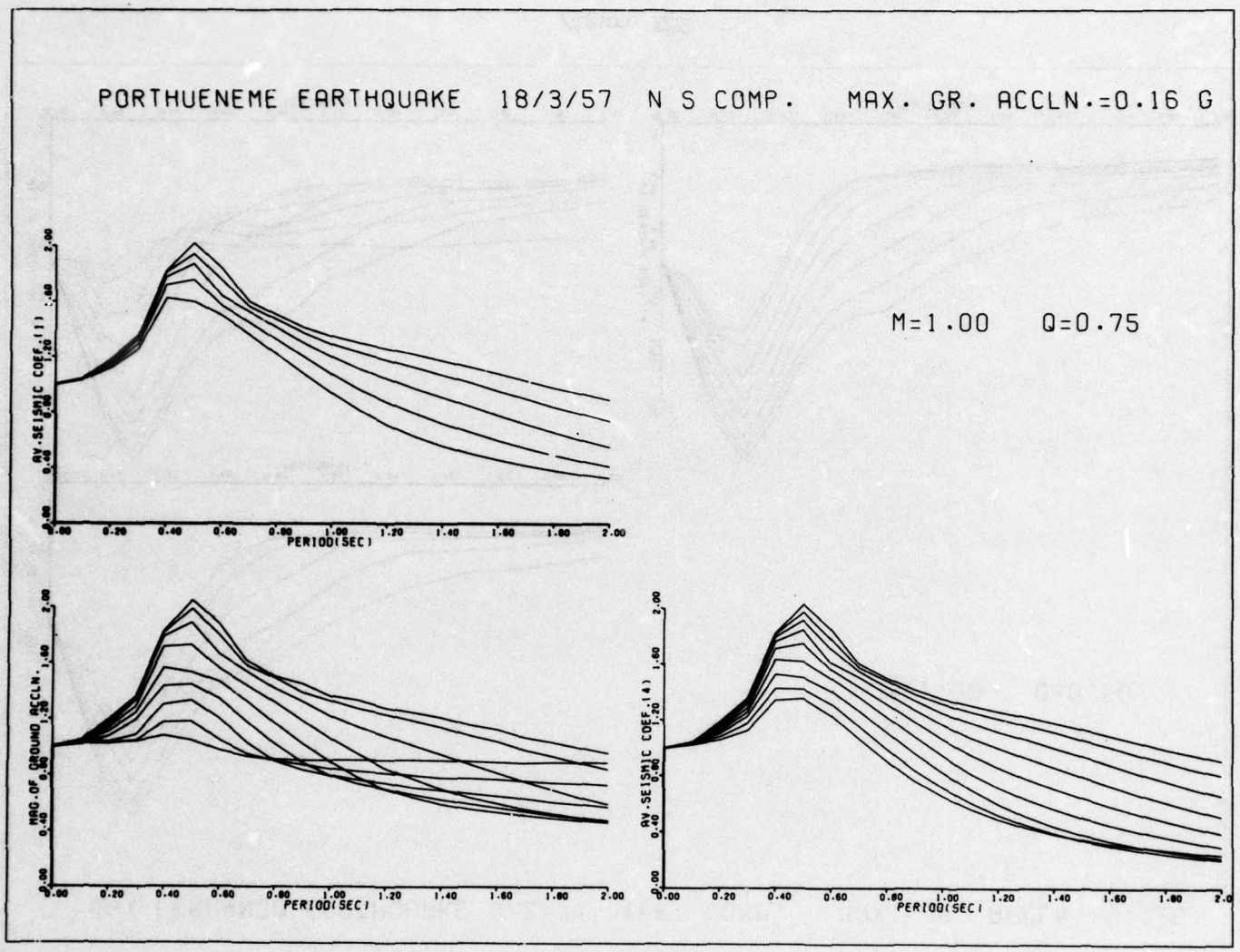
PORTHUENEME EARTHQUAKE 18/3/57 N S COMP. MAX. GR. ACCLN.=0.16 G
M=1.00 Q=0.75
AV.SEISMIC COEF.(I)
PERIOD(SEC)
AVG.OF GROUND ACCLN.
PERIOD(SEC)
AV.SEISMIC COEF.(A)
PERIOD(SEC)

Figure E83

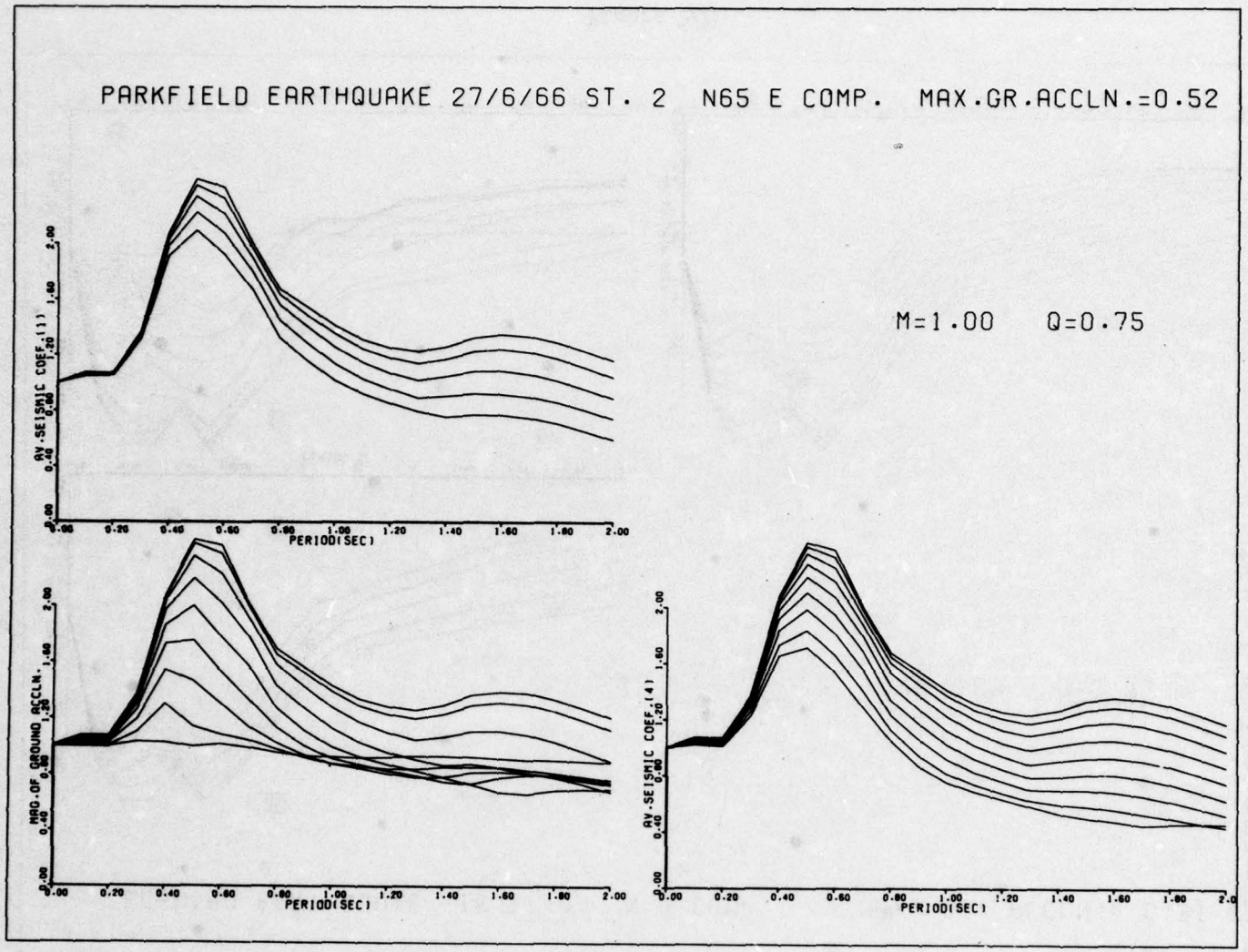
PARKFIELD EARTHQUAKE 27/6/66 ST. 2 N65 E COMP. MAX.GR.ACCLN.=0.52
M=1.00 Q=0.75
AV.SEISMIC COEF.(1)
MAG.OF GROUND ACCLN.
AV.SEISMIC COEF.(4)
PERIOD(SEC)

Figure E84

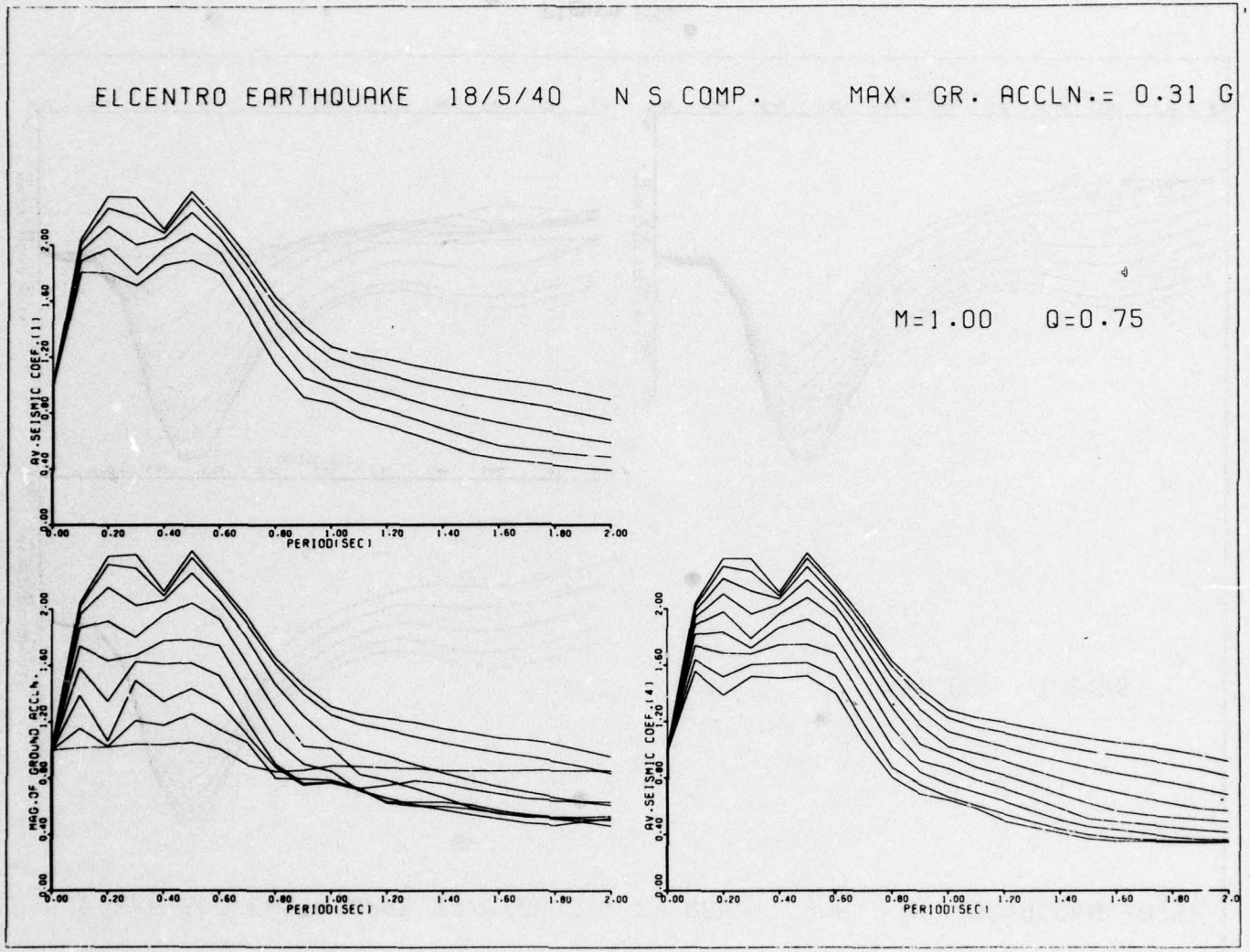
ELCENTRO EARTHQUAKE 18/5/40 N S COMP.
MAX. GR. ACCLN.= 0.31 G
M=1.00 Q=0.75
AV.SEISMIC COEFF.(I)
MAG.OF GROUND ACCLN.
AV.SEISMIC COEFF.(4)
PERIOD(SEC)
0.00
0.20
0.40
0.60
0.80
1.00
1.20
1.40
1.60
1.80
2.00

Figure E85

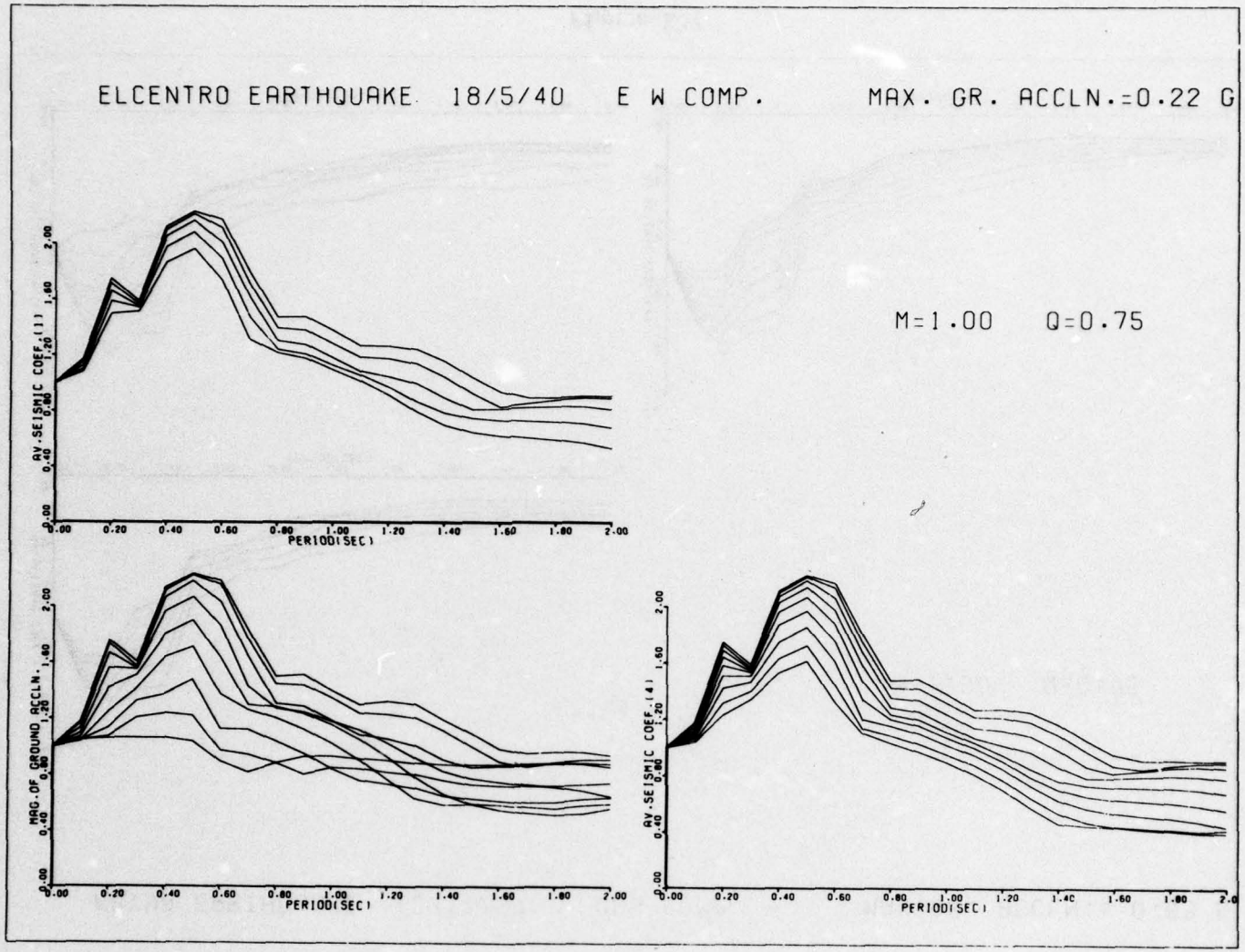
ELCENTRO EARTHQUAKE 18/5/40 E W COMP.
MAX. GR. ACCLN.=0.22 G
M=1.00 Q=0.75
AV.SEISMIC COEF.(1)
MAG.OF GROUND ACCLN.
AV.SEISMIC COEF.(4)
PERIOD(SEC)

Figure E86

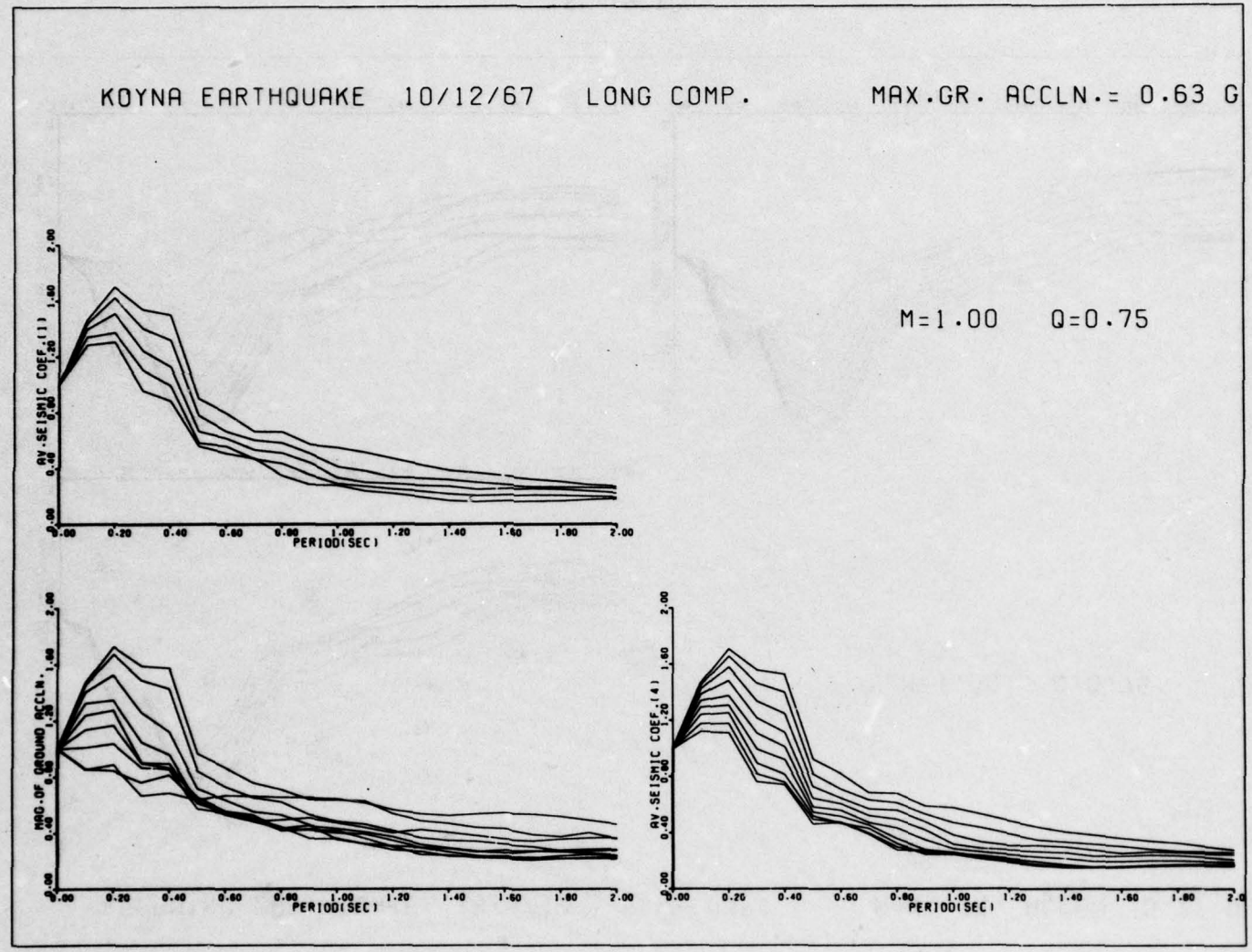
KOYNA EARTHQUAKE 10/12/67 LONG COMP.
MAX.GR. ACCLN.= 0.63 G
M=1.00 Q=0.75
AV.SEISMIC COEF.(1)
PERIOD(SEC)
MAG.OF GROUND ACCLN.
PERIOD(SEC)
AV.SEISMIC COEF.(4)
PERIOD(SEC)

Figure E87

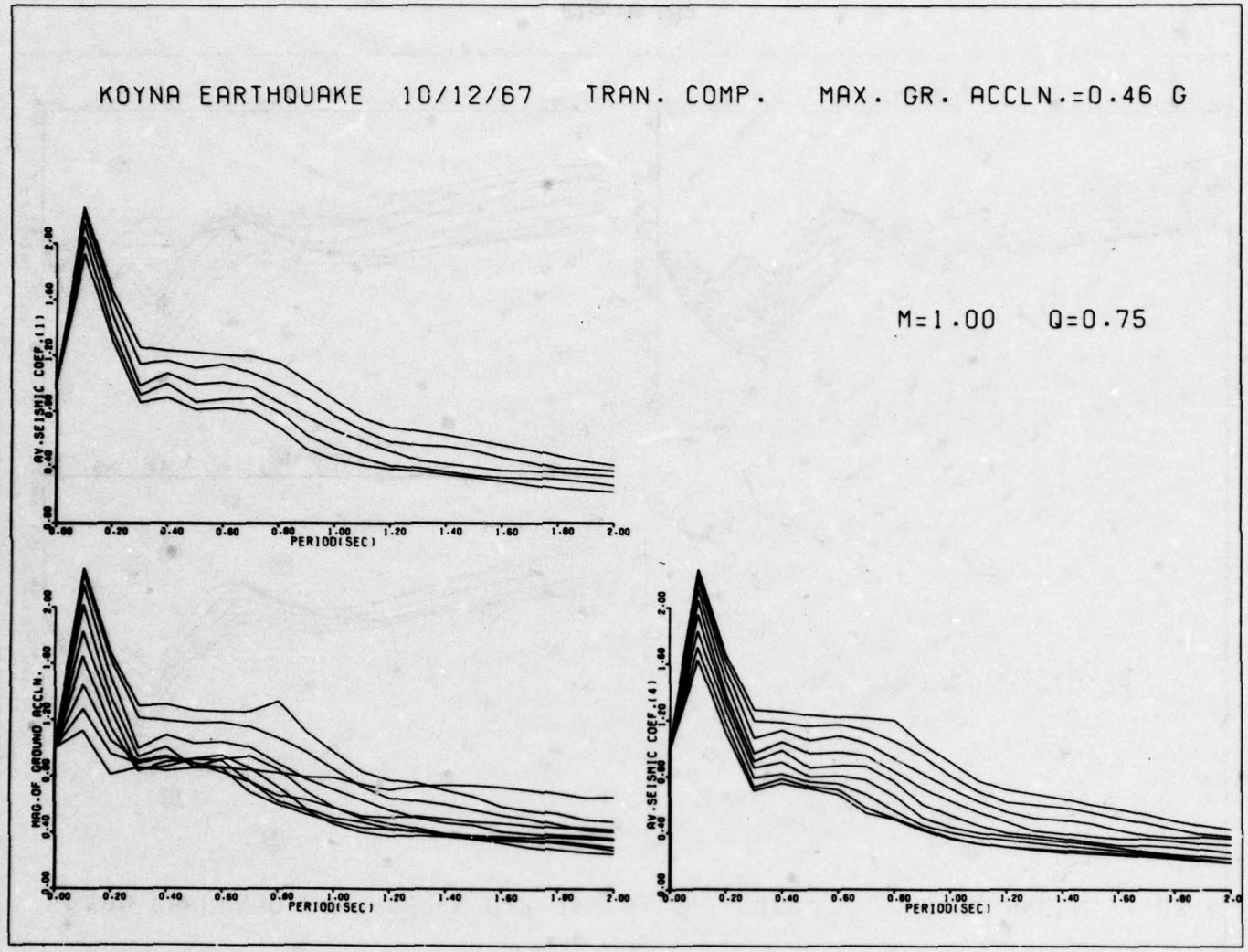
KOYNA EARTHQUAKE 10/12/67 TRAN. COMP. MAX. GR. ACCLN.=0.46 G
M=1.00 Q=0.75
AV.SEISMIC COEF.(1)
MAG.OF GROUND ACCLN.
AV.SEISMIC COEF.(4)
PERIOD(SEC)

Figure E88

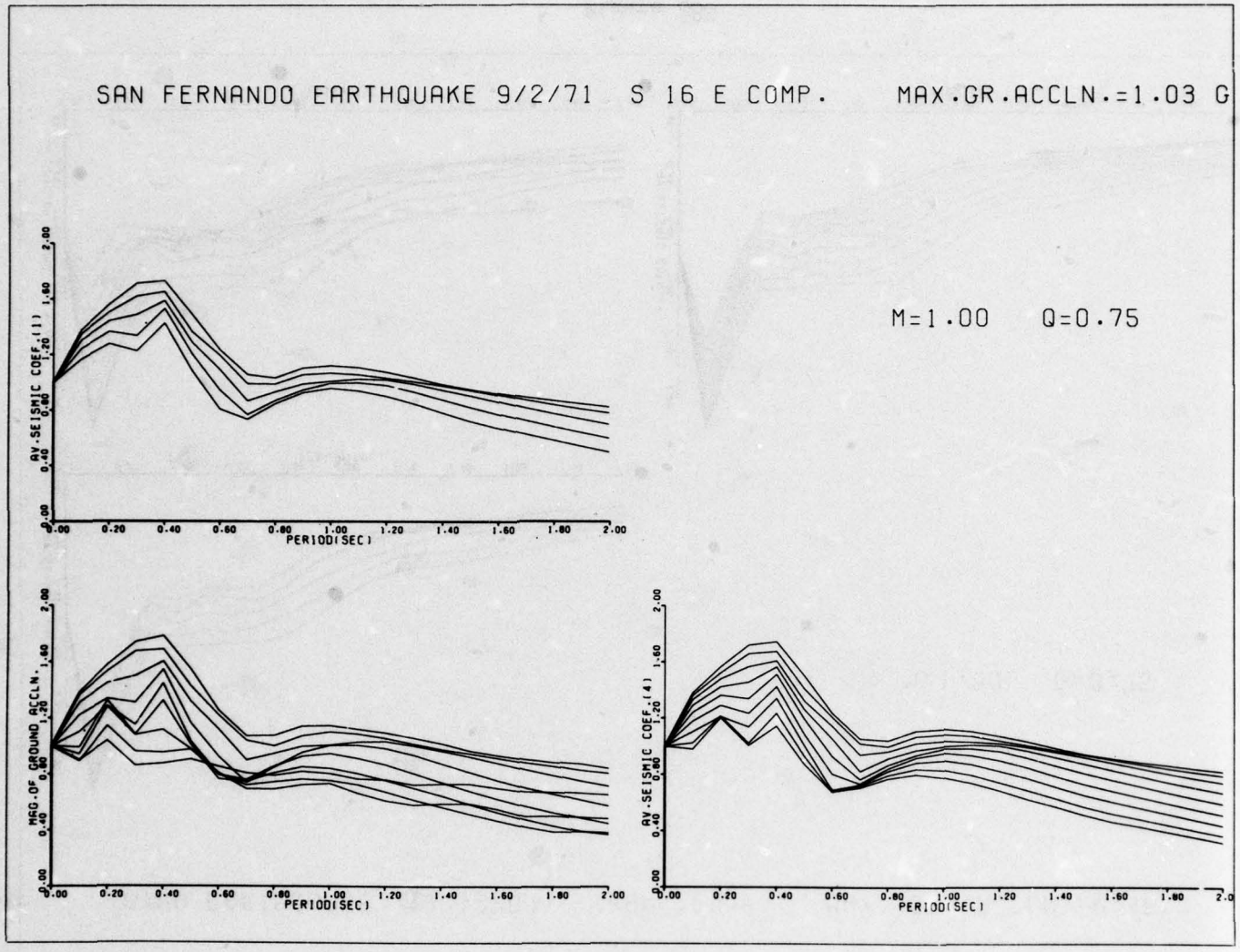
SAN FERNANDO EARTHQUAKE 9/2/71 S 16 E COMP.
MAX.GR.ACCLN.=1.03 G
M=1.00 Q=0.75
AV.SEISMIC COEF.(1)
MAG.OF GROUND ACCLN.
AV.SEISMIC COEF.(4)
PERIOD(SEC)
0.00
0.20
0.40
0.60
0.80
1.00
1.20
1.40
1.60
1.80
2.00

Figure E89

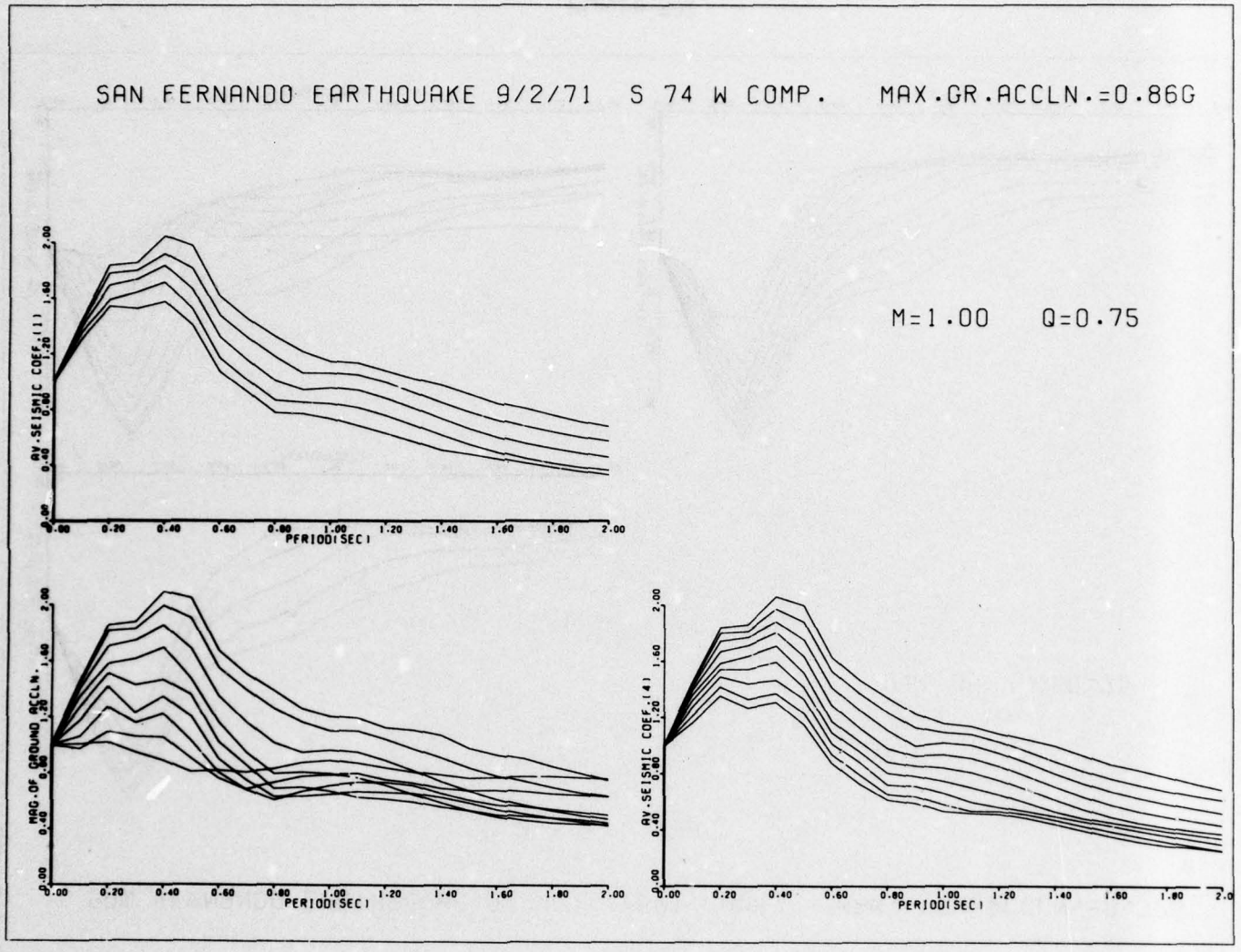
SAN FERNANDO EARTHQUAKE 9/2/71 S 74 W COMP. MAX.GR.ACCLN.=0.86G
M=1.00 Q=0.75
AV.SEISMIC COEF.(1)
MAG.OF GROUND ACCLN.
AV.SEISMIC COEF.(4)
PERIOD(SEC)

Figure E90

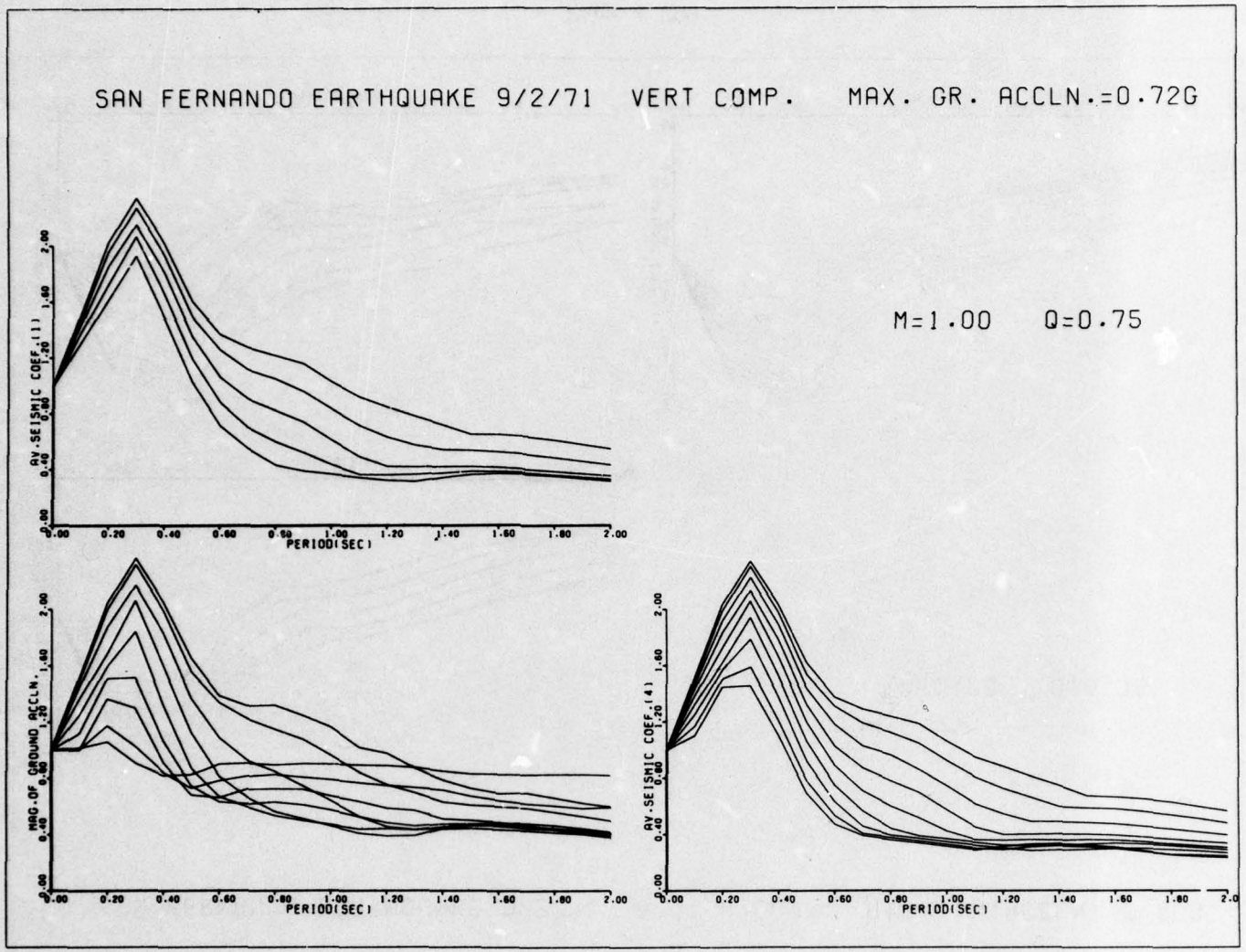
SAN FERNANDO EARTHQUAKE 9/2/71 VERT COMP. MAX. GR. ACCLN.=0.72G
M=1.00 Q=0.75
AV.SEISMIC COEF.(1)
MAG.OF GROUND ACCLN.
AV.SEISMIC COEF.(4)
PERIOD(SEC)
0.00
0.20
0.40
0.60
0.80
1.00
1.20
1.40
1.60
1.80
2.00

Figure E91

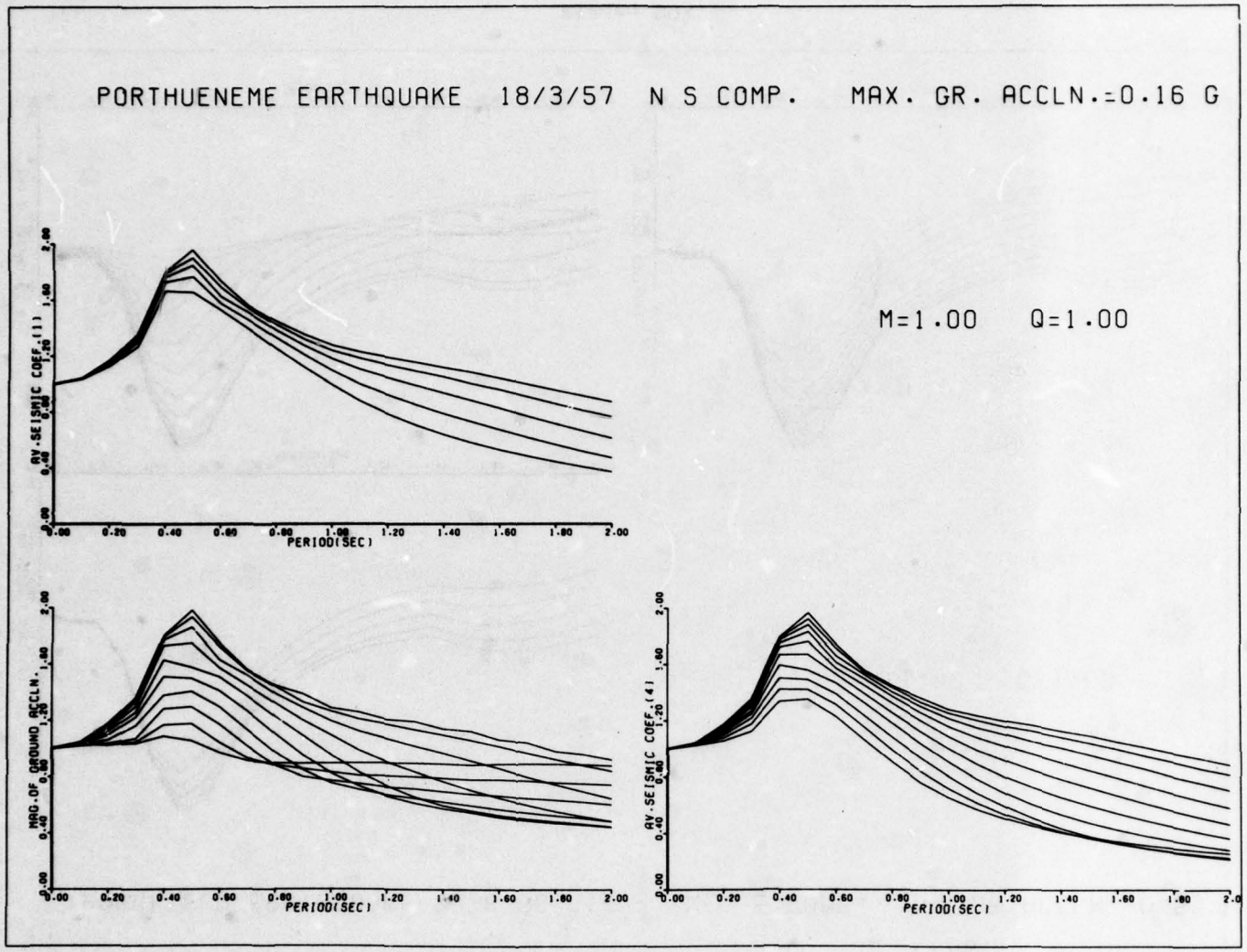
PORTHUENEME EARTHQUAKE 18/3/57 N S COMP. MAX. GR. ACCLN.=0.16 G
M=1.00 Q=1.00
AV.SEISMIC COEF.(1)
MAG.OF GROUND ACCLN.
AV.SEISMIC COEF.(4)
PERIOD(SEC)

Figure E92

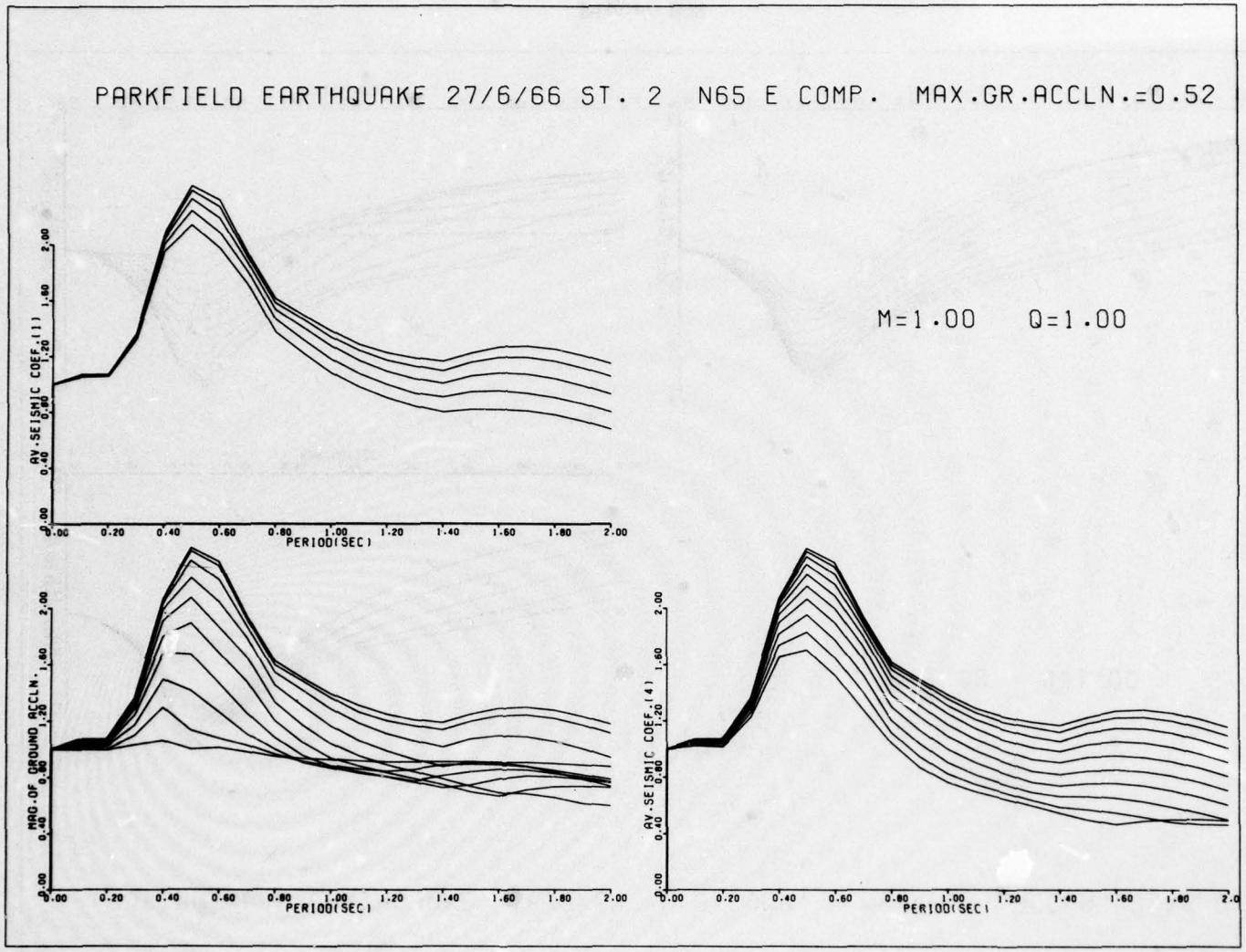
PARKFIELD EARTHQUAKE 27/6/66 ST. 2 N65 E COMP. MAX.GR.ACCLN.=0.52
M=1.00 Q=1.00
AV.SEISMIC COEF.(1)
MAG.OF GROUND ACCLN.
AV.SEISMIC COEF.(4)
PERIOD(SEC)
0.00
0.20
0.40
0.60
0.80
1.00
1.20
1.40
1.60
1.80
2.00

Figure E93

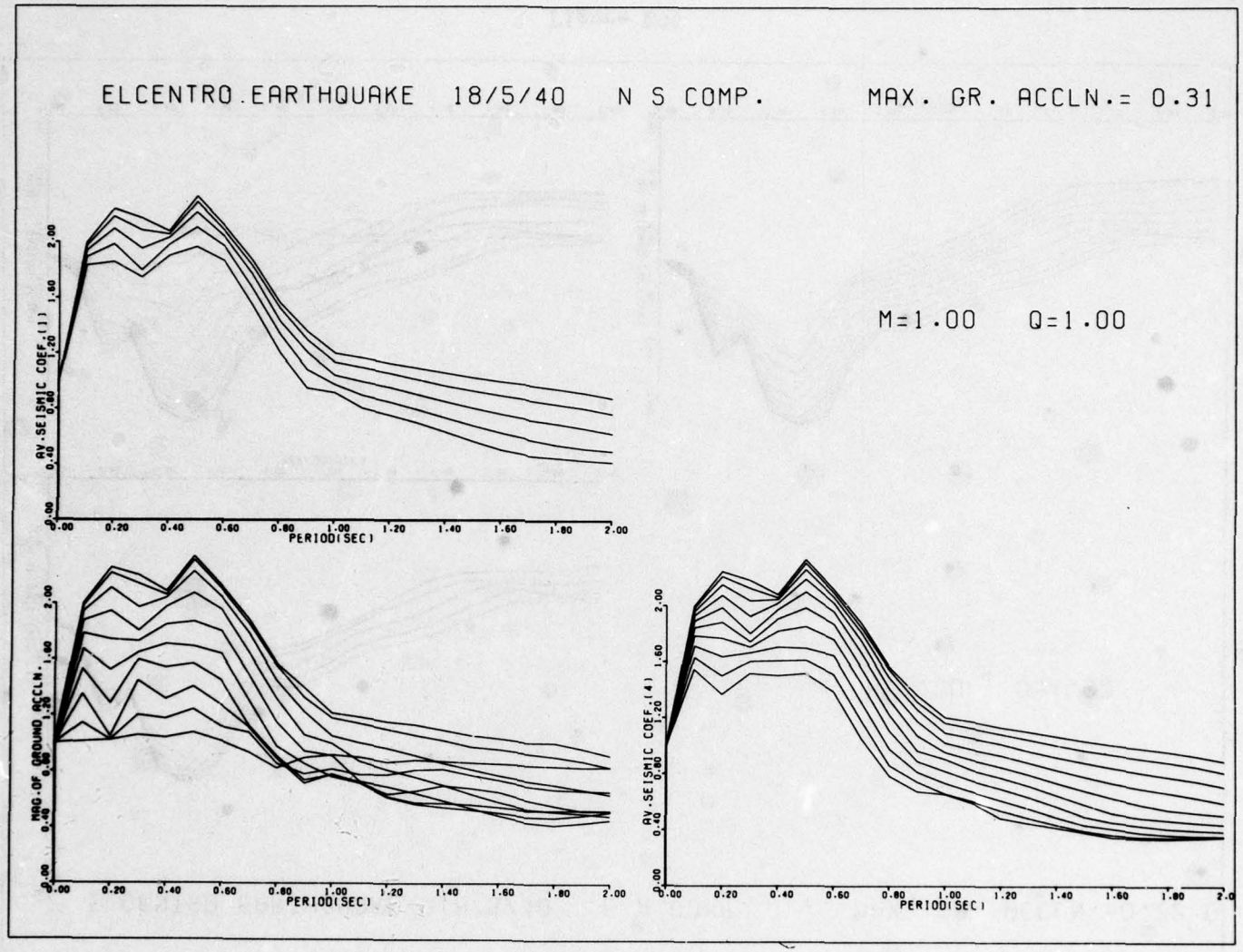
ELCENTRO.EARTHQUAKE 18/5/40 N S COMP.
MAX. GR. ACCLN.= 0.31
M=1.00 Q=1.00
AV.SEISMIC COEF.(1)
MAG.OF GROUND ACCLN.
AV.SEISMIC COEF.(4)
PERIOD(SEC)
0.00
0.20
0.40
0.60
0.80
1.00
1.20
1.40
1.60
1.80
2.00

Figure E94

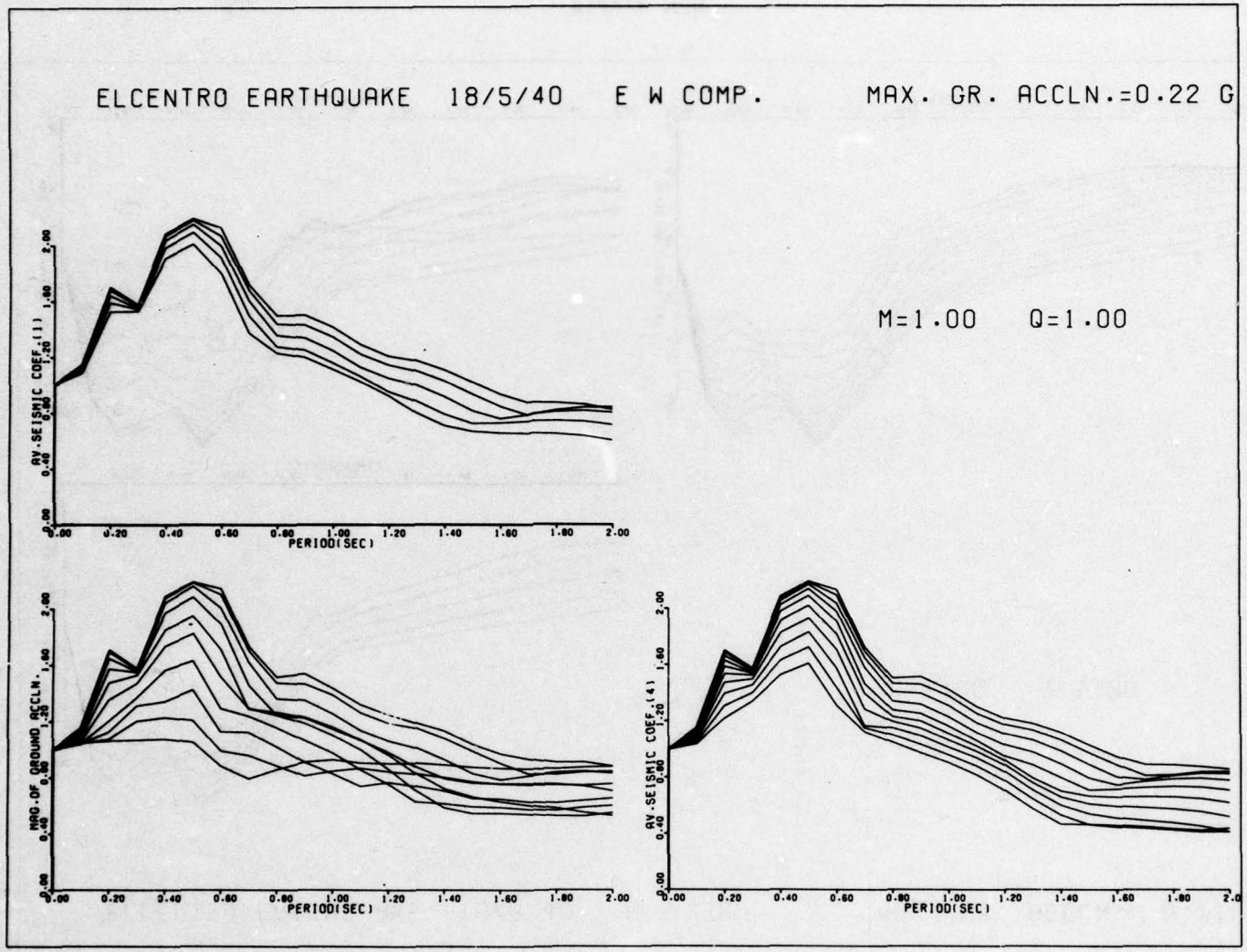
ELCENTRO EARTHQUAKE 18/5/40 E W COMP.
MAX. GR. ACCLN.=0.22 G
M=1.00 Q=1.00
AV.SEISMIC COEF.(1)
PERIOD(SEC)
MAG.OF GROUND ACCLN.
PERIOD(SEC)
AV.SEISMIC COEF.(4)
PERIOD(SEC)

Figure E95

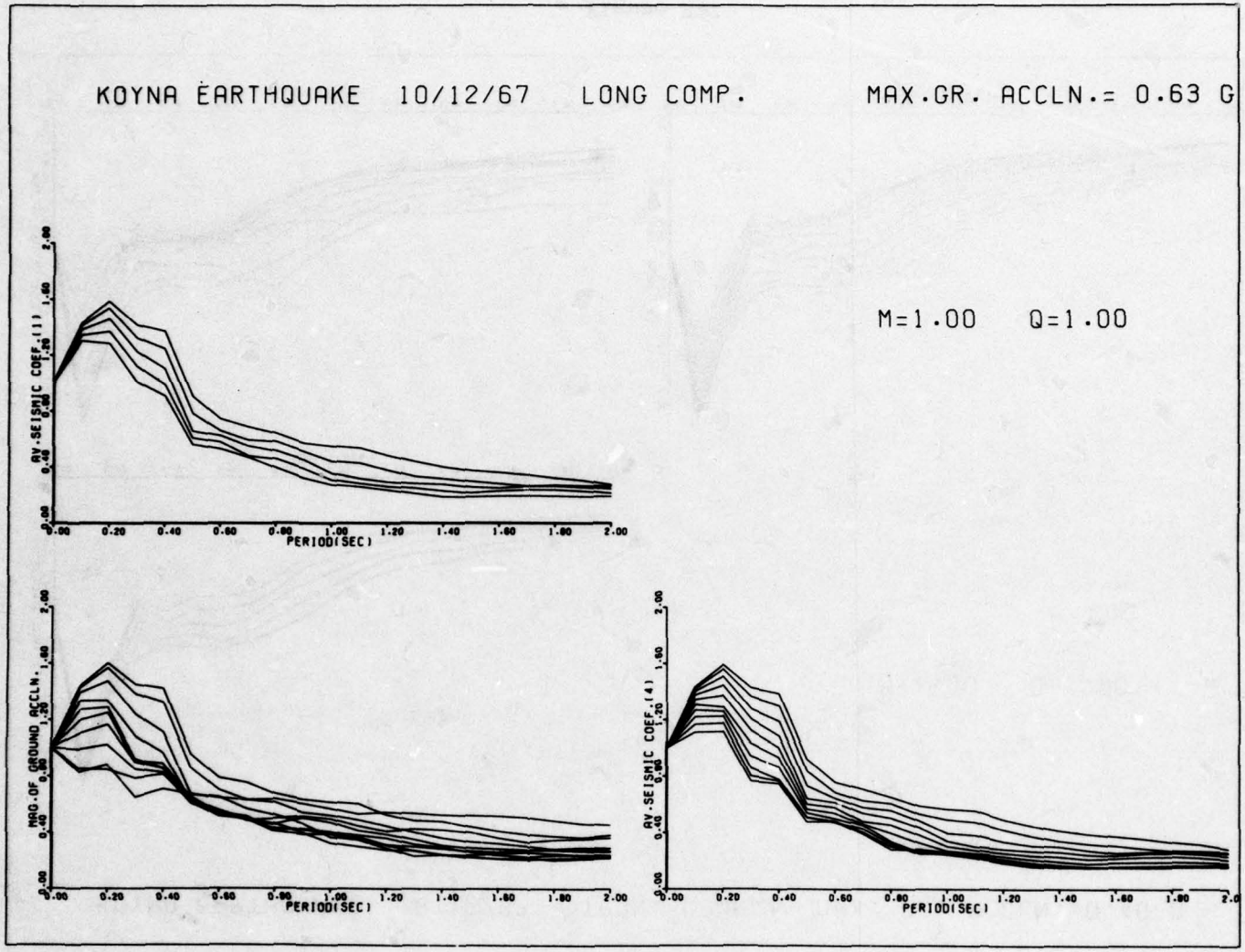
KOYNA EARTHQUAKE 10/12/67 LONG COMP.
MAX.GR. ACCLN.= 0.63 G
M=1.00 Q=1.00
AV.SEISMIC COEF.(I)
MAG.OF GROUND ACCLN.
AV.SEISMIC COEF.(A)
PERIOD(SEC)
0.00
0.20
0.40
0.60
0.80
1.00
1.20
1.40
1.60
1.80
2.00

Figure E96

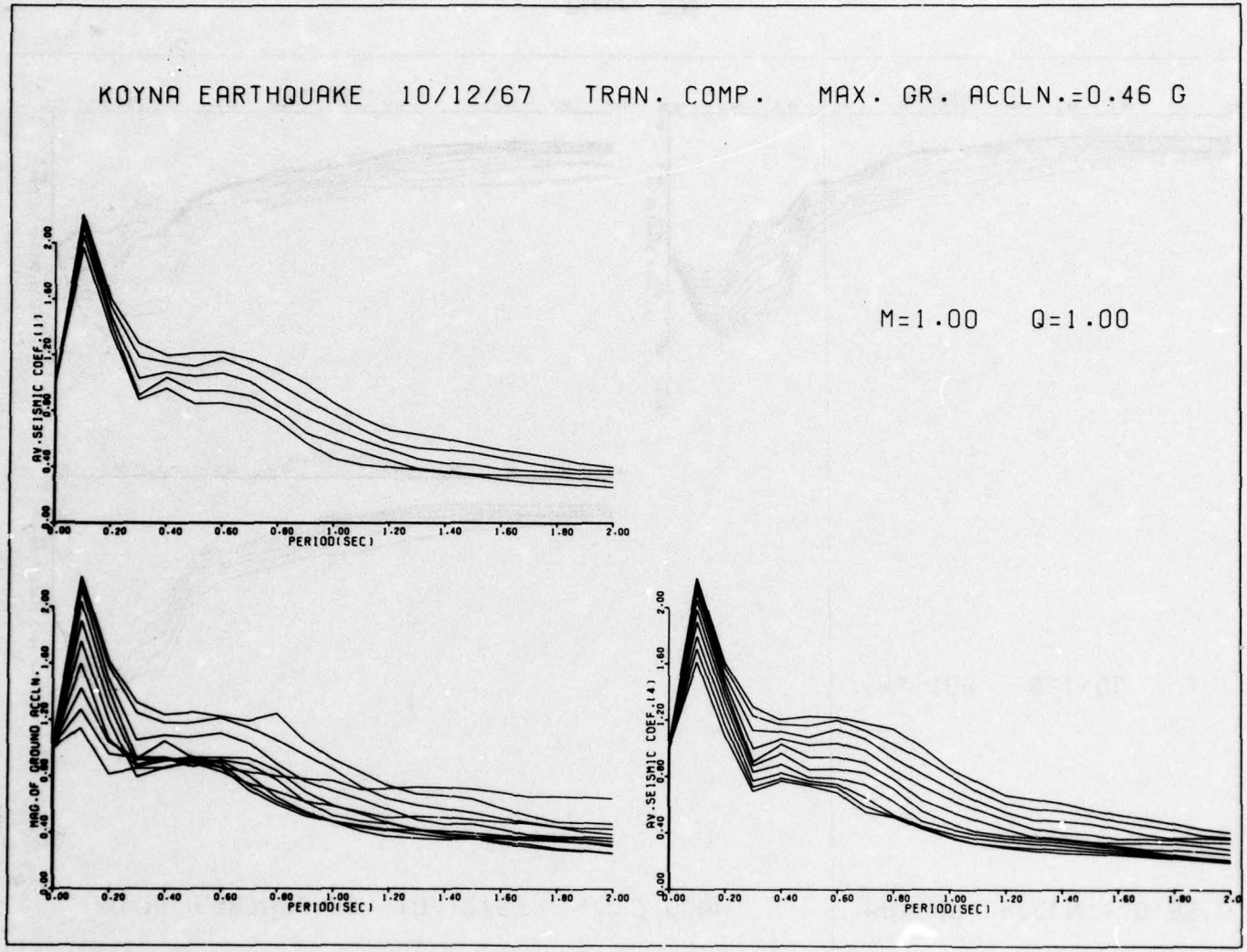
KOYNA EARTHQUAKE 10/12/67 TRAN. COMP. MAX. GR. ACCLN.=0.46 G
M=1.00 Q=1.00
AV.SEISMIC COEF.(1)
MAG.OF GROUND ACCLN.
AV.SEISMIC COEF.(4)
PERIOD(SEC)
0.00
0.20
0.40
0.60
0.80
1.00
1.20
1.40
1.60
1.80
2.00

Figure E97

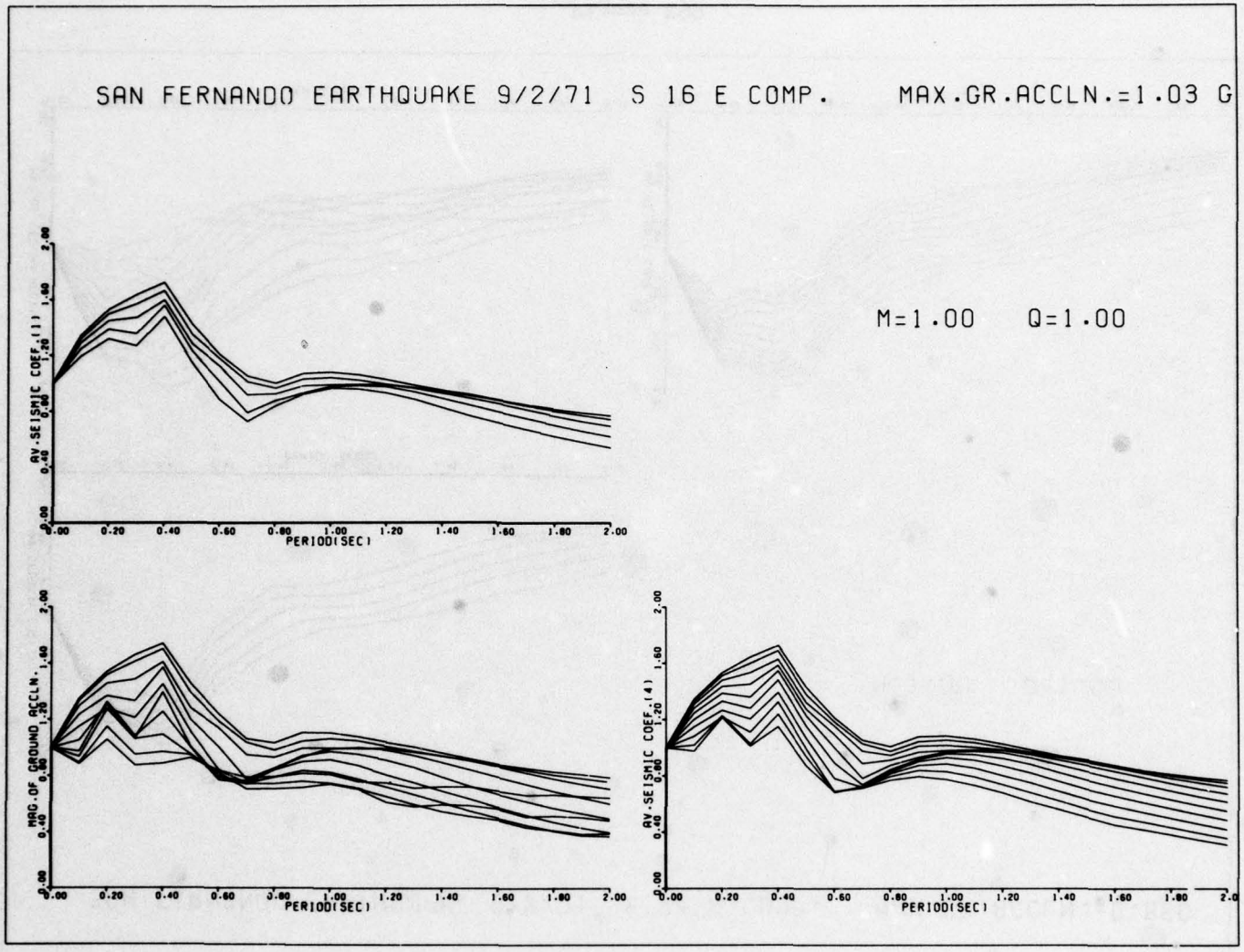
SAN FERNANDO EARTHQUAKE 9/2/71 S 16 E COMP. MAX.GR.ACCLN.=1.03 G
M=1.00 Q=1.00
AV.SEISMIC COEF.(1)
MAG.OF GROUND ACCLN.
AV.SEISMIC COEF.(4)
PERIOD(SEC)
0.00
0.20
0.40
0.60
0.80
1.00
1.20
1.40
1.60
1.80
2.00

Figure E98

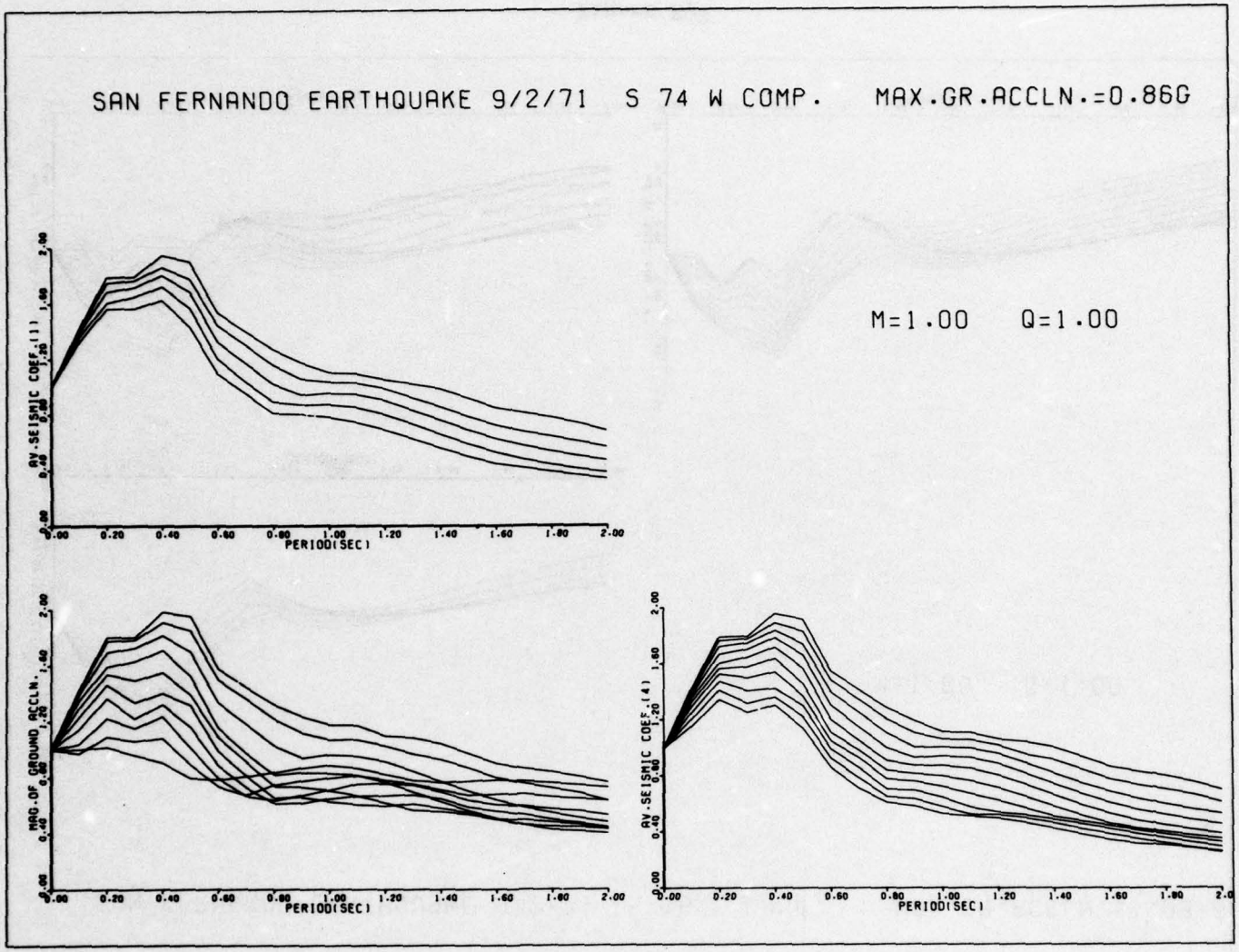
SAN FERNANDO EARTHQUAKE 9/2/71 S 74 W COMP. MAX.GR.ACCLN.=0.86G
M=1.00 Q=1.00
AV.SEISMIC COEF.(1)
MAG.OF GROUND ACCLN.
AV.SEISMIC COEF.(4)
PERIOD(SEC)
0.00
0.20
0.40
0.60
0.80
1.00
1.20
1.40
1.60
1.80
2.00

Figure E99

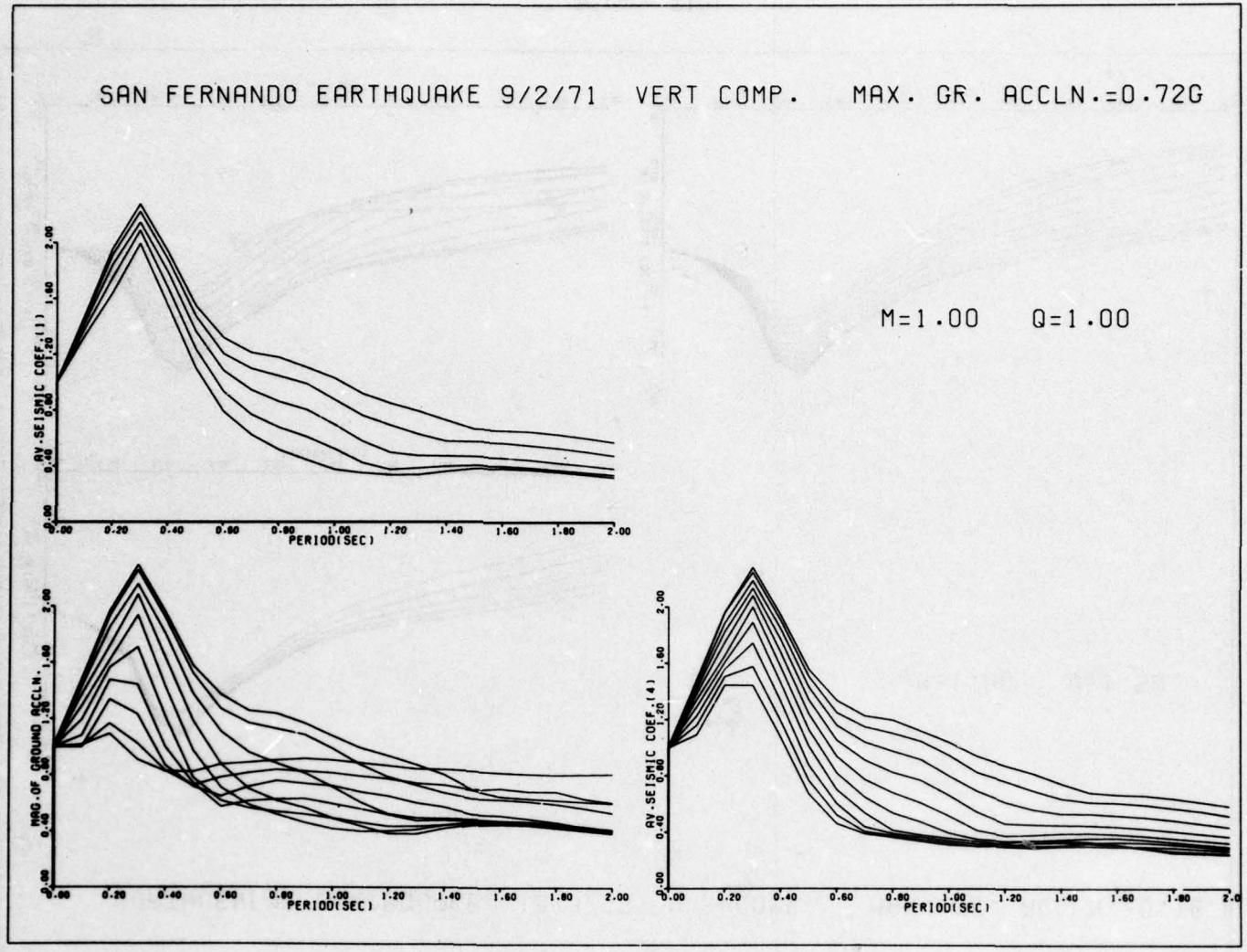
SAN FERNANDO EARTHQUAKE 9/2/71 VERT COMP. MAX. GR. ACCLN.=0.72G
M=1.00 Q=1.00
AV.SEISMIC COEF.(1)
PERIOD(SEC)
MAG.OF GROUND ACCLN.
PERIOD(SEC)
AV.SEISMIC COEF.(4)
PERIOD(SEC)

Figure E100

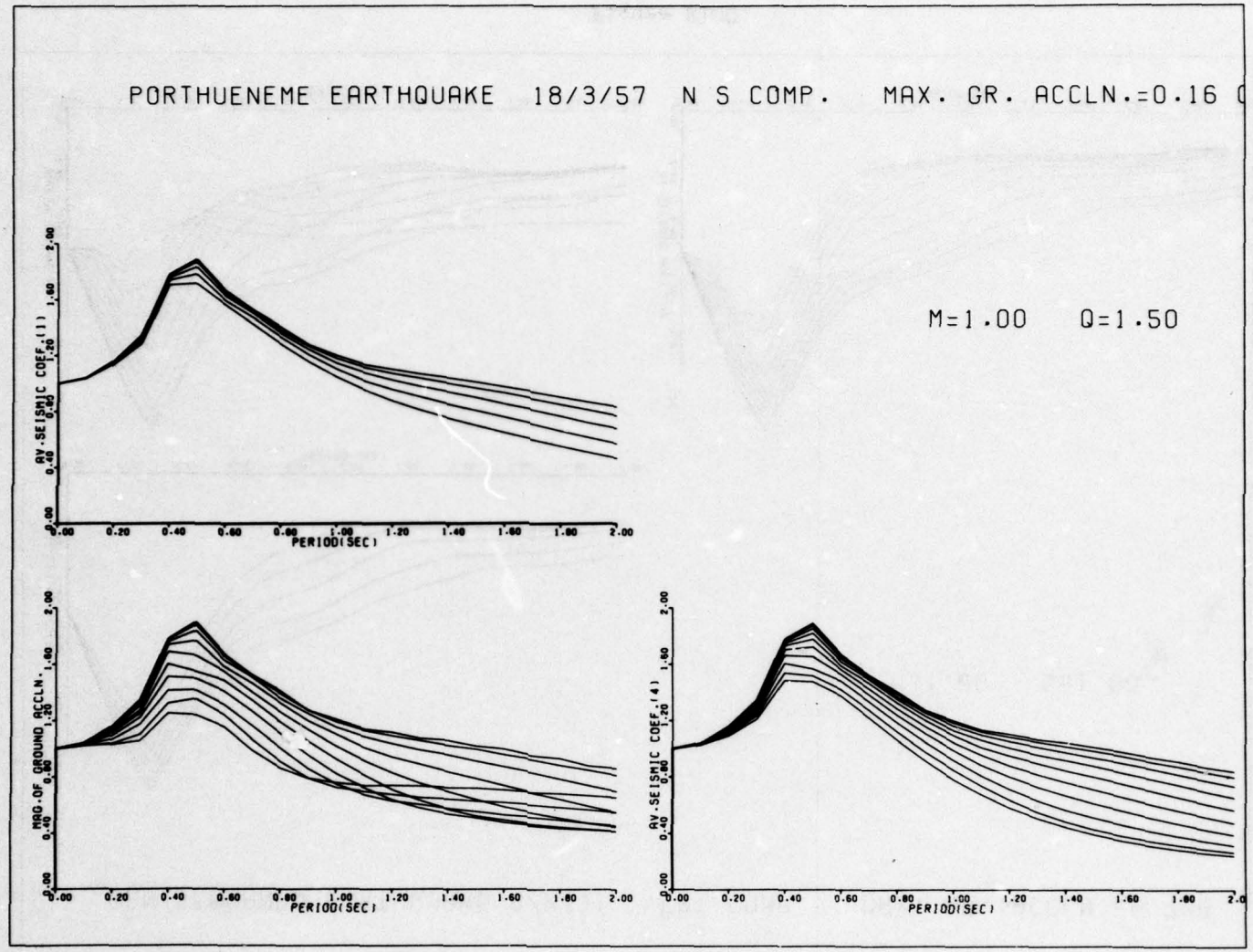
PORTHUENEME EARTHQUAKE 18/3/57 N S COMP. MAX. GR. ACCLN.=0.16 G
M=1.00 Q=1.50
AV.SEISMIC COEF.(I)
MAG.OF GROUND ACCLN.
AV.SEISMIC COEF.(I)
PERIOD(SEC)
PERIOD(SEC)
PERIOD(SEC)

Figure E101

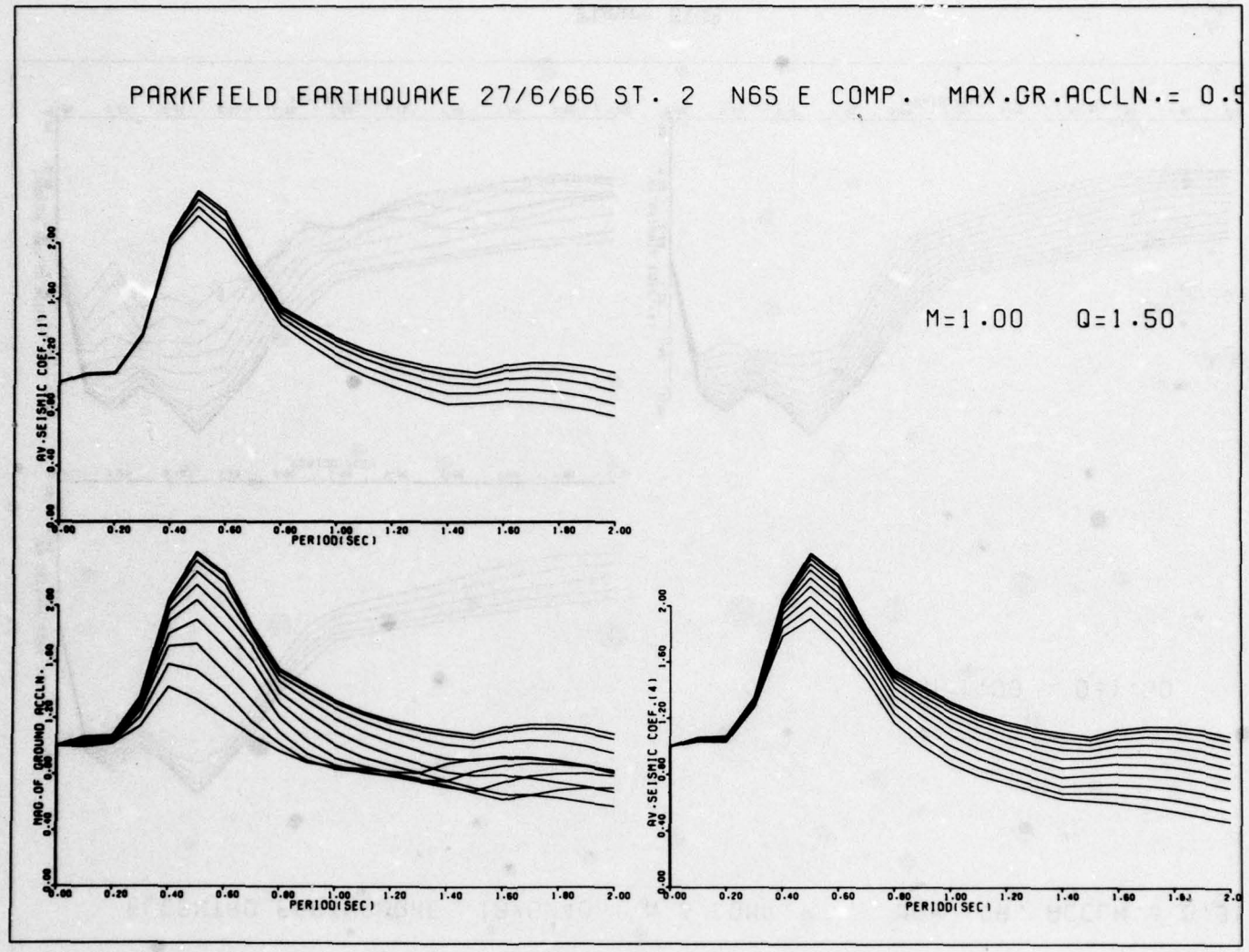
PARKFIELD EARTHQUAKE 27/6/66 ST. 2 N65 E COMP. MAX.GR.ACCLN.= 0.5
M=1.00 Q=1.50
AV.SEISMIC COEF.(1)
PERIOD(SEC)
NAG.OF GROUND ACCLN.
PERIOD(SEC)
AV.SEISMIC COEF.(4)
PERIOD(SEC)

Figure E102

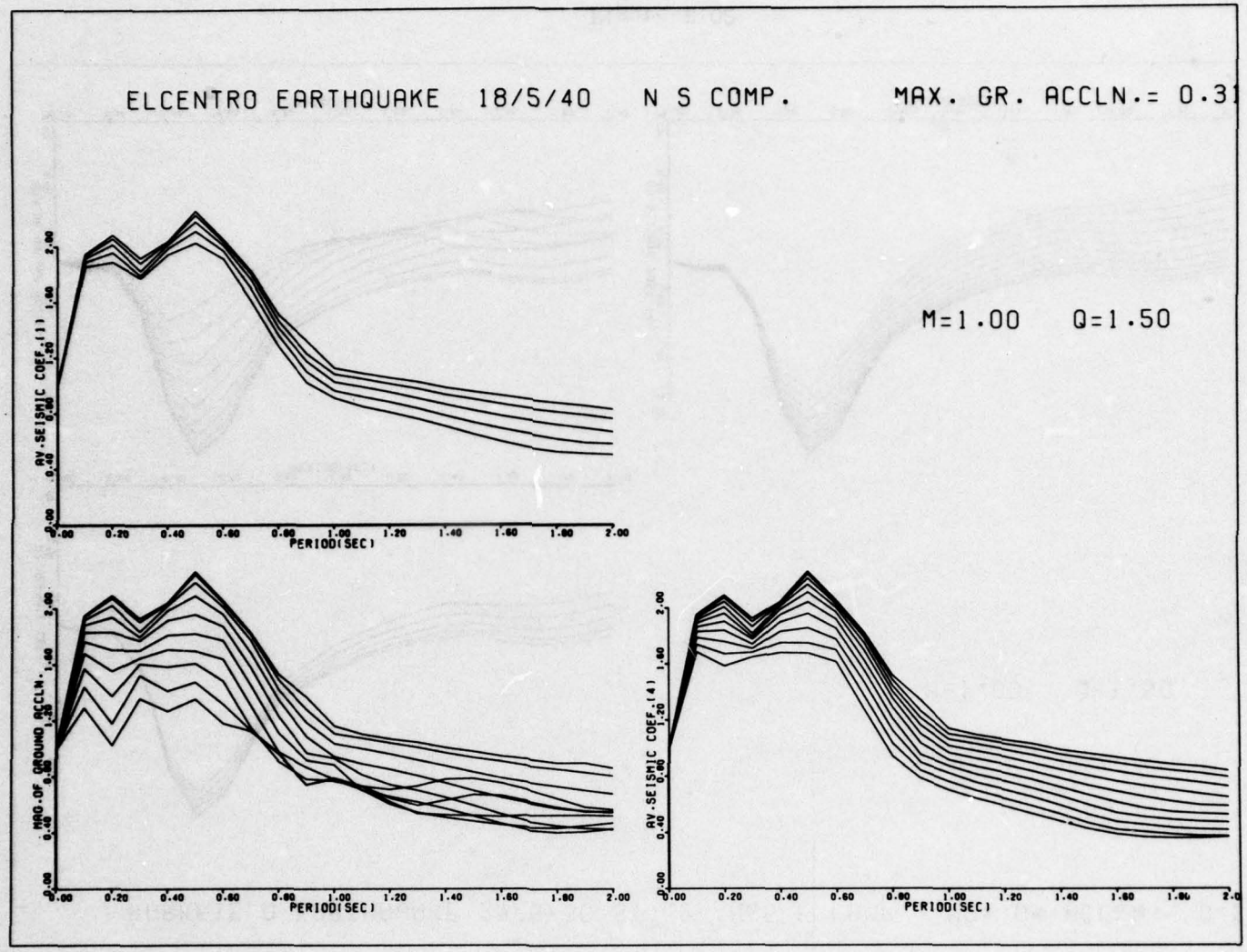
ELCENTRO EARTHQUAKE 18/5/40 N S COMP.
MAX. GR. ACCLN.= 0.31
M=1.00 Q=1.50
AV.SEISMIC COEF.(I)
MAG.OF GROUND ACCLN.
AV.SEISMIC COEF.(4)
PERIOD(SEC)

Figure E103

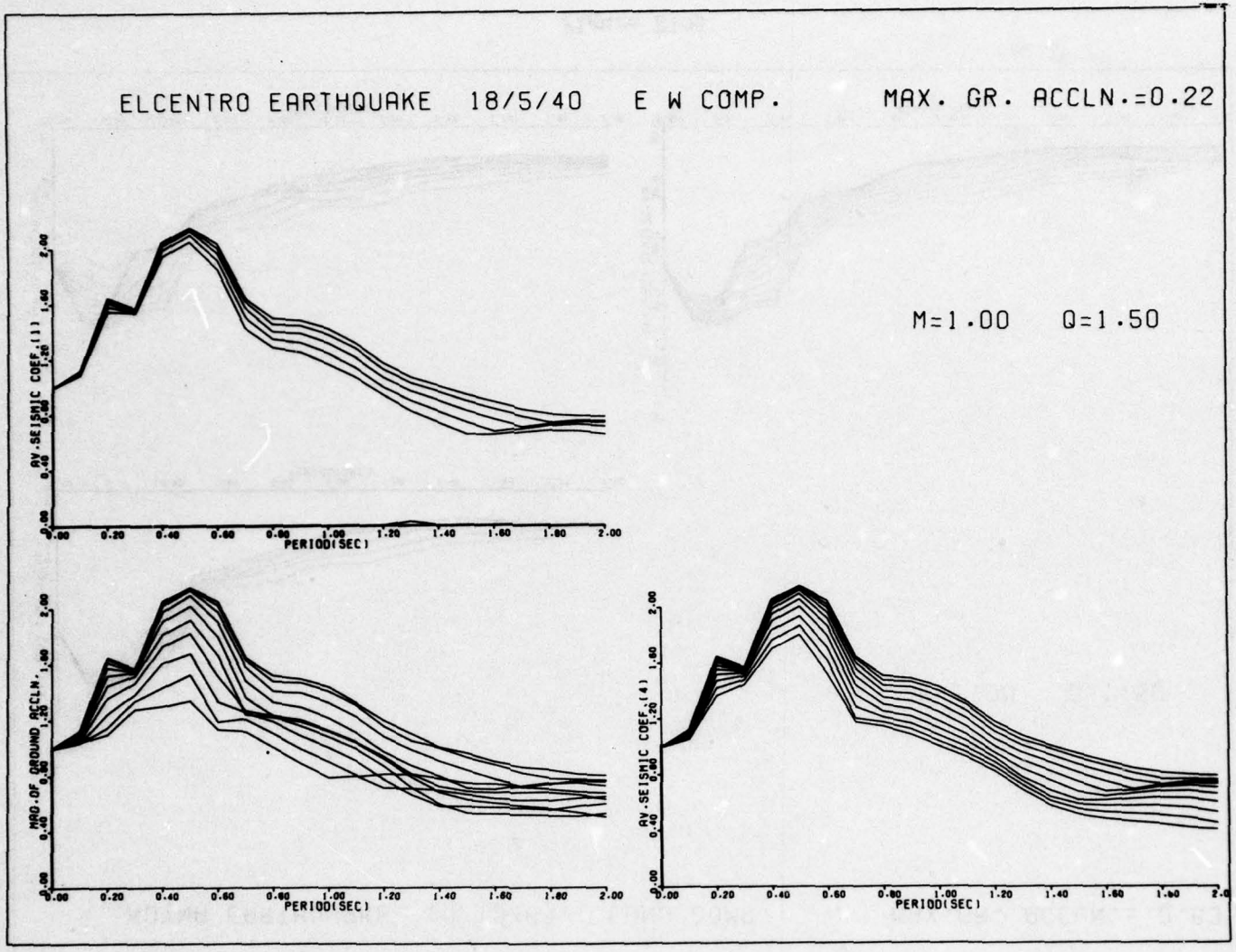
ELCENTRO EARTHQUAKE 18/5/40 E W COMP.
MAX. GR. ACCLN.=0.22
M=1.00 Q=1.50
AV.SEISMIC COEF.(1)
PERIOD(SEC)
MAG.OF GROUND ACCLN.
PERIOD(SEC)
AV.SEISMIC COEF.(4)
PERIOD(SEC)

Figure E104

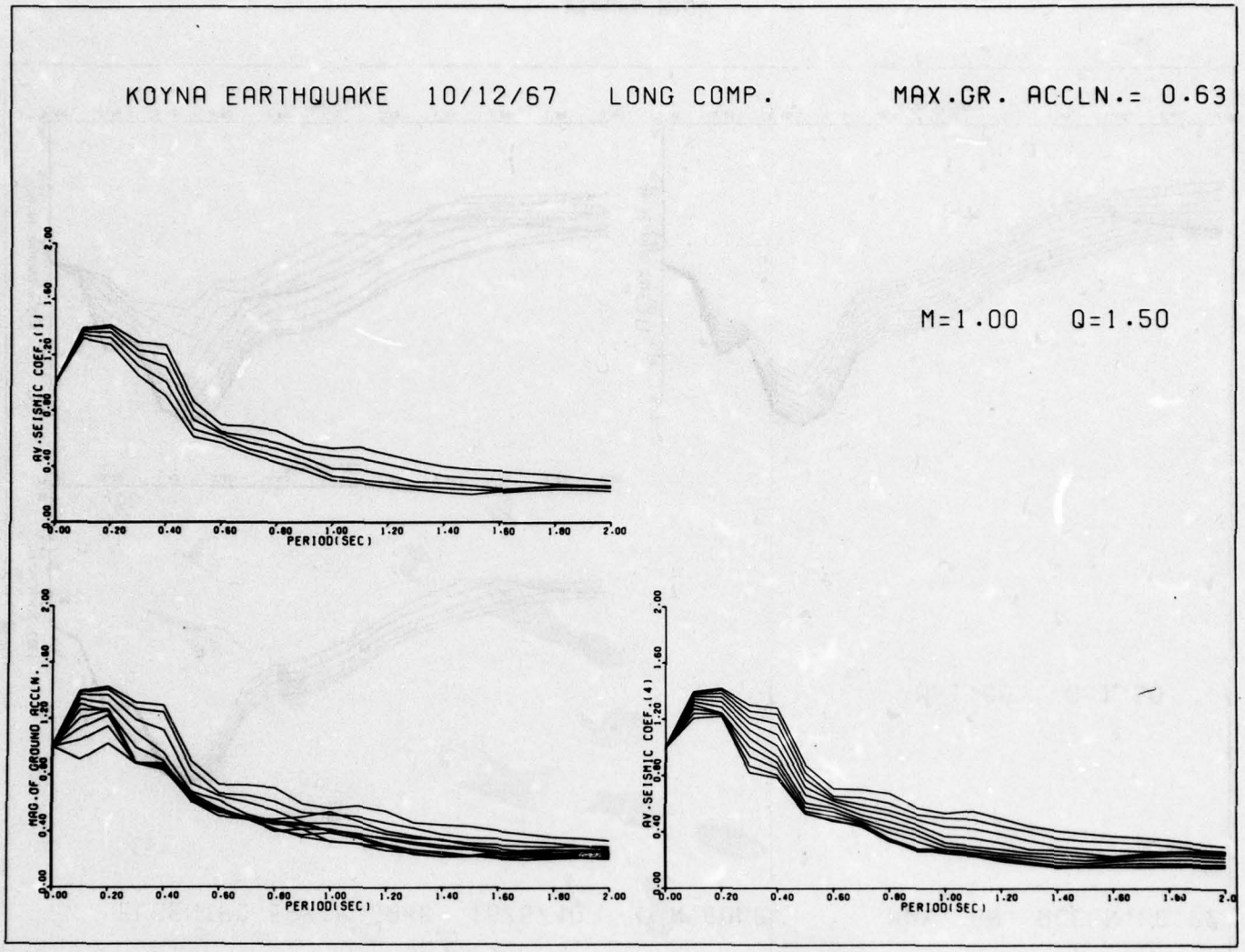
KOYNA EARTHQUAKE 10/12/67 LONG COMP.
MAX.GR. ACCLN.= 0.63
M=1.00 Q=1.50
AV.SEISMIC COEF.(1)
PERIOD(SEC)
MAG.OF GROUND ACCLN.
PERIOD(SEC)
AV.SEISMIC COEF.(4)
PERIOD(SEC)

Figure E105

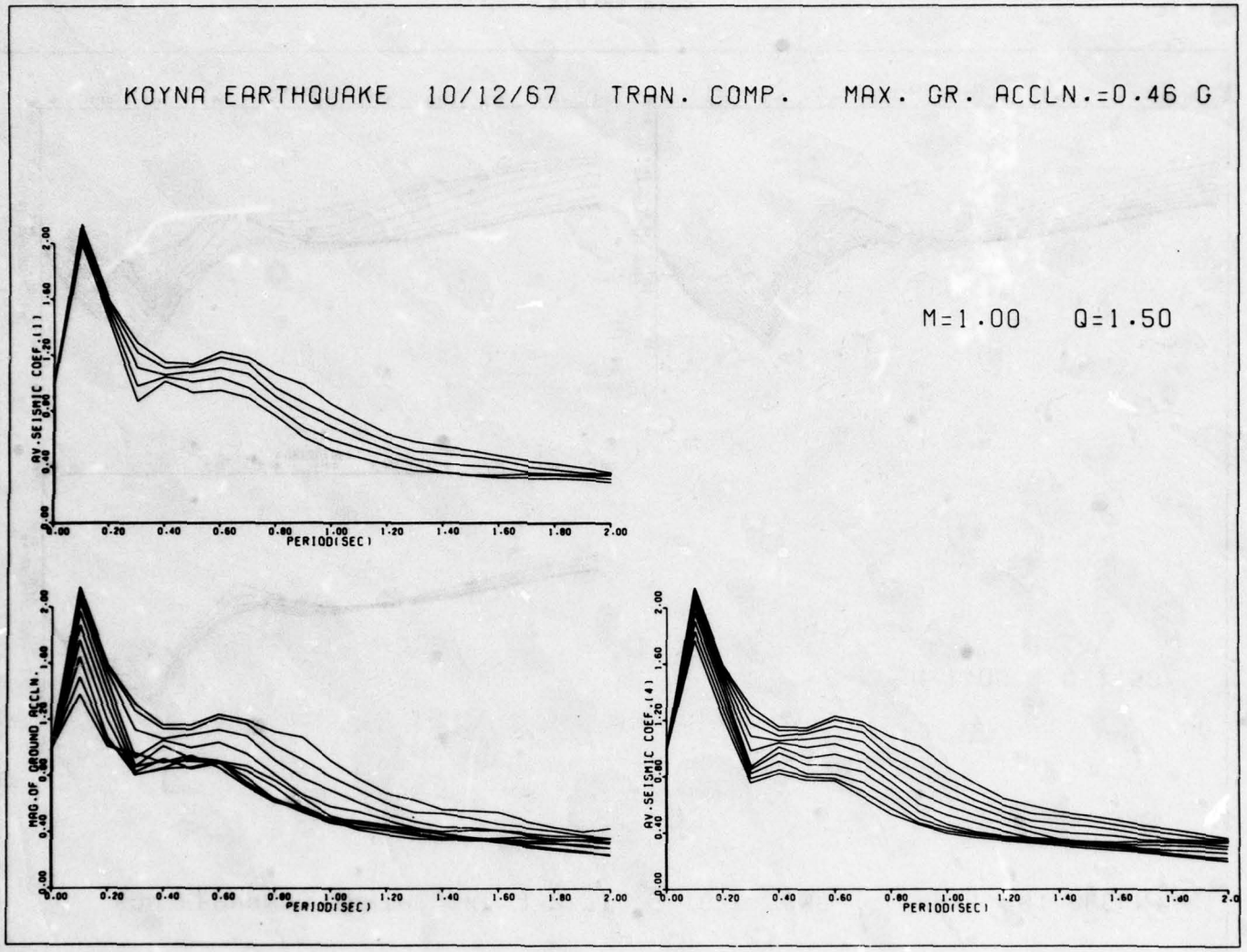
KOYNA EARTHQUAKE 10/12/67 TRAN. COMP. MAX. GR. ACCLN.=0.46 G
M=1.00 Q=1.50
AV.SEISMIC COEF.(I)
MAG.OF GROUND ACCLN.
AV.SEISMIC COEF.(4)
PERIOD(SEC)

Figure E106

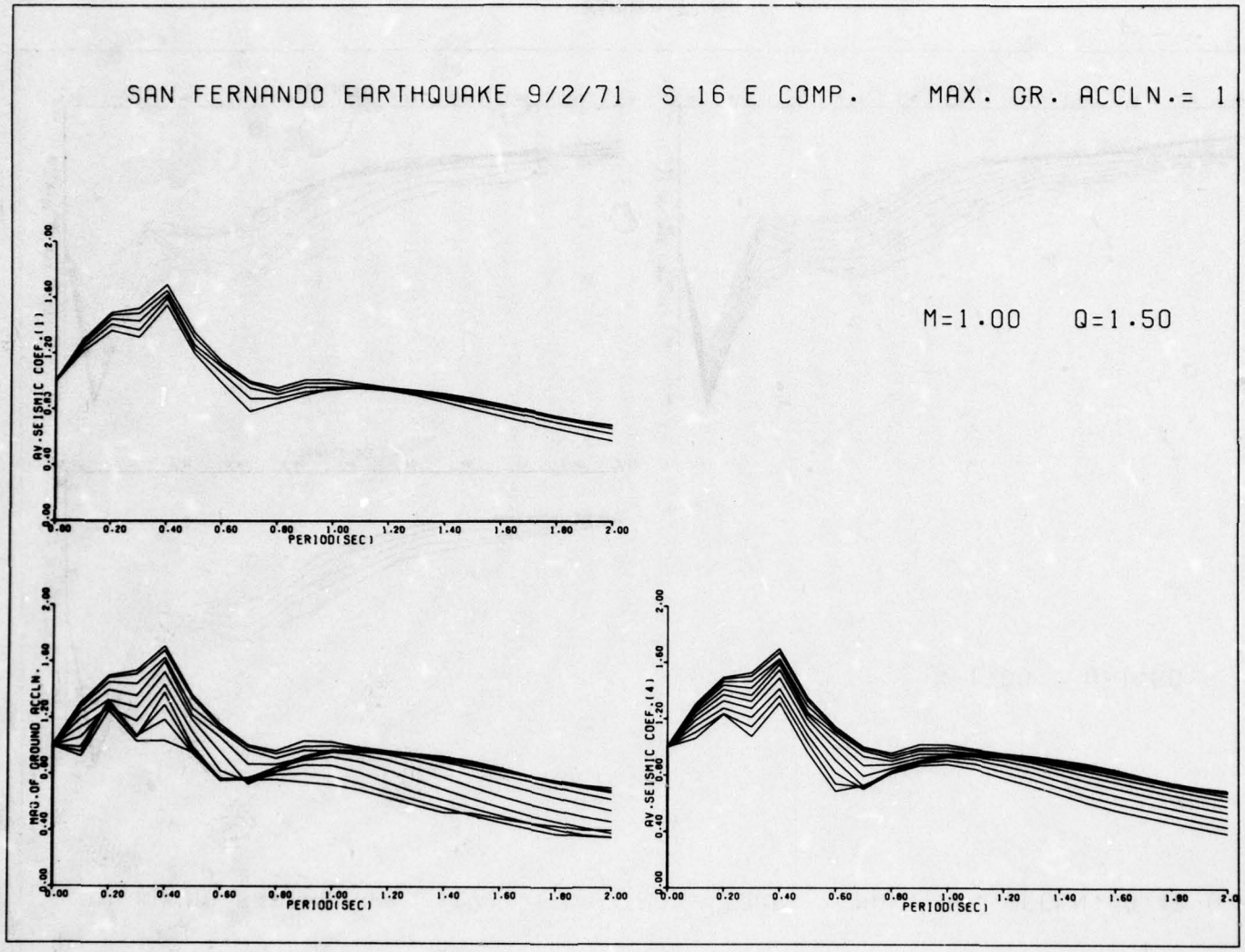
SAN FERNANDO EARTHQUAKE 9/2/71 S 16 E COMP. MAX. GR. ACCLN.= 1
M=1.00 Q=1.50
AV.SEISMIC COEF.(1)
MAG.OF GROUND ACCLN.
AV.SEISMIC COEF.(4)
PERIOD(SEC)
0.00
0.20
0.40
0.60
0.80
1.00
1.20
1.40
1.60
1.80
2.00

Figure E107

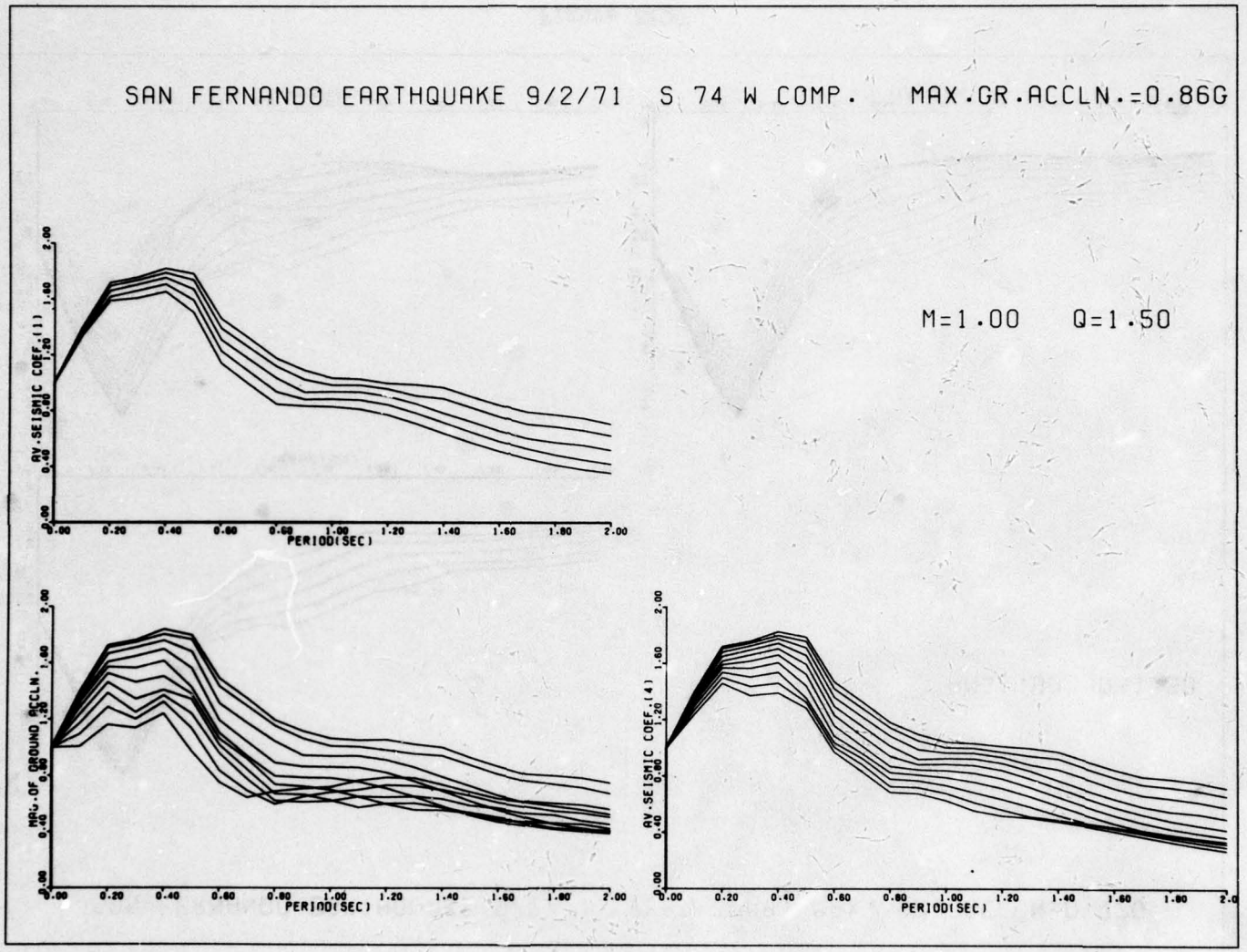
SAN FERNANDO EARTHQUAKE 9/2/71 S 74 W COMP. MAX.GR.ACCLN.=0.86G
M=1.00 Q=1.50
AV.SEISMIC COEF.(1)
NRM.OF GROUND ACCLN.
AV.SEISMIC COEF.(4)
PERIOD(SEC)
0.00
0.20
0.40
0.60
0.80
1.00
1.20
1.40
1.60
1.80
2.00

Figure E108

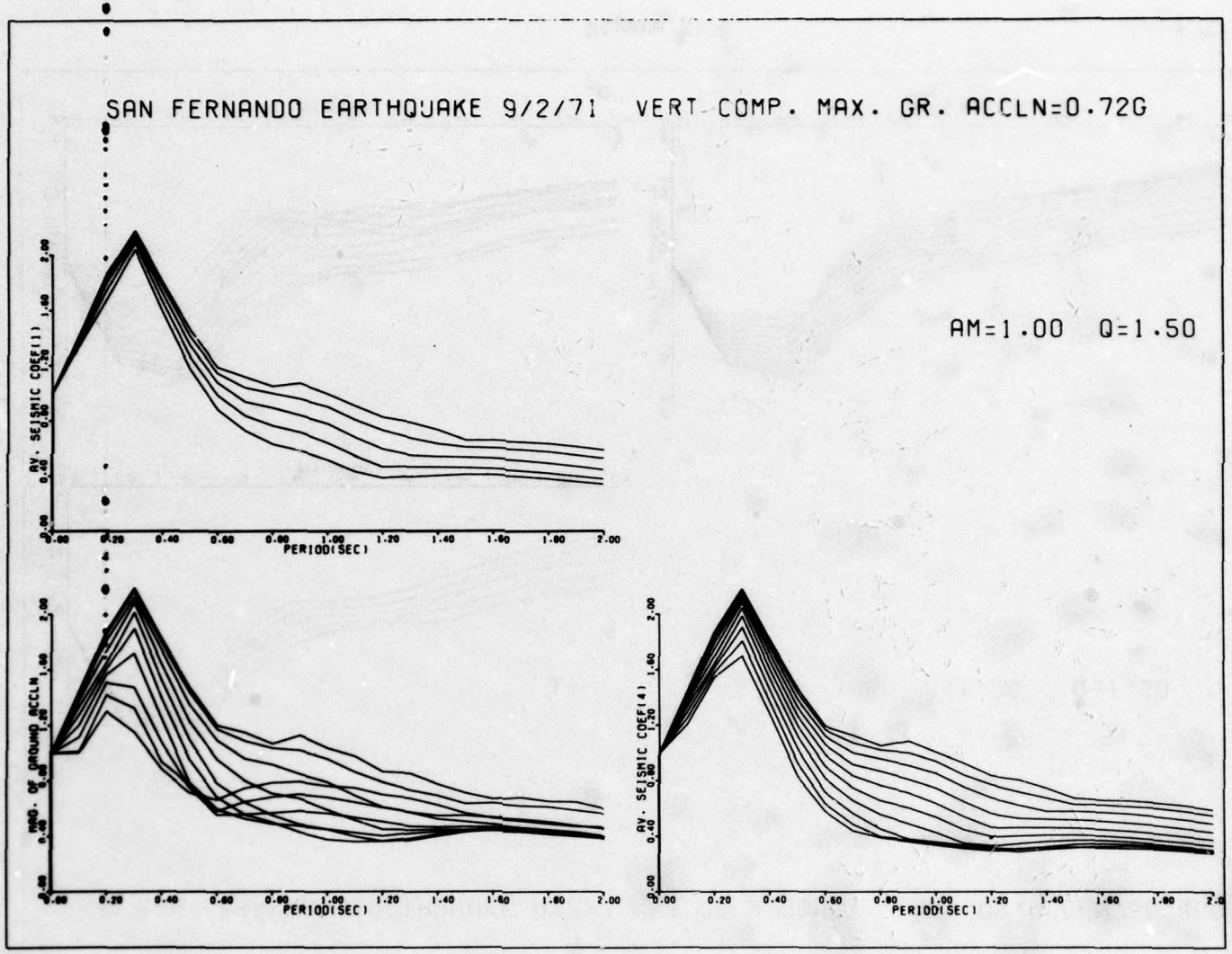
SAN FERNANDO EARTHQUAKE 9/2/71 VERT COMP. MAX. GR. ACCLN=0.72G
AM=1.00 Q=1.50
AV. SEISMIC COEF(1)
AVG. OF GROUND ACCLN
AV. SEISMIC COEF(4)
PERIOD(SEC)

Figure E109

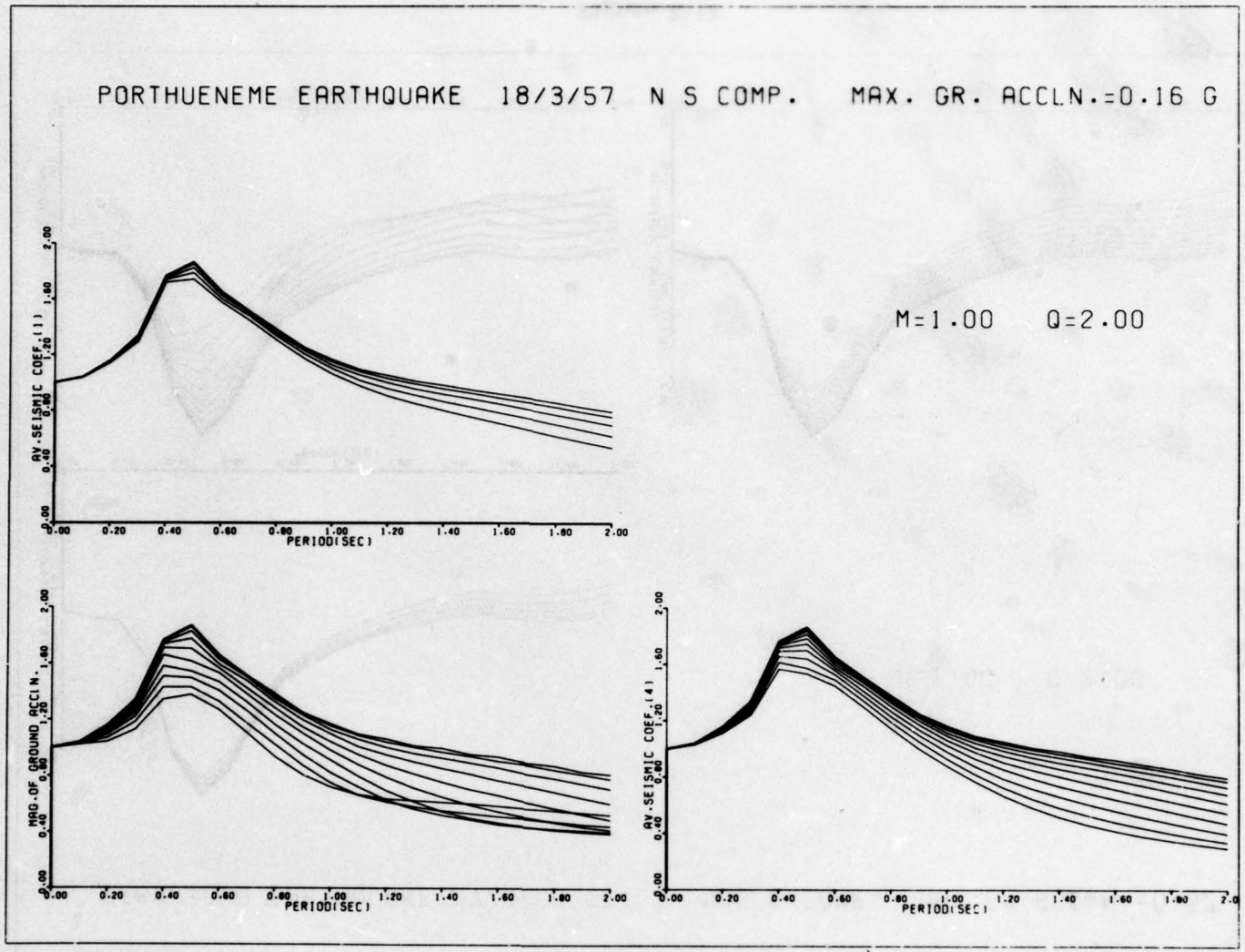
PORTHUENEME EARTHQUAKE 18/3/57 N S COMP. MAX. GR. ACCLN.=0.16 G
M=1.00 Q=2.00
AV.SEISMIC COEF.(1)
MAG.OF GROUND ACCLN.
AV.SEISMIC COEF.(4)
PERIOD(SEC)
0.00
0.20
0.40
0.60
0.80
1.00
1.20
1.40
1.60
1.80
2.00

Figure E110

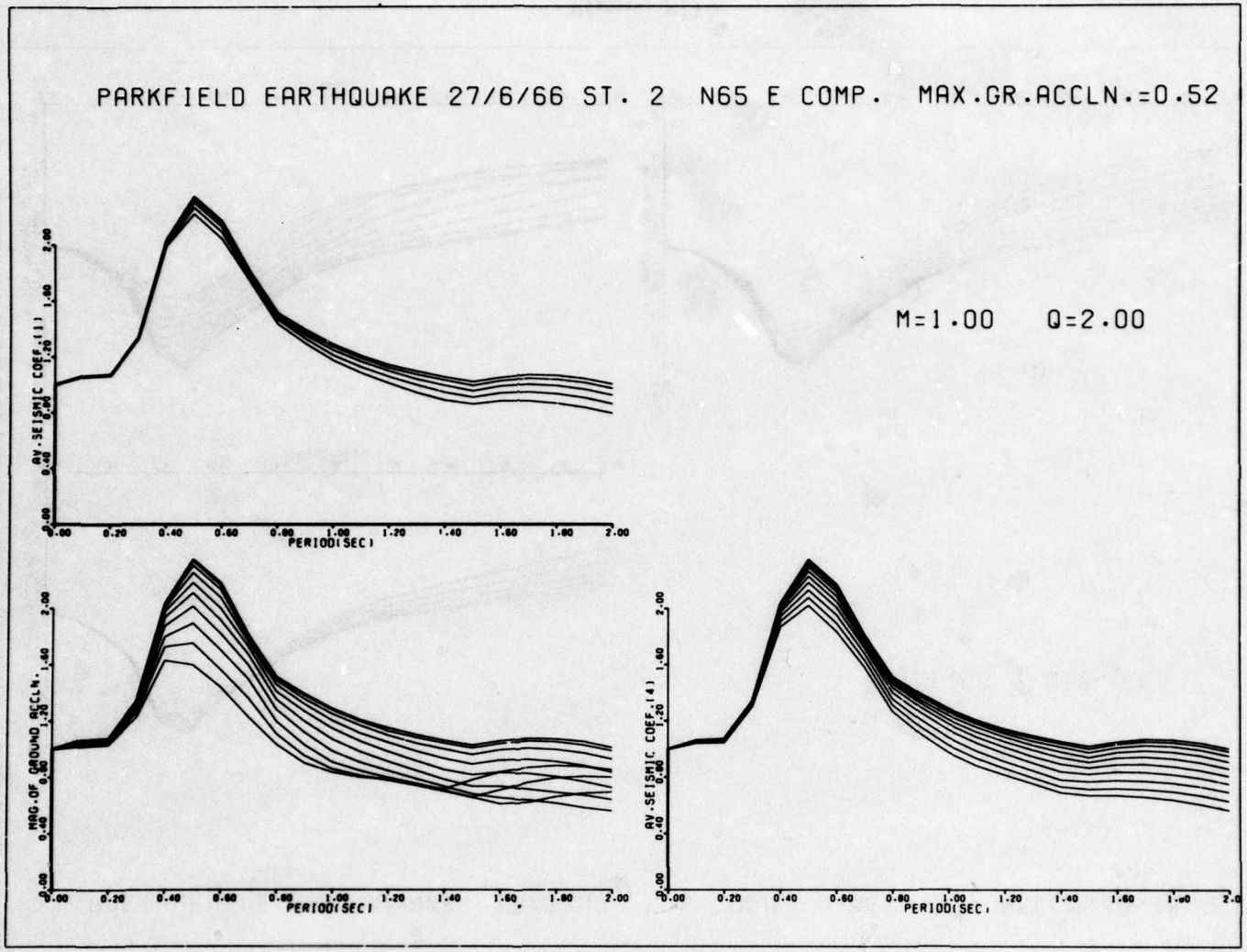
PARKFIELD EARTHQUAKE 27/6/66 ST. 2 N65 E COMP. MAX.GR.ACCLN.=0.52
M=1.00 Q=2.00
AV.SEISMIC COEF.(1)
MAG.OF GROUND ACCLN.
AV.SEISMIC COEF.(4)
PERIOD(SEC)

Figure E111

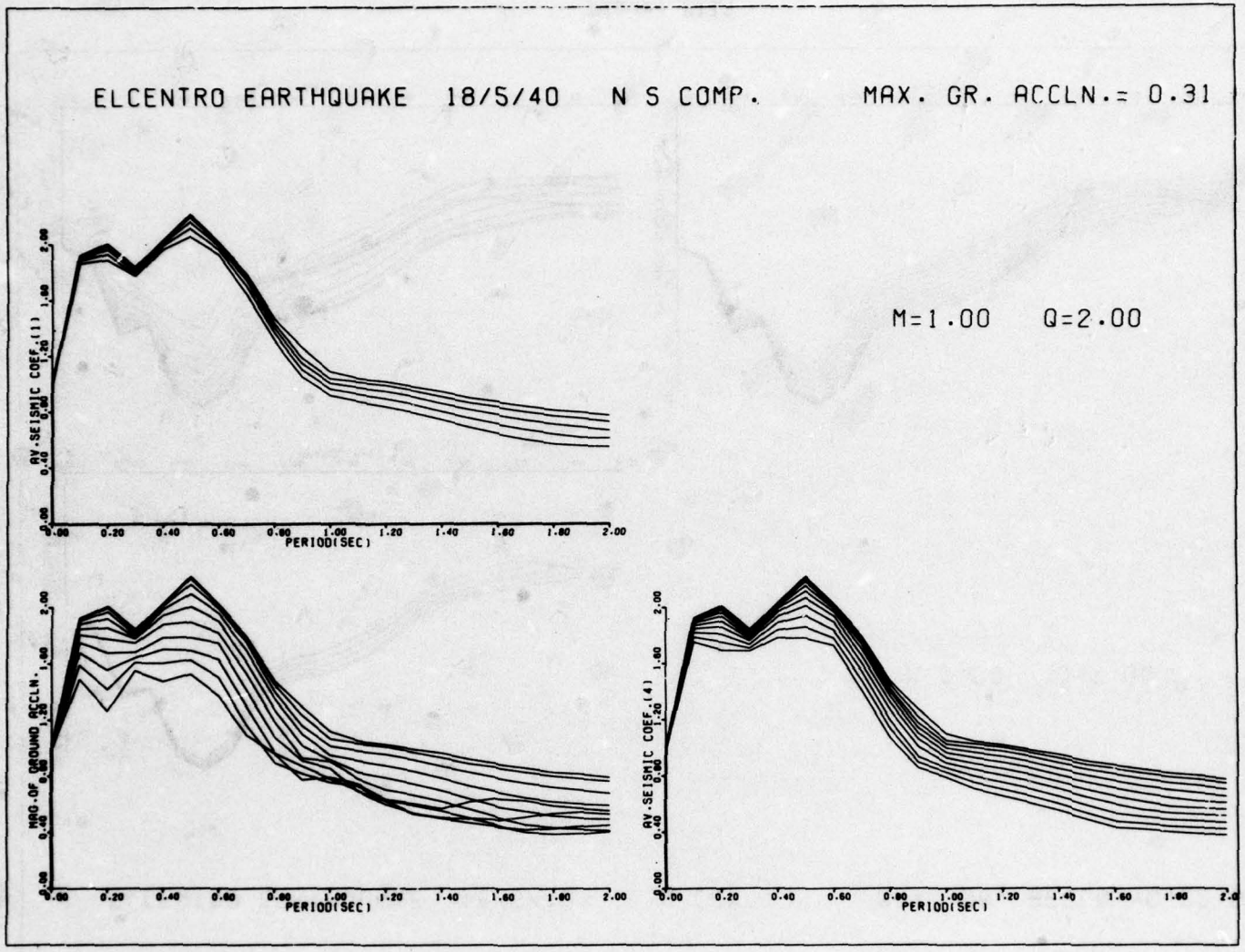
ELCENTRO EARTHQUAKE 18/5/40 N S COMP.
MAX. GR. ACCLN.= 0.31
M=1.00 Q=2.00
AV.SEISMIC COEF.(1)
MAG.OF GROUND ACCLN.
AV.SEISMIC COEF.(4)
PERIOD(SEC)

Figure E112

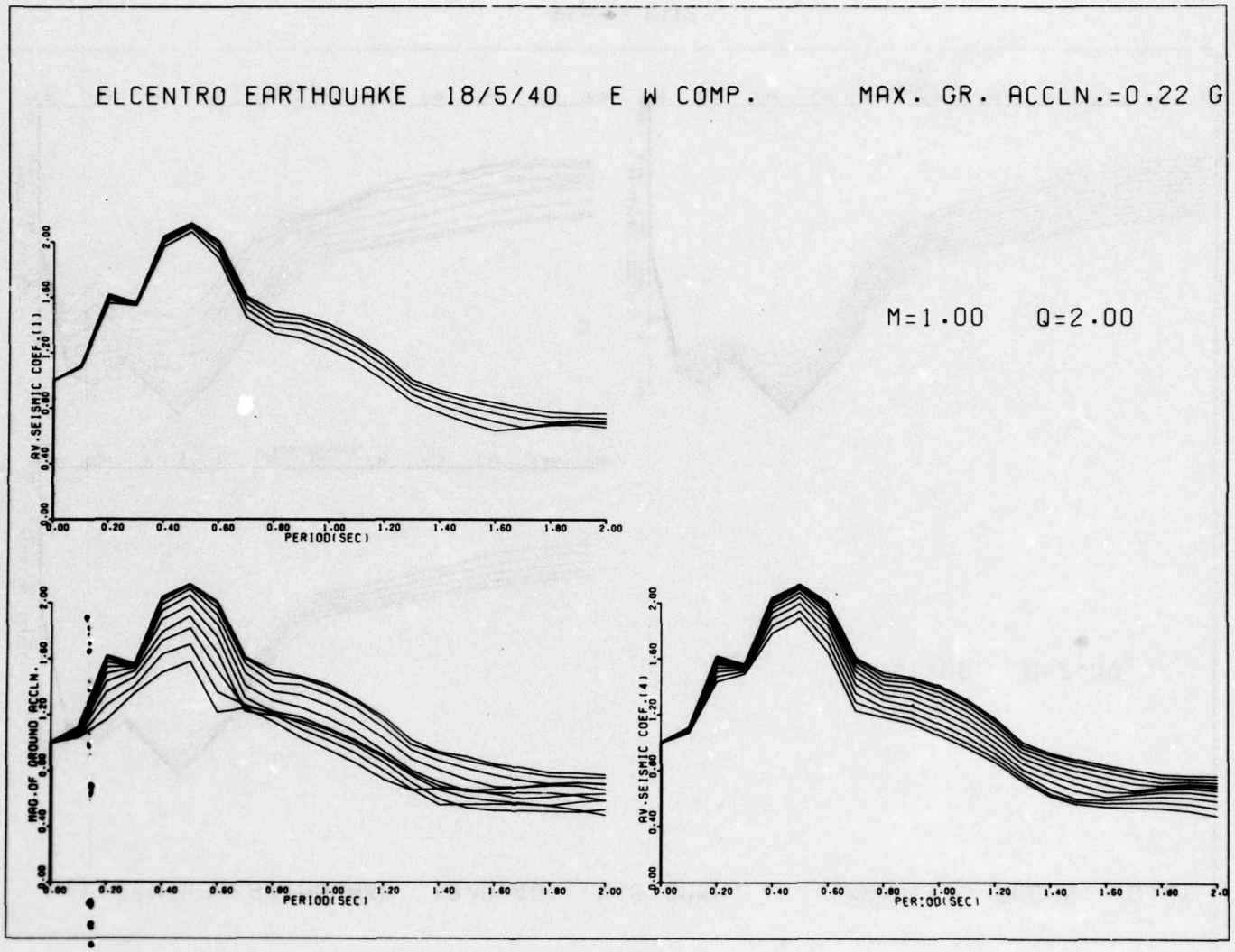
ELCENTRO EARTHQUAKE 18/5/40 E W COMP.
MAX. GR. ACCLN.=0.22 G
M=1.00 Q=2.00
AV.SEISMIC COEF.(1)
MAG.OF GROUND ACCLN.
AV.SEISMIC COEF.(4)
PERIOD(SEC)
0.00
0.20
0.40
0.60
0.80
1.00
1.20
1.40
1.60
1.80
2.00

Figure E113

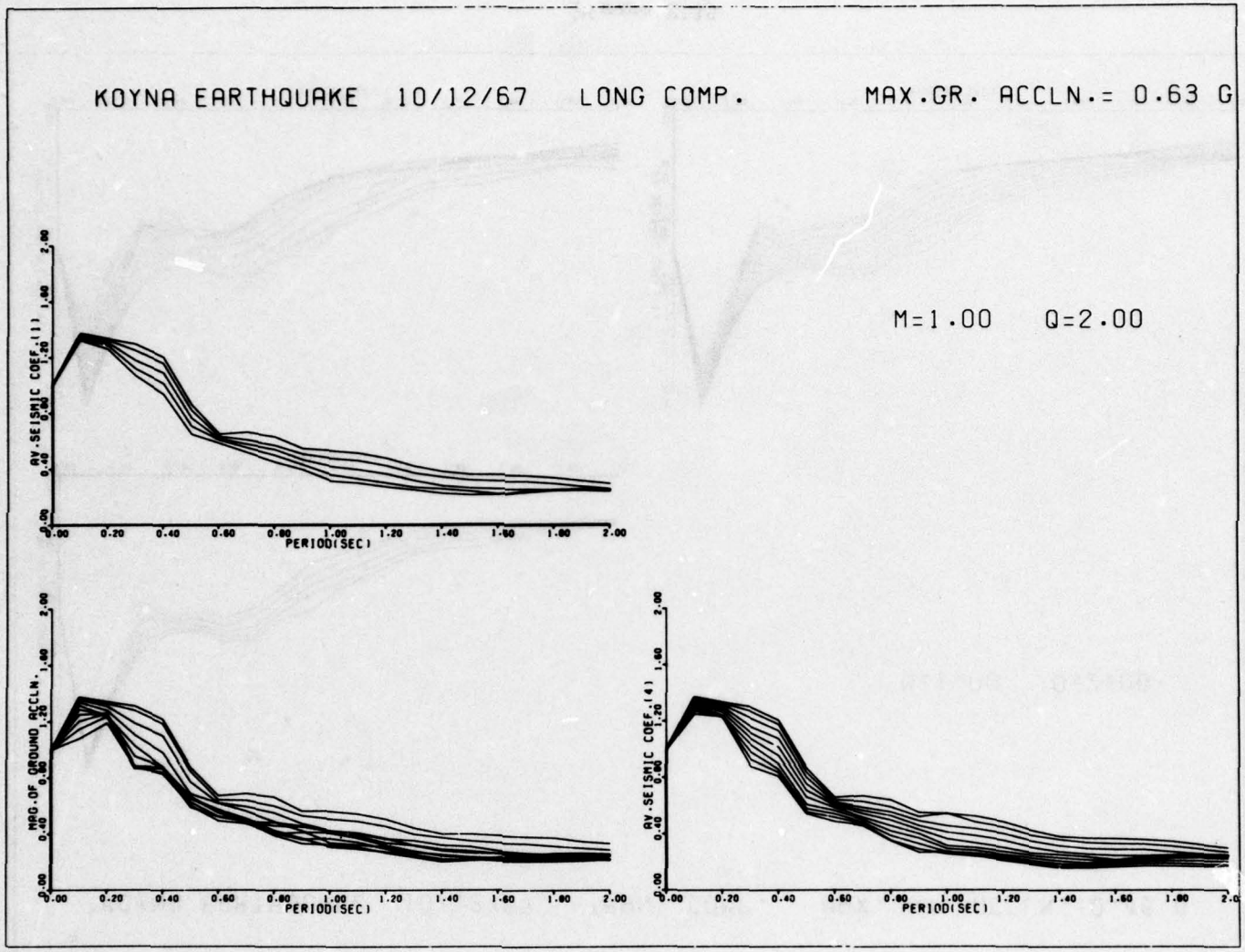
KOYNA EARTHQUAKE 10/12/67 LONG COMP.
MAX.GR. ACCLN.= 0.63 G
M=1.00 Q=2.00
AV.SEISMIC COEF.(1)
PERIOD(SEC)
MAG.OF GROUND ACCLN.
PERIOD(SEC)
AV.SEISMIC COEF.(4)
PERIOD(SEC)

Figure E114

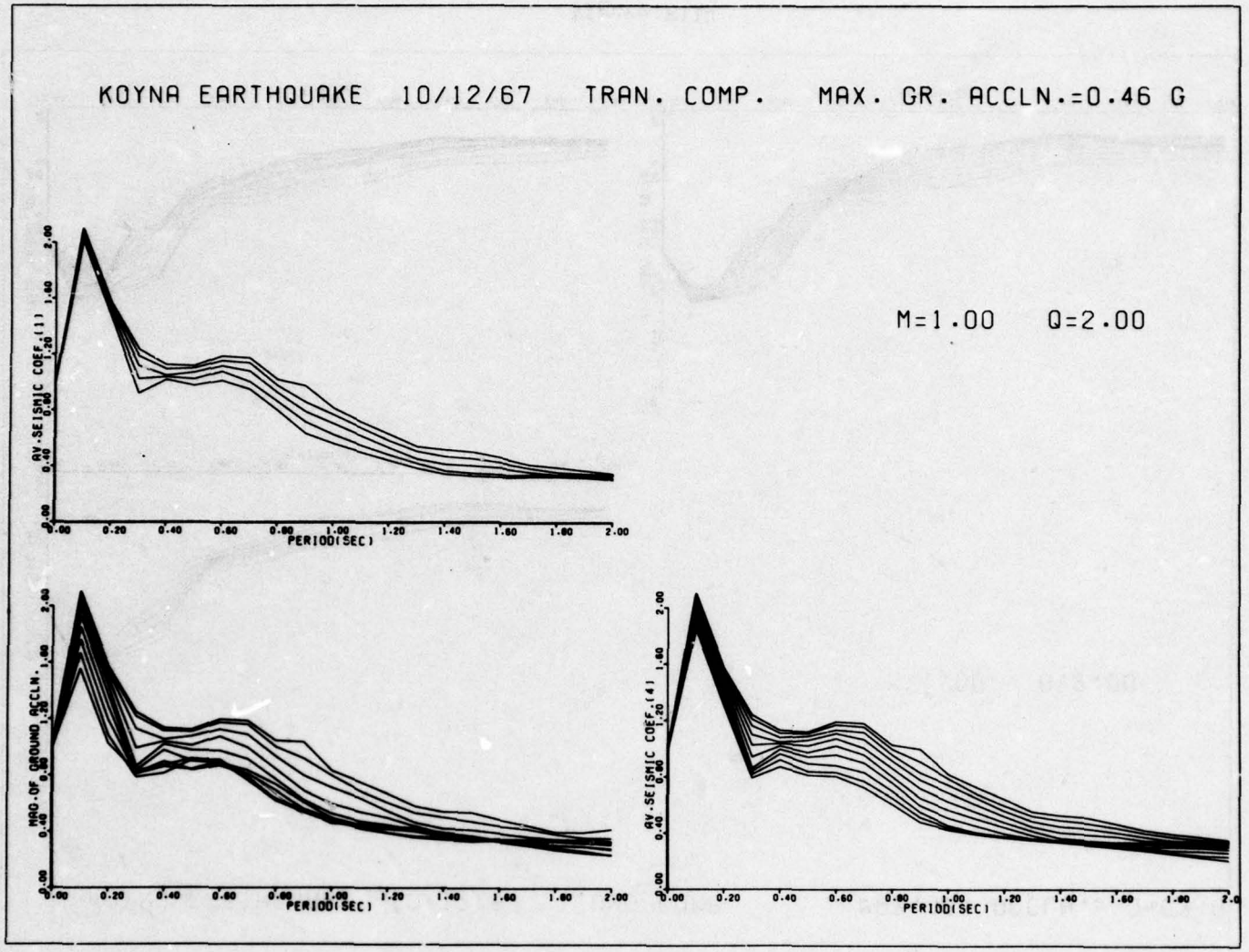
KOYNA EARTHQUAKE 10/12/67 TRAN. COMP. MAX. GR. ACCLN.=0.46 G
M=1.00 Q=2.00
AV.SEISMIC COEF.(1)
PERIOD(SEC)
MAG.OF GROUND ACCLN.
PERIOD(SEC)
AV.SEISMIC COEF.(4)
PERIOD(SEC)

Figure E115

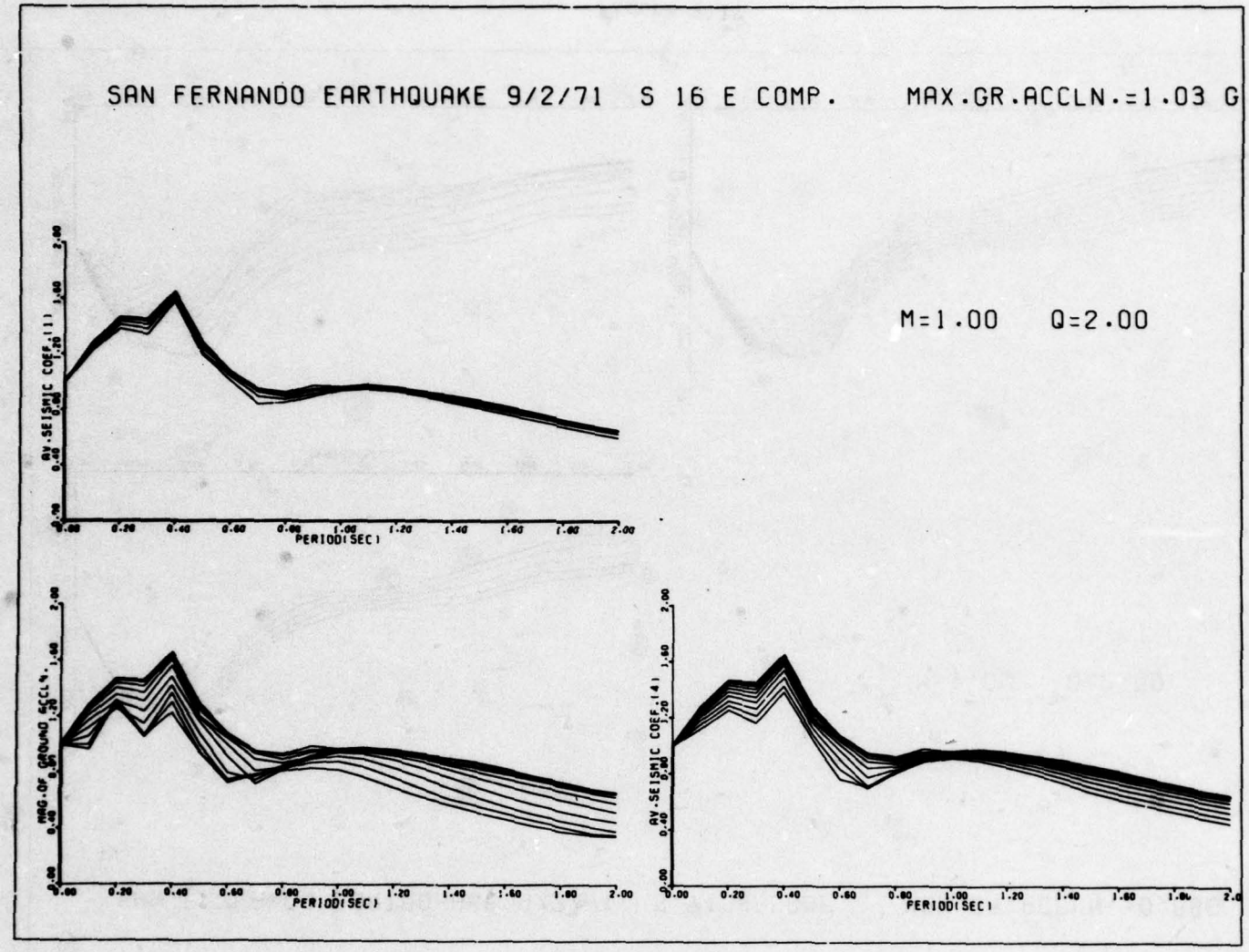
SAN FERNANDO EARTHQUAKE 9/2/71 S 16 E COMP.
MAX.GR.ACCLN.=1.03 G
M=1.00 Q=2.00
AV.SEISMIC COEF.(1)
PERIOD(SEC)
AV.SEISMIC COEF.(4)
PERIOD(SEC)

Figure E116

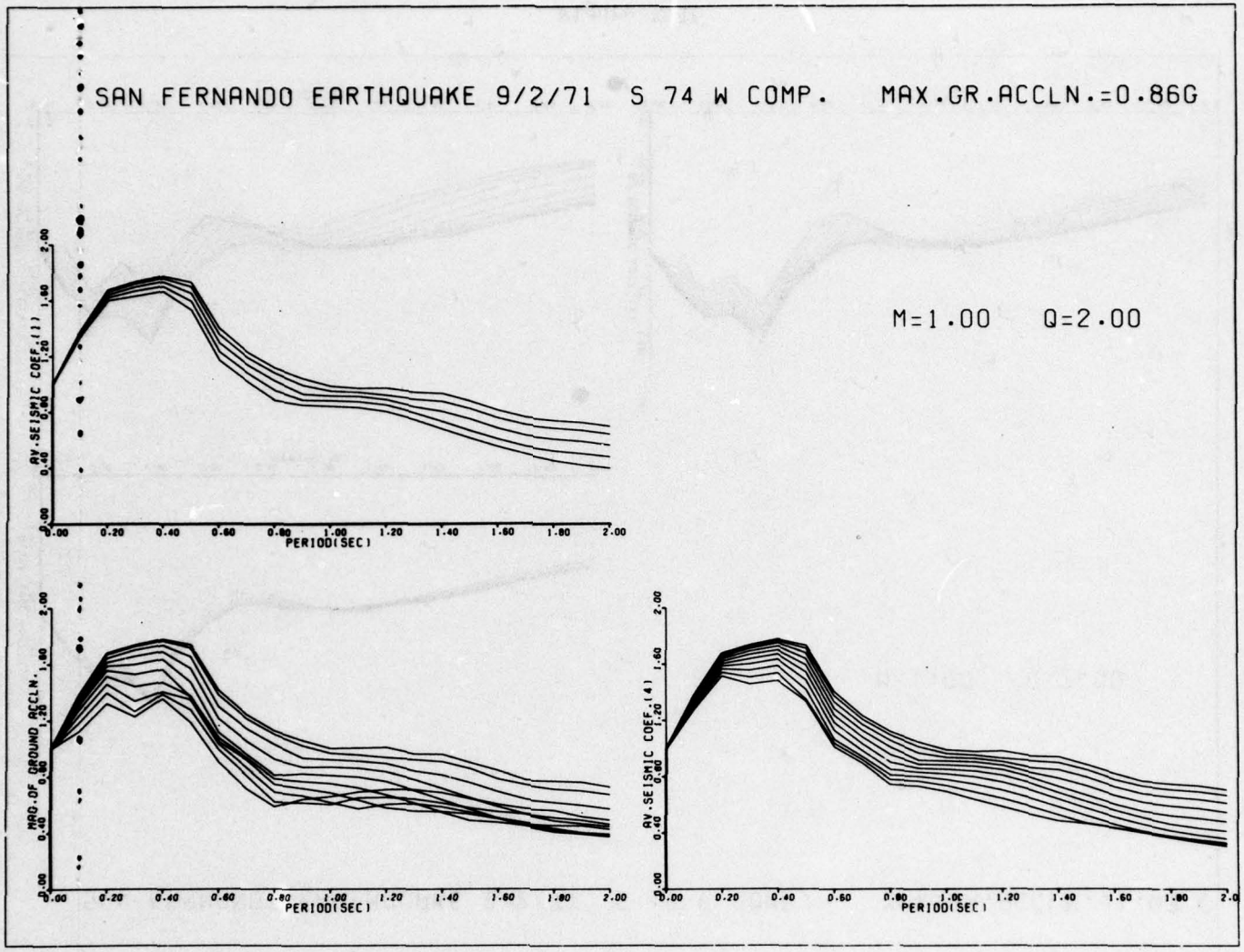
SAN FERNANDO EARTHQUAKE 9/2/71 S 74 W COMP. MAX.GR.ACCLN.=0.86G
M=1.00 Q=2.00
AV.SEISMIC COEF.(1)
PERIOD(SEC)
MAG.OF GROUND ACCLN.
PERIOD(SEC)
AV.SEISMIC COEF.(4)
PERIOD(SEC)

Figure E117

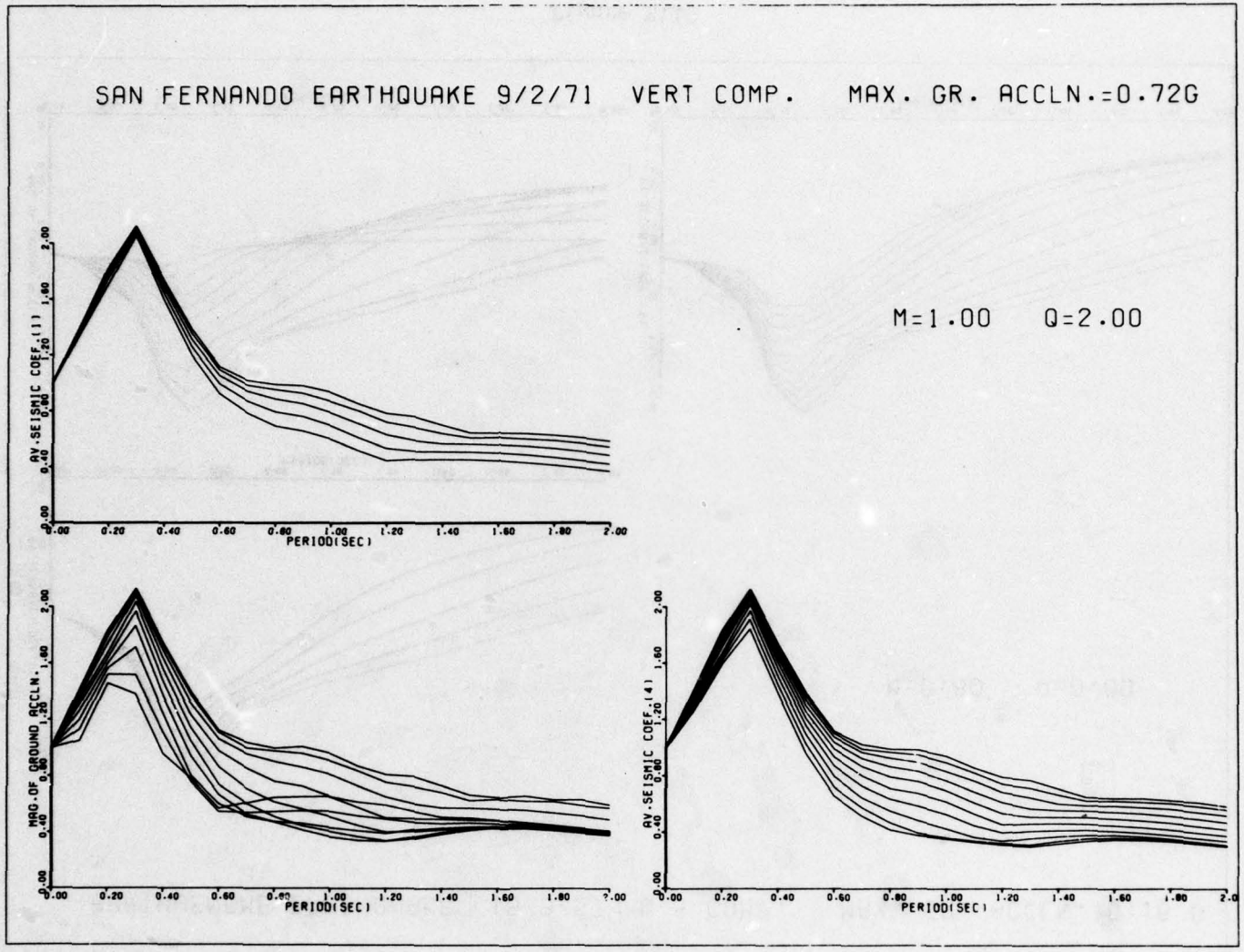
SAN FERNANDO EARTHQUAKE 9/2/71 VERT COMP. MAX. GR. ACCLN.=0.72G
M=1.00 Q=2.00
AV.SEISMIC COEF.(1)
MAG.OF GROUND ACCLN.
AV.SEISMIC COEF.(4)
PERIOD(SEC)

Figure E118

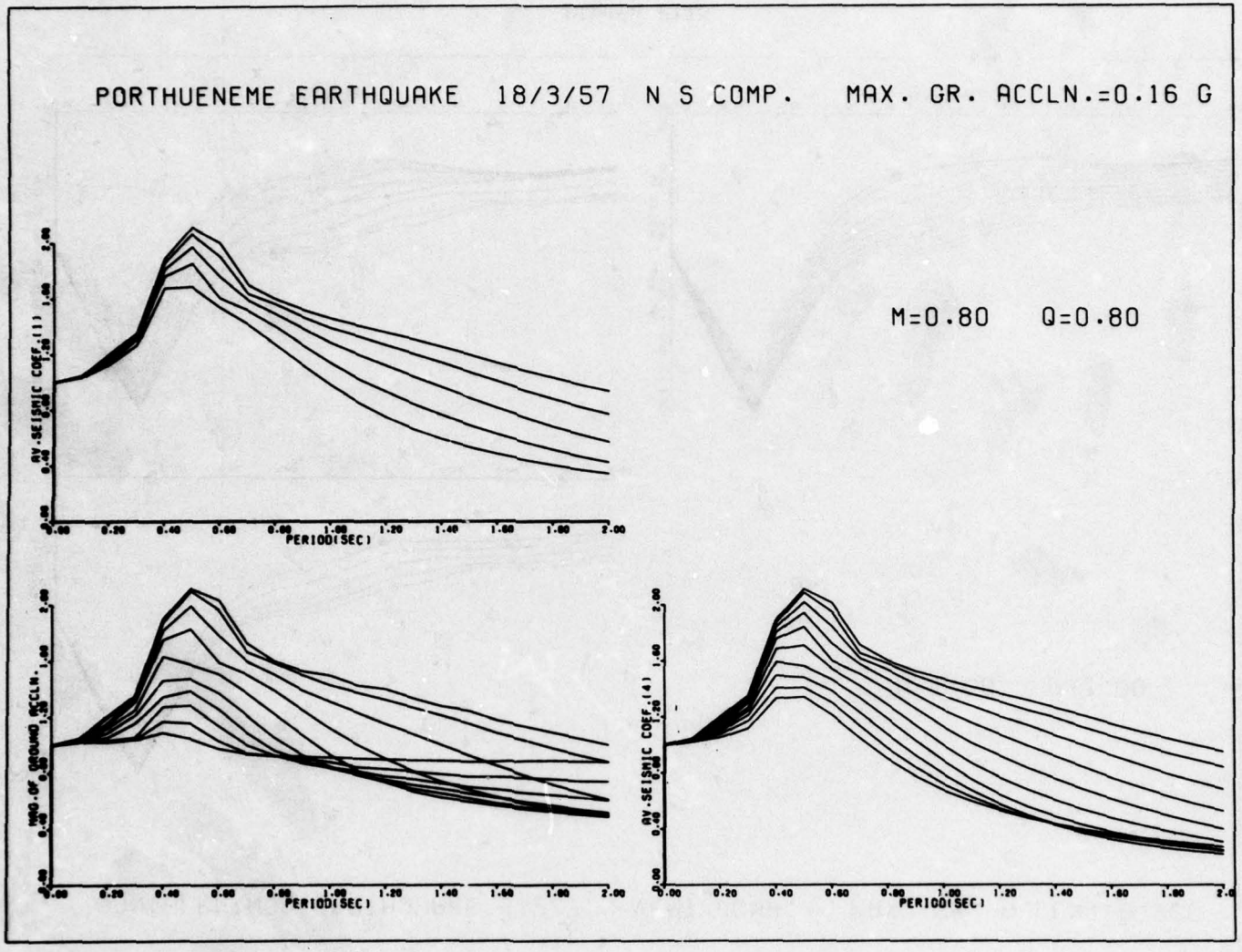
PORTHUENEME EARTHQUAKE 18/3/57 N S COMP. MAX. GR. ACCLN.=0.16 G
M=0.80 Q=0.80
AV.SEISMIC COEF.(I)
PERIOD(SEC)
AV.SEISMIC COEF.(I)
PERIOD(SEC)
AV.SEISMIC COEF.(I)
PERIOD(SEC)

Figure E119

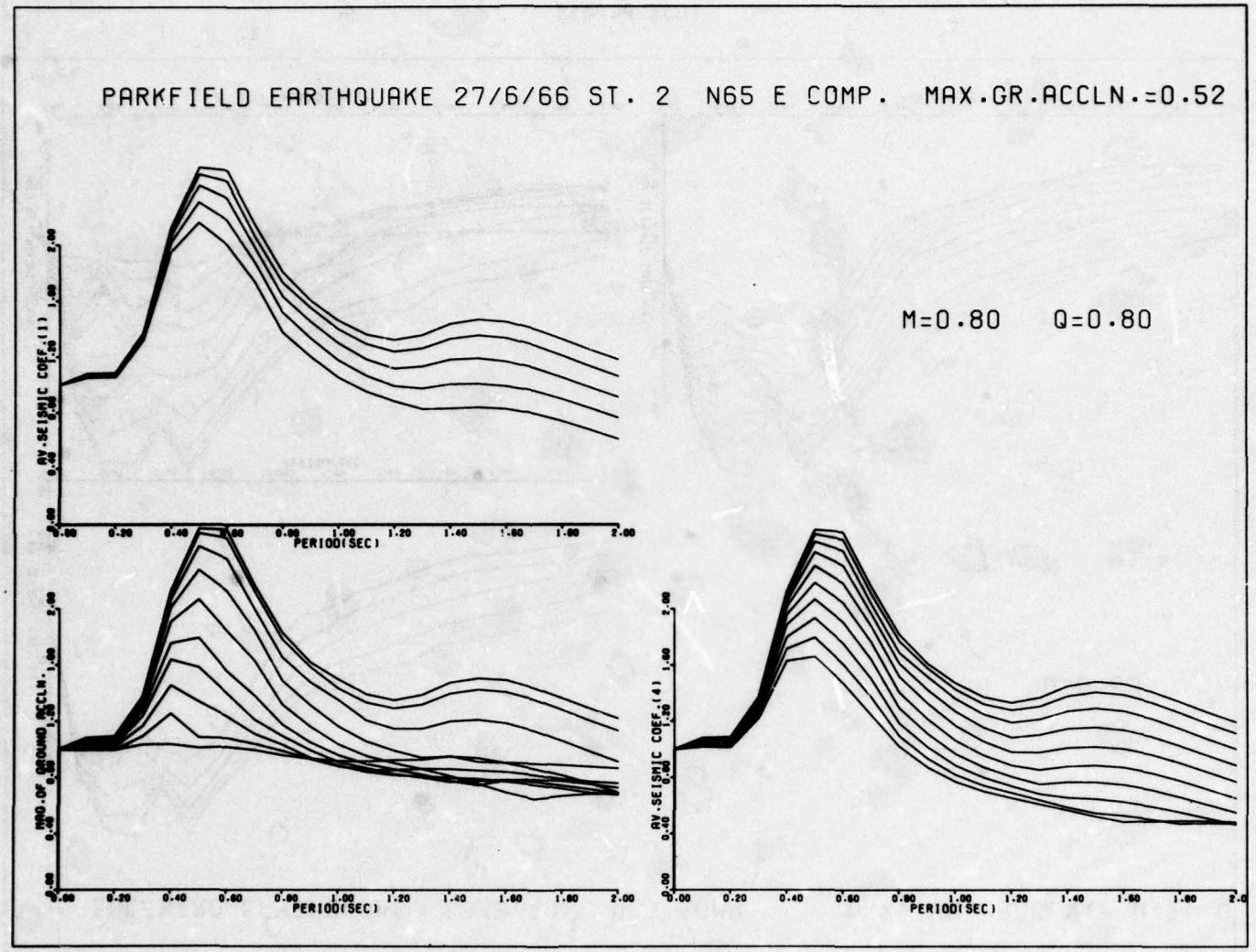
PARKFIELD EARTHQUAKE 27/6/66 ST. 2 N65 E COMP. MAX.GR.ACCLN.=0.52
M=0.80 Q=0.80
AV.SEISMIC COEF.(I)
PERIOD(SEC)
NO. OF GROUND ACCLN.
PERIOD(SEC)
AV.SEISMIC COEF.(4)
PERIOD(SEC)

Figure E120

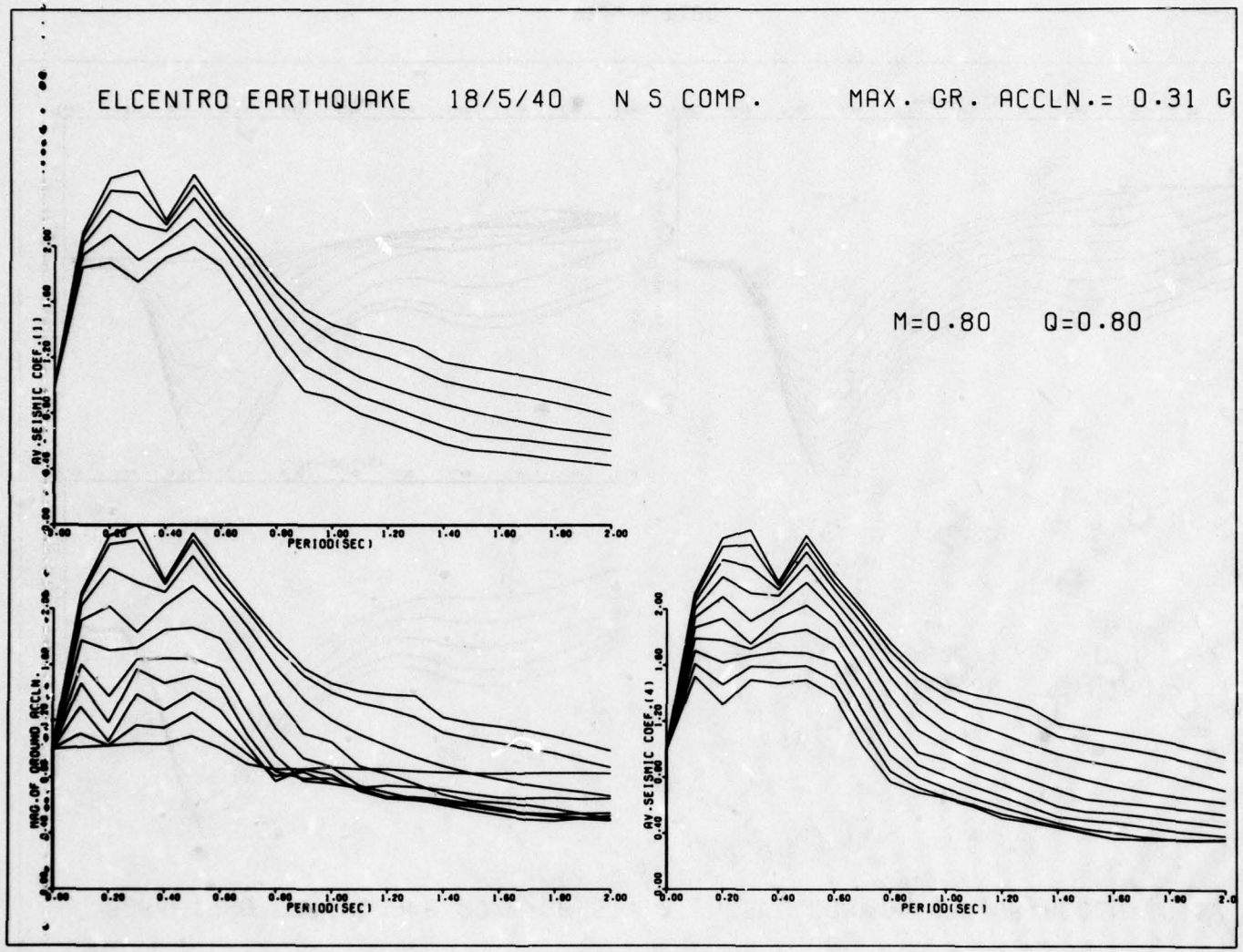
ELCENTRO EARTHQUAKE 18/5/40 N S COMP.
MAX. GR. ACCLN.= 0.31 G
M=0.80 Q=0.80
AV.SEISMIC COEF.(1)
MAG.OF GROUND ACCLN.
AV.SEISMIC COEF.(4)
PERIOD(SEC)
PERIOD(SEC)
PERIOD(SEC)

Figure E121

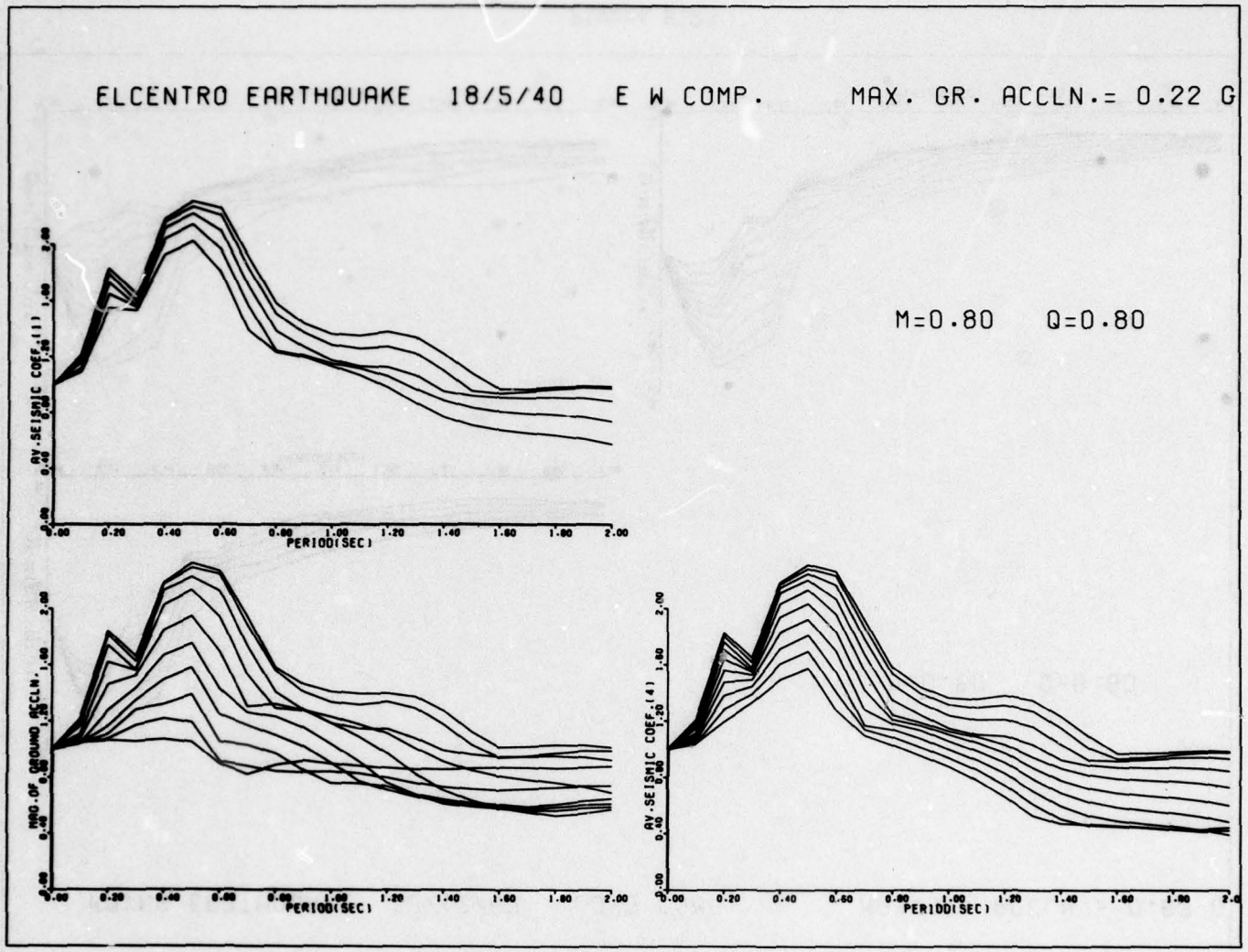
ELCENTRO EARTHQUAKE 18/5/40 E W COMP.
MAX. GR. ACCLN.= 0.22 G
M=0.80 Q=0.80
AV.SEISMIC COEF.(1)
PERIOD(SEC)
NRO. OF GROUND ACCLN.
PERIOD(SEC)
AV.SEISMIC COEF.(4)
PERIOD(SEC)

Figure E122

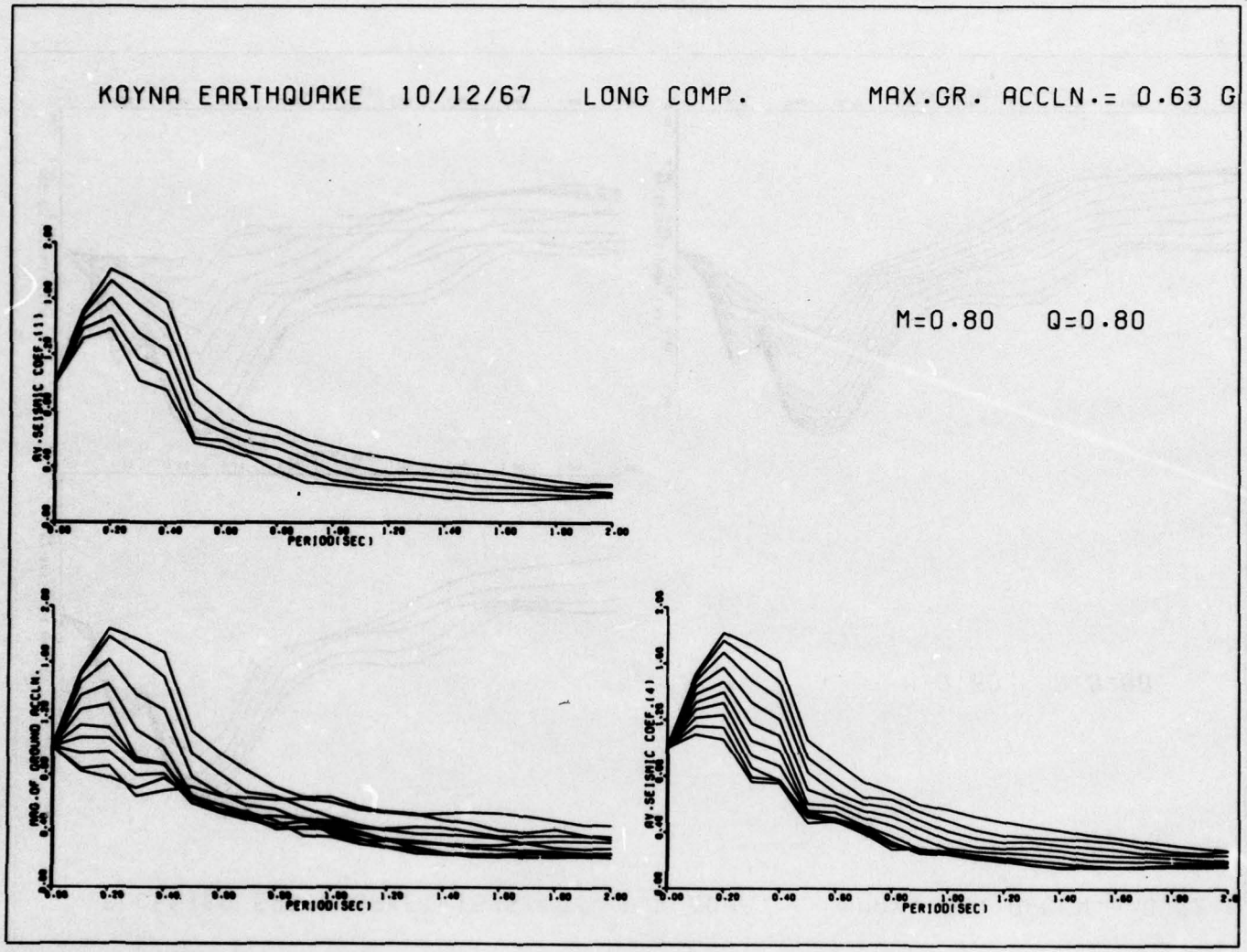
KOYNA EARTHQUAKE 10/12/67 LONG COMP.
MAX.GR. ACCLN.= 0.63 G
M=0.80 Q=0.80
AV.SEISMIC COEF.(1)
PERIOD(SEC)
RMS.OF GROUND ACCLN.
PERIOD(SEC)
AV.SEISMIC COEF.(4)
PERIOD(SEC)

Figure E123

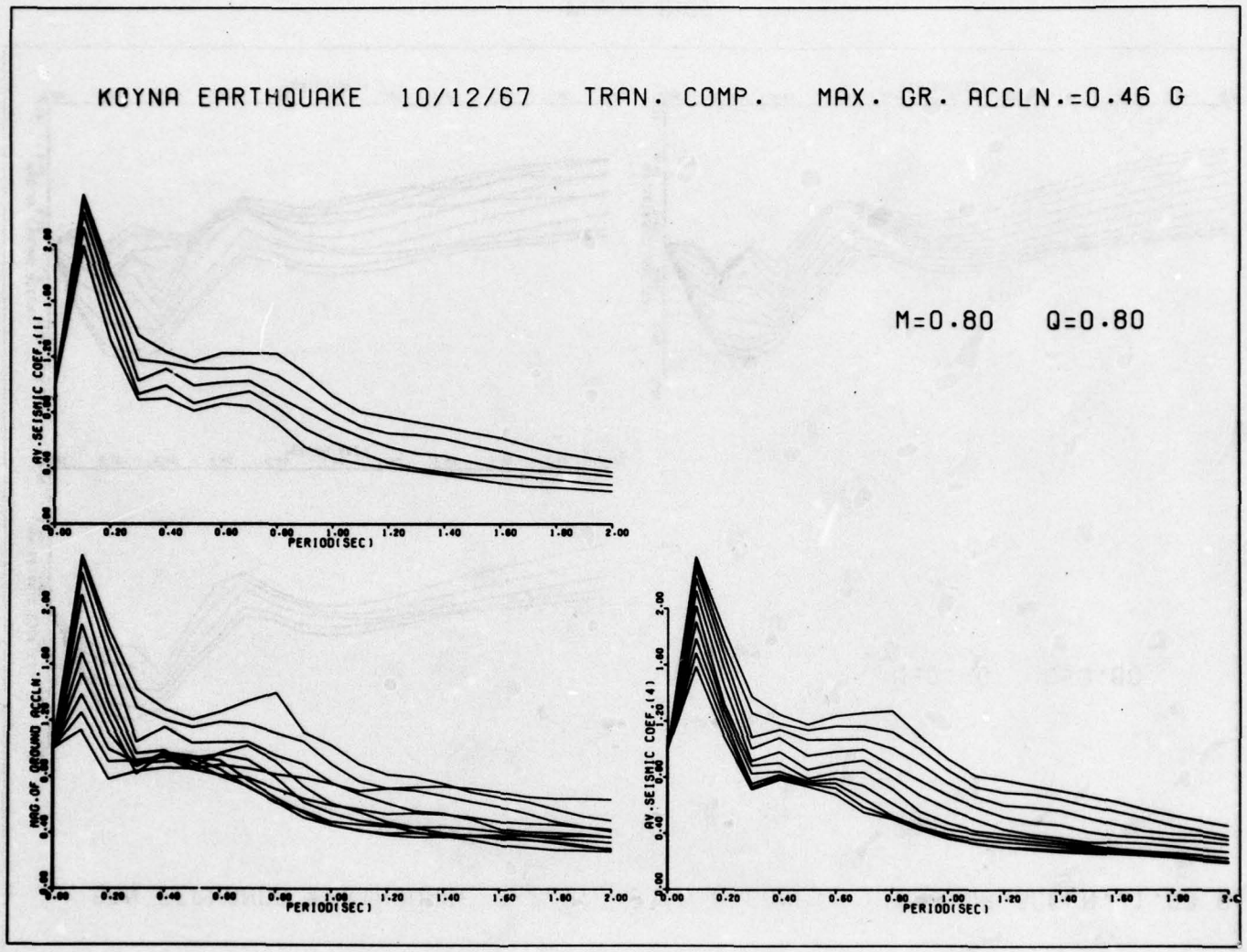
KOYNA EARTHQUAKE 10/12/67 TRAN. COMP. MAX. GR. ACCLN.=0.46 G
M=0.80 Q=0.80
AV.SEISMIC COEF.(1)
AV.SEISMIC COEF.(4)
PERIOD(SEC)
0.00
0.20
0.40
0.60
0.80
1.00
1.20
1.40
1.60
1.80
2.00

Figure E124

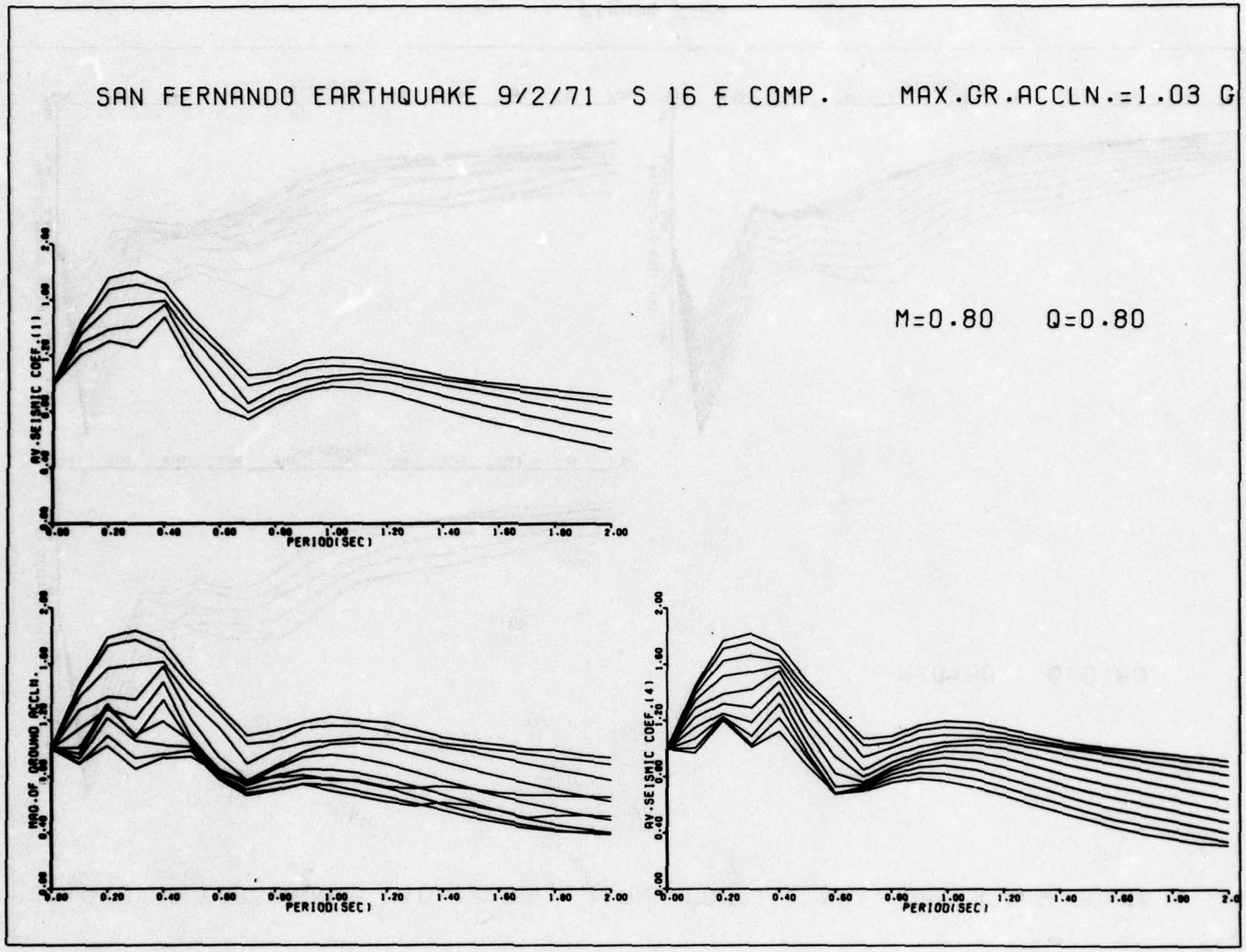
SAN FERNANDO EARTHQUAKE 9/2/71 S 16 E COMP.
MAX.GR.ACCLN.=1.03 G
M=0.80 Q=0.80
AV.SEISMIC COEF.(1)
PERIOD(SEC)
AV.SEISMIC COEF.(4)
PERIOD(SEC)
PERIOD(SEC)

Figure E125

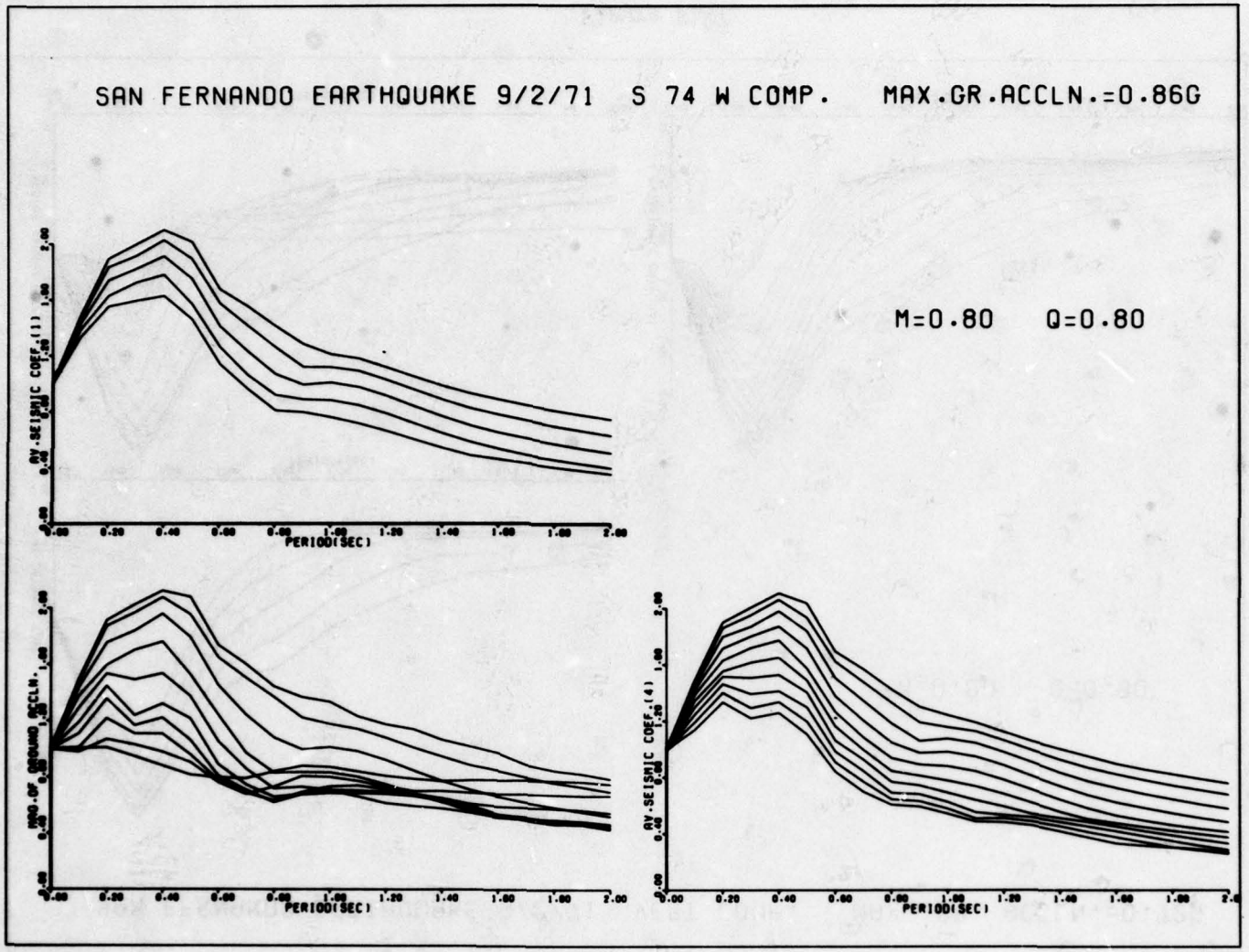
SAN FERNANDO EARTHQUAKE 9/2/71 S 74 W COMP. MAX.GR.ACCLN.=0.86G
M=0.80 Q=0.80
AV.SEISMIC COEF.(1)
PERIOD(SEC)
RMO.OF GROUND ACCLN.
PERIOD(SEC)
AV.SEISMIC COEF.(4)
PERIOD(SEC)

Figure E126

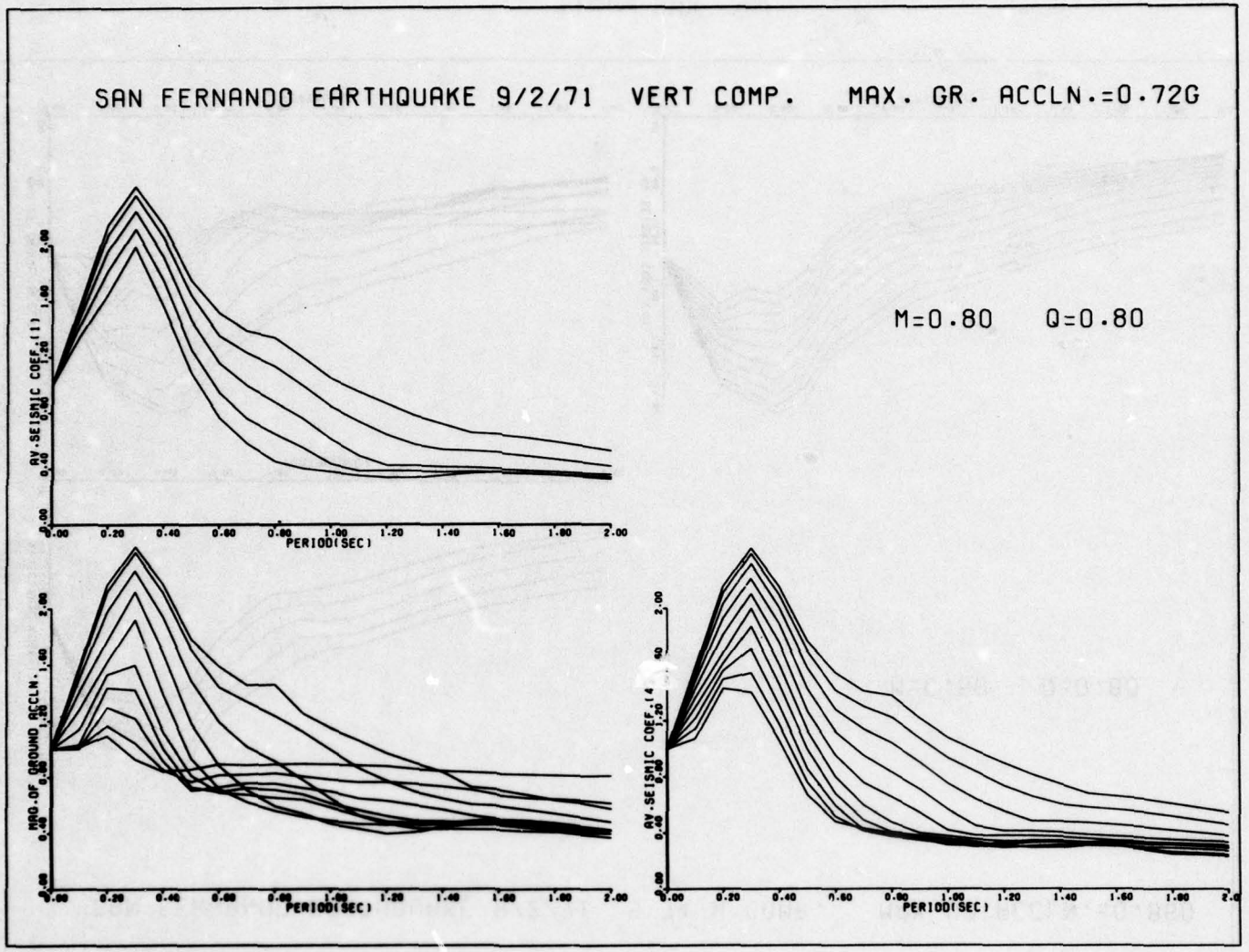
SAN FERNANDO EARTHQUAKE 9/2/71 VERT COMP. MAX. GR. ACCLN.=0.72G
M=0.80 Q=0.80
AV.SEISMIC COEF.(1)
MAG.OF GROUND ACCLN.
AV.SEISMIC COEF.(4
PERIOD(SEC)
PERIOD(SEC)
PERIOD(SEC)

Figure E127

APPENDIX F:

ENVELOPE OF SEISMIC COEFFICIENTS AND POINT ACCELERATION SPECTRA

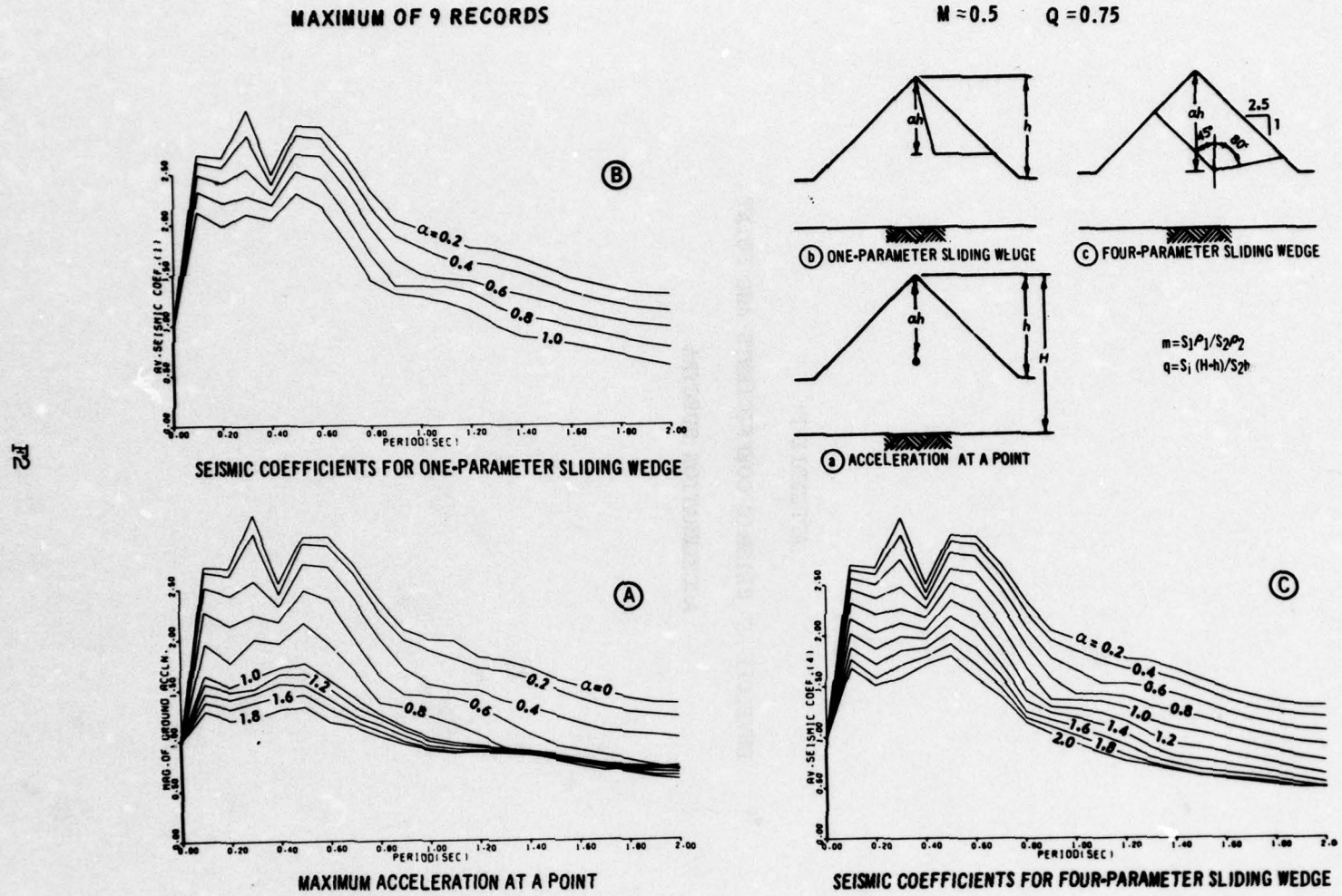
MAXIMUM OF 9 RECORDS
M = 0.5 Q = 0.75
B
a=0.2
0.4
0.6
0.8
1.0
PERIOD(SEC)
SEISMIC COEFFICIENTS FOR ONE-PARAMETER SLIDING WEDGE
ah
h
2.5
1
45°
α
b ONE-PARAMETER SLIDING WEDGE
c FOUR-PARAMETER SLIDING WEDGE
H
m=S1ρ1/S2ρ2
q=Si (H-h)/S2h
a ACCELERATION AT A POINT
A
a=0
0.2
0.4
0.6
0.8
1.0
1.2
1.6
1.8
MAXIMUM ACCELERATION AT A POINT
C
a = 0.2
0.4
0.6
0.8
1.0
1.2
1.4
1.6
1.8
2.0
SEISMIC COEFFICIENTS FOR FOUR-PARAMETER SLIDING WEDGE

Figure F1

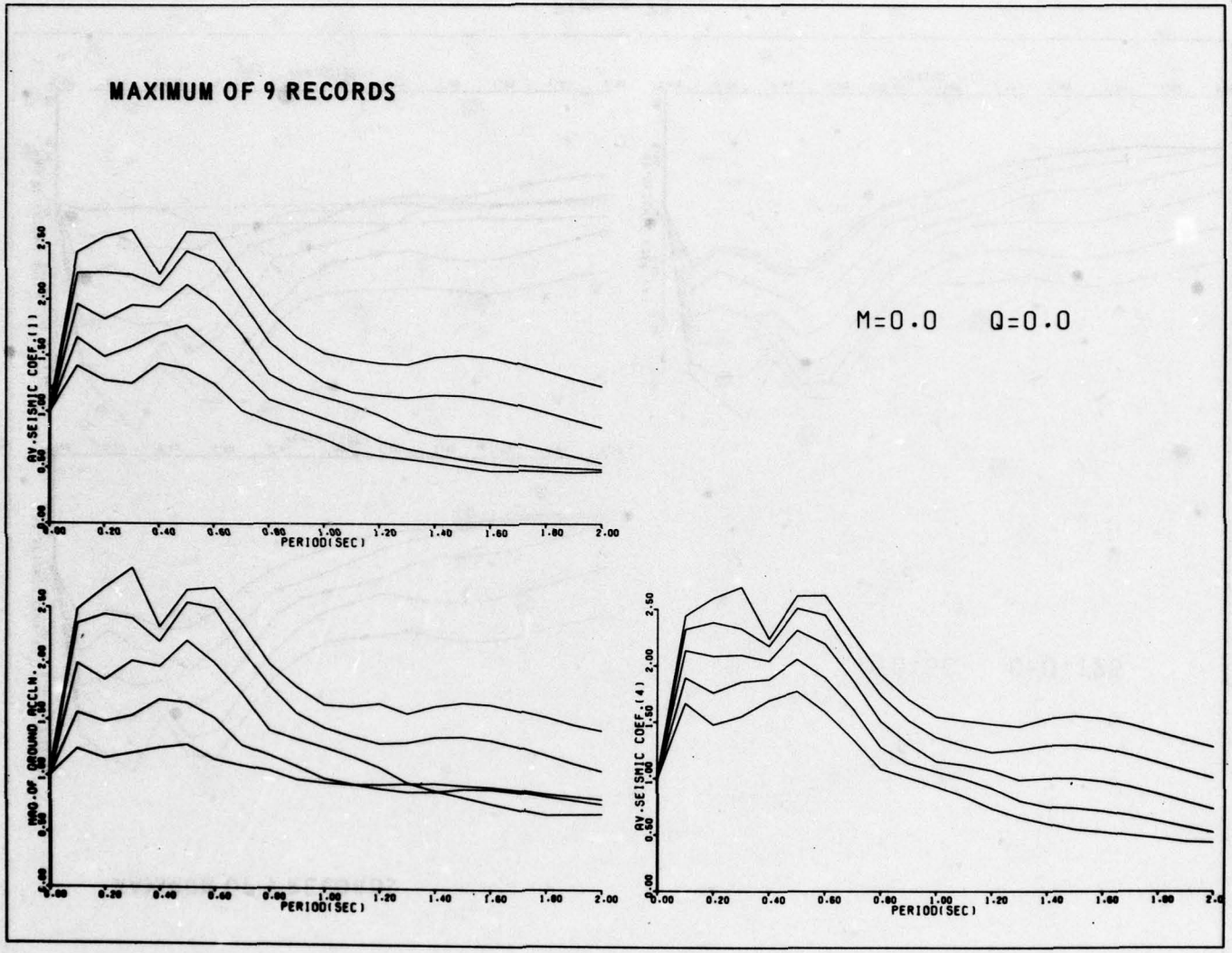
MAXIMUM OF 9 RECORDS
M=0.0 Q=0.0
AV.SEISMIC COEF.(1)
PERIOD(SEC)
AVG.OF GROUND ACCLN.
PERIOD(SEC)
AV.SEISMIC COEF.(4)
PERIOD(SEC)

Figure F2

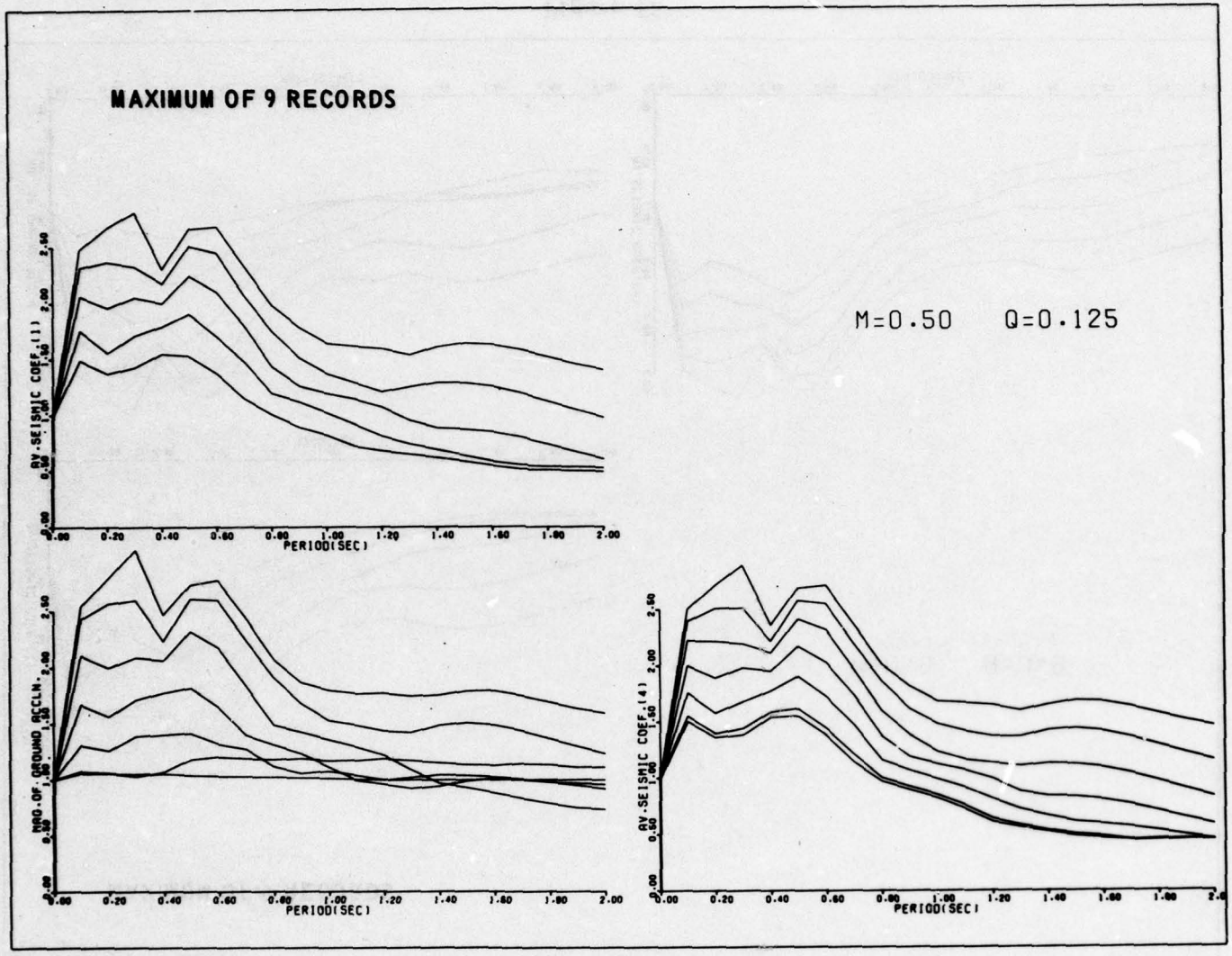
MAXIMUM OF 9 RECORDS
M=0.50 Q=0.125
AV.SEISMIC COEF.(1)
AV.SEISMIC COEF.(4)
MAG.OF GROUND ACCLN.
PERIOD(SEC)

Figure F3

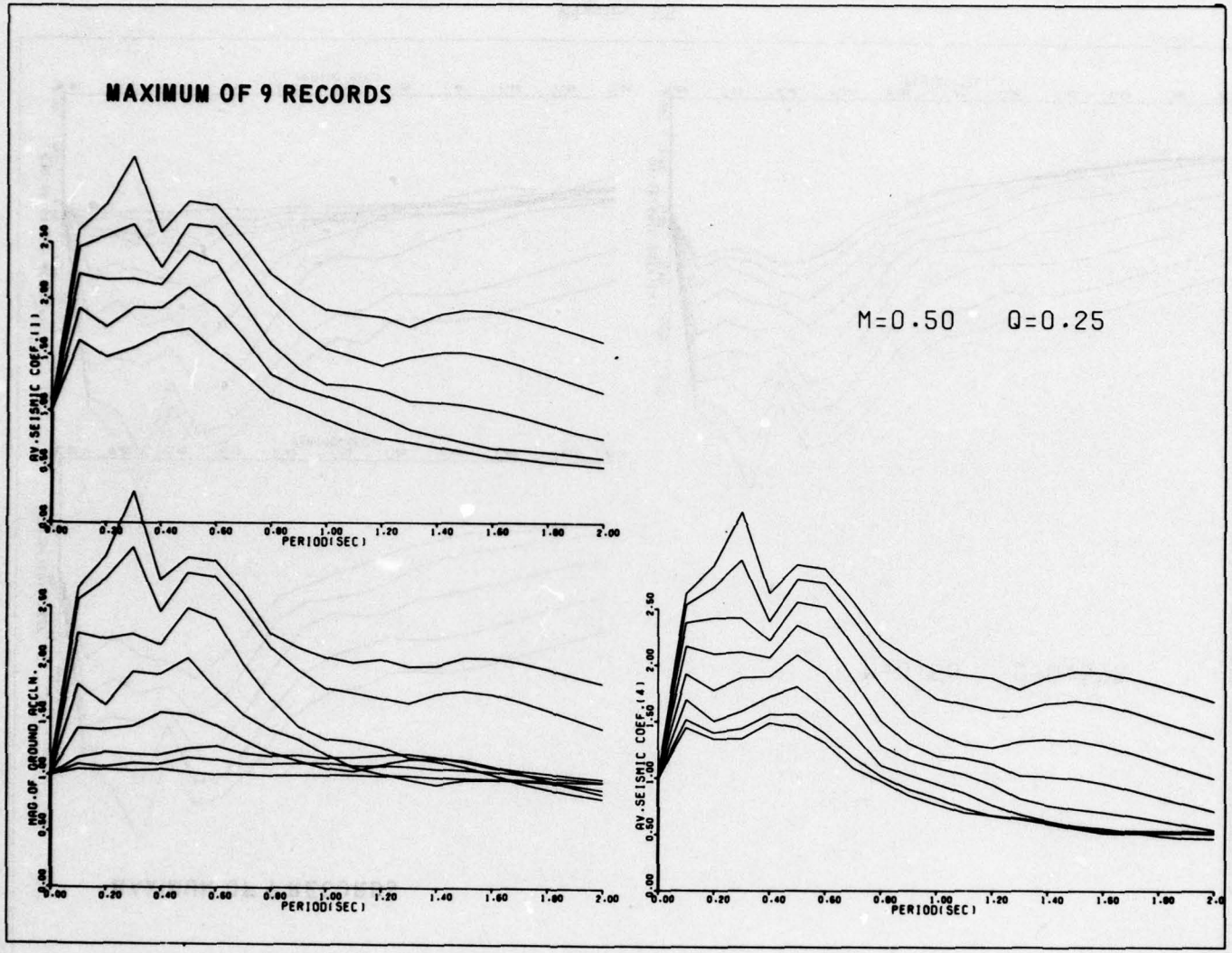
MAXIMUM OF 9 RECORDS
M=0.50 Q=0.25
AV.SEISMIC COEF.(1)
MAG.OF GROUND ACCLN.
AV.SEISMIC COEF.(4)
PERIOD(SEC)

Figure F4

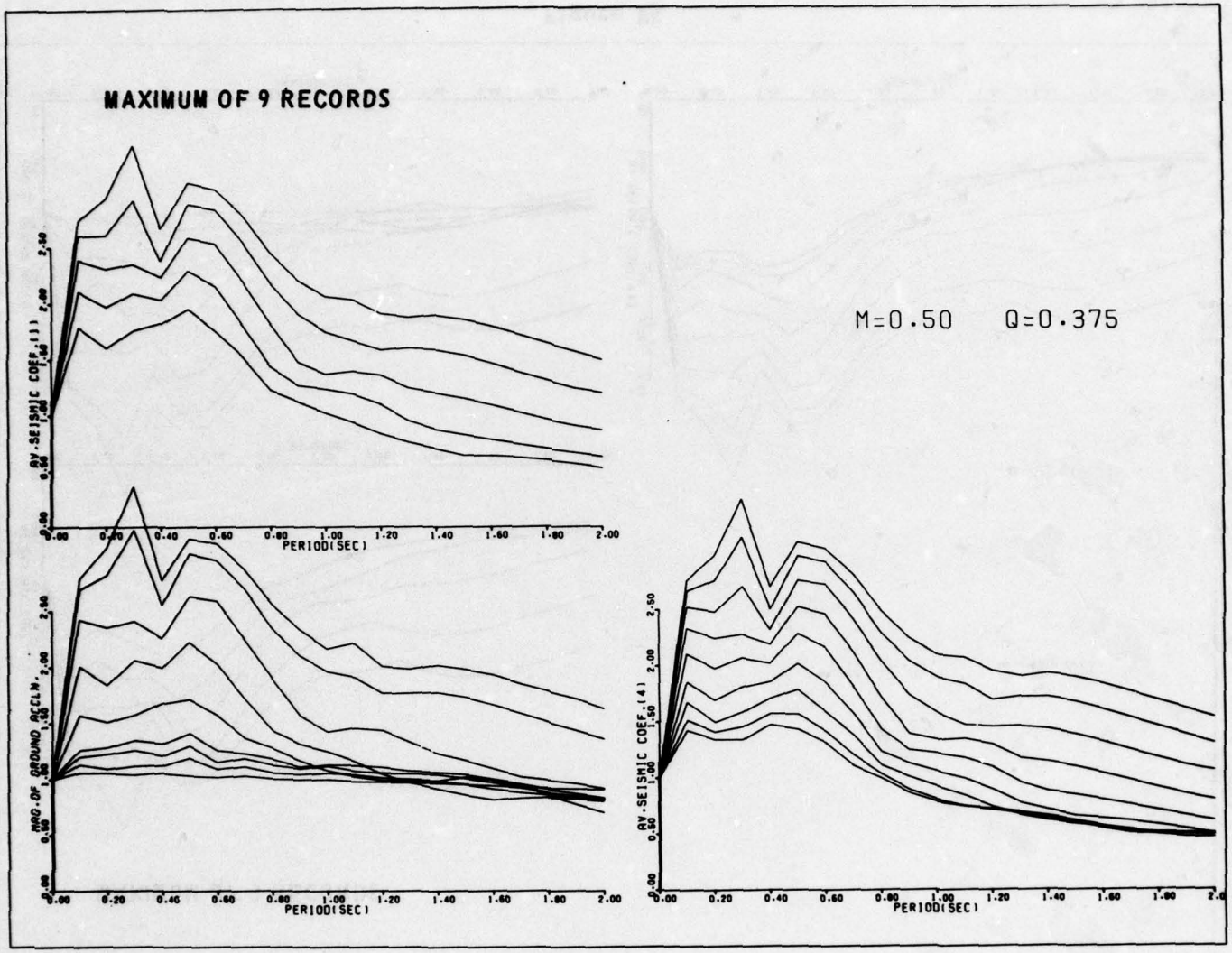
MAXIMUM OF 9 RECORDS
M=0.50 Q=0.375
AV.SEISMIC COEF.(1)
PERIOD(SEC)
AV.SEISMIC COEF.(4)
PERIOD(SEC)
NRO.OF GROUND ACCLN.
PERIOD(SEC)

Figure F5

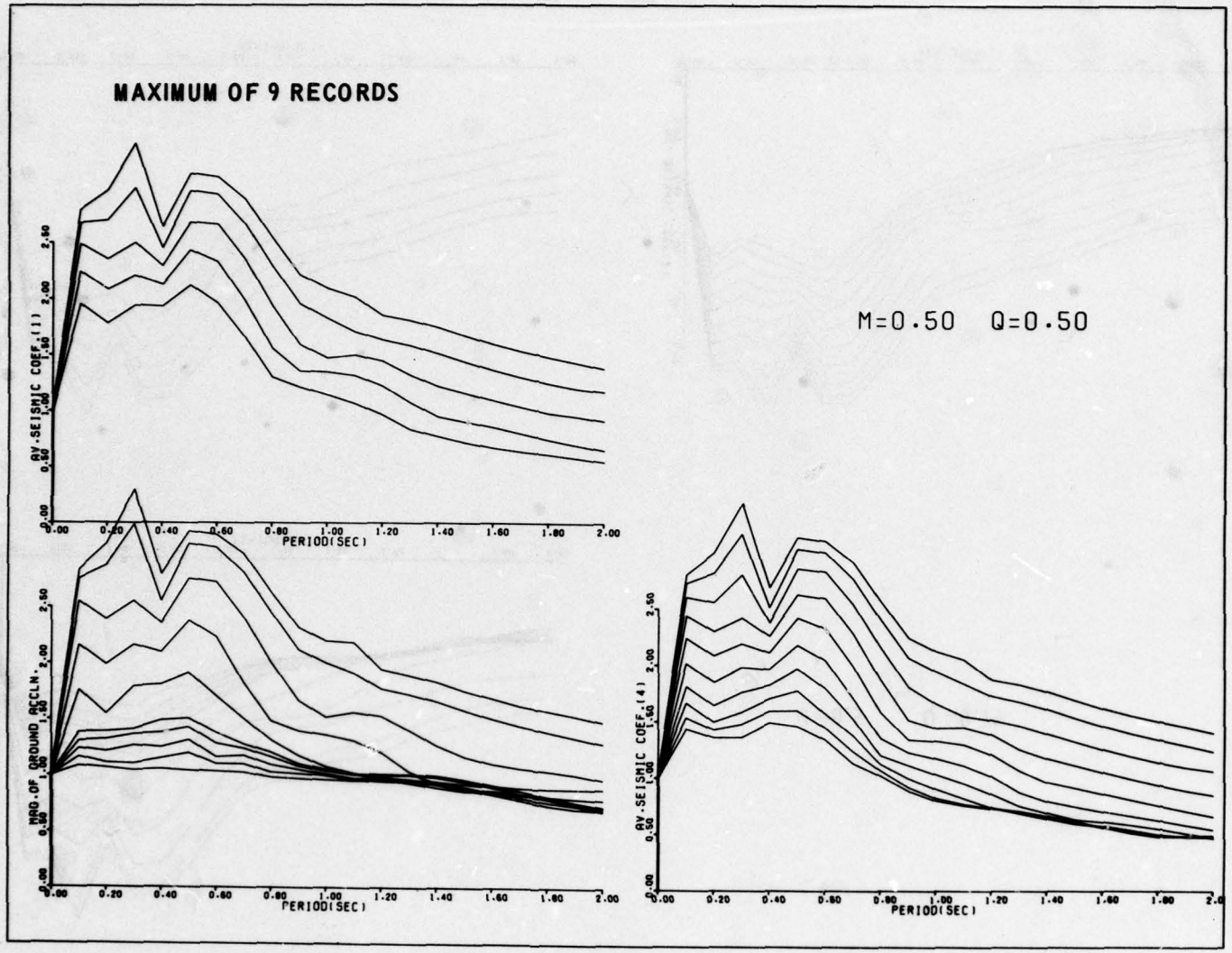
MAXIMUM OF 9 RECORDS
M=0.50 Q=0.50
AV.SEISMIC COEF.(1)
PERIOD(SEC)
MAG.OF GROUND ACCLN.
PERIOD(SEC)
AV.SEISMIC COEF.(4)
PERIOD(SEC)

Figure F6

MAXIMUM OF 9 RECORDS

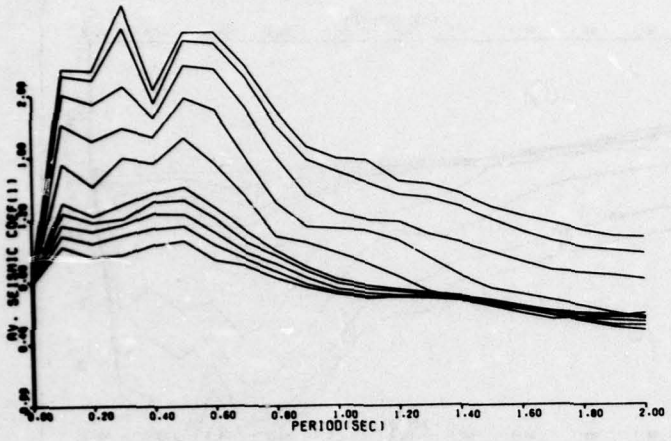

M =0.5 Q =0.75

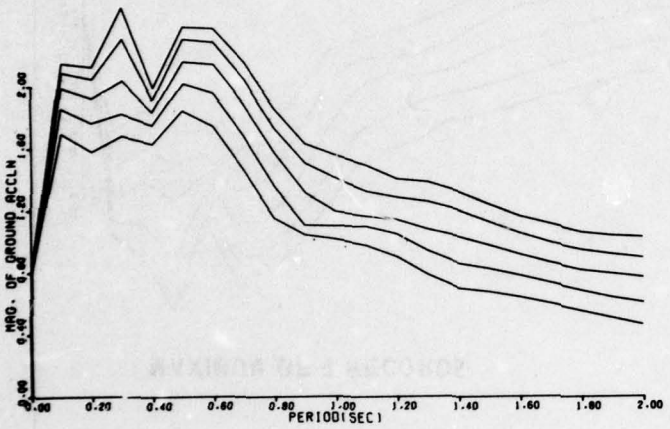

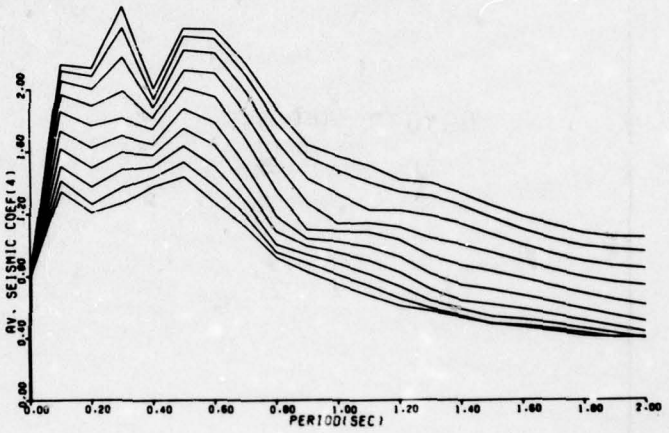

Figure F7

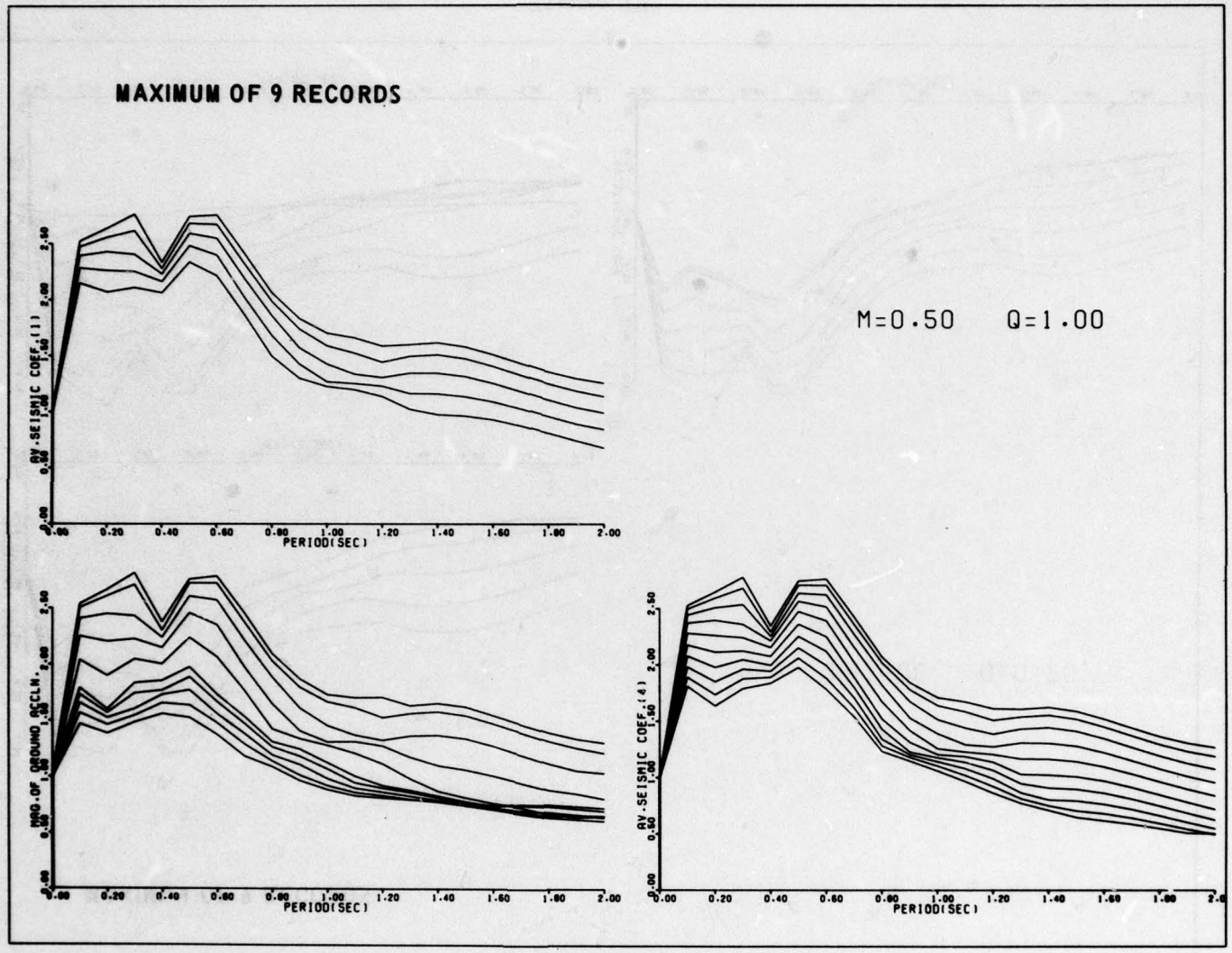
MAXIMUM OF 9 RECORDS
M=0.50 Q=1.00
AV.SEISMIC COEF.(1)
PERIOD(SEC)
AV.SEISMIC COEF.(4)
PERIOD(SEC)

Figure F8

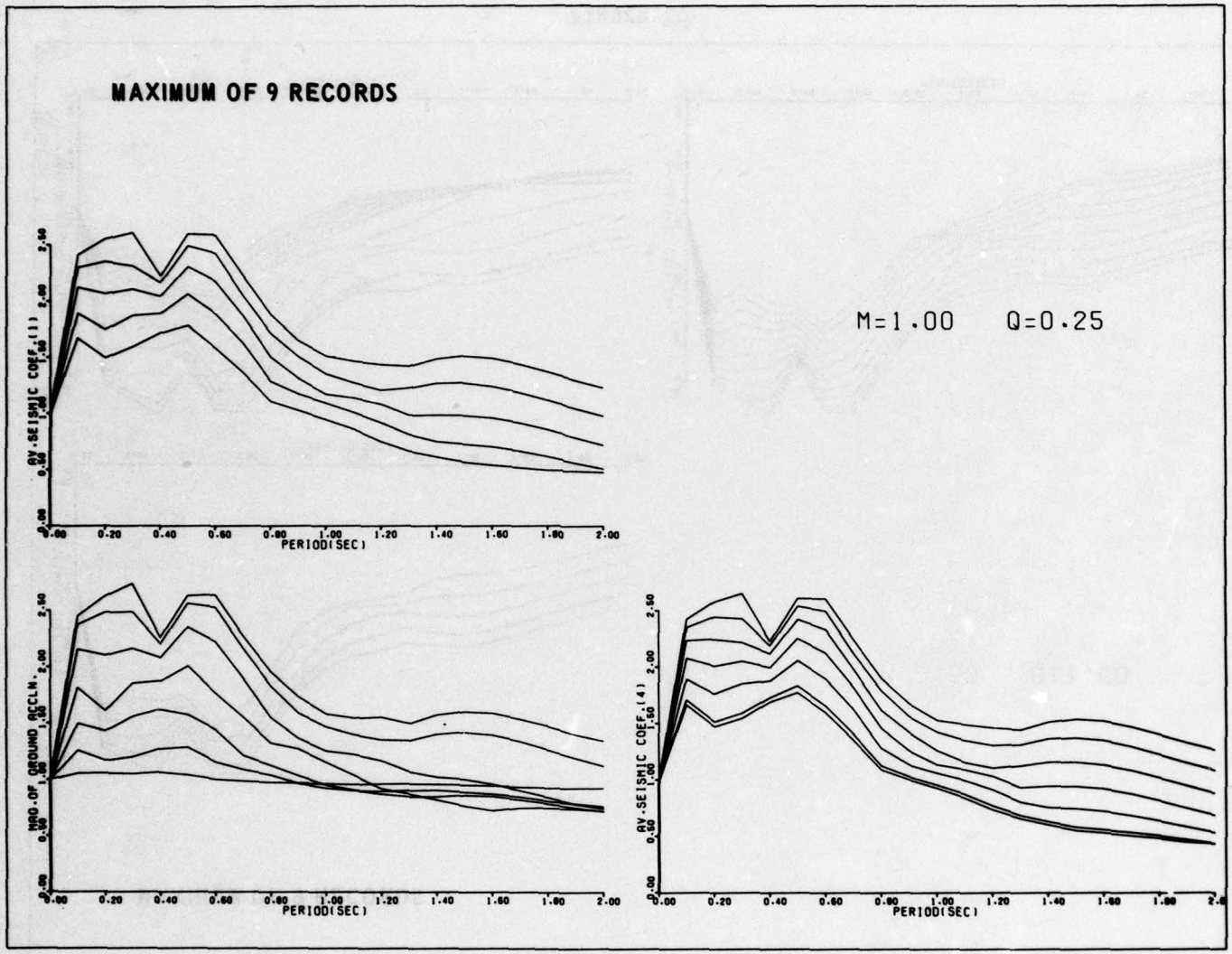
MAXIMUM OF 9 RECORDS
M=1.00 Q=0.25
AV.SEISMIC COEF.(1)
MAG.OF GROUND ACCLN.
AV.SEISMIC COEF.(4)
PERIOD(SEC)
PERIOD(SEC)
PERIOD(SEC)

Figure F9

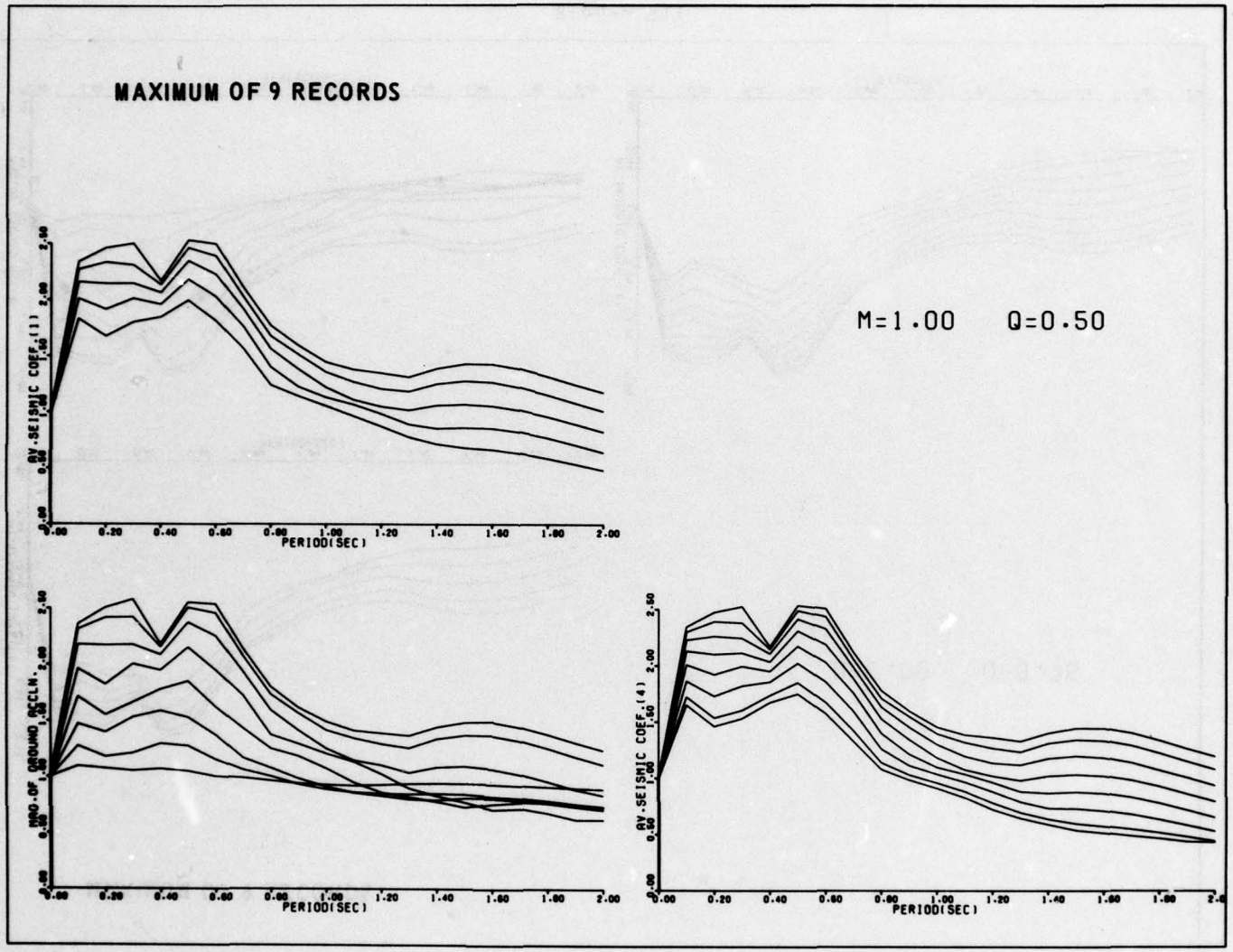
MAXIMUM OF 9 RECORDS
M=1.00 Q=0.50
AV.-SEISMIC COEF.(1)
RMO.OF GROUND ACCLN.
AV.-SEISMIC COEF.(4)
PERIOD(SEC)

Figure F10

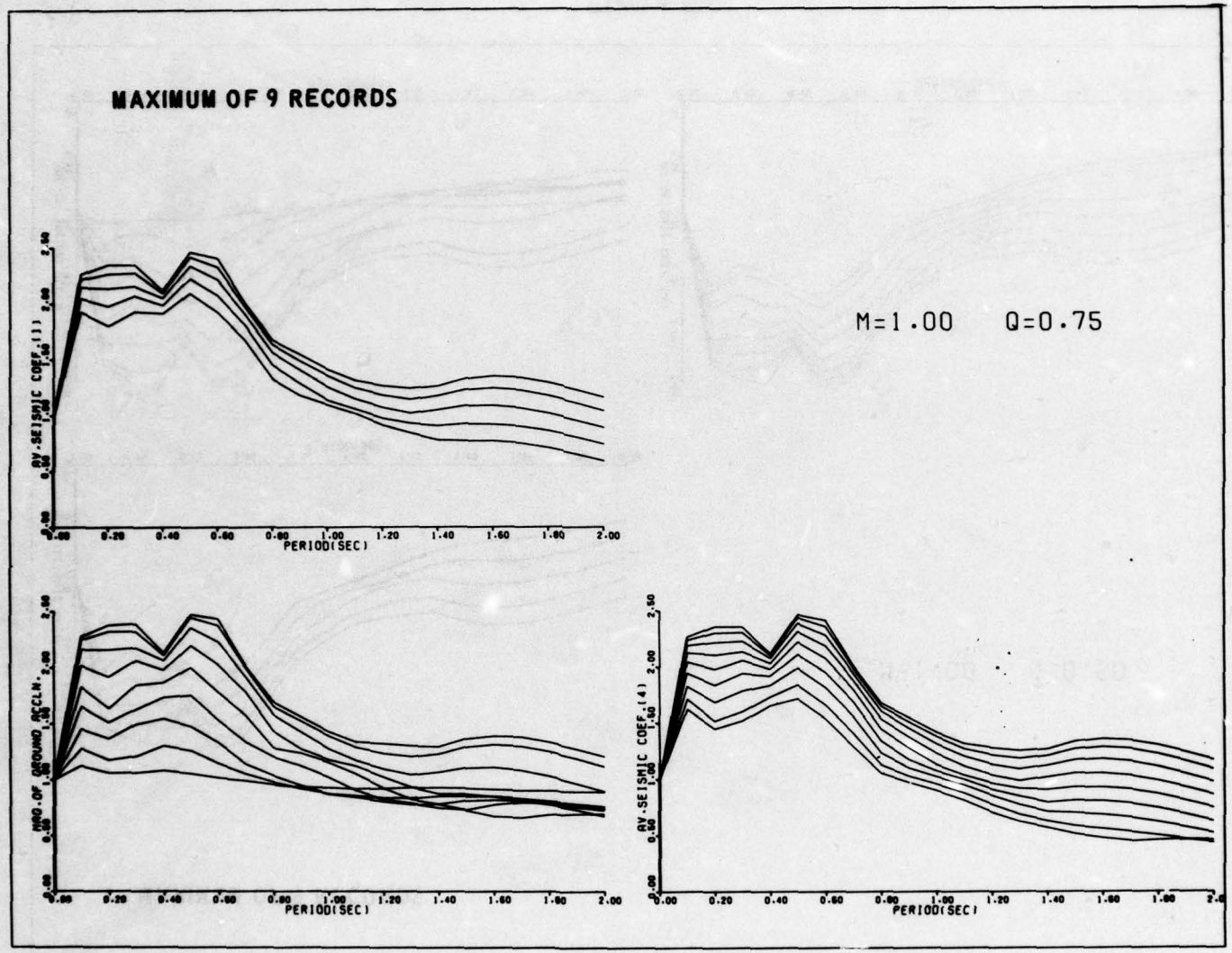
MAXIMUM OF 9 RECORDS
M=1.00 Q=0.75
AV.SEISMIC COEF.(1)
PERIOD(SEC)
MAX. OF GROUND ACCLN.
PERIOD(SEC)
AV.SEISMIC COEF.(4)
PERIOD(SEC)

Figure F11

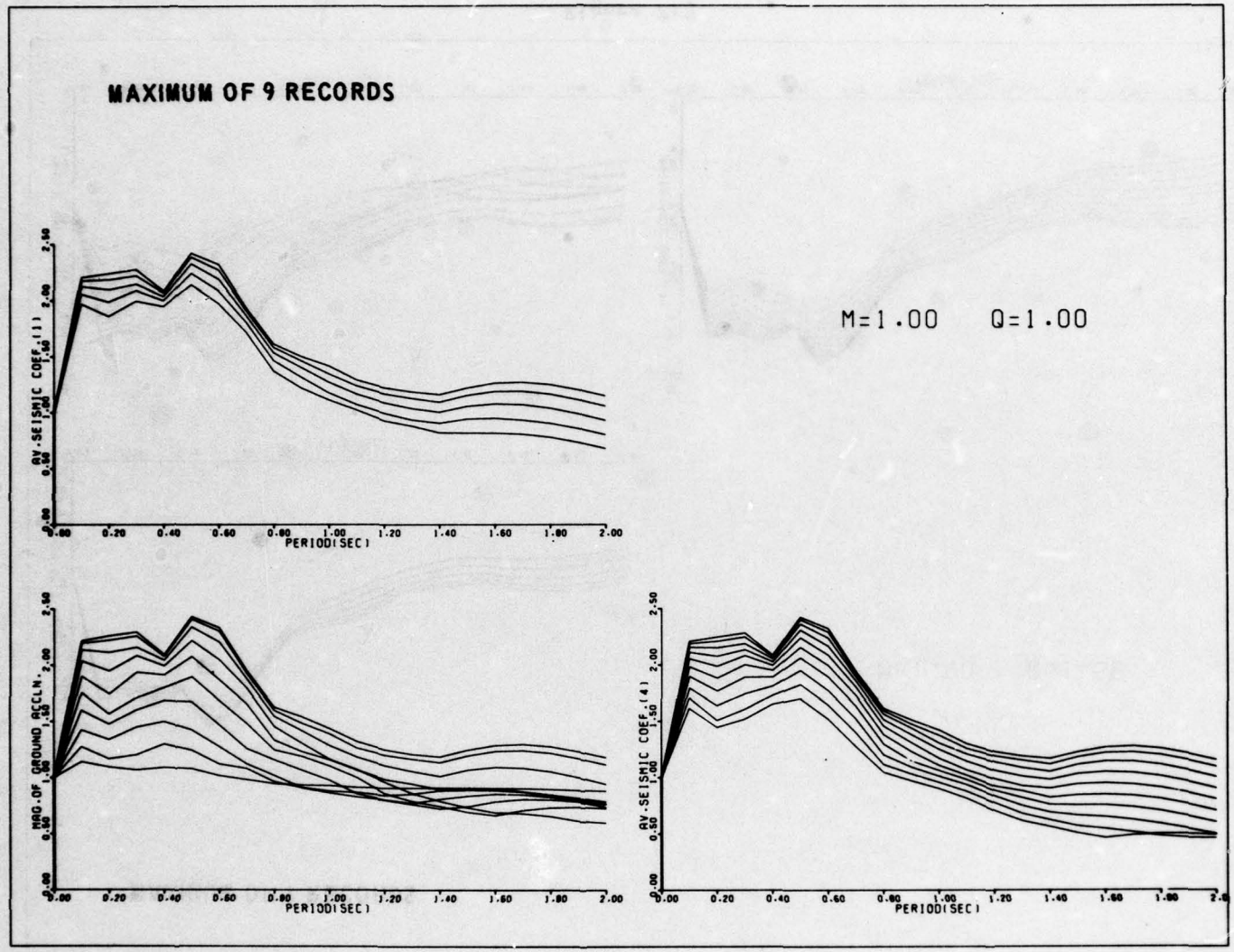
MAXIMUM OF 9 RECORDS
M=1.00 Q=1.00
AV.SEISMIC COEF.(1)
AV.SEISMIC COEF.(4)
MAG. OF GROUND ACCLN.
PERIOD(SEC)
0.00
0.20
0.40
0.60
0.80
1.00
1.20
1.40
1.60
1.80
2.00
0.50
1.00
1.50
2.00
2.50

Figure F12

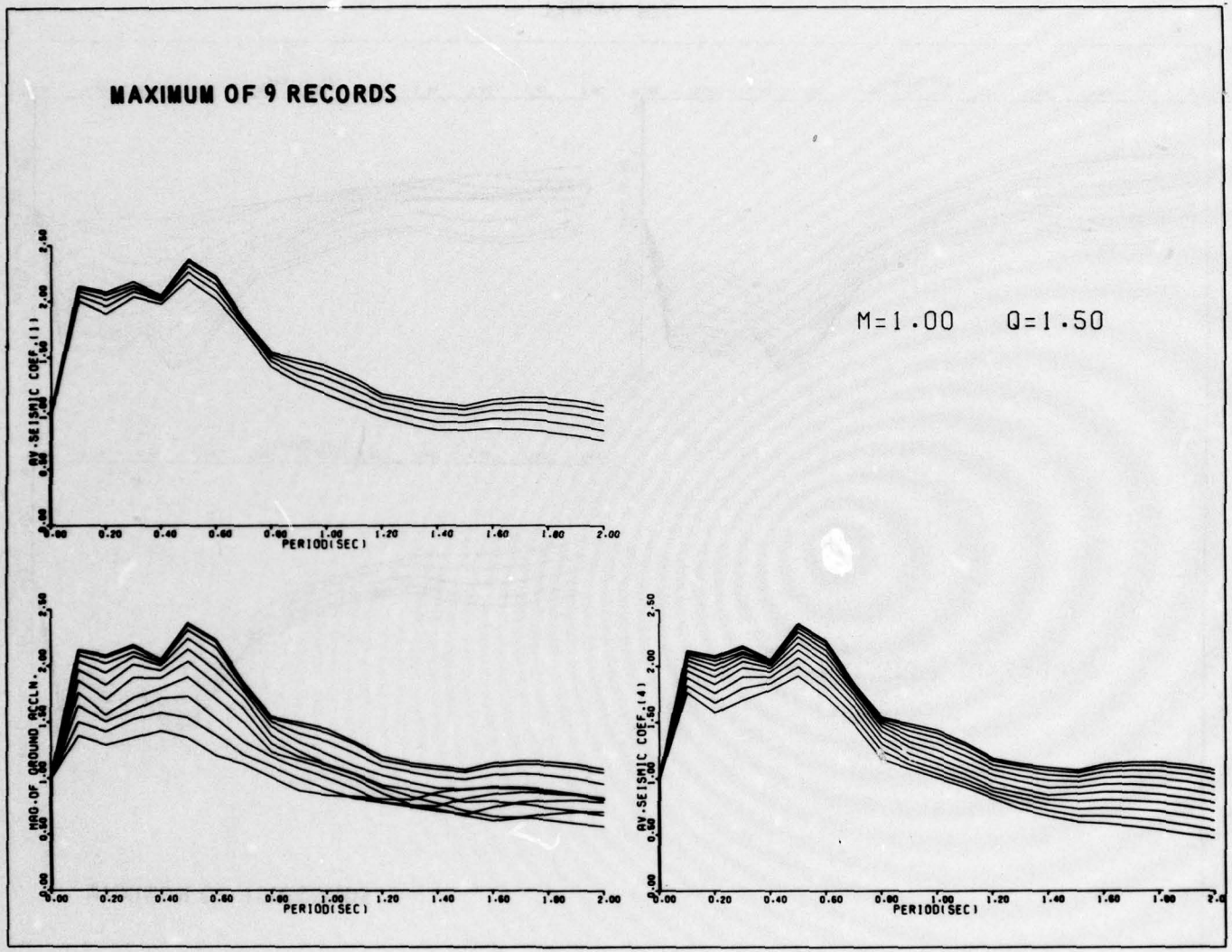
MAXIMUM OF 9 RECORDS
M=1.00 Q=1.50
AV.SEISMIC COEF.(1)
MAG.OF GROUND ACCLN.
AV.SEISMIC COEF.(4)
PERIOD(SEC)
PERIOD(SEC)
PERIOD(SEC)

Figure F13

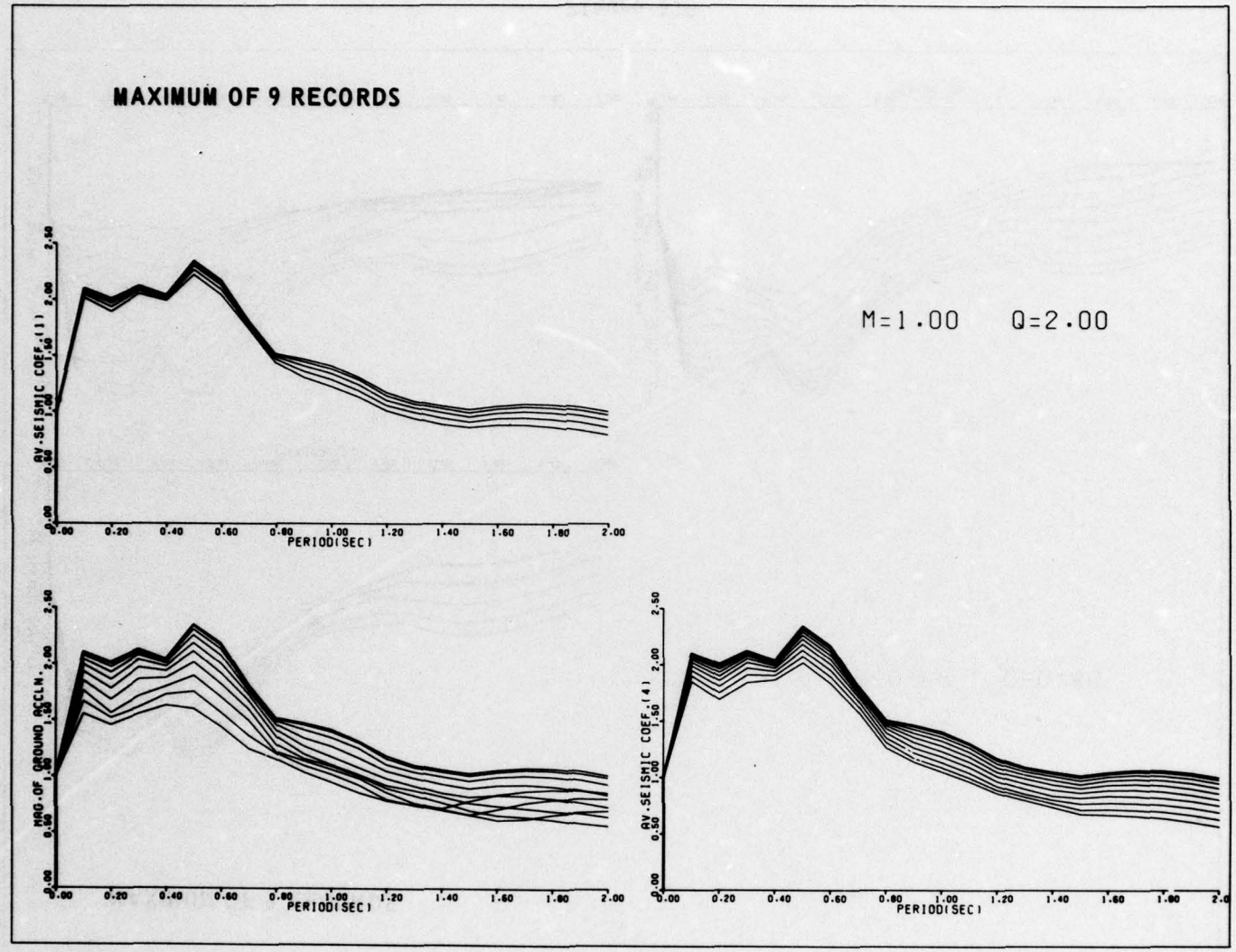
MAXIMUM OF 9 RECORDS
M=1.00 Q=2.00
AV.SEISMIC COEF.(1)
MAG-OF GROUND ACCLN.
AV.SEISMIC COEF.(4)
PERIOD(SEC)
0.00
0.20
0.40
0.60
0.80
1.00
1.20
1.40
1.60
1.80
2.00
0.50
1.50
2.50

Figure F14

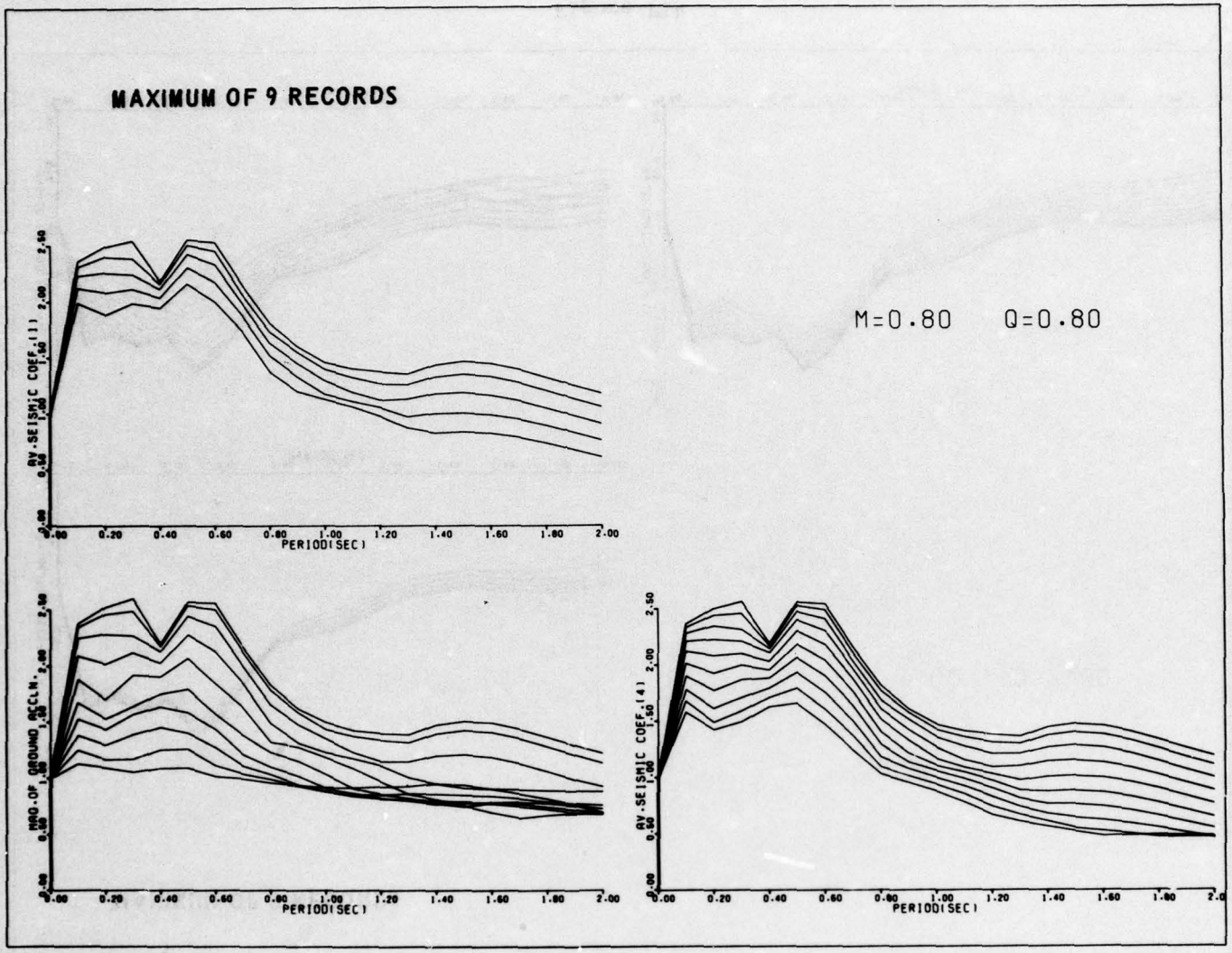
MAXIMUM OF 9 RECORDS
M=0.80 Q=0.80
AV.SEISMIC COEF.(1)
AV.SEISMIC COEF.(4)
MAG.OF GROUND ACCLN.
PERIOD(SEC)

Figure F15

APPENDIX G:

NOTATION

PART II

a_n	The n^{th} root of the equation $J_o(a_n) = 0$
$\bar{a}_n$	n^{th} root of the equation $m \tan q(\bar{a}_n)/J_1(\bar{a}_n)$
b	Width of crest
B	Unknown constant
c	Damping coefficient for both dam and layer
C	Unknown constant
F	Total inertia force
F_{max}	Maximum inertia force
F_1	A function defined in the text
F_2	A function defined in the text
g	Acceleration due to gravity
$\ddot{g}(t)$	Base accelerations
g_{max}	Maximum base acceleration
G_1	Shear modulus of the material of the dam
G_2	Shear modulus of the material of the layer
h	Height of dam
H	Total height from crest of dam to rock level
i	Square root of -1
I_o	Modified Bessel function of order zero
I_1	Modified Bessel function of order one
J_o	Bessel function of the first kind of order zero
J_1	Bessel function of the first kind of order one
K	Average seismic coefficient expressed as a fraction of gravity
$\bar{K}$	Average seismic coefficient expressed as a fraction of the maximum ground acceleration
L	Length of dam
m	The ratio $S_{1\rho 1}/S_{2\rho 2}$
M	Total mass of the sliding body
M_o	A function defined in the text
M_α	Amplification factor, magnitude of ground acceleration
P_o	A function defined in the text
q	The ratio $m(H-h)\rho_2/h\rho_1)$

S_{an}	Response acceleration
S_1, S_2	Shear wave velocity in the dam and in the layer, respectively
t	Time
u_1, u_2	Horizontal displacement of a point in the dam and in the layer, respectively, relative to the rock base
$\dot{u}_1, \dot{u}_2$	Velocity of a point in the dam and in the layer, respectively, relative to the rock base
$\ddot{u}_1, \ddot{u}_2$	Absolute acceleration of a point in the dam and in the layer, respectively
W	Weight of the sliding mass
y	Vertical coordinate
α	The depth of the base of the sliding surface from the crest
λ	Damping as a factor of critical
ρ	Mass density
ρ_1, ρ_2	Mass density in the dam and in the layer, respectively
ϕ	Angle of slope with the horizontal
$\phi_n(y)$	n^{th} mode shape for the dam
$\phi 1_n, \phi 4_n$	Shape function for one-parameter and four-parameter sliding wedge, respectively
$\psi_n(y)$	n^{th} mode shape for the layer
ω_n, ω_{on}	Damped and undamped circular frequency, respectively, of the n^{th} mode of the dam-foundation system

PART III

A	Pore pressure parameter
A_n	Dynamic pore pressure parameter
b	Width of the slice
B	Pore pressure parameter
c'	Cohesion at the base of the slice in terms of effective stresses
$\overline{c}'$	Average cohesion at the side of the slice
c'_i	Cohesion at the base of the slice i
DU_d	Dynamic pore pressure developed under the influence of $k_c W$
E	Total normal force on the side of the slice
E_o	Interslice body force
F	Factor of safety

Part III (Continued)

F_o	Static factor of safety
F_L	Local factor of safety in the side of the slice
h	Height of the section above the slip surface
i	Slice number
k	Seismic coefficient
kW	Horizontal earthquake load
k_c	Critical acceleration
k_o	Coefficient of earth pressure at rest
$\bar{k}_c$	Coefficient of anisotropic consolidation
l	Distance of the point of application of the normal force at the base of the slice from the edge of the slice
N,N'	Normal force at the base of the slice in terms of total stresses and effective stresses, respectively
N_o	Normal force at the base of the slice
PW	Force exerted by the pore water pressure on the side of the slice
T	Shear force at the base of the slice
T_o	Shear force at the base of the slice
u	Pore pressure at the base of the slice
U	Force exerted by the pore water pressure on the base of the slice
W	Weight of the slice
x	Horizontal coordinate
x_g,y_g	Coordinate of the center of gravity of the whole mass
x_m,y_m	Coordinate of the point of application of the normal force
X	Shear force on the side of the slice section
X_o	Interslice body force
Z_i	Height of the point of application of E force above the slip surface
α	Slope of the base of the slice with respect to the horizontal
γ	Density of the material
δ	Slope of the base of the slice with respect to the horizontal
Δu	Change of pore pressure due to cyclic loading

Part III (Continued)

$\Delta\sigma_1$	Change in axial stress
$\Delta\sigma_3$	Change in cell pressure
$\Delta\tau$	Applied cyclic load in simple shear test
λ	An unknown to be determined from the solution
σ	Stress component
σ'	Normal stress at the base of the slice
σ'_{vo}	Vertical consolidation pressure
σ'_{1c}	Axial pressure for consolidaton
σ'_{3c}	Confining cell pressure for consolidation
τ	Shear stress
ϕ'_i	Shear strength parameter at the base of the slice i
$\overline{\phi}'$	Average strength parameter at the edge of the slice

PART IV

c'_{av}	Average cohesion in terms of effective stresses
D	Driving force
k_m	The maximum value of the seismic coefficient
L	Length of sliding block
n'	Average effective normal stress on the slip surface
R	Resisting force
T	Predominant period of an accelerogram or twice the duration of the pulse
U_f	Force due to pore pressure at failure
W	Weight of the sliding block
x	Instantaneous displacement of the sliding block relative to the base
$\dot{x}$	Instantaneous velocity of the sliding block relative to the base
$\ddot{x}$	Instantaneous acceleration of the sliding block relative to the base
x_m	Permanent displacement of the block relative to the base
β	Slope of the sliding plane
τ	Average shear stress on the slip surface

In accordance with letter from DAEN-RDC, DAEN-ASI dated 22 July 1977, Subject: Facsimile Catalog Cards for Laboratory Technical Publications, a facsimile catalog card in Library of Congress MARC format is reproduced below.

Sarma, S K
Response and stability of earth dams during strong earthquakes / by S. K. Sarma, Department of Civil Engineering, Imperial College of Science and Technology, London, U. K. Vicksburg, Miss. : U. S. Waterways Experiment Station ; Springfield, Va. : available from National Technical Information Service, 1979.
82, [188] p. : ill. ; 27 cm. (Miscellaneous paper - U. S. Army Engineer Waterways Experiment Station ; GL-79-13)
Prepared for Office, Chief of Engineers, U. S. Army, Washington, D. C., under Grant Agreement No. DAERO-75-G-010.
References: p. 80-82.

1. Dam stability. 2. Earth dams. 3. Earthquake engineering. 4. Earthquake resistant structures. 5. Earthquakes. I. London. University. Imperial College of Science and Technology. Dept. of Civil Engineering. II. United States. Army. Corps of Engineers. III. Series: United States. Waterways Experiment Station, Vicksburg, Miss. Miscellaneous paper ; GL-79-13.
TA7.W34m no.GL-79-13